LOSS-IN-WEIGHT FEEDING IN CONTINUOUS POWDER MANUFACTURING

by

WILLIAM E. ENGISCH, JR.

A dissertation submitted to the

Graduate School - New Brunswick

Rutgers, The State University of New Jersey

in partial fulfillment of the requirements

for the degree of

Doctor of Philosophy

Graduate Program in Chemical and Biochemical Engineering

written under the direction of

Professor Fernando J. Muzzio

And approved by

_____

_____

_____

_____

_____

New Brunswick, New Jersey

October 2014

ABSTRACT OF THE DISSERTATION

LOSS-IN-WEIGHT FEEDING IN CONTINUOUS POWDER MANUFACTURING

By William E. Engisch, Jr.

Dissertation Director

Professor Fernando J. Muzzio

Processes involving granular material handling are found in many industries, such as pharmaceutical, chemical, catalyst, and food. Significant differences are observed, both between materials as well as between handling methods. Often, special equipment has been developed to monitor, control, and feed these widely varied materials in order to enable the end user to continuously feed or dose the raw powder material so that it can be continuously processed, which has many advantages over batch processing.

To address the difficulties of feeding granular materials, powder feeders are equipped with a variety of tooling that can be used for various rates and powders. Unfortunately most of the sizing and performance knowledge is internal to the feeding equipment manufacturers and is not generally available to the end-user.

In this work, a method for evaluating feeding performance was developed, which allowed for testing that was independent of the type of feeder being evaluated. This method was applied to various feeders to characterize the feeders for the feeding of various powders. In addition, the effects of hopper refilling were quantified and investigated. Finally, the downstream effects were simulated.

For each powder, the fluctuations caused during normal steady state feeding were minimized through tooling and feeder selection. The effects of refill were found to be considerably more significant than the fluctuations associated with steady state feeding. However, optimized refill schedules, easily reduced the deviations to more manageable levels.

In continuous manufacturing systems, the feeders are a potential high risk to content uniformity. The implications of this are investigated from a overarching view of a pharmaceutical direct compression system with a specific focus on regulatory compliance and product quality. Regulatory compliance requires batch definition and raw material traceability, and solutions to both were investigated. The presented options for batch definition are based on the residence time distribution (RTD) of the system, which describes the dispersion of material across the interface between "batches". Raw material traceability was similarly investigated utilizing residence time distribution as a tool.

ACKNOWLEDGEMENTS

Throughout the course of this project, I have been fortunate to have the guidance and encouragement of many individuals. I am very grateful to my advisor, Prof. Fernando Muzzio. Fernando, thank you for all of your time and support, especially with the development and multiple iterations of the many manuscripts. Without your insight, this work would not be possible. I would like to thank the members of my committee, Prof. Marianthi Ierapetritou, Prof. Rohit Ramachandran, and Dr. San Kiang, for their support and feedback.

Many thanks to the National Science Foundation's Engineering Research Center for Structured Organic Particulate Systems (ERC-SOPS) for funding my work and travel, allowing for many great opportunities to interact with others in the field. The many members of the ERC have provided valuable insight that has kept my research focused and relevant to industry. Thank you, all for the great challenging research projects and ideas.

Throughout my graduate studies at Rutgers, I was privileged to have met so many skilled individuals, who have shared their knowledge and encouragement: Dr. Aditya Vanarase, Dr. Alisa Vasilenko, Dr. Juan Osorio, Dr. Yijie Gao, Dr. Matt Metzger, Dr. Atul Dubey, Dr. Eric Jayjock, Pallavi Pawar, Sarang Oka, Abhishek Sahay, and Sara Koynov. I especially would like to thank the undergraduate students that have aided with various laboratory experiments: Daniel Mateo, Shikhar Mohan, Ritesh Shah, Wallace Torres, and Patricia Alvarado. For the sake of brevity, to all those not specifically mentioned, I am also grateful for your support.

I would particularly like to thank my family and closest friends. To my parental units, I have no doubt that your love and support are the strong foundation that I have built on. Finally, to my wife, Elizabeth, your love, encouragement, and patience have been invaluable.

TABLE OF CONTENTS

LIST OF TABLES

LIST OF FIGURES

Chapter 1. INTRODUCTION

1.1 Motivation

Across industry, continuous processing finds widespread application, due to its many technical and economic advantages [1]–[3]. However, in powder–based manufacturing processes that require a high degree of accuracy in product composition, this can be a troublesome proposition. Despite the many potential advantages of continuous "steady state" powder processing, which include smaller scale equipment, enhanced controllability, and reduced labor requirements, powder processing often focuses on suboptimal batch manufacturing, primarily due to lack of understanding of powder flow behavior in continuous manufacturing.

In continuous manufacturing, it is necessary to be able to dose powders consistently and accurately into subsequent unit operations, but for powders the ability to do this is limited by the accuracy of the feeding equipment. Loss-in-Weight feeders have improved the ability to control feedrate and minimize flow variability caused by bulk density changes associated with the emptying of the feeding hopper [4]. This is helpful once a feeding system is setup. Unfortunately, the selection and setup process for a feeding system is typically based on experience and empirical knowledge that is not readily available to the general user.

For loss–in-weight feeders, most of the existing knowledge regarding either (i) the effect of powder properties on flow rate intermittence, or (ii) the effect of feeder design and operation on discharged powder properties, resides with the equipment manufacturers. There has been some published work on improving feeder performance, for instance by

using various devices at the discharge [5], or vibratory hopper agitation [6], but actual specification and sizing is lacking. Feeder tooling selection (screw, discharge screen, etc.) is currently performed using trial and error, and there has been little work focusing on optimizing the feeding of granular materials.

The work presented in this dissertation focuses on the development of a fundamental and practical understanding of the impact of powder material properties, device design, and operating conditions on the variability in powder feed rate and on the effect on discharged powder material properties that can be applied to loss-in-weight powder feeders. This effort started systematically with the development of a method for the characterization of loss-in-weight feeders' performance (Specific Aim I) that could be used to aid in the proper selection of feeder tooling for a given powder at a given feedrate. The steady state performance of the feeders was evaluated for various operating conditions to characterize the baseline performance that could be expected from the feeders when they operated without any significant external disturbances (Specific Aim II). Then the effects of disturbances (specifically the upstream process that results in the refilling of the feed hopper) were evaluated (Specific Aim III). Finally, the downstream effects from fluctuations in the feeder were evaluated with the integration of the feeder into a continuous direct compaction line through the use of RTD modeling (Specific Aim IV). The four specific aims of this dissertation are listed below:

- Aim I: Method development (Chapter 2)
- Aim II: Evaluation of Steady State Feeder Performance (Chapter 3, Chapter 4)
- Aim III: Investigation of the effects of Powder Feeder Refilling (Chapter 5)
- Aim IV: Downstream effects of feeding (Chapter 6)

1.2 Background

1.2.1 Powder Feeding

In the powder handling and processing industries, powder cohesion causes large variability in the flow rate of ingredients fed from powder feeders. This can pass problems of composition and flowrate variability to subsequent unit operations [7]–[11] , making the ability to consistently and continuously feed a powder one of the most important challenges of the overall process. In batch processing, the metering of powder does not depend on the consistency of powder flow as a function of time, but instead depends only on the consistency of the overall amount metered to each batch. On the other hand, continuous manufacturing relies heavily on powder flow consistency as a function of time, therefore increasing the need for properly designed and optimized feeders/dispensers.

The intrinsic nature of powder makes the delivery of a consistent flow rate a challenge. Regardless of the comparisons and similarities to fluid, dry powders flow differently due to the tendency of powder to clump and aggregate, which causes the flowrate of powders to fluctuate even when the overall mean rate remains constant.

1.2.2 Feeders

To feed the many different types of powders with varying degrees of flowability for diverse applications, many powder feeder designs have been developed [12], [13]. Feeding equipment manufacturers try to keep the designs flexible by approaching the feeding equipment as a set of different parts that can be assembled, making the feeders modular and interchangeable. Typical feeders would be designed with the following

parts: hopper, flow aids (optional), weigh platform (optional, but needed for gravimetric control), and a mechanism for dispensing. An example of the modular and interchangeable nature of the feeders is that the same parts may be used by different feeders. The types of feeders are characterized by the mechanism used for dispensing, but other components are equally important in the overall design of a feeding solution.

There are a wide variety of hoppers, feed tooling, weighing platforms, and flow aids that can be used with each feeder type. Together, all these options allow a manufacturer to supply different feeders capable of handling a wide variety of powders with a very large range of achievable feedrates.

1.2.3 Feeding Control Principles

There are two main principles used for controlling the feedrate of a feeder: volumetric and gravimetric. Volumetric feeding is the simplest and least expensive feeding solution. The volumetric feeding principle controls to keep a constant fed volume per unit of time by regulating the speed of the feeding mechanism. This makes this type of feeding reliant on calibration coorelating drive speed and mass feedrate. Feedrate can be described by the following general equation:

$$\dot{m} = \rho_{bulk}\dot{V} \tag{1-1}$$

where ρ_{bulk} is the bulk density and $\dot{V}$ is the volumetric feedrate. In order for the volumetric feeding principle to maintain a constant mass feedrate ($\dot{m}$), the bulk density must remain constant [4]. This is fine where density does not vary, but powders are known to change density depending on the state of consolidation [14]–[16], environmental factors (such as moisture [17]), and changes in powder properties (such as

particle size [14], through segregation or attrition). To compensate for changes in powder density, the gravimetric control principle can be used.

1.2.3.1 Gravimetric Control Principle / Loss-in-Weight

The most significant improvement to continuous feeding is the ability for gravimetric or loss-in-weight control, which uses feedback control to adjust the mass feedrate. This ability to control mass feedrate allows loss-in-weight feeders to greatly improve feedrate control by minimizing flow variability due to density changes associated with the emptying of the feeding hopper [4].

1.2.3.2 Gravimetric controlled Batch feeding

In the case of batch processing, gravimetric control can be achieved by two different methods, gain-in-weight batching (GWB) and loss-in-weight batching (LWB). In GWB, each component is fed into the batch individually by a volumetric feeder controlled by the gain-in-weight (GIW) signal measured by a loadcell-instrumented collecting vessel. This is time consuming, especially when there are a large number of ingredients, because ingredients must be fed in sequence, multiple component streams being added confounds the GIW signal. Alternatively, a batch can have components fed simultaneously in LWB, requiring each feeder to be each instrumented with load cells and loss-in-weight (LIW) controls.

1.2.3.3 Loss-in-Weight

In a continuous system, instrumenting the subsequent unit operation with a loadcell for gain-in-weight control is not a realistic option, due to the need to feed multiple components simultaneously and the continuous nature of powder flow through the subsequent unit operations. So in this case, or in the case of feeding multiple components

in a batch system, loss-in-weight feeding is used. This enables the ability to monitor the feedrate of each component individually.

Although there may be small differences between the manufacturer's algorithms used in loss-in-weight control, the general design and methods are the same. All loss-in-weight feeders consist of three parts [6]: volumetric feeder, weighing platform (load cell), and gravimetric controller (see Figure 1). The volumetric feeder is mounted on top of a weighing platform that measures the mass of the feeder and its powder hopper. As the feeder feeds powder, the gravimetric controller acquires a signal from the loadcell in the weighing platform as a function of time. Using the difference in weight measured by the platform divided by time, the controller can determine the instantaneous feedrate, which is compared to the desired setpoint. The controller controls the feedrate by adjusting the mechanism that dispenses the powder from the feeder. The mechanism that is used to dispense the powder can include [12], [13]: screw [18], vibration [19], belt [20], and rotary valve [21]. Regardless of type, the theory of gravimetric loss-in-weight control and the function of the feeder remains the same.

Most manufacturers can provide a variety of paired weighing platforms to accommodate the need for high resolution loss-in-weight data used for control. This ensures that an appropriately sized loadcell is selected for the desired feedrate setpoint. In some cases the weighing platforms consist of multiple loadcells in order to accommodate feeders with differing geometries or larger sizes.

1.2.4 Improving feeding accuracy

There has been a small amount of work focused on improving the uniformity of feeding rate by improving the discharge of screw feeders, updating feeding control algorithms [22]–[24], or designing an entirely new type of feeder.

Kehlenbeck modified the discharge of screw feeders in a variety of ways. See Figure 1.2. He modified the standard dosing tube by adding dents and holes on the tube so that material left the feeder radially from the screw rather than in the typical axial direction. Attachments were added at the end of the dosing tube, including a grid shaped screen, a star shaped screen, a rotating rotor that sliced the powder, and a rotating star shaped screen. It was discovered that screen and rotor attachments at the end of the feeding tube displayed larger improvement than modifying the dosing tube [5]. Tardos used a vibrating hopper to improve the performance of a screw feeder [6]. Figure 1.3 shows how the standard deviation of feedrate decreased for increasing amplitude of vibration. Vibration helps to generate flow [25], [26] within hoppers, which aids in the uniform filling of flights of screws in feeders. Other flow aids that could be included in feeder designs due to their ability to improve hopper flow are internal stirring, external paddle agitation on a flexible wall [27], and gas assisted flow [28].

1.2.5 Refill

Under its standard gravimetric mode of operation, a loss-in-weight (LIW) feeder's controller compares the observed gravimetric feedrate to the user-defined setpoint. Depending on the deviation from setpoint, the controller may send a new signal to the feeder to change the speed. However, since the feeder hopper has a finite volume, a continuous process requires periodic refill of the feed hopper. It has become common

industrial practice to replenish the feeder when it reaches the lowest level that the manufacturer would recommend for operation. For the refill process, it is typically recommended to initiate filling at around 20% fill level and continue until the hopper fill level reaches 80%. [29], [30] However, during this refill time and a short settling time thereafter (typically about 10-15 seconds) [29], [31]–[33], the feeder operates in volumetric mode and does not monitor nor control the gravimetric feedrate, opening the possibility for deviations from setpoint. Even if the feeder screw continues to rotate at a constant speed, a potential source of deviation occurs when the incoming material compresses the bed of powder within the hopper, thereby increasing the density in the hopper, causing over-feeding [34]. Another source of deviation occurs when the material becomes aerated by the refill procedure. When this occurs, the powder behaves like a liquid and flows through the screws uncontrollably [32].

Although there have been no journal articles published on improving performance during the refill of gravimetric feeders, there have been a few patents created by manufacturers that attempt to address this limitation of using a continuous feeder that will eventually require refill. [34]–[36]

In US Patent 4524886 (See Figure 1.4), Wilson and Loe use values stored during the emptying of the feed hopper to control the screw speed during refill [34]. This is also the current method used in the K-Tron manufactured feeders. Although this is a method that can potentially work in a slow refill process, this method has problems when refill times are very short. This is briefly mentioned in the K-Tron operations manuals for their twin-screw feeders suggesting that the “Refill Array” feature only be enabled for refill methods that are longer than 15 seconds in duration [31].

US Patent 6446836 (See Figure 1.5) by Aalto and Bjorklund addresses the problem by using redundant replenishment hoppers instrumented with load cells [35]. When the gravimetric feeder requires replenishment, one of the hoppers receives a signal to refill. The other replenishment hopper remains isolated from the gravimetric feeder, and is replenished with material from a pneumatic refill system. The subsequent feed hopper refill will be handled by this recently refilled replenishment hopper. The loadcells connected to each isolated replenishment hopper pass the rate of refill signal to the dispensing gravimetric feeder's controller. This removes the uncertainty of the rate of the refill stream from the replenishment hopper, enabling the feeder to operate in a modified gravimetric mode throughout the refill process.

Wilson and Bullivant discuss in US Patent 4579252 (See Figure 1.6) a method that bypasses the issue altogether. They use a second feeder to feed while the original one is refilled [36]. Although this method may have the best results, it also has the disadvantage of the expense of a secondary gravimetric feeding system and the additional space required around a downspout that may already be crowded by other feeders supplying different components.

1.2.6 Continuous Manufacturing in the Pharmaceutical Industry

Pharmaceutical manufacturing has a long history of developing and manufacturing drug product in batches. This production technique was used for industrial chemicals and other consumer products long before the industrial revolution (18th century) when an initial shift from batch to continuous processing occured. Due to continuous process advantages, today the majority of commodity chemicals, petrochemicals, food, and consumer products are manufactured continuously, leaving pharmaceuticals behind,

which are still made with traditional batch processes. Many sources have suggested that pharmaceutical manufacturing has been frozen in time due to regulatory requirements that generate large amounts of paperwork causing huge monetary cost in production delays resulting from even minor manufacturing changes (See, for example, a Wall Street Journal article on this topic [37]). This has lead to fearful, conservative cultures within the industry, which would rather remain steadfast with old and familiar technology rather than evolve with new technologies that improve the industry.

With the goal of modernizing and spurring technological improvement in the regulation of pharmaceutical manufacturing and product quality, in August 2002 the Food and Drug Administration (FDA, http://www.fda.gov) launched a regulatory modernization initiative, meant to encourage early adoption of new technological advances, facilitate industry application of modern quality management techniques, encourage implementation of risk-based approaches, ensure regulatory policies are based on state-of-the-art science, and enhance the consistency and coordination of drug quality regulatory programs. [38] A series of guidances have since been published, which further encourage significant changes to processes used to manufacture pharmaceuticals. The FDA has published the initial Process Analytical Technology (PAT) Framework [39], which supports the move from static batch processing to more dynamic approaches that mitigates the risk of producing poor quality product. The International Conference on Harmonization (ICH, http://www.ich.org) implemented a trio of quality guidances; Q8(R2), Q9, and Q10 [40]–[42], which introduced valuable new concepts such as quality by design (QbD).

Although the regulatory guidances describe in detail what is necessary, they provide little explanation of how to accomplish them. To begin filling in this gap, the International Society for Pharmaceutical Engineering (ISPE, http://www.ispe.org) launched the Product Quality Lifecycle Implementation (PQLI) initiative in 2007. This initiative aims to provide practical solutions for implementation challenges of the ICH guidances [43]–[45], while still recognizing that there are multiple satisfactory ways to address the concepts described in the guidelines [43]. However, there is little focus on providing solutions that directly apply to continuous processing.

1.3 Figures for Chapter 1

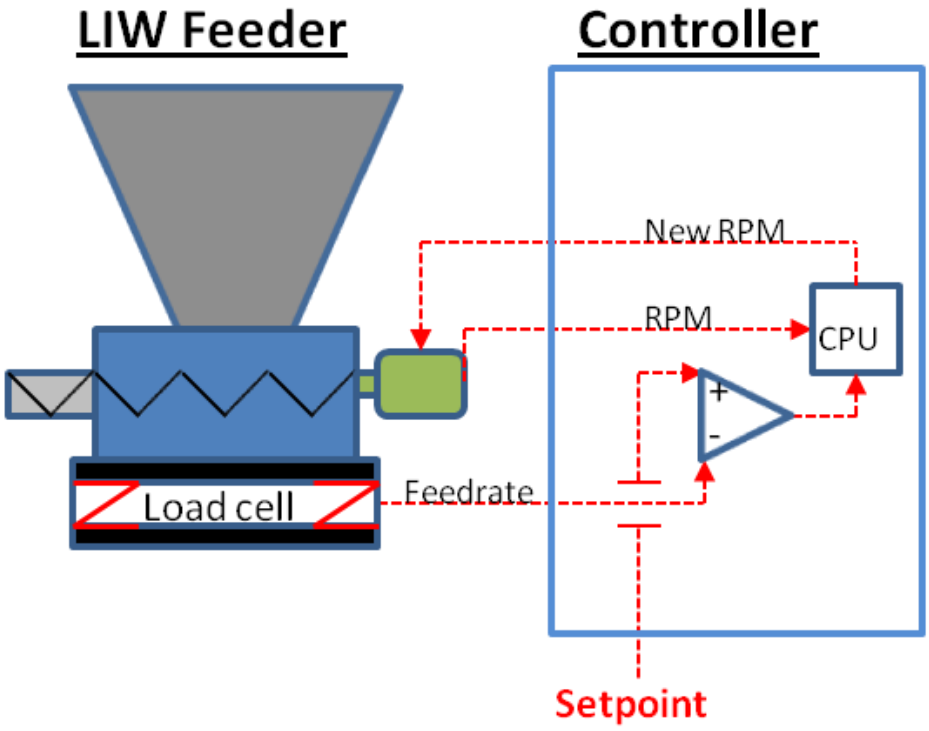

Figure 1.1: Diagram of the main components of a loss-in-weight feeder. A volumetric feeder is mounted on a load cell with a feedback controller monitoring and controlling feedrate.

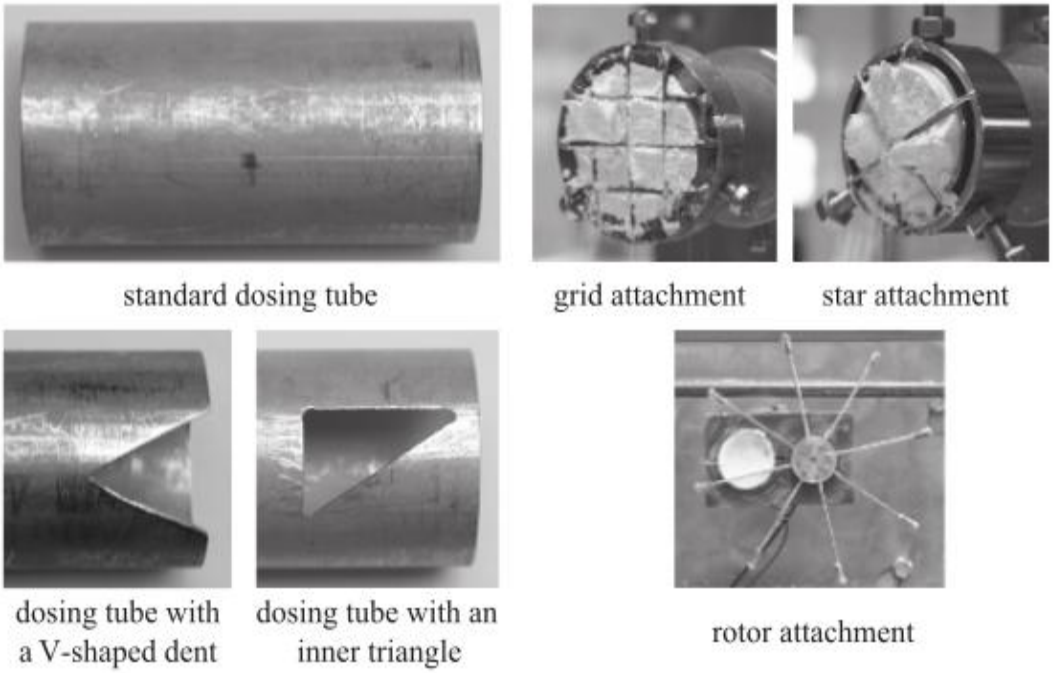

a.

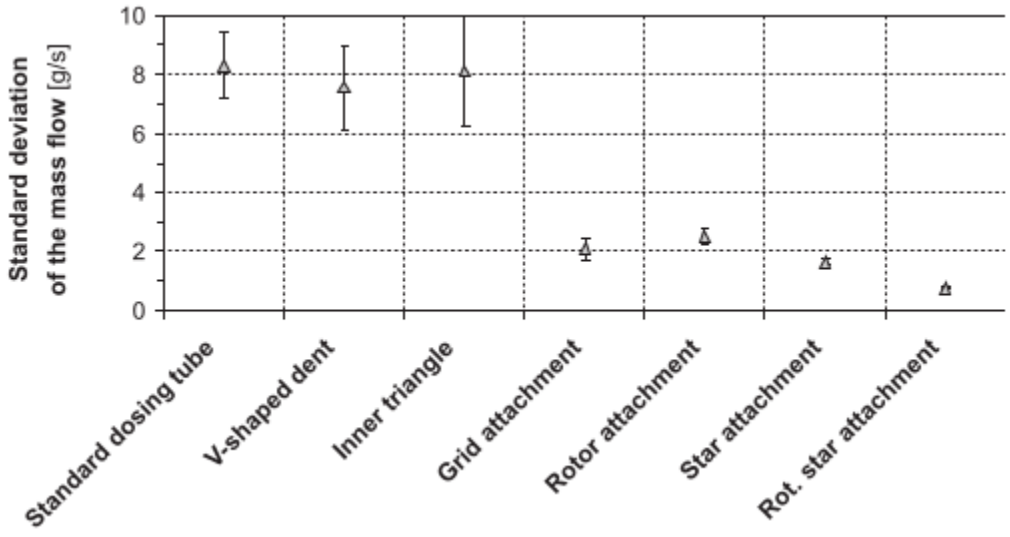

b.

Figure 1.2: a.) Attachments used by Kehlenbeck *et al* to improve feeding constancy. b.) The standard deviation of mass flow results for the various feeding attachments. [5]

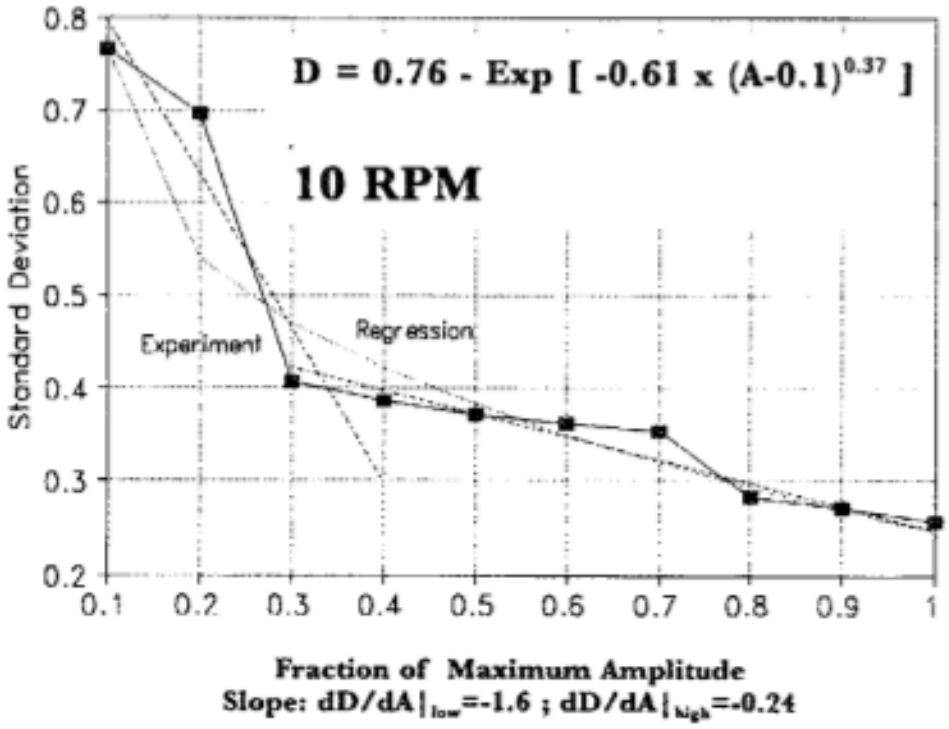

Figure 1.3: Standard deviation versus vibration amplitude for a screw feeder as displayed in the results by Tardos *et al.*[6]

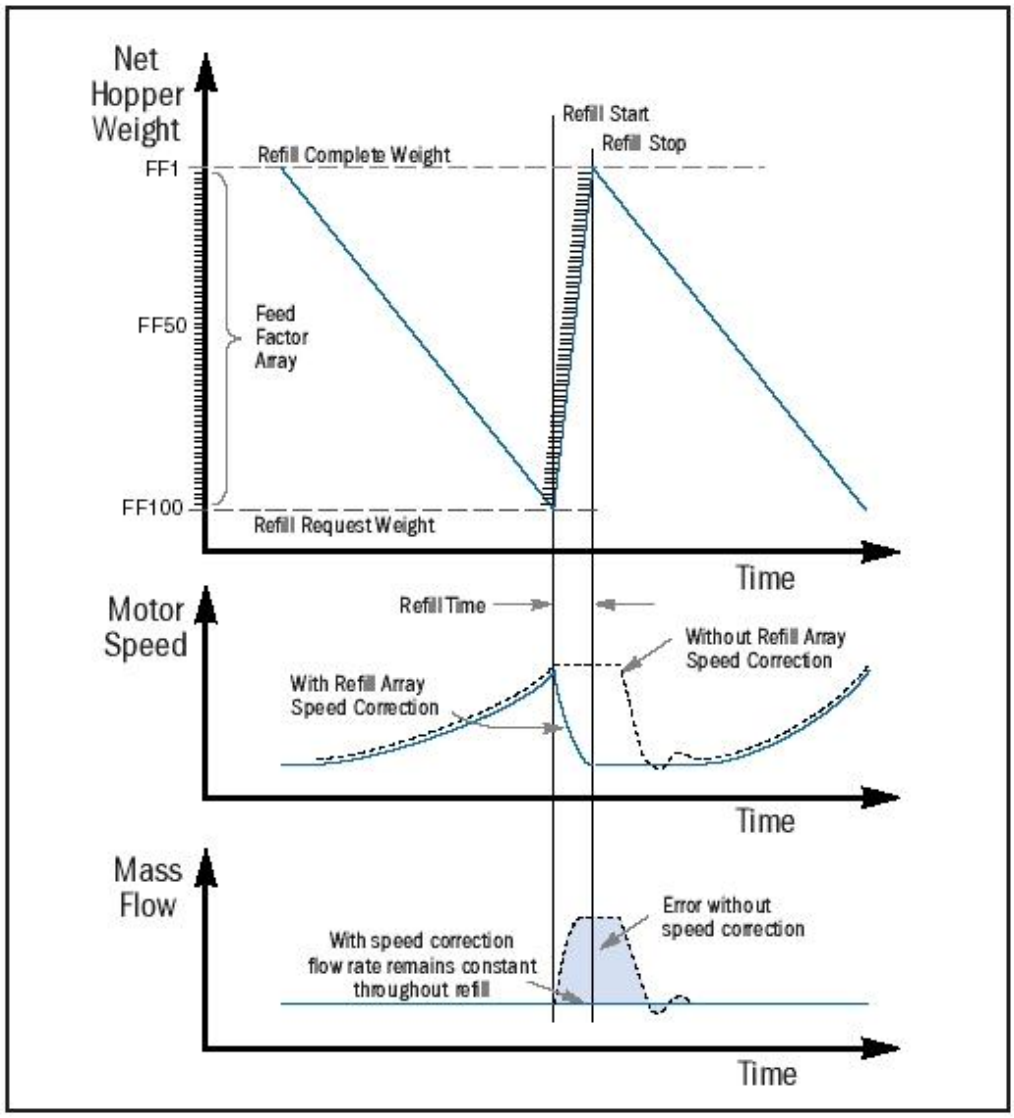

Figure 1.4: Depiction of the feed factor array described in the patent by Wilson and Loe [34]

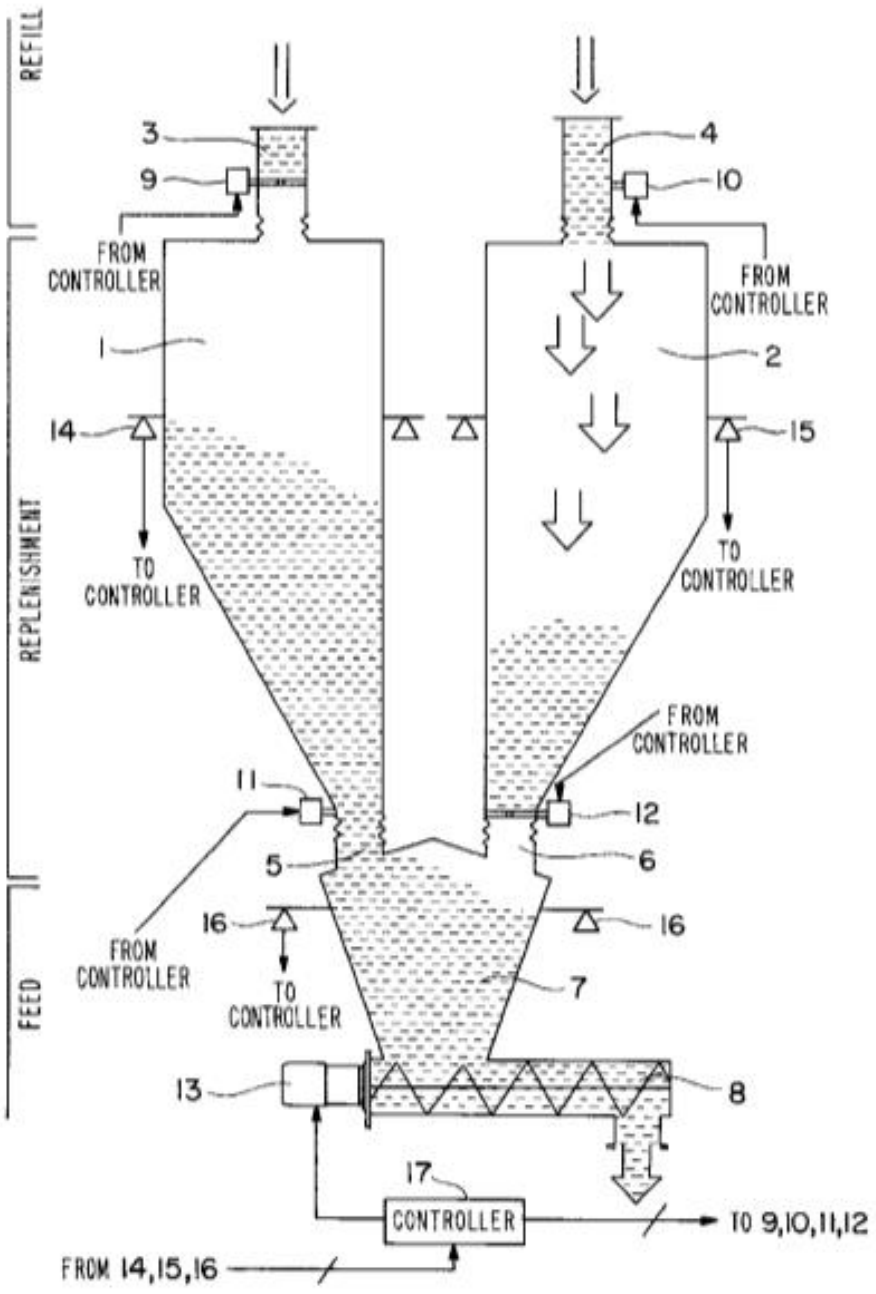

Figure 1.5: Depiction of the redundant and loadcell-instrumented replenishment hoppers described in the patent by Aalto *et al* [35]

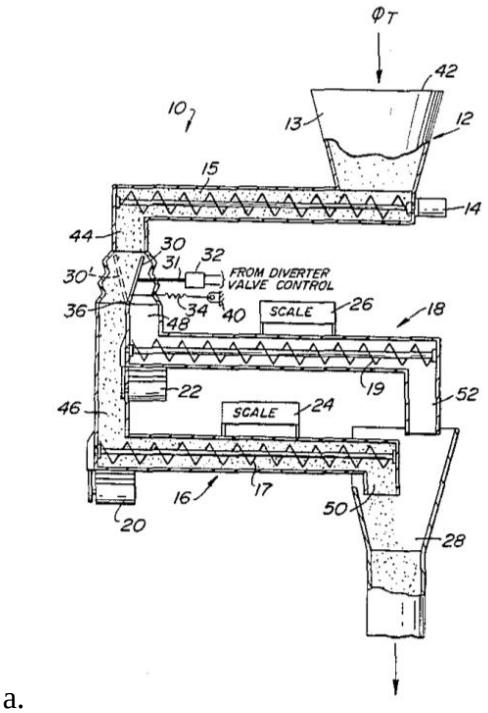

a.

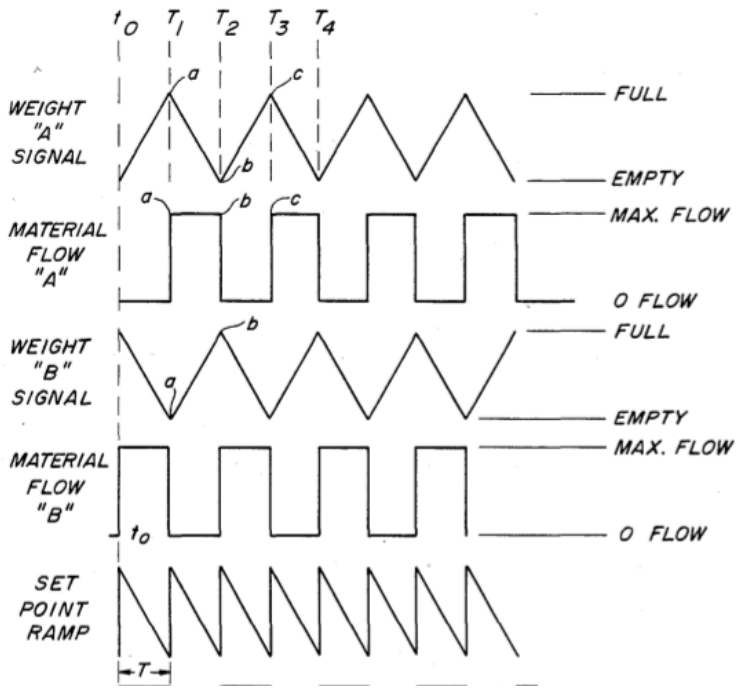

b.

Figure 1.6: a.) Depiction of the redundant feeder and b.) control signals described by Wilson *et al* [36]

Chapter 2. METHOD FOR CHARACTERIZATION OF LOSS-IN-WEIGHT FEEDING EQUIPMENT

2.1 Summary

Loss-in-weight feeders have improved the ability to control feedrate and minimize flow variability caused by bulk density changes associated with the emptying of the feeding hopper [4]. This is helpful once a feeding system is set up. Unfortunately, the selection and setup process for a feeding system is typically based on experience and empirical knowledge that is not readily available to the general user. For loss-in-weight feeders, most of the existing knowledge regarding either (i) the effect of powder properties on flow rate intermittence, or (ii) the effect of feeder design and operation on powder properties, resides with the equipment manufacturers. There has been some published work on improving feeder performance, for instance by using various devices at the discharge [5], or vibratory hopper agitation [6], but actual specification and sizing information is lacking. Feeder tooling selection (screw, discharge screen, etc.) is currently performed using trial and error methods, and there has been little work focusing on optimizing the feeding of materials.

This chapter focuses on the development of a method for the characterization of loss-in-weight feeders that can be used to aid in the proper selection of feeder tooling for a given powder at a given feedrate. The method includes the experimental setup and procedure for collecting feeding data and the data filtering and data analysis methods that are used to obtain useful values for comparison. The experimental procedure is a multiple step process that involves running the feeder in both volumetric and gravimetric modes.

Volumetric studies are performed to determine capacity, followed by gravimetric studies, which are used to determine overall performance. The performance data for each condition is analyzed using relative standard deviation and also analysis of variance (ANOVA). The method is validated and applied to evaluate performance in the full operational range of the K-Tron KT35 loss-in-weight feeder for three pharmaceutical grade powders.

After a brief description of materials and equipment (Section 2.2), the developed method is introduced in Section 2.3, and then used to evaluate performance of the K-Tron KT35 loss-in-weight feeder for three pharmaceutical grade powders (Section 2.4). Conclusions are described in Section 2.5.

2.2 Materials and Equipment:

2.2.1 Materials

The powder materials used in the experiments are listed in Table 2.1. These pharmaceutical powders were chosen to test a range of cohesiveness and flowability in the feeder characterization experiments. Flowability of each powder is quantified through the use of the flow index measured from a Gravimetric Displacement Rheometer (GDR) and the dilation value is obtained from a simple drum tumbler. [46]–[49] The GDR consists of a cylinder mounted on a hinged lever arm supported by a load cell. As the cylinder on the GDR rotates, the material dilates and forms avalanches as it tumbles. The standard deviation from the load cell of the GDR is proportional to the size of avalanches formed at various speed settings, and this standard deviation is used to compute the flow index. The dilation number is calculated from the ratio of the initial

consolidated powder bed volume and the equilibrium powder bed volume while flowing in a tumbling drum. A higher flow index and/or dilation number indicates that the powder is more cohesive and harder to flow.

2.2.2 Schenck Accurate AccPro II with 7 kg Load Cell (Catch Scale)

A Schenck Accurate AccPro II was used as a "catch scale" for characterization of the loss-in-weight feeders' performance. A catch scale is needed because the internal load cells used in gravimetric loss-in-weight feeders use different filtering algorithms to pre-treat the gravimetric signal, which may not allow for accurate performance comparison between different feeders. AccPro II is a PC Excel program that obtains weight readings from a 7 kg strain gage load cell through the Schenck DISOBOX summing box. The DISOBOX uses a 24 bit Analog Devices A/D converter to obtain the weight readings every 0.1 seconds. These readings are obtained and stored by the AccPro II application. Although the AccPro software includes a built-in data analysis that runs in real time as the catch scale is collecting, only the raw 0.1 second readings are used for post-processing and analysis. The AccPro II catch scale was chosen as a catch scale as it was large enough to handle the typical feedrates of the K-Tron KT35 feeder, but still has a high resolution that can catch the small variations associated with feeding powders. In general, typically the smallest acceptable available scale should be used as the resolution will typically be the highest in similar quality scales. A scale chosen for this application needs to also have very fast response and settling time.

2.2.3 K-Tron KT35 Loss-in-Weight Feeder

The K-Tron KT35 twin screw loss-in-weight feeder was designed to handle a large range of pharmaceutical powders, including those with very poor flowability, which are often

lumpy and tend to build bridges. The design consists of a modular twin-shaft feeder mounted on a sanitary weigh bridge. There are a variety of feeding screws and discharge screens, which allows one to feed a large range of bulk powder materials. Figure 2.1 displays the K-Tron KT35 feeder with the Schenck Accurate AccPro II catch scale, and Figure 2.2 displays a representative sample of feeder tooling for the KT35 feeder. At the bottom of the feed hopper is a bowl containing a horizontal agitator that helps fill the flights of the feed screws. The agitation speed is set at 17% of the feed screw speed. The gearbox controlling the screws is a type B with a gear ratio of 6.7368:1 combined with a motor with a maximum speed of 2000RPM. At 100% of the motor speed, the screw rate is 297 RPM (327 RPM @ 110% is also achievable by over-speeding).

2.3 Methodology

Determining the performance of a powder feeder includes an experimental setup to collect feed stream data, filtering noise, and analysis. Of the many benefits of a method for characterizing loss-in-weight powder feeders, the most significant is a means of determining differences in feeding performance that can be used to optimize the feeder and tooling selection. Quantified feeding performance also provides general users of feeding equipment an additional tool to validate that the feeder is performing according to the feeder's controller displays. The gravimetric control of the loss-in-weight feeder involves a significant amount of noise filtering, and as a result, the process variables displayed by the feeder's controller often appear more consistent than they actually are. In addition, a poor or erroneous calibration of the loss-in-weight feeder's loadcell will cause the controller to display a feedrate that is offset from the actual feedrate.

2.3.1 Experimental Setup

Characterization experiments were performed by using the Schenck AccPro II scale to record the weight of powder dispensed by the feeder every 0.1s for all tests. A 9" diameter and 9" height bucket was used to collect the samples. Figure 2.3 shows a graphical representation of the experimental setup used for monitoring feedrate and determining steady state performance. The feeders were placed on a sturdy lab bench. The catch bucket and scale were placed on a separate lower stand with the bottom of the bucket at 10" below the outlet of the feeder. When a bucket becomes full, it is quickly replaced by an empty bucket. Due to the sensitivity of the load cells in the equipment, careful consideration was taken to isolate and minimize outside disturbances on the feeders and catch scale. In determining equipment placement and filtering methods, the various general considerations listed in the work by Erdem have been taken into account [50]. Most importantly, a curtain was placed around the setup to minimize effects from air currents.

In addition to catch scale data, the feeder process values were recorded, including screw drive speed and hopper fill level. The data from each feeder was compared to the data obtained from the catch scale. Testing proceeded with first determining the volumetric capacity of the feeder operating at various volumetric speeds (without engaging the feeder gravimetric control system). Following this, the testing of gravimetric performance was performed by monitoring the feedrate from the feeder for more than 30 minutes. A time longer than 30 minutes was chosen so that there would be a sufficient data for statistical comparison. As volumetric capacity testing only requires an estimated average feedrate, these tests can be short, with only achievement of a steady state

required (or as close to it as possible) for a given set of experimental parameters (powder, tooling, screw speed, hopper fill level)

2.3.2 General Volumetric Test Run Procedure

The general procedure for the volumetric capacity experiments is as follows:

1. Calibrate the catch scale.
2. Fill the feeder to 100% of the maximum hopper fill level.
3. Run tests with volumetric set points at 10%, 20%, 50%, 80% and 90% of the control magnitude or screw speed.

Volumetric mode is not the typical operation of the feeder and as such, the equipment may not have settings to select the speed of the screw manually. The K-Tron feeder used in this experiment required manually setting the initial feed factor to 100 kg/hr. After manually setting this value, the volumetric set points could be entered directly with the default units of kg/hr signifying % screw speed. The initial feed factor is the control value that refers to the capacity of the feeder at 100% of the control magnitude. This is the initial feed factor, as the feed factor often changes slowly with hopper fill level. When running in gravimetric mode, the feeder will continually correct the feed factor.

2.3.3 General Gravimetric Test Run Procedure

The general procedure for the characterization experiments is as follows:

1. Calibrate the feeder and catch scale.
2. Fill the feeder to 100% of the maximum fill level.

3. Find the maximum feed rate for each experimental combination (powder, screw type, screens, agitation rate, agitation depth), and use this for the initial feed factor controller value.
4. Run tests with set points at 20%, 50% and 80% of the maximum controllable speed with initial fill level at 100% of the maximum fill level.

The maximum controllable feedrate for each feeder can also be determined as the result of the built-in auto feed factor calibration program of the feeder's controller, rather than running volumetric capacity tests. This returns the value of the initial feed factor, which is the estimated feed rate at 100% of the screw speed that is used to control the feeder. An issue with using the built-in auto feed factor calibration program of the feeder is that if the relationship between the average feedrate and volumetric screw speed is not linear, the estimated feed factor could have some error, as it assumes a linear relation to extrapolate the value. Although a non-linear relationship is not very common for free flowing powders, it becomes more common with powders that are cohesive and are unable to consistently fill the flights of the screw at higher rotation rates.

The feed factor is used primarily for a volumetric reference point for the feeder and may be used whenever the feeder may need to be run in volumetric mode. A feeder running in gravimetric mode will occasionally switch to volumetric mode in instances where gravimetric control is impossible, such as during refilling of the feed hopper or when the feeder is "bumped".

The initial calibration of the feeder and catch scale load cells is of utmost importance, because if either of them is miscalibrated then the values collected from these load cells

would be meaningless. Miscalibration of the feeder load cell has an additional implication since the feeder uses this signal for control. If this is incorrect, the feeder will misinterpret changes in weight, thus controlling to a different value than setpoint. This is a common mistake made when the wrong units are used for a check weight. This can be quite confusing to an operator that enters a desired setpoint of 5 kg/hr which is then displayed on the controls of the feeder, yet the actual feedrate being fed is 5 lbs/hr (or 2.27 kg/hr). Unless checked with a correctly calibrated catch scale, or until the calibration is rechecked with a check weight, it may go unnoticed until problems are discovered downstream.

The initial filling of the feeder is important as there is often a substantial change in the screw filling at lower fill levels. To avoid this issue altogether, it is recommended to fill the feeder close to maximum for testing, thereby ensuring that the minimum operation level is exceeded. Most feeding manufacturers state that this minimum is ~20% hopper fill level, but this is dependent on powder properties and may vary.

2.3.4 Analysis and Filtering

The data collected from a catch scale is gain-in-weight information that can be used similarly to how the controller in a loss-in-weight feeder extracts useful values of feedrate from the loss-in-weight signal of the feeder's built-in load cells. To analyze the data, the mass dispensed every 1 second is used to calculate the fed material mass for the interval. From this data, the average feedrate ($\dot{m}_i$) can be calculated for each 1 second (Δt) interval:

$$\dot{m}_i = \frac{\Delta m_i}{\Delta t} \tag{2-1}$$

From all the mass flowrates at each interval, a distribution can be determined; and from this distribution, the standard deviation (σ) and relative standard deviation (RSD) can be calculated:

$$\sigma = \sqrt{\frac{\sum_{i=1}^{n}(\dot{m}_i - \overline{\dot{m}})}{n-1}} \tag{2-2}$$

$$RSD = \frac{\sigma}{\overline{\dot{m}}} \tag{2-3}$$

where $\overline{\dot{m}}$ is the arithmetic mean mass feedrate of the distribution and n is the number of samples in the distribution.

2.3.5 Data Analysis: Discrete Fourier Transform:

Using the feedrate data that was obtained through gain-in-weight information collected by the catch scale, it is possible to investigate the frequency of fluctuations through the use of Fourier Transform methods. This requires the transformation from the time domain to the frequency domain and it is based on the Fourier Transform:

$$S_x(f) = \int_{-\infty}^{\infty} x(t) e^{-j2\pi ft}\, dt \tag{2-4}$$

(Forward Transform)

$$x(t) = \int_{-\infty}^{\infty} S_x(f) e^{j2\pi ft}\, df \tag{2-5}$$

(Inverse Transform)

where x(t) is the time domain representation of the feedrate signal, $S_x(f)$ is the frequency domain representation of the feedrate signal, and $j = \sqrt{-1}$.

To digitally compute the Fourier Transform from a discrete and noncontinuous set of values, such as the signal data collected from the catch scale, a numerical integration called a discrete Fourier transform (DFT) must be performed to approximate the true Fourier Transform. The DFT of the feedrate data is computed using a fast Fourier transform (FFT) algorithm in Matlab based on the FFTW library [51].

$$X(k) = \sum_{j=1}^{N} x(j)\omega_N^{(j-1)(k-1)} \tag{2-6}$$

(Forward Transform)

$$x(j) = (1/N)\sum_{k=1}^{N} X(k)\omega_N^{-(j-1)(k-1)} \tag{2-7}$$

(Inverse Transform)

where $\omega_N = e^{(-2\pi i)/N}$ is an N th root of -1.

By using Fast Fourier Transform on the feedrate data collected during the characterization test runs, it is possible to obtain power spectra. In Figure 2.4, several of these power spectra are shown. The sources of the dominating frequencies of this twin screw feeder are not obvious due to interactions between the two screws and the agitator. Table 2.2 shows the rotation rates and frequencies associated with the percent screw speed for both the screws and agitator. At 20% the rotation rate of each of the screws is approximately 60 RPM with a frequency of 1 Hz. For Fast Flo Lactose, this could be the reason for the peak at 1 Hz, but neither Avicel 102 nor Ceolus display this peak, but

instead have a peak at ~1.5 Hz. The frequency of the agitator is a little less than 0.5 Hz, which could cause the peak that is seen in each of these powders. At 50% of the maximum screw speed, the frequency is about 2.5 Hz, which again relates to one of the peaks in the Fast Flo Lactose, but again neither the Avicel 102 nor the Ceolus display this peak. At this screw speed, the agitator would have a frequency of ~0.9 Hz, which could cause the peak that is observed at ~1 Hz. There are multiple frequencies that contribute to feedrate variability, and feeding behavior varies depending on the powder that is fed and the feeder tooling being used, making the feed stream from a feeder a very complex data series.

2.3.6 Data Filtering

During the analysis, in order to eliminate disturbances in the feedrate data caused by refilling, machine startup/shutdown, etc., the data is filtered by rigorously removing disturbances from the original data set. As an initial rough filtering method, 3 seconds of data are removed before and after each disturbance (total of 6 seconds in addition to the perceived duration of the disturbance), as this allows adequate time for the equipment to settle after a disturbance. Disturbances can be detected in the data set by setting appropriate bounds to the acceptable data. Since the feeder is under gravimetric control, the feedrate should not be deviating more than 10% from the setpoint. This is a modest set of bounds, as the feeder controls the feedrate much more tigthly than this criterion. Thus, these bounds will detect significant physical disturbances to the catch scale, such as bucket change-overs.

By comparing the distribution of the original unfiltered data with the filtered data, it is possible to further optimize the filtering procedure. The initial filtering of an extra 6

seconds in addition to each disturbance results in a roughly filtered data set that has an average feedrate that is an initial estimate of the quasi-steady behavior and a standard deviation that is relatively close to the true value. The ideal filter uses the mean and standard deviation of the filtered data, so an iterative procedure with this initial estimate is needed. The bounds used for each iteration are three standard deviations about the average. After each iterative pass, increasingly better estimates of the mean and standard deviation are calculated. After several filtering passes, the iterative filter self tunes and results in a final average and standard deviation that is unchanging with additional filter passes and is representative of the data without the outlying datapoints caused by disturbances. Shown in Figure 2.5 is the average feedrate and standard deviation calculated after each filtering iteration for a sample data set.

The average and standard deviation of the unfiltered data set could also be used as a first pass, but if there are many disturbances this will result in an initial estimate that may not be close to the true value. In addition, this will require many passes before the average and standard deviation of feedrate approach a limit as is shown in Figure 2.6. In data sets where the data collection system was heavily perturbed, it may never converge.

Figure 2.7 shows a sample set of unfiltered catch scale data with a disturbance at ~60 seconds into the set, when a bucket became full and was replaced with a new empty one. Figure 2.8 shows the data after filtering. After filtering out disturbances, the leftover data is representative of the quasi-steady behavior of the feeder. The “steady state” distribution of the feed rate data is obtained with the feeder operating in gravimetric loss-in-weight mode. The example presented in Figure 2.8 shows feedrate data as a function of time and its respective distribution, which for properly filtered data approaches a

Gaussian curve. There are two important parameters for performance that can be gathered from steady feedrate signal data: spread of the data (standard deviation), ideally as narrow as possible; and deviation of the average from the setpoint, ideally zero.

In order to be able to use the standard deviation as a means to compare different feed rate data sets, it is highly advantageous to verify that the data sets have a normal distribution. This is important, as a normal distribution can be simply described with two values, the average and the standard deviation. Moreover, knowledge of the existence of a parametric distribution with accurately estimate parameters enables the use of a limited data set for the prediction of the frequency of extreme deviations.

Figure 2.9 shows two sample distributions of catch scale data collected from the K-Tron KT35 with the coarse concave self-cleaning twin screws feeding different powders at different rates. Figure 2.9a displays data that was collected with a coarse square discharge screen with the feeder feeding Fast Flo lactose at 70 kg/hr. Figure 2.9b shows data obtained when the feeder was feeding Avicel 102 through a fine square discharge screen at a rate of 105 kg/hr. Both distributions have a Gaussian shape, which is confirmed by the linear probability plots. A normal Gaussian fit for the data reduces the need of descriptive variable to only two: average and standard deviation. Comparing the two distributions shows that the differences in average and standard deviation are visually apparent and significant.

2.3.7 Experimental Conditions Examined

The parametric space for the K-Tron KT35 feeder was sampled using twelve tooling configurations, three powders, and three feedrate setpoints. Figure 2.10 provides a

graphical representation of the experimental design used for the characterization of this K-Tron KT35 feeder. For the feeder tooling, there are four sets of twin screws (coarse concave, fine concave, coarse auger, and fine auger) and three screen configurations (coarse square screen, fine square screen, and without the use of a screen) for a total of twelve feeder tooling (screws and screens) combinations. The concave screws are specially designed and shaped to be self-cleaning, with the flights of the pair of screws interspersed very closely to each other. The auger screws are not self cleaning, and therefore it is possible for a highly cohesive material to adhere to the screws, filling part of the flight with material that does not get dispensed and reducing the overall theoretical throughput of the screw pair. At each of these configurations, the feeder performance was characterized at three different setpoints (20, 50, 80% of maximum flowrate for a given feeder tooling configuration) using the three pharmaceutical-grade powder: 316 Fast Flo Lactose, Avicel PH-102, and Ceolus KG-802. Thus, a total of 108 experimental combinations (4 screws * 3 screen configurations * 3 test speeds * 3 powders) were tested for the characterization of this feeder.

2.4 Results and Discussion:

2.4.1 Determination of Volumetric Capacity:

The volumetric capacity was obtained for each powder (FastFlo Lactose, Avicel 102, and Ceolus) and each tooling combination. A few of the resulting volumetric capacity plots are displayed in Figure 2.11. The volumetric speed setpoints were 10, 20, 50, 80, and 90% of the maximum speed of the screws. These speeds were chosen to sample the whole range of the feeder including those points that are outside of the typical operating range of 20-80%.

An important observation from the volumetric capacity plots in Figure 2.11 is the relationship between the volumetric capacity and the volumetric setpoint. In all of the cases tested in this study the relationship was linear, which suggests the powders fill the flights of the screws consistently. This also signifies that the feed factor calibration for volumetric operation can be calibrated or calculated from a linearly fitted volumetric capacity chart. These charts are also useful for determining sizing of screws as the range of capacity for the various combinations of screws and discharge screens are different. In the following gravimetric study, the capacities found for the volumetric setpoints of 20%, 50%, and 80% are used for the gravimetric setpoints.

Although the volumetric capacity plots were linear, there are some common causes for inconsistent flight filling. Some powders that are very cohesive may present hindered filling of the screws flights at higher feedrates due to bridging over the screws. This can cause phenomena such as hopper "rat holes", or in extreme cases complete bridging above the screws. Under such conditions no material would enter the screw, thereby stopping the flow. Figure 2.12 displays an example of "rat holing" in a Schenck PureFeed loss-in-weight feeder. Other causes that could result in inconsistent screw filling include the screw becoming coated with powder or powder density changes. Figure 2.13 shows screw coating of the auger (not "self-cleaning") twin screws with a very cohesive powder, which had the tendency to coat all the exposed metal surfaces of the feeder.

There were a few unexpected failures in the volumetric capacity studies. Although Fast Flo Lactose ran for all tooling conditions and speed settings, Avicel 102 and Ceolus overloaded the motor of the feeder for some settings when run with the fine square

screen. Avicel 102 only caused a motor overload problem at the highest speed setting (90%) when used in combination with the coarse auger twin screw (CAS), which are the highest throughput screw. As 80% was the highest speed tested in the gravimetric studies, this did not affect the range of study for the gravimetric testing. For Ceolus, both the coarse auger twin screw and the fine auger twin screw had a motor overload error with the fine square screen and could not be run, and thus were not tested in the gravimetric performance testing with the fine square screen. The reason for these motor overloads is that as the screws were pushing powder through the screens, and since the screen added resistance, the powder was compressed, which greatly increased the torque needed to continue pushing the powder through the holes of the screen. To avoid damage to the feeder and its tooling, the feeder shuts down with an overload alarm if the torque becomes too high.

2.4.2 Gravimetric Performance:

A complete parametric set of characterization runs was performed for the K-Tron KT35 twin screw feeder. This included every combination of 3 screen conditions (no screen, coarse square screen, and fine square screen), 4 paired sets of screws (coarse concave, fine concave, coarse auger, and fine auger) and the 3 powders at the 3 feedrate setpoints. Both FastFlo Lactose and Avicel 102 were fed successfully through their entire tested range of speed setpoints for all combinations of feeder tooling. Ceolus, on the other hand, did not run for either of the auger twin screws with the fine square screen due to a motor overload.

To test for reproducibility of results of the data, all of the runs with Avicel 102 were repeated. Analysis of variance (ANOVA) is a statistical tool that can determine the

significance of differences in the gravimetric performance data based on the potential sources of change to the performance such as: screw, discharge screen, and screw speed. A sample ANOVA for the Avicel 102 in the K-Tron KT35 is shown in Table 2.3, with a sampling of some of the standard deviation as a function of average feedrate in Figure 2.14 and relative standard deviation as a function of feedrate in Figure 2.15.

The ANOVA shows that for the K-Tron KT35 feeding Avicel 102, the speed is the most influential source for change in feeder performance and has a statistically significant effect ($F > F_{critical}$ or a $P < \alpha$). The screw is also found to be statistically significant. Following this is the screen, which is not shown as a statistically significant variable, but would likely be found to be significant with the collection of more extensive data. These effect on relative standard deviation may not apply universally to all powders or to all feeding equipment, as this is just descriptive of the data that was analyzed in this ANOVA. With some powders, the screen may become a very significant source of performance change.

Figure 2.14 shows the standard deviation as a function of average feedrate for the KT35 feeder when feeding Avicel 102 for several combinations of screws and screens. As speed increases the absolute standard deviation increases significantly as there is more variability at the higher feedrate. This is important, but typically higher rates will have higher acceptable variability, which can be expressed a percentage of the feedrate.

Figure 2.15 shows the same data plotted as relative standard deviation (RSD), which is the standard deviation normalized by the average feedrate. A plot of RSD as a function of feedrate can be used to select the best available feeder tooling for an application. For

Avicel 102 in the K-Tron KT35, this plot could be used to choose the best performing tooling for any specific desired feedrate in the tested range. This can be done by selecting the set of tooling that has the lowest RSD at any feedrate. As the coarse auger screws (CAS) with no screen (NoS) has the highest RSD values, it would only be used for high rates that the other screws cannot achieve. The fine concave screw (FCS) with no screen (NoS) could be used for lower feedrates as the other displayed plots have RSD values that are higher at feedrates less than ~100 kg/hr. For the intermediate speeds between ~100 and 200 kg/hr either of the other options, coarse concave screw (CCS) with the coarse square screen (CSqS) or the coarse auger screw (CAS) with the fine square screen (FSqS) would be appropriate, as the relative standard deviations are very similar for both.

2.5 Conclusions:

A method for characterization of loss-in-weight feeders was proposed and verified using experimental results. In this method, a catch scale was used to monitor the feedrate of material dispensed from the loss-in-weight feeder. The feeder was monitored as it ran in two different modes: volumetric (constant screw speed) and gravimetric (variable screw speed based on feedback control).

Fast Fourier transforms were used to obtain power spectra for the feedrate data obtained during feeder characterization trials. Although for the K-Tron KT35 this data was found to be quite complex due to the interactions of the screws and the agitator, it can still be quite useful in determining the frequencies of the fluctuations of the feedrate. This frequency data can be useful in determining characteristic times of the feeder that could potentially be used in pairing the feeder to other unit operations.

In volumetric mode, the feeder was tested for a wide feeding range of 10 to 90% of the screw speed. This was used to determine the relationship between screw speed and feedrate. When this relationship is linear, the uptake and filling of the flights of the feed screws is consistent and reliable. If the relationship is non-linear, this can indicate that there are inconsistencies in screw flight filling, which can lead to poor feeding performance. Powder bridging is the primary reason for inconsistent flight filling of the feed screws. Powder adhering and coating the screws can also change the effective flight volume and can lead to inconsistent flight filling.

Volumetric capacity trials were used to determine gravimetric setpoints for the gravimetric trials. Gravimetric testing was performed for the K-Tron KT35 with setpoints that would result in screw speeds that fall within the manufacturer's recommended range of 20-80%. By post process filtering and analysis it was possible to fit the data to a normal distribution that allows the performance to be quantified by two values: average feedrate and standard deviation of feedrate. This allows the performance to be compared between the different gravimetric trials with different feed tooling and powders.

ANOVA of the feeder characterization data was used to determine significance of effects (feeder tooling, powder, and speed) on feeder performance. The significance of screw, screen, and speed may vary with powder. For instance, a free flowing powder may not have as significant a screen effect as a very cohesive powder that may be prone to forming clumps that may be broken up by a discharge screen.

As there is need, and there are many options, for optimizing feeding systems, being able to detect differences in feeding performance is of utmost importance. The method presented here, based on using a catch scale, greatly improves feed tooling selection. With the characterization method described, a database of feeder performance and powder properties could potentially generate a predictive model such that feed tooling can be selected based on desired feedrate and measured powder properties rather than trial and error.

2.6 Figures for Chapter 2

Figure 2.1: K-Tron KT35 feeder with Schenck Accurate AccPro II catch scale.

Figure 2.2: K-Tron KT35 feeder tooling. Consists of 4 sets of twin screws: fine concave screw (FCS), coarse concave screw (CCS), fine auger screw (FAS), and coarse auger screw (CAS). There are two screen: fine square screen (FSqS) and coarse square screen (CSqS). The feeder can also be run without a screen (NoS).

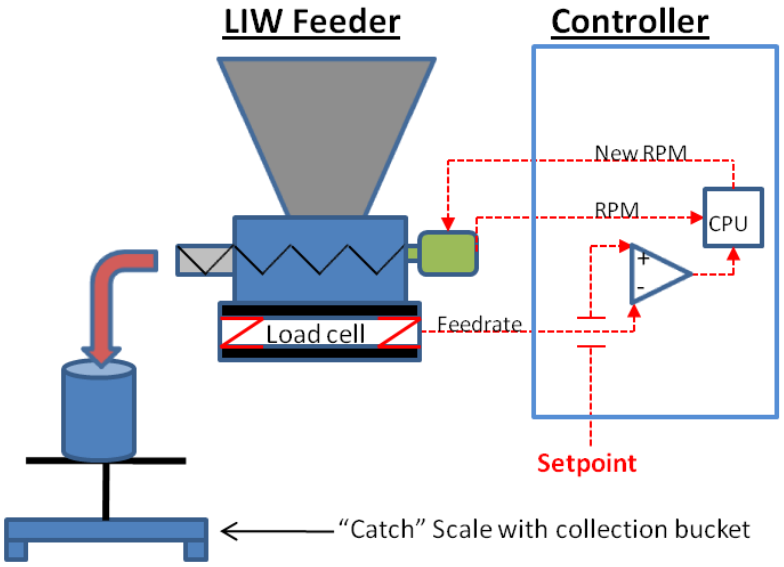

Figure 2.3: Loss-in-weight feeder characterization setup for monitoring feedrate and determining steady state performance. The catch scale is used to collect gain-in-weight data from the outlet of the feeder.

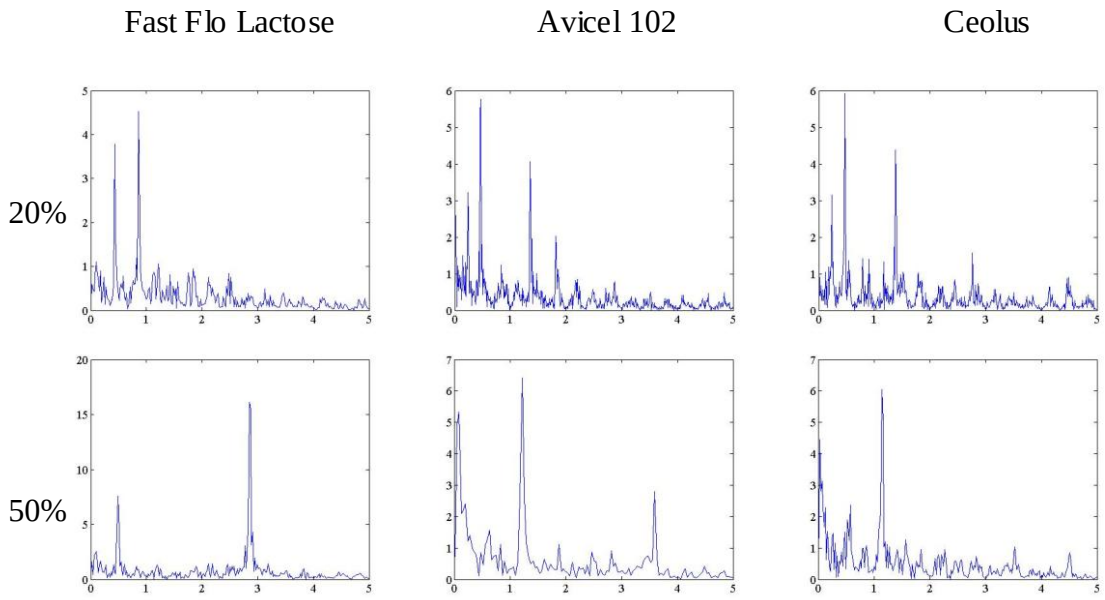

Figure 2.4: Fast Fourier transforms of the feedrate data for the powders (from left to right): Fast Flo Lactose, Avicel 102, and Ceolus fed from the K-Tron KT35 feeder with the coarse auger screws and no screen. The top row is for 20% and the bottom row is 50% of the maximum screw speed. All are run at their respective gravimetric setpoints.

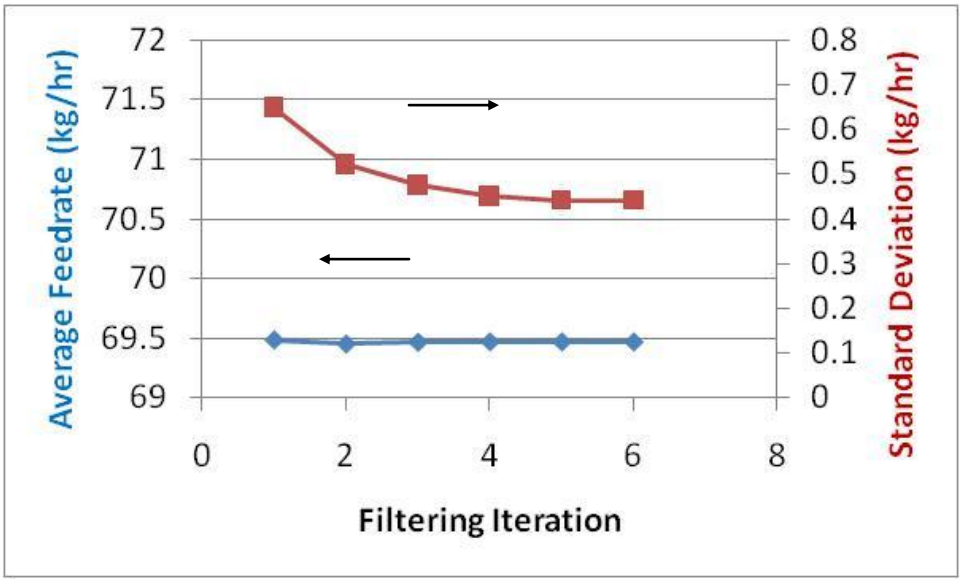

Figure 2.5: Applying the initial filtering with +/-10% bounds quickly finds the average feedrate from the feedstream data. Backing up the initial filtering with iterative +/-3σ rapidly causes standard deviation to come to a limit.

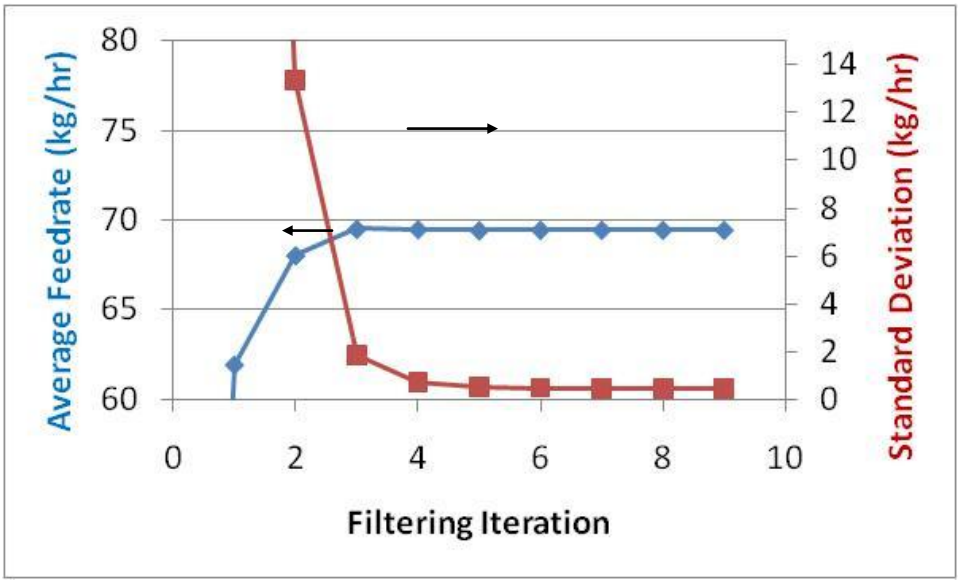

Figure 2.6: Using iterative filtering with bounds of +/-3σ with the poor initial values of average feedrate and standard deviation being calculated from the unfiltered data involves numerous extra filtering iterations than starting with better selected initial values.

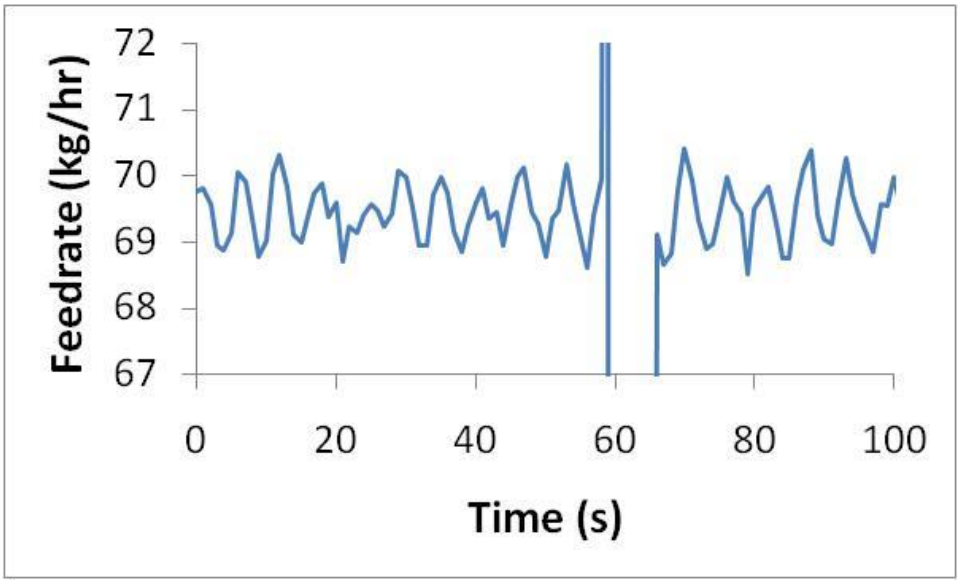

Figure 2.7: Sample 1 second interval catch scale data before any applied filter with a catch bucket change at ~60 seconds.

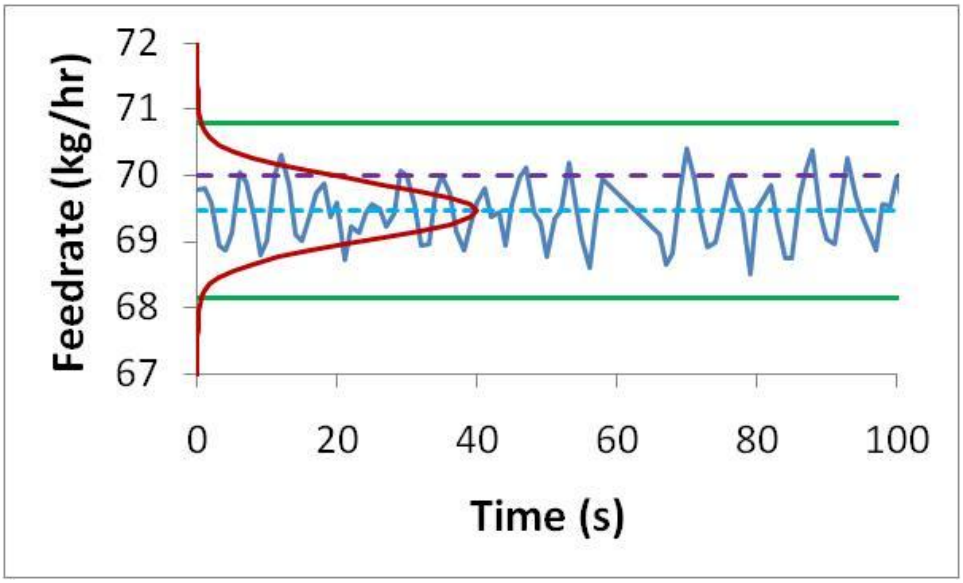

Figure 2.8: Sample filtered 1 second interval catch scale data (Blue) with its normal fitted distribution (Red). Also marked with a horizontal line is the mean value (Light Blue), the setpoint (Purple), and the ±3σ (Green).

a.

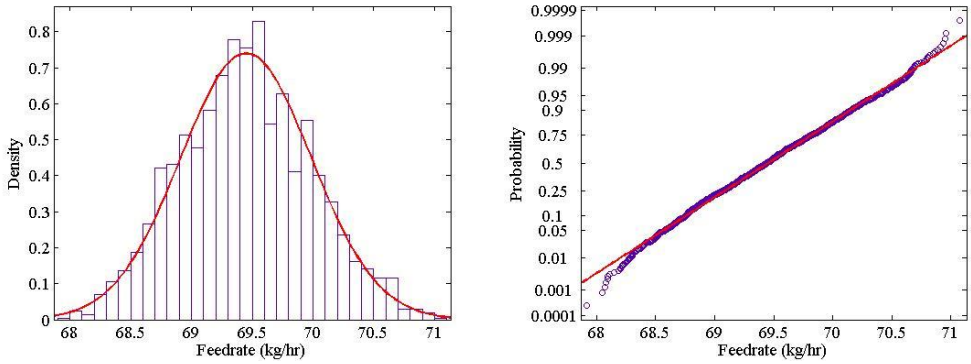

b.

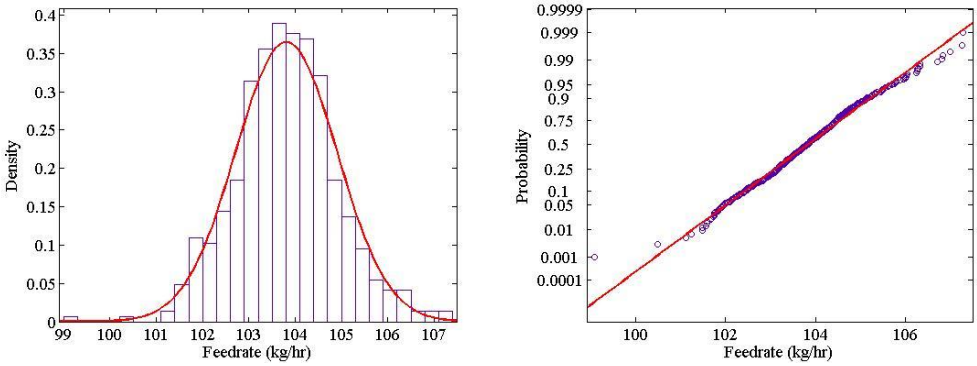

Figure 2.9: Normal Gaussian distributions and normal probability plots for the K-Tron KT35 loss-in-weight feeder characterization trials. The top plots (a.) are for feeding FastFlo Lactose at 70 kg/hr with the coarse concave "self-cleaning" twin screws and a coarse square screen, and the bottom plots (b.) are for Avicel 102 with the coarse concave screws and the fine square screen feeding at 105kg/hr.

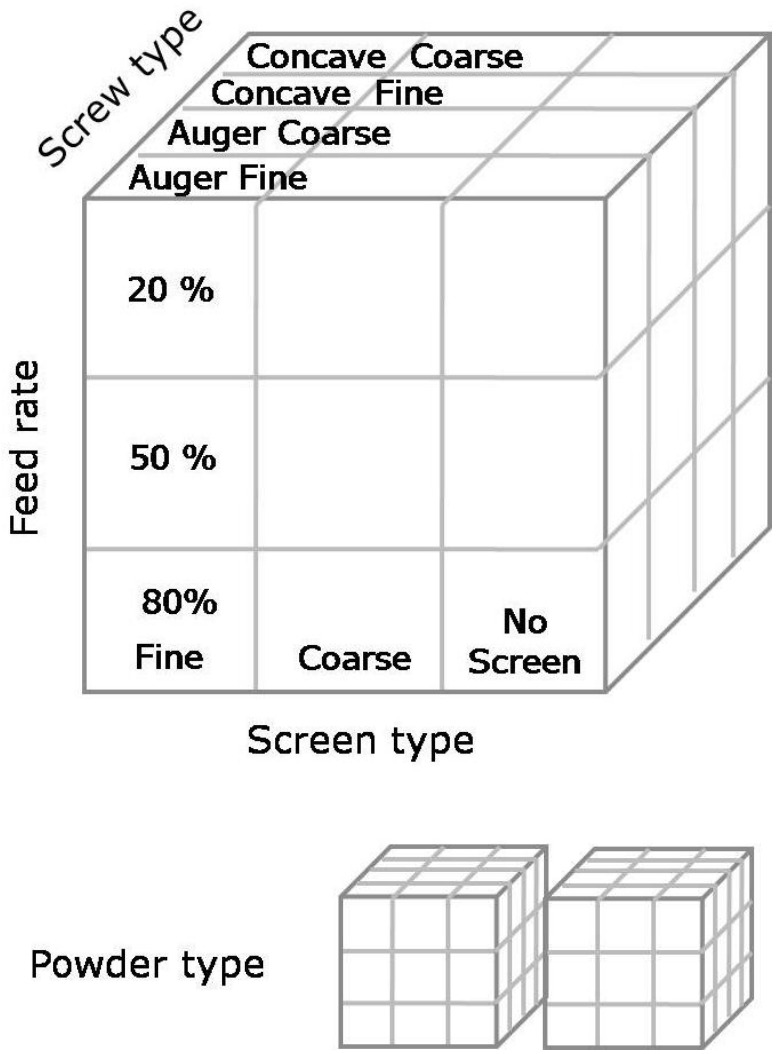

Figure 2.10: Sample visual representation of the characterization combinations for the K-Tron KT35 feeder.

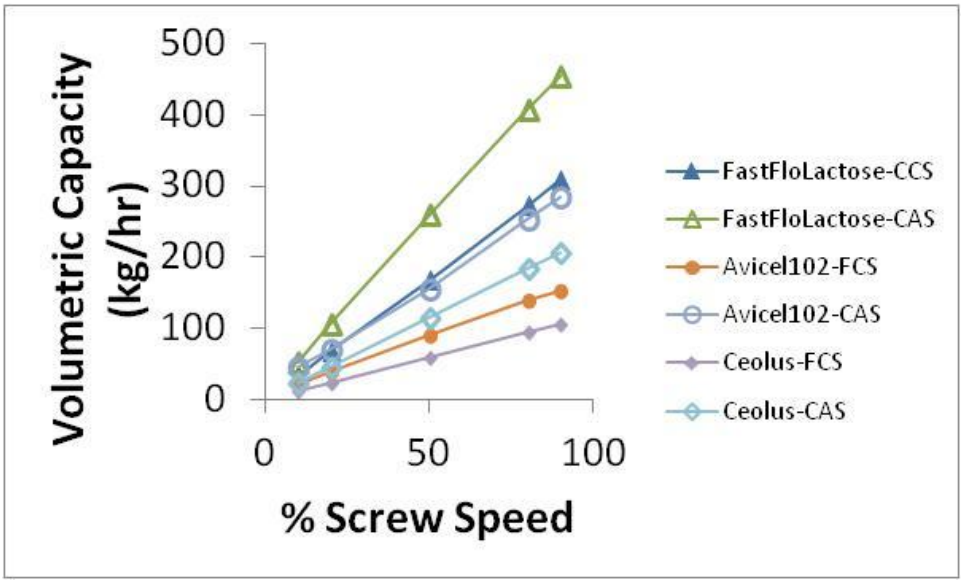

Figure 2.11: Volumetric capacity for the various combinations of feeder screws and powders.

Figure 2.12: "Rat holing" and bridging shown in the hopper of a Schenck Accurate Purefeed feeder feeding a very cohesive powder.

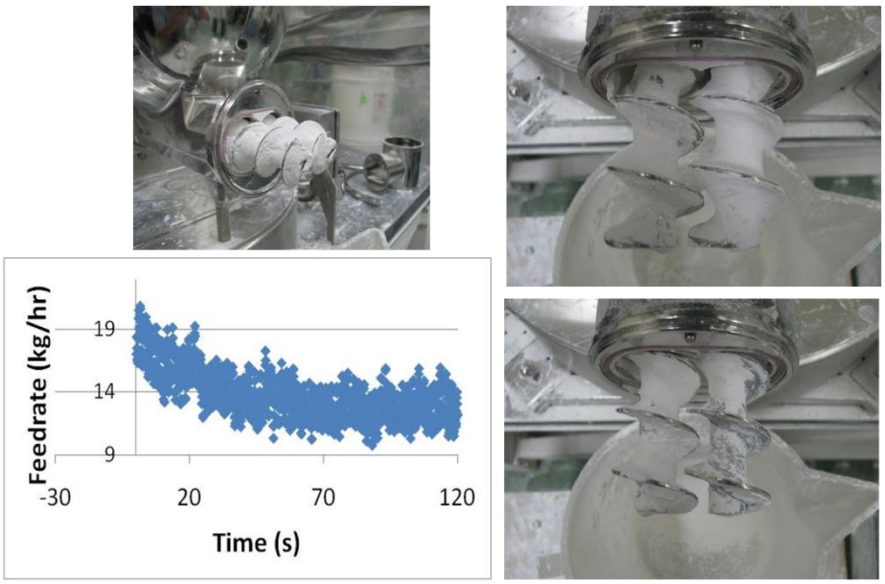

Figure 2.13: K-Tron KT35's fine auger twin screws become coated with zinc oxide material which reduces the feedrate by reducing the effective flight volume of the screws.

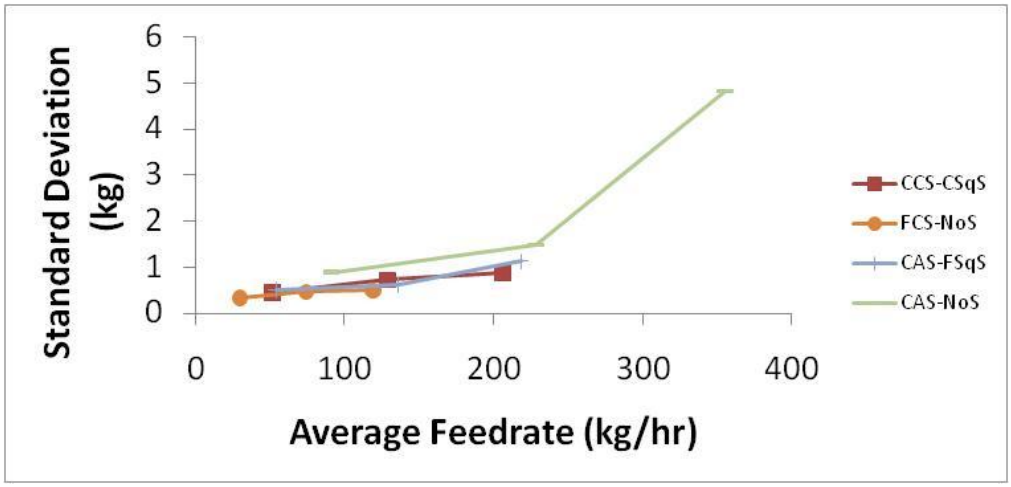

Figure 2.14: Standard deviation plotted as a function of average feedrate of the KT35 feeder characterization data for Avicel 102.

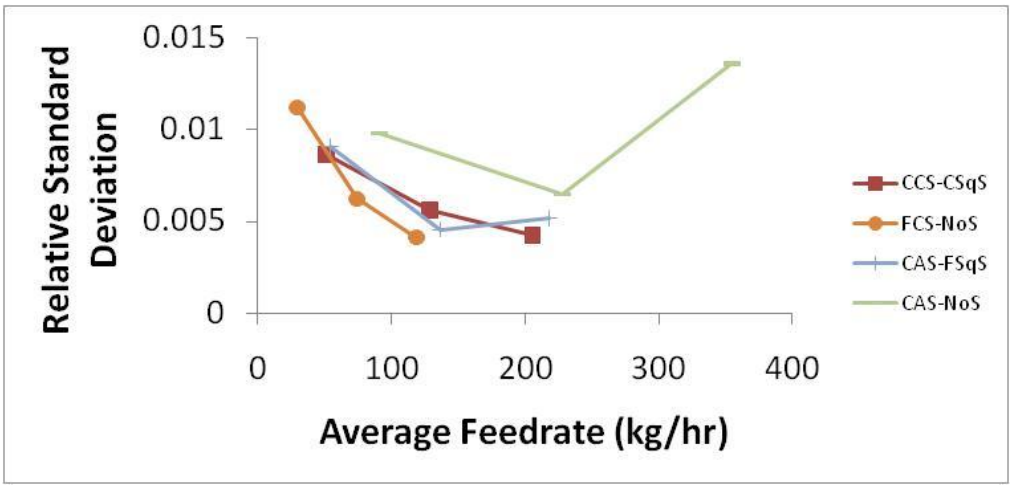

Figure 2.15: Relative standard deviation (RSD) plotted as a function of average feedrate of the KT35 feeder characterization data for Avicel 102.

2.7 Tables for Chapter 2

Table 2.1: Pharmaceutical powders

Name	Flow Index	Dilation	Density	Average Particle Size (μm)	Vendor
316 Fast Flo Lactose	27.8	10	0.58	100	Foremost
Avicel PH-102	38	15	0.30	100	FMC Biopolymer
Ceolus KG-802	49.2	22	0.21	50	Asahi-Kasei

Table 2.2: Rotation rate of screws and agitator for the KT35 with corresponding frequencies

	Screw		Agitator		
%	Rotation Rate (RPM)	Frequency (Hz)	Rotation Rate (RPM)	Frequency (Hz)	Doubled Frequency (Hz)
10	29.7	0.49	5.0	0.08	0.17
20	59.4	0.99	10.1	0.17	0.34
50	148.4	2.47	25.2	0.42	0.84
80	237.5	3.96	40.4	0.67	1.35
90	267.2	4.45	45.4	0.76	1.51

Table 2.3: ANOVA of Avicel 102 feeder characterization data with interactions (n=2 and α=0.05)

Source	df	SS	MS	F	P	Fcrit	
Screw	3	4.14E-05	1.38E-05	3.794	0.018	2.866	significant
Screen	2	2.34E-05	1.17E-05	3.213	0.052	3.259	
Speed	2	2.99E-04	1.50E-04	41.180	4.96E-10	3.259	significant
Screw*Screen	6	5.11E-05	8.52E-06	2.343	0.052	2.364	
Screw*Speed	6	5.48E-05	9.13E-06	2.512	0.039	2.364	significant
Screen*Speed	4	2.26E-05	5.65E-06	1.554	0.208	2.634	
Screw*Screen*Speed	12	6.63E-05	5.52E-06	1.519	0.162	2.033	
Error	36	1.31E-04	3.64E-06				
Total	71	6.90E-04					

Chapter 3. LOSS-IN-WEIGHT FEEDING TRIALS CASE STUDY: PHARMACEUTICAL FORMULATION

3.1 Summary

While the great majority of pharmaceutical products are produced through batch manufacturing, recent years have witnessed a growing interest in continuous manufacturing methods. Relative to other industries, the pharmaceutical industry has been slow in adopting modern manufacturing approaches, often citing regulatory uncertainty [3], [39] as the main reason. However, in recent years, industry and academia have engaged in many studies to demonstrate the benefits of continuous manufacturing processes and to create reliable methods for their design, optimization, and control. [1], [3], [52]–[59]

One of the key issues in powder-based continuous manufacturing is the need to feed accurately poorly flowing raw ingredients at the ratios needed for a given formulation. In a continuous system, if the feed rate of one ingredient changes even for a brief period of time, the resulting perturbation in concentration of the process stream will propagate downstream [7]–[10], potentially leading to out of specification product units. Hence, the ability to feed powder consistently and continuously is often regarded as one of the critical requirements of the overall process. While for large scales of operation and for freely-flowing powders (i.e., most granulations) this is generally not a difficult feat, at the small flowrates associated with typical pharmaceutical processes (0.5-100 Kg/hr), inaccuracies in feeding rates of dispensed component feedstreams need to be carefully addressed and minimized.

Singh *et al* [56], [60] describes a flexible multifunction continuous manufacturing platform (being developed at the ERC-SOPS) which aims to provide side-by-side the multiple processing routes for the continuous manufacturing of tablets: direct compaction (DC), wet granulation (WG), and dry granulation (DG). In this chapter, we are primarily interested in direct compression, where the powders are fed, blended, and compressed into tablets without a granulation step. The feeding process is the same among all processing routes. A typical direct compression process, adapted for continuous manufacturing, is shown in Figure 3.1. The overall process for the formulation consists of 4 main unit operations: feeding, delumping (milling), blending, and compaction. As shown in Figure 3.1, feeding is the first step and consists of several different feeders. Variations and inaccuracies at this step are magnified and complicated by the number of feeders used.

In this chapter, a case study is presented, where a commercial formulation is investigated in order to develop a feeding regime that enables a continuous manufacturing process. As the optimal feeding configuration (tooling selection) for any powder is based on both feedrate and powder properties, it is important to rigorously test and investigate each component separately. This involves determining the constraints in feeder and feeding tooling for each individual component in the formulation, testing potentially successful configurations, and comparing the feeding performance between the different configurations. This ensures that when the components are fed simultaneously, the resulting feed streams will combine with minimal fluctuations in the ratios required by the formulation.

The optimized feeding regime was determined for a formulation containing the following components: a proprietary active pharmaceutical ingredient (API), Prosolv HD90, crosspovidone, magnesium stearate, and silicon dioxide. Feeding configurations for Prosolv HD90 and crosspovidone were optimized with minimal difficulty, mainly due to their free-flowing behavior. The API, although relatively free-flowing, had some tendencies to clog in discharge screens, which caused it to be incompatible with several of the smaller aperture screens. Magnesium stearate presented some challenges due to its shear sensitivity and its tendency to coat metal tooling. Silicon dioxide had issues with adhesion due to its light density and strong electrostatic behavior. These problems were successfully addressed, as explained below. Although the results presented here are formulation specific, the approach used is applicable to any formulation.

3.2 Equipment

3.2.1 Feeders

The feeders used in these feeding trials are the KT35, KT20, and MT12 (See Figure 3.2 and Table 3.1) by K-Tron (Sewell, NJ). All of these feeders are based on gravimetric control principles and use loss-in-weight data to control the feedrate. They are all twin-screw feeders, consisting of a twin-screw driven feeder mounted on a weigh bridge. For each feeder, there are several feeding screws and discharge screens available (see Figure 3.3), allowing the feeding of bulk powder materials with a large range of cohesions at a wide range of feedrates. Although there are multiple methods for improving feeding performance through feeder modification [5], [6], only standard tooling available through the feeder manufacturer was used in this study.

Each feeder has a different set of tooling that is only compatible with that feeder type and size. Each of the feeders has their own set of 4 different twin screws: coarse concave (CCS), coarse auger (CAS), fine concave (FAS), and fine auger (FAS). Each of these screws is specific to a single feeder model, as each has a different diameter: 35mm for the KT35, 20mm for the KT20, and 12mm for the MT12. Coarse and fine screws have different capacities, which are determined by the size of the pockets created by the pitch of the screws. The concave screws have a "self-cleaning" function, which is useful when feeding "sticky" powders that will otherwise adhere to the metal tooling, reducing throughput and performance. The auger screws do not have this "self-cleaning" ability, but have the advantage of higher capacity.

Each feeder has multiple discharge screens that can be paired with the different sets of screws (see Table 3.2). The K-Tron KT35 has 3 screen conditions: coarse square screen (CSqS), fine square screen (FSqS), and no screen (NoS). The K-Tron KT20 has 4 screen conditions: coarse square screen (CSqS), medium square screen (MSqS), fine square screen (FSqS), and no screen (NoS). The K-Tron MT12 has 5 screen conditions: Coarse Square Screen (CSqS), Fine Square Screen (FSqS), Coarse Slotted Screen (CSlS), Fine Slotted Screen (FSlS) and No Screen (NoS). The function of the screens is two-fold. They can be used to break up clumps for cohesive powders, and can also be used for very free-flowing powders to create back-pressure that holds the material from freely flowing from the feeder.

3.2.2 Catch Scale

As described in Chapter 2, a Schenck Accurate AccPro II "catch scale" was used to characterize feeder performance. This was the same system described in Chapter 2. The

notable difference was a 1 kg strain gage loadcell was added to measure the very small feedrates of the K-Tron MT12. For the larger feedrates of the K-Tron KT20 and KT35, the 7 kg strain gage loadcell was still used.

3.3 Method for characterizing gravimetrically controlled feeding performance

The steady state feeding performance of each feeder was evaluated using the relative standard deviation index. This information can be used to select the best feeder tooling for a given powder at a given feedrate. Characterization experiments were conducted using the catch scale to record the weight of powder delivered by the feeder at the highest resolution possible of the catch scale. The method has been extensively detailed in a Chapter 2 [61]. The main difference in the feeder characterization method is the range of setpoints that were used. The desired setpoints to be tested depend on the reason for testing. If testing is performed to determine the limits of the feeder for a given powder, the rates may be set on the entire screw speed range of the feeder, such as: 10%, 20%, 50%, 80%, 90% and 100% of the overall screw speed. The corresponding gravimetric setpoints are determined through volumetric testing at each of these screw speeds. Alternatively, and in the case of this study, the feedrate setpoints are defined by the ranges required for the throughput capacities of the formulation: 80%, 100% and 125% of the nominal capacity of 30 kg/hr.

The feeders were mounted on a sturdy surface and the catch scale was placed on a separate lower stand, effectively isolating the catch scale from any vibrations that might emanate from the feeder. If and when the container on the scale became full, it was replaced by an empty one. Data collection was “paused” during this contained exchange

so that this disturbance did not affect the results. Due to the sensitivity of the load cells in the equipment, careful consideration was taken to isolate and minimize outside disturbances on the feeders and catch scale. In addition, samples were taken to test for the effect of feeding on the powders. The powder samples were used to investigate for potential changes to powder properties in a Freeman Technology FT4 powder testing system using the compressibility and shear cell tests.

3.3.1 Analysis

The raw data from the catch scales was extracted using the Excel export option from the catch scale software package. To analyze the data, the powder exiting the feeder was collected over a period of 1 second and its mass was used to calculate the fed material mass for the interval. From all the mass flowrates at each interval a distribution can be created, and the standard deviation (σ) and relative standard deviation (RSD) can be calculated. After modest filtering to remove irrelevant disturbances (as described in detail in Chapter 2 [61]), the standard deviation and the average feedrate was calculated and used for comparison of feeding performance for the different data sets.

Unless there are very large oscillations, the distributions of feedrate from the feeders have a near Gaussian distribution like the one shown in Figure 3.4b. Significant uniform oscillations would result in a distribution that is more 'U' shaped. Figure 3.5b shows the resulting distribution created from large oscillations in feedrate (Figure 3.5a) which can be compared to a sine wave function (Figure 3.5c) and its characteristic 'U' shaped distribution (Figure 3.5d). As this is non-optimal operation of the feeders and may lead to process instabilities, it should be avoided when possible.

3.4 Conditions examined in this study

The throughput requirements for each powder are directly related to the powder formulation, which is shown in Table 3.3. The nominal overall set point feedrate for the process studied here is 30 kg/hr. The range of interest for the feeding trials is 80% to 125% of this nominal formulation throughput. Using these values and the formulation feedrate, ranges for each component can be easily calculated. Although the feeders are often capable of much larger ranges, the range of 80% to 125% of the nominal formulation throughput was chosen such that the performance measured is maximally relevant to the formulation of interest under the conditions relevant to the actual manufacturing process. The target gravimetric feedrates were converted to corresponding volumetric feedrates based on approximate bulk densities. These volumetric feedrates were then compared with the volumetric capacities of the feeder and tooling configurations to narrow the choice of configurations to those feeders and tooling combinations that could potentially achieve the desired range of flows. These are potentially achievable configurations, because 100% screw flight filling is unlikely and this may reduce the overall throughput that is actually achievable with any specific tooling configuration. It is also important that any single tooling configuration can achieve the entire desired range of flows.

Testing of the feeding consistency was performed for 3 setpoints: nominal (100%), 80% and 125%. Using a nominal formulation throughput of 30 kg/hr, the following Table 3.4 shows the feedrates for each component to be tested. The bottom part of Table 3.4 shows the conversion from gravimetric feedrates (kg/hr) to approximate volumetric feedrates (dm^3/hr).

Assuming close to ideal filling of the screws, the appropriate feeder and screws for testing can be determined. The theoretical volumetric capacity for each feeder is shown in their respective Table 3.5-Table 3.7. The calculated volumetric feedrates for each powder should be compared to the theoretical volumetric capacities of the feeders to determine potential feeding configurations that need to be tested. The volumetric capacity of any set of screws follows the equation:

$$\dot{v} = \omega * V_{rotation} * \varepsilon_{fill} \qquad (3\text{-}1)$$

where ω is the rotation rate, $V_{rotation}$ is the volume dispensed per revolution, and ε_{fill} is the flight fill fraction. The fill fraction accounts for incomplete or non-ideal filling with powders that do not easily fill the flights of the screw. For ideally flowing powders, the fill fraction equals 1, meaning that the powder completely fills the volume of the flights in the screws.

An initial set of experiments was designed with the major components, Active Pharmaceutical Ingredient (API) and Prosolv HD90, being tested with the K-Tron KT20 and the minor components, Crospovidone and Magnesium Stearate, being tested with the K-Tron MT12.

3.4.1 ProSolv HD90

ProSolv HD90 is a high density silicified microcrystalline cellulose filler that promotes good flow and good compaction properties on a formulation for direct compression. In this formulation, it is the main excipient used, with a desired flowrate range from 10.64 kg/hr to 16.62 kg/hr (21.7 to 33.9 dm^3/hr), which falls on the upper end of the capacity of the K-Tron KT20, but on the lower end of the K-Tron KT35. This means that, assuming

ideal flight filling of the screws, the powder flowrates can be achieved on both feeders. This excipient is very free flowing and the powder easily fills the flights of the screws. To feed at the upper end of the throughput of the KT20, both sets of the higher throughput coarse screws were tested: coarse concave screws (CCS) and coarse auger screws (CAS). Both of the smaller throughput fine screws were deemed unable to achieve the high feedrates needed for ProSolv HD90 in this formulation. Four discharge screen conditions were available to be paired with each of the screws: coarse square screen (CSqS), medium square screen (MSqS), fine square screen (FSqS), and no screen (NoS).

For the feeding in the K-Tron KT35, the two fine sets of screws were used: fine concave screws (FCS) and fine auger screws (FAS). There are only two screens that can be used with the KT35, so there are three discharge screen conditions that were tested: coarse square screen (CSqS), fine square screen (FSqS), and no screen (NoS).

3.4.2 Active Pharmaceutical Ingredient (API)

Since this is a commercial product, the API identity is not disclosed here. The material is free-flowing with a particle size distribution with the following properties: d_{10} of 70 µm, d_{50} of 214 µm, and d_{90} of 447 µm. The desired flowrate range for API was 12.48 to 19.51 kg/hr (20.5 to 32 dm^3/hr), which once again fell on the upper range of the K-Tron KT20, but on the lower end of the K-Tron KT35. Therefore, both the coarse concave screws (CCS) and coarse auger screws (CAS) were appropriate for testing on the KT20. After some initial tests, it was found that the API material built up on the coarse auger screws, which can impact feeding performance, also creating traceability and maintenance concerns. From the throughput range of the CAS, it would appear that these

screws would be able to handle this feeding task, but in practice this may not be the case, as the overall capacity will be reduced as the material adheres within the flights of the screws. In addition, stagnant material caught in the screws will have an extremely long residence time, which may lead to material degradation and/or the need to clean the tooling very often. Thus, it was decided to use only self-cleaning screws to ensure that these stagnant zones and material buildup did not occur. The coarse concave screws were paired with all of the screen conditions of the KT20.

3.4.3 Colloidal Silicon Dioxide (Silica)

Colloidal silicon dioxide is a glidant that is used in low quantities to improve flow of the blend. Its low density, high cohesion, and electrostatics properties make it a very difficult material to handle as it will adhere to many surfaces and flows poorly. The desired flowrate range for colloidal silicon dioxide, 218 to 341 g/hr (5.5 to 8.5 dm^3/hr) falls in the mid to low range of the throughput of the K-Tron KT20. The ability of this powder to flow into the flights of the screws and fully fill them was unknown, but it was expected to be a challenge, so a broad range of tooling was initially screened for compatibility. All of the screens were found to be incompatible with the silica since the extra surfaces created extra buildup of silica at the feeder's discharge. The auger screws were also not an option as this could potentially lead to stagnant areas within the flights of the screws. The fine screws were unable to deliver the capacity needed for the entire desired feedrate range due to the material being unable to fully fill the flights of the screws. This left, as the only option for the K-Tron KT20 feeder, the coarse concave screws without a screen. The powder was also tested in the K-Tron KT35 with coarse

concave screws, expecting that the larger feeder could improve flight filling consistency due to the use of much larger screws.

3.4.4 API and Silica Preblend

As explained above, preliminary testing of the colloidal silicon dioxide demonstrated that this material would adhere to screws, screens, and the downspout for all conditions tested. Thus, it was decided to test both a preblend of colloidal silicon dioxide with the API in addition to testing each of these components individually. Since the silicon dioxide is a minor component, the feeding range for these trials is similar to the API feeding trials, meaning that the same feeder and tooling combinations should be investigated. It was unknown whether the preblended API and silica would adhere to the flights of the coarse auger screws, so these were also tested for compatibility and performance.

3.4.5 Magnesium Stearate

Magnesium stearate is used in small amounts as a lubricant to enable release of the compacted tablets from the tooling of a tablet press. This powder is easily sheared, and also tends to coat other powders and metal surfaces. Both of these properties contribute to giving MgSt its lubricant functionality. However, these properties also make MgSt a challenging material to handle, as it tends to coat metal tooling and tends to be shear sensitive. The desired flowrate range for magnesium stearate was 0.177 to 0.2777 kg/hr (1.3 to 2 dm^3/hr), which is in the middle to upper range for the capacity of the K-Tron MT12. As initial testing with magnesium stearate showed it had a tendency to coat the metal tooling, it was tested only with the "self-cleaning" screws: coarse concave screws (CCS) and fine concave screws (FCS). Five screen conditions were available to be

paired with both of these screws: coarse square screen (CSqS), fine square screen (FSqS), coarse slotted screen (CSlS), fine slotted screen (FSlS), and no screen (NoS).

Since manual refilling of the K-Tron MT12 may be difficult due to the need to refill it relatively often, testing was also carried out using the K-Tron KT20 feeder, which has a much larger hopper. This feeder was only tested for the fine concave screws (FCS), because the coating issue required self-cleaning screws and the low feedrate required fine screws. Once again, all four screen conditions were tested.

3.4.6 Crospovidone

Crospovidone is used in small amounts in tablet formulations as a disintegrant. The desired flowrate range for crospovidone, 0.480 to 0.750 kg/hr (1.5 to 2.2 dm^3/hr), falls on the upper range of the MT12 and on the lower end of the KT20. Initial testing in the K-Tron MT12 revealed that the upper end of the range could not be achieved consistently, so testing was limited to the KT20. The reason the MT12 was unable to achieve the upper end of the desired feedrate setpoint may have been due to fluctuations in density or flight filling. Self-cleaning screws were needed in order to remove the potential material buildup on the screws. This left a single pair of screws to be tested in the KT20, the fine concave screws (FCS). These screws were paired with all four screen condition options: coarse square screen (CSqS), medium square screen (MSqS), fine square screen (FSqS), and no screen (NoS).

3.5 Results

3.5.1 ProSolv HD90

Acceptable performance was achievable in both tested feeders: KT35 and KT20. The feeding performance is shown in Figure 3.6. In the KT35, performance is quickly divided into two sets of observations with very different performance values. In the poorly performing set, characterized by higher RSD values, the oscillations are due to the powder flowing too freely with respect to the tooling. This causes pulsations as the screws turn, due to the powder emptying or flushing out of each flight of the screws with each rotation. This situation is greatly improved by using the concave screws that have smaller pockets, and thus smaller pulsations. Discharge screens also contributed to performance improvement by holding the powder in the screw flights and not allowing it to flush out freely.

As the desired throughput of the Prosolv HD90 fell on the lower end of the KT35, performance was also examined in the smaller KT20 feeder. Performance of the two feeders (KT35 and KT20) is compared in Figure 3.7a,b,, suggesting that the KT20, in general, is a better fit for the throughput, but comparable performance can be achieved with the KT35 with the proper tooling selections. In the KT20, it was found that the best configuration was the coarse concave "self-cleaning" screws (CCS) with the coarse square screen (CSqS).

To determine the actual magnitude of feedrate variations, not just their relative impact, the feedrate data can be plotted with respect to time and can be compared to variations observed for multiple feeder and tooling combinations. Figure 3.8 a, b, c show the

feedrate as a function of time for several configurations. To demonstrate the importance of the sampling interval and the impact of averaging, each of these figures show the actual sampled feedrate data (sampling time of 0.1 seconds) as well as moving averages for several time intervals. Figure 3.8a shows a poorly performing condition in the KT35 using the fine auger screw. This results in very large oscillations. In Figure 3.8b, the magnitude of the oscillations is decreased using the fine concave screws, but the frequency is similar. Figure 3.8c, which shows data obtained using the smaller KT20, demonstrates that the magnitude of deviations is further reduced, but in addition the frequency of oscillations is increased. This represents a significant improvement, since higher frequency oscillations will be more effectively filtered by axial mixing in the blenders and other processing units downstream of the feeders.[62]

Figure 3.10 further highlights the importance of the sampling interval when reporting relative standard deviation of a feedrate. Figure 3.10a is a rescaled version of the plot shown in Figure 3.8a, which is the feeding data from the K-Tron KT35 feeding ProSolv without a screen. This condition leads to very large, almost sinusoidal oscillations. In this figure, moving averages are plotted for 0.1s intervals, which is the sampling interval of the data collection. If the sampling frequency is reduced, the sampling interval would be larger and result in data points like those shown in Figure 3.10b. For the sampling intervals larger than 1 second, there is an inability to detect the actual oscillatory nature of the feedrate.

When the sampling or moving average interval is increased, the relative standard deviation quickly decreases as shown in Figure 3.10c. A common but misleading practice that is often used by feeding equipment manufacturers is to use a relative

standard deviation for a 60s interval, which results almost always in very low levels for RSD. Considering that the next unit operation for this manufacturing process is a continuous blender that may have a residence time shorter than 60s, using a sampling interval this long is both conceptually wrong and potentially misleading. A sampling interval should be short enough to detect fluctuations that are pertinent to the process, which means that sampling needs to be much faster than the residence time of the subsequent unit operations.

Figure 3.9 shows the performance data for the KT20 for each screen condition: no screen (NoS), coarse square screen (CSqS), medium square screen (MSqS), and fine square screen (FSqS). For each condition, it is shown that the two screws perform in similar manner. Main differences are observed only with the use with the coarse square screen at all feedrate setpoints, and when using no screen for high speeds. The data suggests that the coarse concave screw performs slightly better, but as the screens become finer the effect from the screw type becomes less important. As a whole, these differences in performance shown in the KT20 can be considered minor.

3.5.2 Active Pharmaceutical Ingredient (API)

Figure 3.11 shows the feeding performance results from the feeding the API powder in the K-Tron KT20. For some of the screens, testing with this material resulted in autoshutdown alarms in the feeder, which is meant to prevent damage to the equipment. The cause of this run time failure was that the openings in the screen were too small for the rates that were needed and so the powder could not pass through the screen fast enough, resulting in clogging and ultimately compaction of the powder in the discharge tube. This raised the torque needed to rotate the screws, which is how the feeder detected

the problem. The screens incompatible with the API were the medium square screen (MSqS) and the fine square screen (FSqS). See Table 3.14.

Due to the incompatibilities that were shown with some of the screens, it was concluded that API would be best fed without discharge screens, thereby avoiding the potential for feeder alarm from the clogging of the screens. While the feedrates could potentially be fed in the K-Tron KT35, larger screws often require discharge screens. After observation of the compatibility problems with the discharge screens in the K-Tron KT20, feeding in the KT35 with discharge screens was determined to be non-viable.

3.5.3 Colloidal Silicon Dioxide (Silica)

Colloidal Silicon Dioxide was anticipated to pose the largest feeding challenges. As mentioned, this material is very low density and has intense electrostatic properties, which causes it to display a strong tendency to adhere to the downspout on the outlet of the feeder. Thus, the plan was to test this material with the largest array of tooling options, but tooling compatibility quickly reduced the available options. Moreover, in an attempt to suppress the effect of electrostatics, the discharge of the feeder was instrumented with a static eliminator. The static eliminator consisted of an ion generator and a small air flow, which could contribute to eliminate static charge development and reduce the tendency of the material to adhere to the feeder. Figure 3.12a shows the buildup of material that occurred without the static eliminator and Figure 3.12b shows the assembly of the static eliminator attached to the outlet of the feeder. In Figure 3.13a,b, the effect of the static eliminator was examined. It is shown that there is more material adhering to the feeder without the static eliminator. However, while the problem was reduced, it was not eliminated; even when a static eliminator was used, there was still

significant material buildup. This was considered unacceptable, as the material sticking at the feeder discharge would eventually fall into the mixer, intermittently raising the concentration of silica in the formulation, resulting in product containing higher silicon dioxide content than the formulation specification.

In Figure 3.14, the feeding performance of the silicon dioxide in both the KT20 and KT35 is shown. The effect of using the static eliminator is also shown. Use of the static eliminator showed an improvement in feeding performance. In addition, the more consistent flight filling of the larger screws in the KT35 also caused improvements in the feeding performance as compared to the smaller screws of the KT20. Use of a metal surface coating, Impreglon, also showed a significant improvement. Based on performance alone, it was possible to feed the material and minimize variability. However, it must also be considered that during the short runtime of the experimental feeding trials, material that built up on the feeder did not fall out of the downspout. In longer runs used for commercial manufacturing, this would indeed happen, causing spikes in the silica feedrate. Thus the feeding performance observed in Figure 3.14 may not be representative of what would be observed in a long-running process. As such, it was concluded that silica should not be fed as a pure component, and that instead it should be either eliminated from the formulation or preblended with another ingredient, such as the API.

3.5.4 API and Silica Preblend

Figure 3.15 shows the feeding performance results from the feeding of the API and silica preblend in the K-Tron KT20. Similar to the pure API trials, tests utilizing the fine square screen (FSqS) resulted in autoshutdown alarms in the feeder. See Table 3.15.

Differing from the API, the preblend was compatible with the medium square screen (MSqS), which is due to the addition of the colloidal silicon dioxide that improved flow.

Due to the incompatibilities that were shown with some of the screens, it was concluded that API / silica preblend would be best fed without discharge screens, thereby avoiding the potential motor overload alarm caused by the clogging of the screens. The performance between screws without screens was concluded to be similar, although the coarse concave screws are preferred as they eliminate the potential for material buildup within the flights of the screws, even though no material buildup was observed during these trials.

3.5.5 Magnesium Stearate

As mentioned, Magnesium stearate is a lubricant known to have a tendency to coat and smear on metal parts. As such, it was decided that all the testing for this powder would be carried out with concave self-cleaning screws. The feeding performance of MgSt for the MT12 is displayed in Figure 3.16. In general, the tooling did not play a large role in the feeding performance of MgSt. The fine concave screw performed the best. There was not a significant improvement from the usage of screens, so it was concluded that the best performance would be obtained without a screen.

When testing in the larger KT20 feeder, it was noticed that the control magnitude of the feeder drifted. It was also noticed that the feeding performance changed as a function of time, as seen in Figure 3.17. In the figure, the order of the runs was, first, without screen (NoS), then another shorter run without screen, then a run using the coarse square screen (CSqS), the medium square screen (MSqS), and the fine square screen (FSqS).

Subsequently, the run without the screen was repeated. After each run, it was noticed that the drive command decreased from start to finish. This time-dependent behavior is most likely caused by the long residence time of the powder in the hopper. As the hopper size is much larger for the KT20, this leads to repetitive shearing due to the hopper agitation.

This led to the investigation of long runs with this powder in order to determine long term performance, which is shown in Figure 3.18 in both feeders. With the KT20, the feeder performance became worse over time, which can be shown by the increasing RSD. For the MT12, there was a slight increase in RSD, but it was not nearly as large as shown by the resulting horizontal plot for the MT12 in Figure 3.18. The sudden dips in RSD shown for the MT12 correspond to the hopper refills which occurred at ~70 minutes and ~120 minutes, indicating that it is a change in powder behavior.

The difference between the KT20 and MT12 in the drifting behavior of the RSD for magnesium stearate may be due to a residence time difference (as the KT20 is much longer), but it may also be due to design differences affecting how the hoppers are agitated. The KT20 uses a horizontal axis with an over-under rotation, located at the bottom of the powder bed, which may lead to very intense shear. Due to the smaller size, the MT12 has much less powder, but also uses an agitator that rotates along the vertical axis of the hopper, acting in a stirring motion resulting in less shearing against the downward weight of the entire bed.

When comparing the KT20 and MT12's long term performance, it is quite obvious that the MT12 performs better. The one main advantage to the KT20 is that it has a larger

hopper and will not require refills as often which makes for a refill scheduling that is easier to maintain.

3.5.6 Crospovidone

Crospovidone is fed at a low rate in the KT20. Figure 3.19 shows the feeding performance from the KT20. This powder fed relatively easily with no significant problems being observed in feeding performance. Using the RSD vs. feedrate plot, the best performing tooling combination can be easily determined. The lowest RSD across the desired feedrate range is displayed by the fine concave screws (FCS) and the medium square screen (MSqS).

3.5.7 Effects of feeding conditions on powder flow properties

Each powder was tested in the Freeman Tech FT4 powder rheometer before and after feeding in order to detect any changes in the powder caused by the feeding process. Two tests were used: compressibility and the shear cell test. An example of the compressibility test for Prosolv HD90 is shown in Figure 3.20. Compressibility is a bulk property that is measured in the FT4 by conditioning the powder followed by slowly compressing, while letting entrained air escape. Compressibility can indicate whether a powder is cohesive or free flowing [63]–[65]. The compressibility for this powder was found to be low (~7%) which indicates that it is a free flowing powder. Minor differences between the fed and unfed powder were observed, but the effect of tooling was not found to be statistically significant. All of the powders in the formulation had similar plots with the same conclusion that the effect of feeding on the discharged powder properties, if any, was independent of feeder tooling. This means that the selection of optimal feeder and tooling was independent of changes to the powder flow properties.

However, since feeding does increase the compressibility of the pure components, this needs to be considered, when characterizing the rest of the downstream processes.

An example of the shear cell test results for the Prosolv HD90 is shown in Figure 3.21. As all of the plots also overlap, there is no significant difference due to the powder feeding process. This same result and conclusion also applied to the other powders in the formulation. Significant changes in shear cell results would have been expected if the powders were extremely shear sensitive as the feeders do not heavily shear the materials.

3.6 Conclusions

This study was for a specific formulation, but the same methods used can be applied to other formulations. The process for tooling optimization can be described with the following list of steps:

1. Select potential feeders and tooling
2. Screen the tooling for compatibility issues
3. Test compatible conditions and monitor feedrate

Initial selection of the feeders to be tested was based on the theoretical volumetric throughput of the different tooling configurations for the feeders. The ability of a feeder to achieve these volumetric throughputs depends on the powder properties of the powder. If the powder does not flow easily in the flights of the screws, the flight fill fraction will be less than ideal and the theoretical throughput will be higher than actual throughput.

During gravimetric feeding trials, selection of the proper sampling interval is very important. An interval that is too long relative to the subsequent processing will not adequately detect fluctuations. When recording relative standard deviation the sampling

time is needed for reference as relative standard deviations with differing sampling intervals cannot be compared fairly.

After potential feeders and tooling are selected, the testing should be narrowed to only compatible tooling. Tooling can be found to be incompatible for several reasons based on powder properties.

- Screws tend to fail due to material adhering within the flights or in the case of flight filling issues. If material is adhering within the screws, this will be observed after running the feeder with the selected screw when the feeder is disassembled and the screws are visible. If this problem observed, then self-cleaning concave screws should be used. In the presence of flight filling issues, the feeder will run at a higher RPM than the theoretical rate, which may not be a problem unless the feeder is running at the top screw speed. In extreme cases, which were not observed in the tested formulation, powder bridging in the hopper leads to "rat holing" or tunneling. Such cases may lead eventually to no powder entering the flights of the screws. Larger screws or even larger flights tend to improve flight filling.
- Screens tend to fail with very cohesive and/or shear sensitive materials. With free flowing materials, screens create an extra barrier that prevents material from flooding out of the feeder. With cohesive materials they serve to break up clumps of material into a more smooth flowing stream. Because they still act as a barrier even with cohesive materials or shear sensitive materials, they increase the overall shear on the material and also the holes in the screen may clog with cohesive

material. An additional failure occurs for materials that tend to adhere to surfaces, as this adds another surface that material can deposit.

There are other non-tooling dependent problems that could potentially affect the long term performance of a continuous process. Significantly, it is important to minimize the amount of material that adheres to surfaces. For the case study discussed here, these effects are most critical for the colloidal silicon dioxide. This is a common ingredient used in many formulations. Feeding of this powder as a pure component proved to be very unreliable. Thus, it is recommended that the colloidal silicon dioxide be preblended with another ingredient that is thus used as a carrier. In most formulations, the best choice of this carrier is likely to be the API, since the usual purpose of adding silicon dioxide, a glidant, is to improve API flow properties. For the process of interest here, preblending of silica would enable the process to be carried out using 4 feeders dispensing each material into the blender: API / silica preblend, Prosolv HD90, Magnesium Stearate, and Crosspovidone.

3.7 Figures for Chapter 3

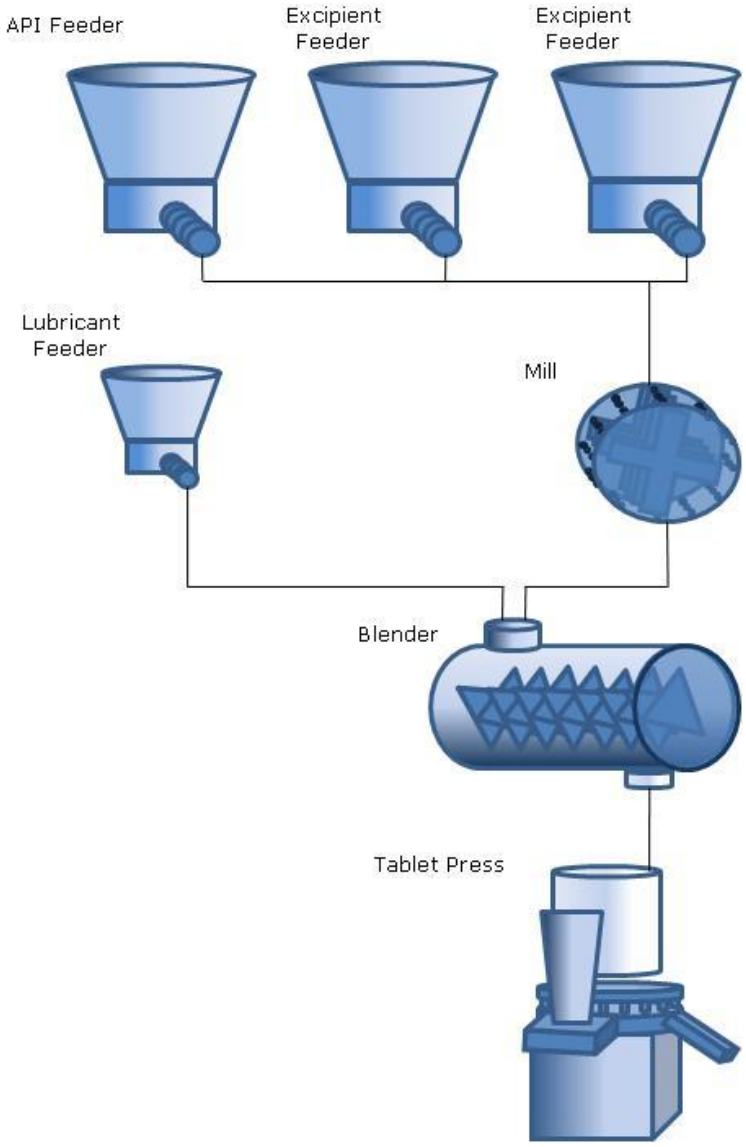

Figure 3.1: Diagram of a direct compression continuous process

Figure 3.2: K-Tron KT35 feeder with Schenck Accurate AccPro II catch scale, K-Tron KT20 feeder, and K-Tron MT12 feeder.

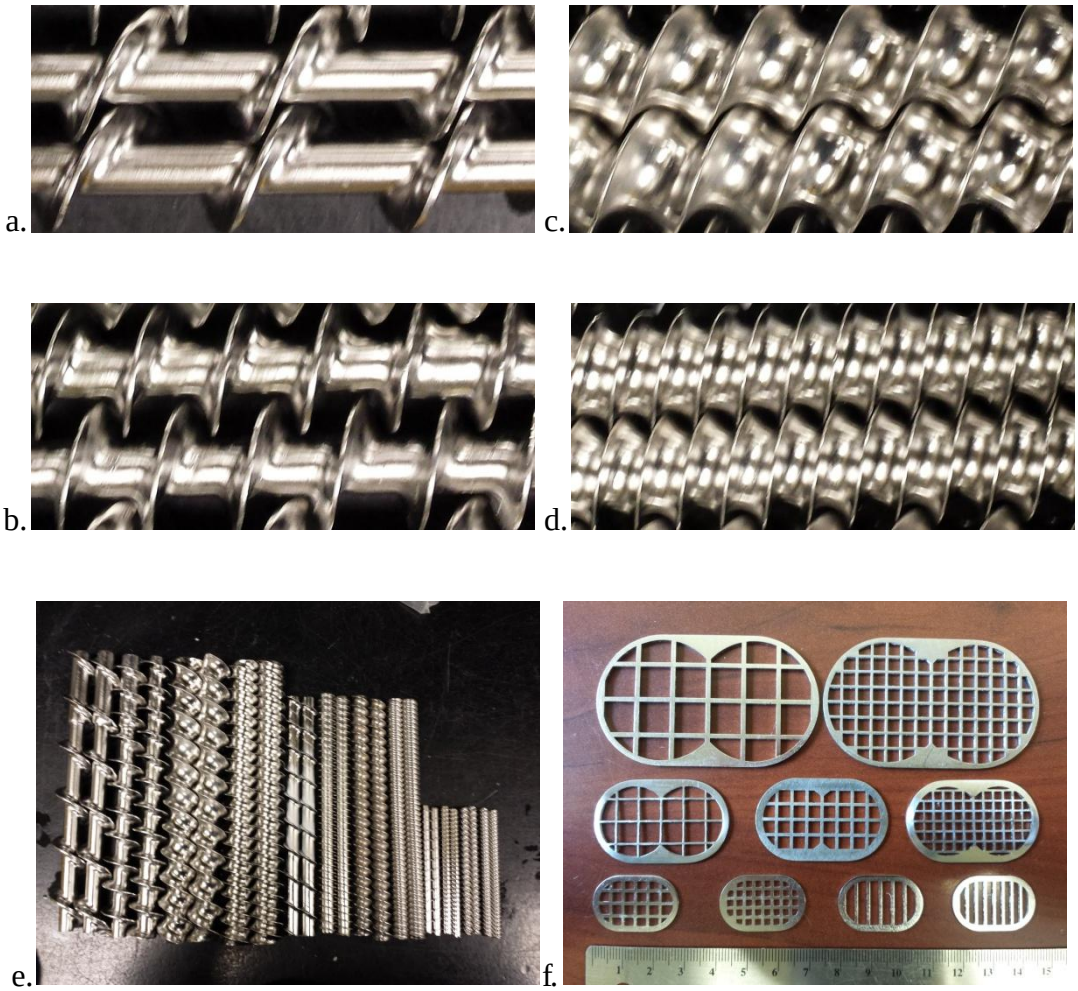

Figure 3.3: K-Tron twin-screw feeder tooling. Each feeders tooling consists of 4 sets of twin screws: a) coarse auger screw (CAS), b) fine auger screw (FAS), c) coarse concave screw (CCS), and d) fine concave screw (FCS). e) The screws from each feeder are only compatible with that feeder as they are different sizes. f) The screens for all the feeders are displayed together for comparison. KT35 has two screens (top): fine square screen (FSqS) and coarse square screen (CSqS). The KT20 has three screens (middle): fine square screen (FSqS), medium square screen (MSqS), and coarse square screen (CSqS). The MT12 has four screens (bottom): fine square screen (FSqS), coarse square screen (CSqS), fine slotted screen (FSlS), and coarse slotted screen (CSlS). All of the feeders can also be run without a screen (NoS)

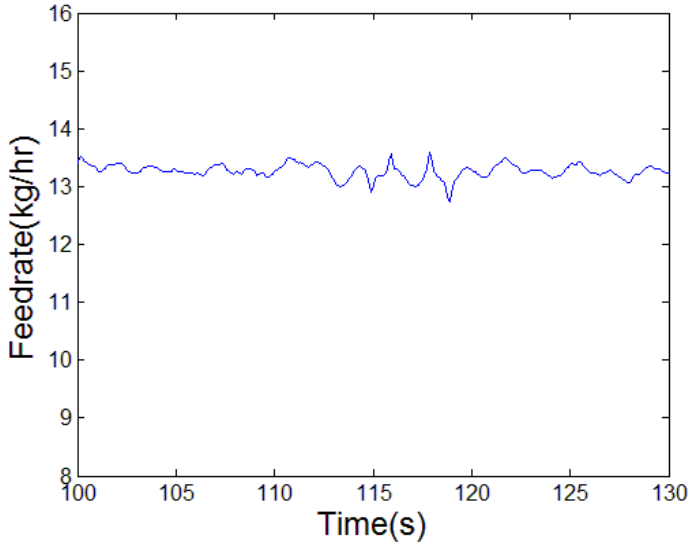

a.

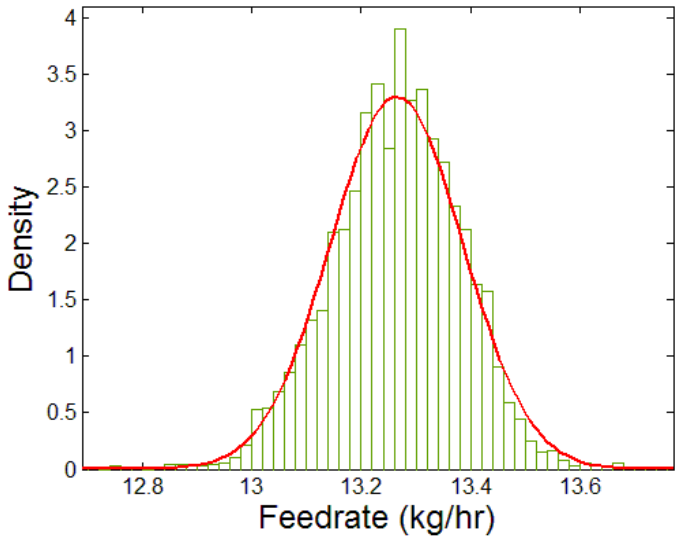

b.

Figure 3.4: a) Time series data and b) probability distribution function (PDF) for the KT20 with Coarse Concave Screws (CCS) and Medium Square Screen (MSqS) feeding Prosolv at 13.3 kg/hr.

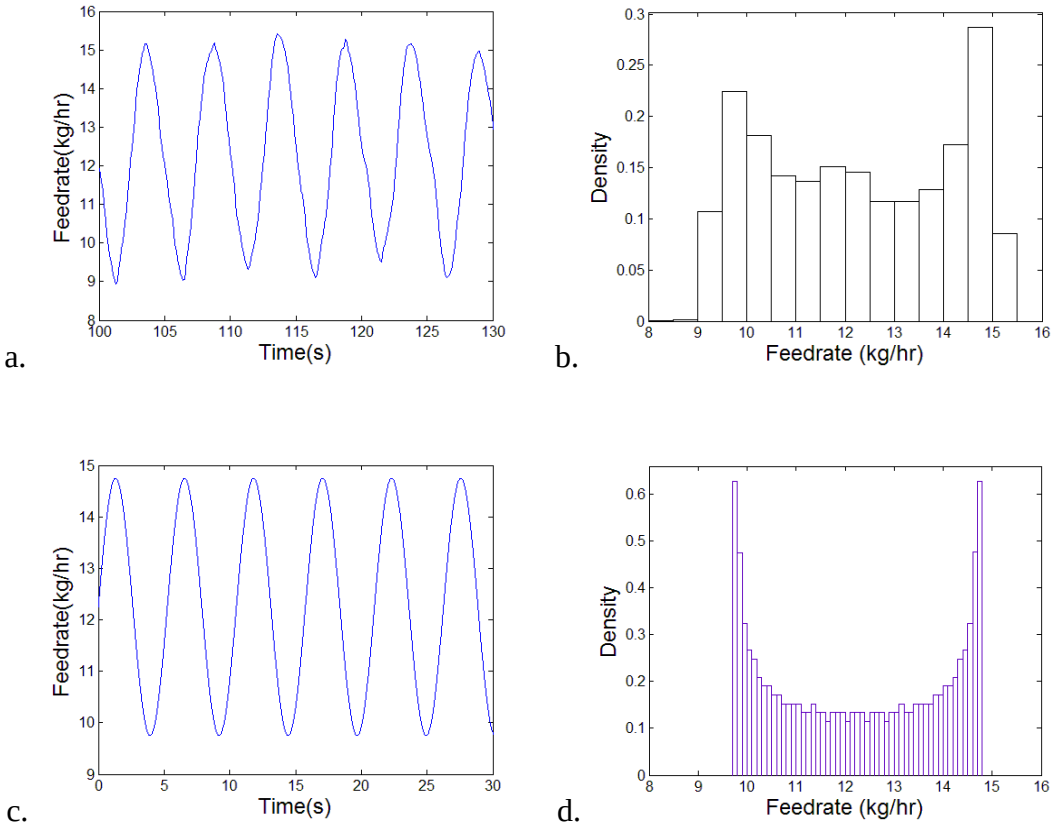

Figure 3.5: a) Time series data and b) probability distribution function (PDF) for the KT35 with Fine Auger Screws (FAS) and No Screen (NoS) feeding Prosolv at 13.3 kg/hr. For comparison, c) Simulated Sine wave and d) its PDF.

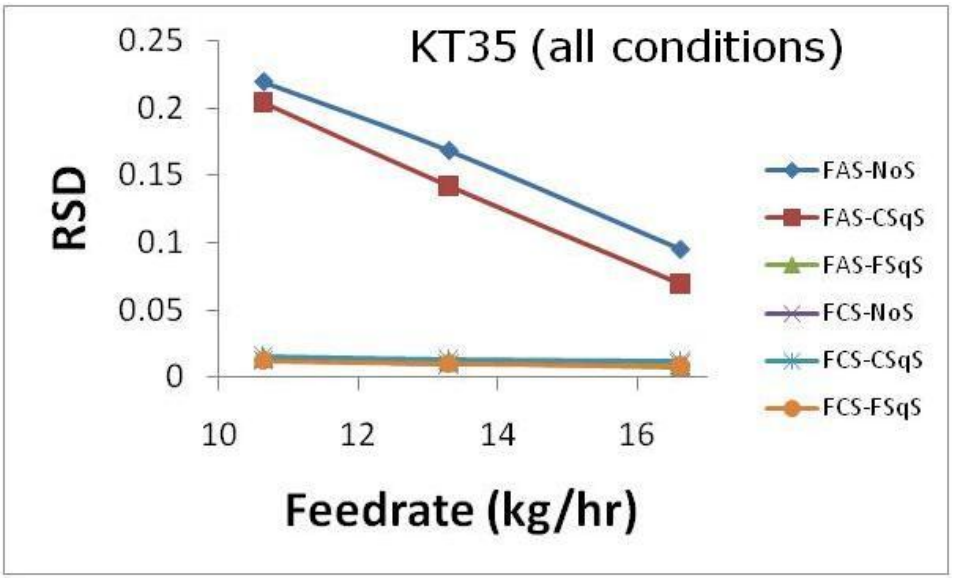

Figure 3.6: Feeding performance as RSD as a function of feedrate for the KT35 feeding Prosolv HD90. See Figure 3.7a for a rescaled plot showing the best conditions.

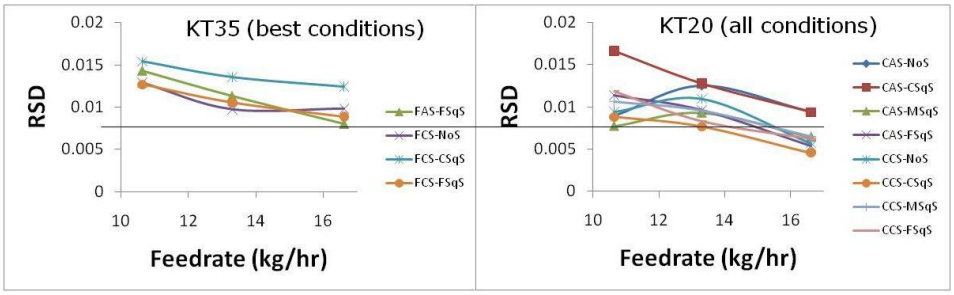

Figure 3.7: Feeding performance of Prosolv HD90 being fed by (a) KT35 and (b) KT20

a.

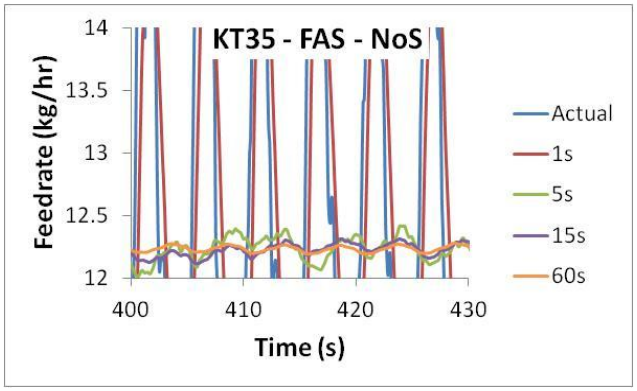

b.

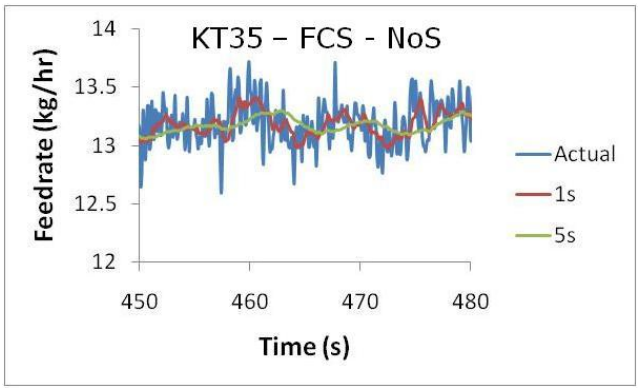

c.

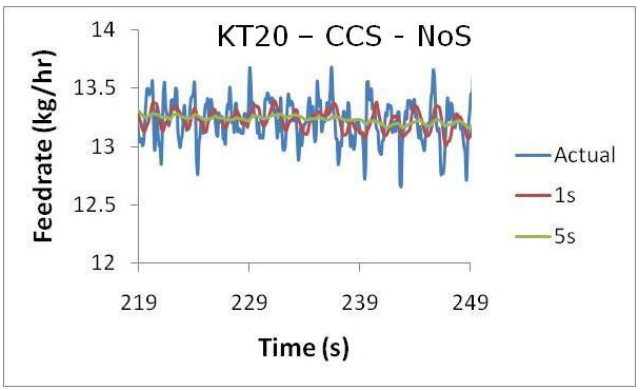

Figure 3.8: Feedrate data as a function of time for the feeding of Prosolv HD90 being fed from (a) KT35 with fine auger screws and no screen, (b) KT35 with fine concave screws and no screen, and (c) KT20 with coarse concave screws and no screen.

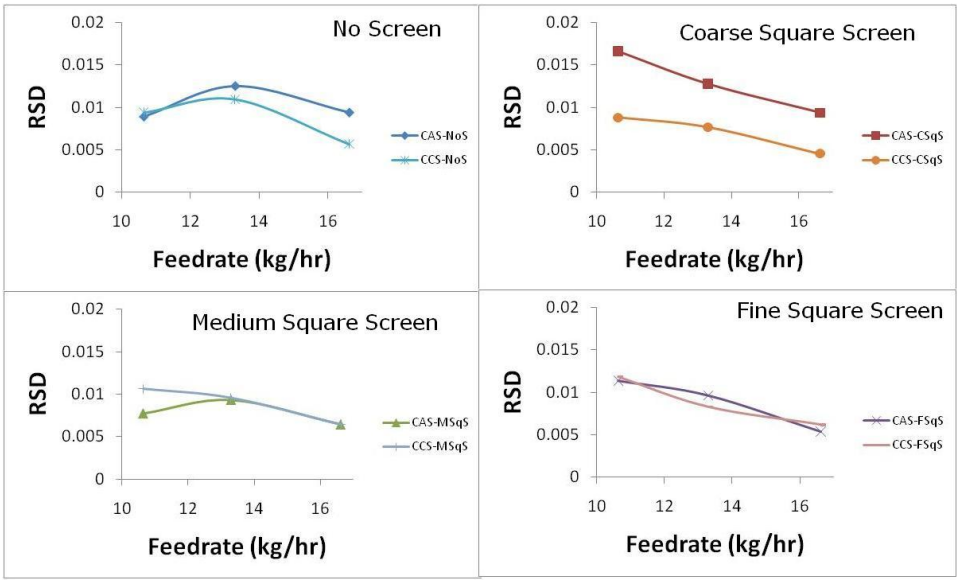

Figure 3.9: Feeding performance of KT20 feeding Prosolv HD90.

a.

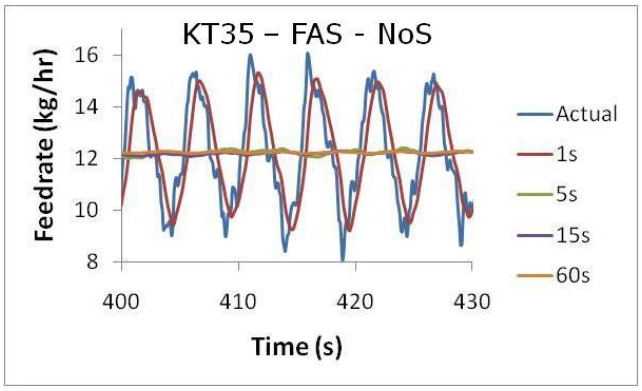

b.

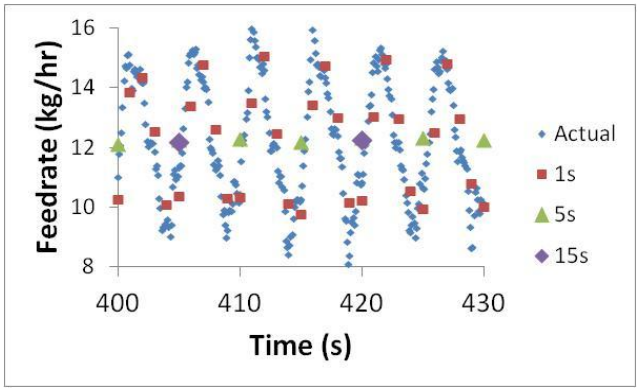

c.

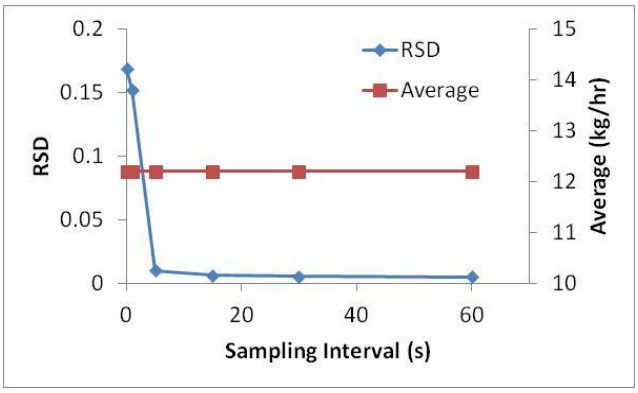

Figure 3.10: Feedrate data as a function of time for the feeding of Prosolv HD90 being fed from KT35 with fine auger screws and no screen displayed (a) using different moving averages and (b) using simulated sampling intervals. (c) The effect of sampling interval on relative standard deviation (RSD).

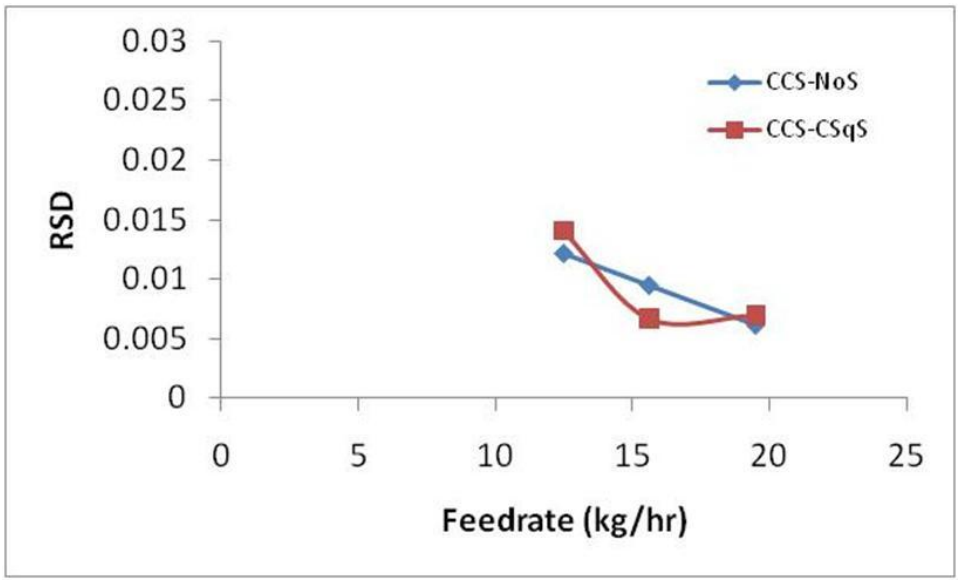

Figure 3.11: Feeding performance of pure component API fed by the K-Tron KT20

Figure 3.12: Picture of feeder (a) without static eliminator and (b) with static eliminator

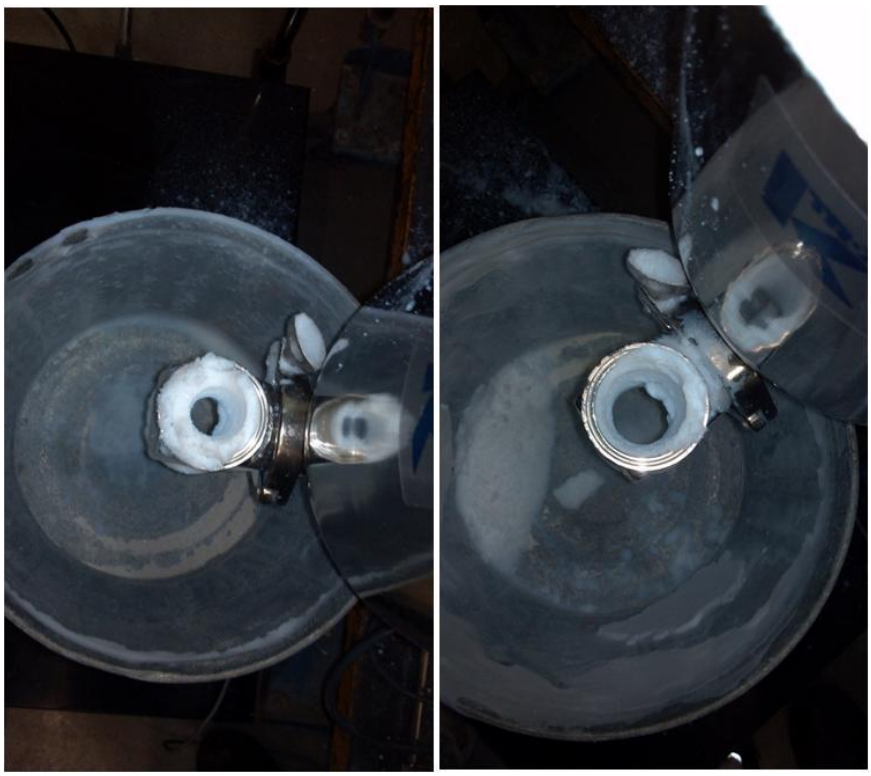

Figure 3.13: Picture of silicon dioxide buildup for (a) without static eliminator and (b) with static eliminator

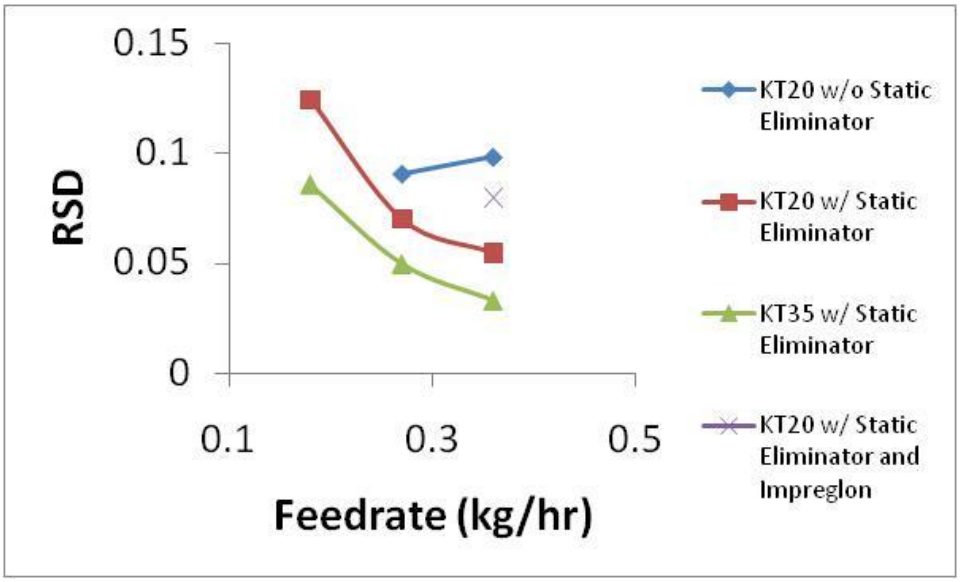

Figure 3.14: Feeding performance of both KT35 and KT20 feeders feeding silicon dioxide

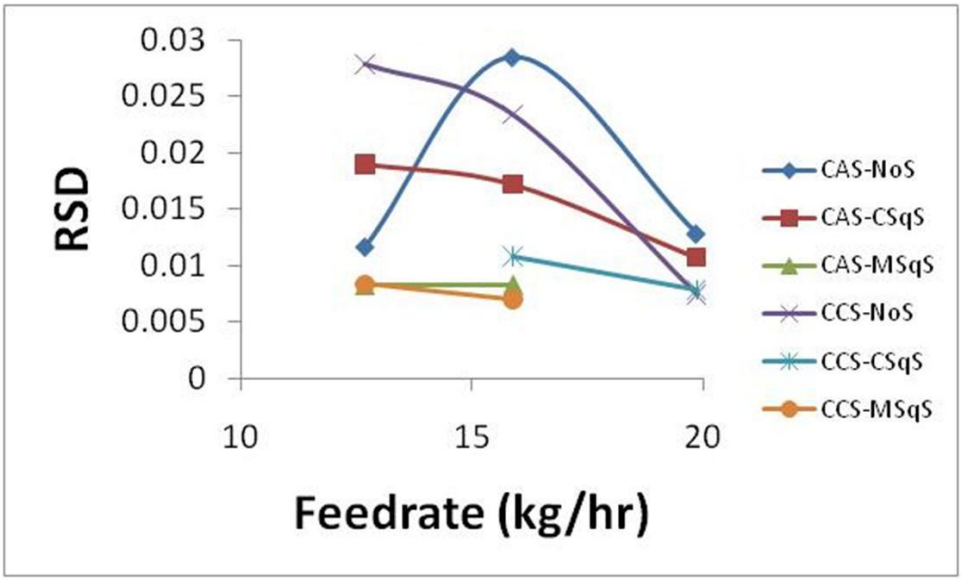

Figure 3.15: Feeding performance of API / Silica blend fed by the K-Tron KT20

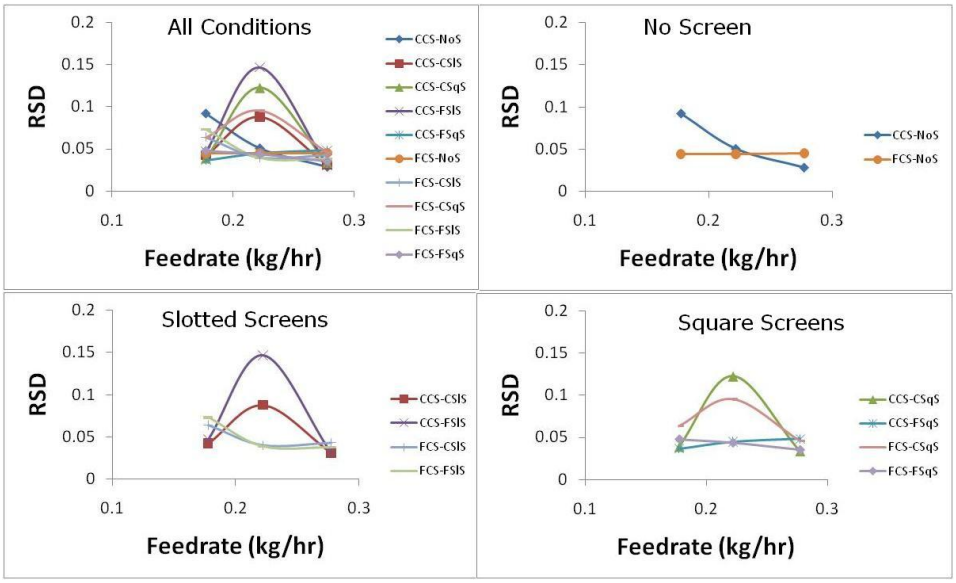

Figure 3.16: Feeding performance of MT12 feeding magnesium stearate

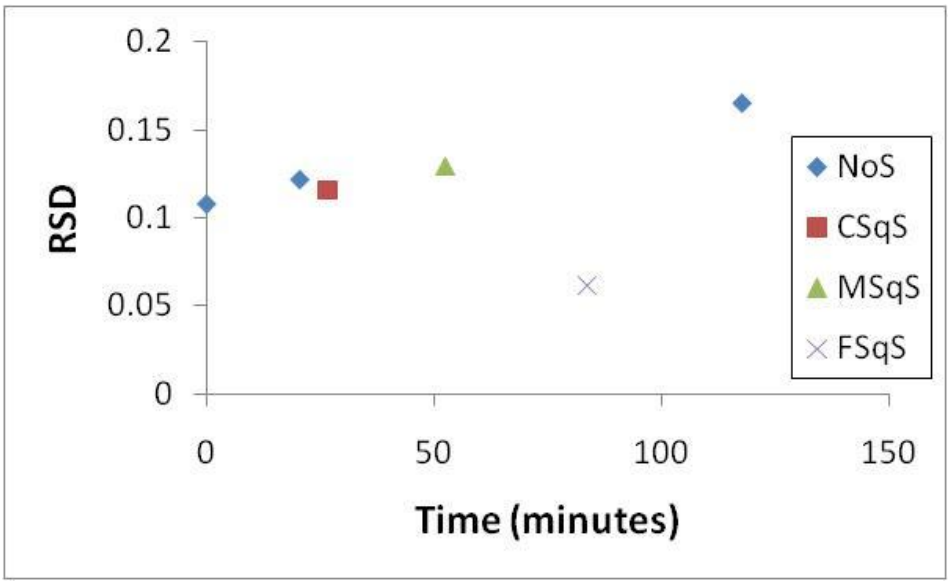

Figure 3.17: Feeding performance of KT20 feeding magnesium stearate at nominal feedrate

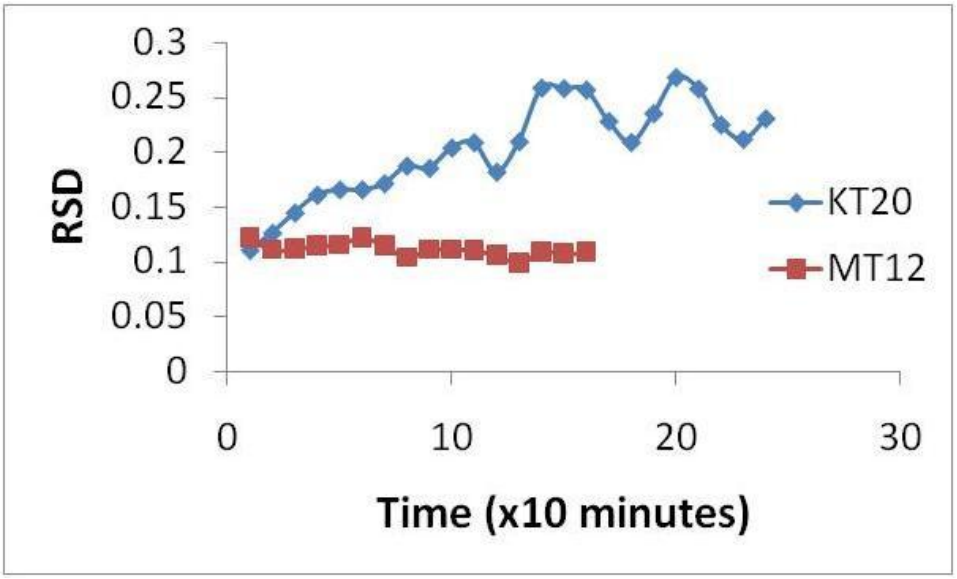

Figure 3.18: Long term feeding performance for the feeding of magnesium stearate being fed by KT20 and MT12

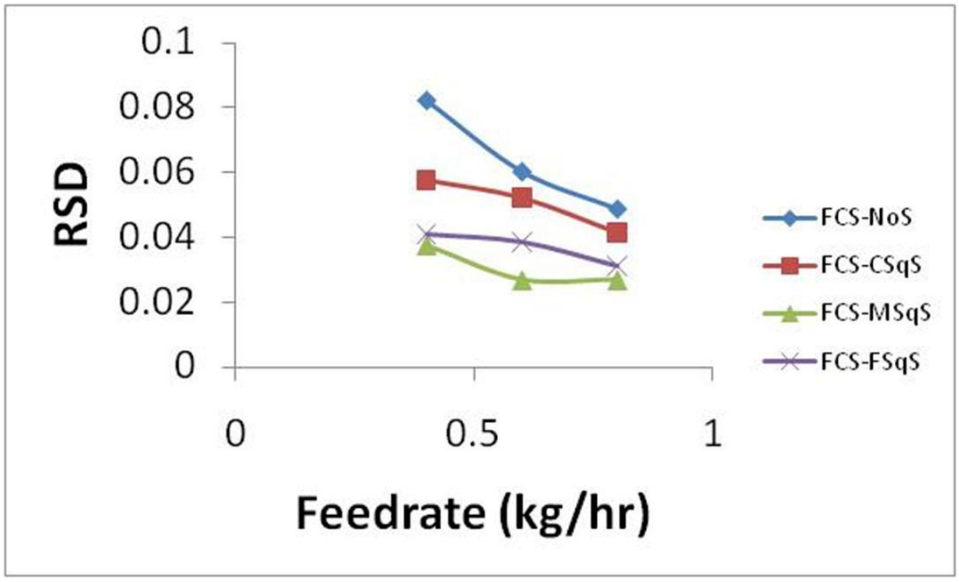

Figure 3.19: Feeding performance for the KT20 feeding crospovidone

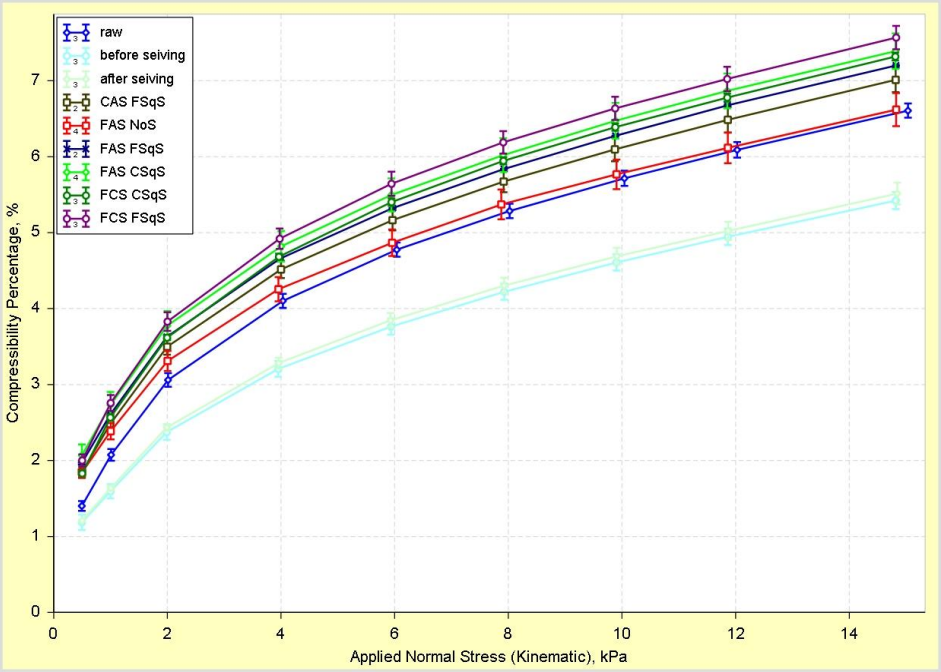

Figure 3.20: Freeman Tech FT4 compressibility results for Prosolv HD90 being fed with various feeder tooling. No significant effect of feeder configuration was found.

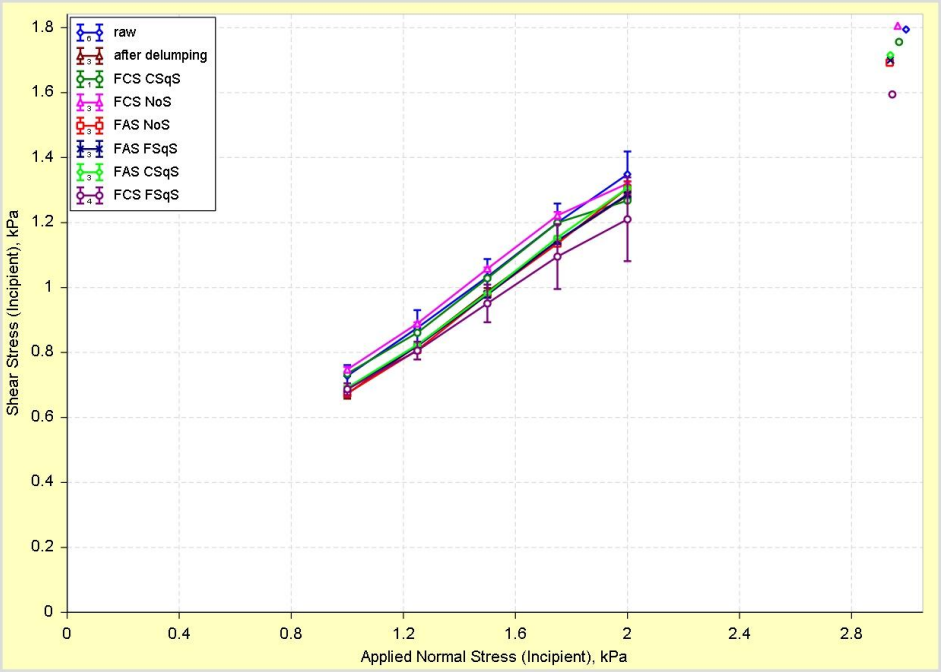

Figure 3.21: Freeman Tech FT4 shear cell test results for Prosolv HD90 being fed with various feeder tooling. No significant effect of feeder configuration was found.

3.8 Tables for Chapter 3

Table 3.1: Feeder capacity of K-Tron feeders

Model	Volumetric Throughput (dm^3/hr)		Gravimetric Throughput (kg/hr)*		Hopper Capacity	
	Low	High	Low	High	dm^3	kg*
K-Tron KT35	1.8	2500	0.9	1250	25	12.5
K-Tron KT20	0.1	200	0.05	100	25	12.5
K-Tron MT12	0.04	4	0.02	2	2	1

*Gravimetric Throughput assumes a bulk density of 0.5 kg/dm^3.

Table 3.2: List of available screens for each K-Tron feeder model

Feeder	CSqS	MSqS	FSqS	CSlS	FSlS	NoS
KT35	X		X			X
KT20	X	X	X			X
MT12	X		X	X	X	X

Table 3.3: Formulation

Component	Manufacturer	Function	% w/w
API		Active	52.02
Prosolv HD90	JRS Pharma	Filler	44.33
Colloidal Silicon Dioxide (Cab-O-Sil M5P)	Cabot	Glidant	0.91
Crospovidone (Polyplasdone XL-10)	ISP	Disintigrant	2
Magnesium Stearate (Grade 5712)	Mallinckrodt	Lubricant	0.74
		Total	100

Table 3.4: Component gravimetric and calculated volumetric feedrates

Component	API	Prosolv HD90	Colloidal Silicon Dioxide	Crospovidone	Magnesium Stearate
% w/w	52.02	44.33	0.91	2	0.74
Nominal Feedrate (kg/hr)	15.606	13.299	0.273	0.6	0.222
80%	12.485	10.639	0.2184	0.4800	0.1776
100%	15.606	13.299	0.2730	0.6000	0.2220
125%	19.508	16.624	0.3413	0.7500	0.2775
Density (kg/dm3)	0.61	0.49	0.04	0.33	0.14
Volumetric Rates (dm3/hr)					
80%	20.47	21.71	5.46	1.45	1.27
100%	25.58	27.14	6.83	1.82	1.59
125%	31.98	33.93	8.53	2.27	1.98

Table 3.5: Volumetric Capacity for the K-Tron KT35

Screw	Volumetric Feedrate (dm^3/hr)		RPM	
	MIN	MAX	MIN	MAX
Coarse Concave Screw (CCS)	62	849	24	327
Coarse Auger Screw (CAS)	64	882	24	327
Fine Concave Screw (FCS)	21	294	24	327
Fine Auger Screw (FAS)	23	310	24	327

Table 3.6: Volumetric Capacity for the K-Tron KT20

Screw	Volumetric Feedrate (dm^3/hr)		RPM	
	MIN	MAX	MIN	MAX
Coarse Concave Screw (CCS)	2.5	34	12	170
Coarse Auger Screw (CAS)	2.7	37	12	170
Fine Concave Screw (FCS)	0.93	13	12	170
Fine Auger Screw (FAS)	1	14	12	170

Table 3.7: Volumetric capacity of the K-Tron MT12

Screw	Volumetric Feedrate (dm^3/hr)		RPM	
	MIN	MAX	MIN	MAX
Coarse Concave Screw (CCS)	0.1	4	0.5	100
Coarse Auger Screw (CAS)	0.1	4	0.5	100
Fine Concave Screw (FCS)	0.04	2.2	0.5	100
Fine Auger Screw (FAS)	0.04	2.2	0.5	100

Table 3.8: Feeder testing configurations for Prosolv HD90

KT20		Prosolv HD90 80%	100%	125%
CCS	CSqS	X	X	X
	MSqS	X	X	X
	FSqS	X	X	X
	NoS	X	X	X
CAS	CSqS	X	X	X
	MSqS	X	X	X
	FSqS	X	X	X
	NoS	X	X	X
FCS	CSqS			
	MSqS			
	FSqS			
	NoS			
FAS	CSqS			
	MSqS			
	FSqS			
	NoS			

KT35		Prosolv HD90 80%	100%	125%
CCS	CSqS			
	FSqS			
	NoS			
CAS	CSqS			
	FSqS			
	NoS			
FCS	CSqS	X	X	X
	FSqS	X	X	X
	NoS	X	X	X
FAS	CSqS	X	X	X
	FSqS	X	X	X
	NoS	X	X	X

Table 3.9: Feeder testing configurations for API

KT20		API 80%	100%	125%
CCS	CSqS	X	X	X
	MSqS	X	X	X
	FSqS	X	X	X
	NoS	X	X	X
CAS	CSqS			
	MSqS			
	FSqS			
	NoS			
FCS	CSqS			
	MSqS			
	FSqS			
	NoS			
FAS	CSqS			
	MSqS			
	FSqS			
	NoS			

Table 3.10: Feeder testing configurations for colloidal silicon dioxide

KT20		Colloidal Silicon Dioxide		
		80%	100%	125%
CCS	CSqS			
	MSqS			
	FSqS			
	NoS	X	X	X
CAS	CSqS			
	MSqS			
	FSqS			
	NoS			
FCS	CSqS			
	MSqS			
	FSqS			
	NoS			
FAS	CSqS			
	MSqS			
	FSqS			
	NoS			

KT35		Colloidal Silicon Dioxide		
		80%	100%	125%
CCS	CSqS			
	FSqS			
	NoS	X	X	X
CAS	CSqS			
	FSqS			
	NoS			
FCS	CSqS			
	FSqS			
	NoS			
FAS	CSqS			
	FSqS			
	NoS			

Table 3.11: Feeder testing configurations for API and silicon dioxide preblend

KT20		API & Silica Blend		
		80%	100%	125%
CCS	CSqS	X	X	X
	MSqS	X	X	X
	FSqS	X	X	X
	NoS	X	X	X
CAS	CSqS	X	X	X
	MSqS	X	X	X
	FSqS	X	X	X
	NoS	X	X	X
FCS	CSqS			
	MSqS			
	FSqS			
	NoS			
FAS	CSqS			
	MSqS			
	FSqS			
	NoS			

Table 3.12: Feeder testing configurations for magnesium stearate

MT12		Magnesium Stearate		
		80%	100%	125%
CCS	CSqS	X	X	X
	FSqS	X	X	X
	CSlS	X	X	X
	FSlS	X	X	X
	NoS	X	X	X
CAS	CSqS			
	FSqS			
	CSlS			
	FSlS			
	NoS			
FCS	CSqS	X	X	X
	FSqS	X	X	X
	CSlS	X	X	X
	FSlS	X	X	X
	NoS	X	X	X
FAS	CSqS			
	FSqS			
	CSlS			
	FSlS			
	NoS			

KT20		Magnesium Stearate		
		80%	100%	125%
CCS	CSqS			
	MSqS			
	FSqS			
	NoS			
CAS	CSqS			
	MSqS			
	FSqS			
	NoS			
FCS	CSqS	X	X	X
	MSqS	X	X	X
	FSqS	X	X	X
	NoS	X	X	X
FAS	CSqS			
	MSqS			
	FSqS			
	NoS			

Table 3.13: Feeder testing configurations for crospovidone

KT20		Crospovidone		
		80%	100%	125%
CCS	CSqS			
	MSqS			
	FSqS			
	NoS			
CAS	CSqS			
	MSqS			
	FSqS			
	NoS			
FCS	CSqS	X	X	X
	MSqS	X	X	X
	FSqS	X	X	X
	NoS	X	X	X
FAS	CSqS			
	MSqS			
	FSqS			
	NoS			

Table 3.14: Changes to the API feeding trials. Tests marked with "InC" were found to be incompatible

KT20		API		
		80%	100%	125%
CCS	CSqS	X	X	X
	MSqS	InC	InC	InC
	FSqS	InC	InC	InC
	NoS	X	X	X
CAS	CSqS			
	MSqS			
	FSqS			
	NoS			
FCS	CSqS			
	MSqS			
	FSqS			
	NoS			
FAS	CSqS			
	MSqS			
	FSqS			
	NoS			

Table 3.15: Changes to the API / silica preblend feeding trials. Tests marked with "InC" were found to be incompatible

KT20		API & Silica Blend		
		80%	100%	125%
CCS	CSqS	X	X	X
	MSqS	X	X	X
	FSqS	InC	InC	InC
	NoS	X	X	X
CAS	CSqS	X	X	X
	MSqS	X	X	X
	FSqS	InC	InC	InC
	NoS	X	X	X
FCS	CSqS			
	MSqS			
	FSqS			
	NoS			
FAS	CSqS			
	MSqS			
	FSqS			
	NoS			

Chapter 4. OPTIMIZING GRAVIMETRIC FEEDING OF ZINC OXIDE

4.1 Summary

As discussed in previous chapters, metered dosing of granular materials is relatively unexplored and there is a broad lack of understanding of the effect of both the properties of incoming materials on the feeding process and the effect of the feeding process on the properties of material discharged into subsequent processing units. To further complicate matters, numerous grades of materials are often available for selection. Grades of a given powder (i.e., fume silica) may vary in numerous powder properties, including: moisture content [66], [67], particle size distribution [68]–[70], morphology [69], and impurity concentrations [66], [69], all of which might contribute to the overall processability and bulk powder behavior. There are no studies that specifically examine the effects of material grades as it pertains to feeding. When grade is unimportant, then the selection of a raw material can be completely economically driven, but this determination still requires an understanding of both the effect of incoming material properties and processing. Only if these effects are negligible or can be controlled, can a purely economic decisions for the selection of raw materials be warranted.

As previously mentioned in Chapter 1, Kehlenbeck *et al.* have shown that attachments at the discharge of screw-driven feeders can improve feeding performance [5]. However, these studies were limited to a single powder and did not consider the effect of the feeding process on the powder. As attachments add to the amount of shear imparted to fed material, attachments may be incompatible with some shear sensitive materials. Tardos *et al.* improved feeding performance of different powders through the use of

vibration and observed that different powders have different feeding behavior [6], but once again the effect of the feeding process on powder properties was not recorded.

This chapter presents a loss-in-weight feeding case study that used zinc oxide obtained from two manufacturers. The goals of the study were to test the feasibility of using screw-driven loss-in-weight feeding technology for the metered dosing of zinc oxide, to determine the differences in feeding performance for two different grades of zinc oxide, as well as to determine the effect of the feeding process on the zinc oxide powder. Zinc oxide is used for these studies as it is a good example of a material that has many different grades, has processing sensitivity [71], is used across various industries (plastics, ceramics, lubricants, paints, ointments, fire retardants, etc.) with many prospective future applications [72], [73], so that an improved understanding of material selection would be very beneficial.

Previous work with zinc oxide by Meissner *et al.* showed that zinc oxide powder with fine particle size distributions have a peculiar behavior of spontaneous pelletization when the loose powder is tumbled over. It was observed that this phenomenon would occur for relatively small particles (0.25 micron and less), whereas relatively large particles (1 micron and larger) would only form weak agglomerates. [74] A small extent of processing can result in the quality of zinc oxide powders to change significantly, which means that the powder is shear sensitive and processing considerations must be carefully characterized and understood.

A similar particle size based behavior was investigated by Al-Tounsi *et al.* where decreasing particle size resulted in increased strength of zinc oxide compacts. [70] As

with any process, there are a number of material properties that may play a role in the overall outcome of any process making measurement and material characterization crucial. However, this is only feasible with process understanding, which will narrow measured material properties to those identified as significant rather than broad measurement of all possible material properties.

4.2 Materials

The materials chosen for this study are two grades of zinc oxide that show different flow behavior: Norzinco CF8 and Grillo Pharma8. Observations made from previous handling of the materials indicate that Norzinco CF8 is a worse-flowing material than the Grillo Pharma8, although these two zinc oxide materials are often used interchangeably. The Norzinco zinc oxide is the more shear-sensitive of the two materials, but both are known to display compressive and shear effects caused by processing and handling.

Typically, during a material selection process, the main defining attribute of the powder used for selection would be "grade", which for zinc oxide is based on purity, compositions, specific surface area, and sometimes the process by which it is made. [73] Often there are several available products that can fit the specifications defined by the application. The two different zinc oxide materials were chosen due to their similar manufacturer specifications that would make them acceptable candidates for many of the same applications. The two materials selected for comparison in this study were made by a similar indirect method (“French Process”), have the same specified surface area of 8 m^2/g, have the same purity (99.9%), and similar compositions of impurities (See Table 4.1). As specified by the manufacturers, these two materials would seem virtually indistinguishable or fully interchangeable, yet previous experience and visual inspection

of the powders during processing reveal that their flow behavior and shear sensitivity are quite different.

Initial testing to quantify the flow behavior of the materials was carried out in the "gravimetric displacement rheometer" (GDR). This device consists of a tumbling drum mounted on a hindged lever arm, supported by a load cell, that measures the change in center of mass as a result of avalanching material inside the drum. The standard deviation taken from the load cell signal in the GDR is proportional to the size of avalanches formed at various speed settings, and this standard deviation is used to compute the flow index [46]–[49]. In the GDR, it was observed that the Norzinco CF8 powder spontaneously agglomerated (see Figure 4.1), but the Grillo Pharma8 did not exhibit this same behavior. Additionally, both materials heavily coated the tumbling drum of the GDR, reducing reproducibility, making the test only adequate in differentiating between the two materials as the Norzinco powder would form large agglomerates, but the Grillo material would not. The GDR testing equipment was unable to sufficiently measure material property changes caused due to processing effects from the feeding equipment, because the GDR measurements were confounded by the changes to the powders caused by tumbling within the GDR.

Formation of weak agglomerates caused by tumbling is common for zinc oxide powders with particle size greater than 1 micron [74], which is the case for both materials (See Figure 4.2), however the Grillo material did not exhibit this behavior. Figure 4.2 shows that the particle size distributions (PSD) for both zinc oxide powders have similar means, yet have significantly different dispersity. The Grillo material's PSD is narrower than the Norzinco powder's PSD. Considering the tendency for agglomerates formed from

monodisperse particles to be weaker [75], it is likely that the Grillo material's agglomerates are broken by the stresses caused by tumbling, whereas the Norzinco powder's agglomerates do not, but instead grow larger.

Pre and post-feeding analysis of the materials was performed using the Freeman FT4 powder rheometer to examine changes displayed by the powders under some of the feeding treatments. The Freeman FT4 has a suite of tests that measure various powder properties that can be related to processability or to determine shear sensitivity.

4.3 Equipment

4.3.1 Loss-in-weight feeders

All the feeders tested in the feeding trials reported here were designed to handle powder with a large range of flow properties, including those with very poor flowability, which tend to be lumpy and form bridges. The feeders tested here for steady state flow rate variability were the Gericke GLD87, the Gericke GAC232, and the KTron KT35. All of the feeders are screw dispensing loss-in-weight feeders, which use gravimetric control to maintain the feedrate at a desired setpoint.

4.3.1.1 KTron KT35 Loss-in-Weight feeder (Small/Mid Feeder)

The KTron KT35 (see Figure 4.3a) twin screw Loss-in-Weight feeder's design consists of a modular twin-shaft feeder mounted on a sanitary weigh bridge. There are several feeding screws and discharge screens available, which allows feeding a large range of bulk powder materials (see Figure 4.3b and c for a picture of the feeder tooling for the KT35 feeder). At the bottom of the feed hopper is a bowl containing a horizontal double-bladed agitator, which helps fill the flights of the feed screws. The agitation speed is set

at 17% of the feed screw speed. The gearbox controlling the screws is a type B with a gear ratio of 6.7368:1, combined with a motor with a maximum speed of 2000 RPM. At 100% of the motor speed, the screw rate is 297 RPM (327 RPM @ 110% is also achievable by over-speeding). [31]

4.3.1.2 Gericke GLD87 Feeder (Small Gericke Feeder)

The Gericke GLD87 (see Figure 4.4) feeder is a single screw device designed with a counter-weight and an oil dampening system to maintain a high level of accuracy with robustness. The agitation in the feeder comes from a horizontally rotating 4-bladed screw filler that forces material into the screw flights from above as well as a vertically rotating hopper agitator that rotates closely to the hopper walls in a stirring motion that keeps material from bridging within the hopper. Interchangeable discharge nozzles allow for a large range of interchangeable metering screws of different diameters that can achieve a range of discharge rates from 0.05 to 600 liters / hour. For the feeding trials reported here the screw tested had a metering size of 3. The maximum rotation rate of the dosing screw is 220 RPM with a typical operating range of 44 to 176 RPM (20 to 80% of the maximum), which enables the gravimetric control to adjust screw speed.

4.3.1.3 Gericke GAC232 Feeder (Large Gericke Feeder)

The Gericke GAC232 (see Figure 4.5) is the largest feeder tested here. It is a single screw device, which has an agitator that rotates concentrically around the dispensing screw. The interchangeable screws and nozzles allow for an even larger operating range than the GLD87, from 1.3 to 27000 liters / hour. The screw size tested for this feeder had a size of 8, which has a feeding rate range from 160 to 3200 liters / hr. The maximum

rotation rate of the screw is 157 RPM with the operating range from 32 to 126 RPM (20 to 80% of the maximum).

4.3.2 Catch Scales

As in chapter 2, a "catch" scale was used to measure the output flow of the feeders. This device was needed because each gravimetric loss-in-weight feeder uses a different filtering algorithms, which may not allow for accurate comparison between different feeders (or even reliable measurements). Although the scales have software that may include built-in data analysis that runs in real time as the catch scale is collecting a sample, only the raw mass readings are used for post-processing and analysis. For each feeder, the catch scale was chosen based on availability as well as to maximizing the resolution of the collected data. This basically requires the smallest (best resolution) acceptable available scale to be used in each case. All of the scales used were "catch" scales with a very fast response and settling time.

4.3.2.1 Schenck Accurate AccPro II

A Schenck Accurate AccPro II was used as a "catch scale" to characterize the KTron KT35 feeder's performance. AccPro II uses a PC Excel program that obtains weight readings from a 7 kg strain gage load cell through the Schenck DISOBOX summing box. The DISOBOX uses a 24 bit Analog Devices A/D converter to obtain the weight readings every 0.1 seconds. These readings are obtained and stored by the AccPro II application.

4.3.2.2 Mettler Toledo scales

A Mettler WMHA15 was used for the small Gericke GLD87 feeder, and a Mettler WMHC600 was used for the large Gericke GAC232. The Mettler WMH scales are

platform scales that communicate via RS232/422 to a Labview program, which monitors the load cell every 1 second for a maximum of 15 minutes.

4.4 Methodology

4.4.1 Characterization of Steady State feeding performance

The steady state feeding performance of a feeder can be used to aid in the proper selection of feeder tooling for a given powder at a given feedrate. The method used to analyze feeding performance is a two step process involving determination of volumetric capacity and gravimetric performance testing. Characterization of volumetric capacity requires measuring the capacity of the feeder at various set screw speeds, whereas the gravimetric studies are used to determine overall performance of the feeder while it is running under gravimetric control. The performance data for each condition is evaluated and compared using the relative standard deviation of the feed rate. To further analyze the data, a Fourier transform is used to obtain the power spectrum of the flow rate data, which can be used to determine frequencies of the dominating components of noise in the feedrate signals.

4.4.1.1 Steady State feeding performance

The characterization experiments were conducted using an appropriate "catch" scale to record the weight at the highest resolution for all tests. Due to the sensitivity of the load cells in the equipment, careful consideration was taken to isolate and minimize outside disturbances on the feeders and catch scale. In determining equipment placement and filtering methods, the various general considerations listed in the work by Erdem were taken into account [9]. Before any experiments were performed, the load cells in the

catch scales and the loss-in-weight feeders were calibrated. The feeders were mounted on a sturdy surface and the catch scale setup was placed on a separate lower stand, which reduced interference on the catch scale caused by vibrations in the feeder (see Figure 4.6). A container on the "catch" scale was used to collect the samples. When the container on the scale become full, it was replaced by an empty one. Data collection was "paused" during each container change so that this disturbance did not affect data analysis.

As mentioned, the Schenck Accurate AccPro II with a 7kg load cell was used for the KTron KT35 feeder. The Gericke feeders were at a different facility, where the available scales were different. For the smaller feedrates, using the Gericke GLD87 feeder, a higher resolution Mettler WMHA15 with a 15 kg maximum load was used. A higher capacity Mettler WMHC600 with a 600 kg maximum was used for the larger feedrates of the GAC232 to collect material in a big bag placed in a crate. The larger capacity of the WMHC600 had an effect on the overall resolution of the scale, but it was suitable as the fluctuations were much larger than the resolution of the scale due to the much larger discharge tube and larger flights of the screw for the larger feeder.

Any unexpected behavior (such as electrostatic charging, noise during feeding, compaction, etc.) noticed during testing was recorded, and where applicable, pictures were taken. Other potential problems such as abrasion of the seals, which can cause long term issues, were also monitored. Where relevant, samples were taken for offline measurements.

4.4.1.1.1 Volumetric Capacity

Feeders were first tested in volumetric mode. The main goal of the volumetric tests was to determine capacity at each of the tested volumetric speeds. Five volumetric setpoints were investigated for each combination of feeding tooling in the feeders: 10, 20, 50, 80, and 90% of the maximum volumetric screw speed. These five conditions were chosen to examine the entire working range of the feeder and to determine the dependence of the capacity on screw speed. Volumetric tests were conducted for a short time, 2-5 minutes, to prevent hopper fill and density changes to cause testing to drift from the original feedrate capacity.

4.4.1.1.2 Gravimetric Performance

Following the volumetric trials, gravimetric performance was evaluated by monitoring the feedrate from the feeder for 15 minutes (~900 one-second data points, which is the minimal sampling time for the Labview program used with the Mettler scales). A time of 15 minutes was chosen so that there would be a sufficient number of data points for meaningful statistical comparison between conditions as well as to verify sustained performance for an extended period of time. Three gravimetric setpoints were evaluated, which were the gravimetric equivalent setpoint of the 20, 50, and 80% volumetric setpoints obtained from the volumetric capacity tests previously performed. Initial fill level was at the maximum. The gravimetric mode of the feeder automatically adjusted for changes in the flight filling of the screw caused during hopper emptying.

The maximum controllable feedrate for each feeder was also determined using a built-in calibration program of the feeder's controller rather than running volumetric capacity tests. This returned the value of the initial feed factor, which is the estimated feed rate at

100% of the screw speed. The issue with using the built-in calibration program of the feeder is that it assumes a linear relation between the average feedrate and volumetric screw speed. If the actual relation is not linear, the estimated feed factor will contain errors.

4.4.1.1.3 Analysis

The raw data from the "catch" scales used for analysis was obtained via an Excel export from the catch scale software package. The mass at every 1s was used to calculate the fed material mass. Dividing this fed material mass by the 1 second time interval resulted in the average feedrate for that 1 second interval. The standard deviation and average of the feedrate was calculated and used for comparison of the different data sets. Fast Fourier Transform of the feedrate data was used to investigate the frequency of the variance in the feeding signal.

In order to eliminate disturbances caused by refilling, machine startup/shutdown, etc., the data was filtered by rigorously removing disturbances from the original data set. Before and after each disturbance, 3 seconds of data were removed, allowing adequate time for settling after a disturbance. By comparing the distribution of the original unfiltered data with the filtered data it is possible to further optimize the filtering, which was detailed in Chapter 2 [61]. After filtering out disturbances, the left over data represents the steady state behavior of the feeder.

The steady state distribution of the feed rate data, which was obtained for the feeders operating in gravimetric loss-in-weight mode, is illustrated in Figure 4.7. This figure shows feedrate data as a function of time, and its respective fitted Gaussian distribution.

There are two important parameters for performance that can be gathered from feedrate signal data: spread of the data (standard deviation) and deviation of the average from the setpoint.

At higher screw rotation rates the distributions from all the feeders were found to be Gaussian. However, for lower screw speeds, a non-Gaussian distribution was often observed, as shown in Figure 4.8. This figure shows the feedrate distributions created from the Gericke GLD87 feeding Norzinco powder at three different feedrate setpoints: 14.2kg/hr, 30.2kg/hr, and 46.9kg/hr. At the lowest feedrate setpoint, the feedrate distribution is skewed into a partially U-shaped distribution. As the screw speed was increased, the oscillations decrease, and the distribution becomes more Gaussian.

This behavior was common for both single screw feeders: Gericke GLD87 (See Figure 4.9a) and Gericke GAC232 (See Figure 4.9b). The distributions from the K-Tron KT35 operating at 20% screw speed did not have this same behavior, but instead had a Gaussian shape (See Figure 4.9c). However, further reduction of the screw speed, when using the auger screws, caused the K-Tron feeder to display a similar U-shaped feedrate distribution (See Figure 4.10a). Low screw rotation rates often lead to sinusoidal oscillations (See Figure 4.10b), which causes the majority of instantaneous feedrate data points to lie on the outer ranges of the distribution, resulting in a U-shaped distribution.

Filtering and removal of data during refill is important, because during refill a loss-in-weight feeder operates in volumetric mode. Under such conditions, the feeder does not control and compensate for fluctuations in flight filling of the dispensing screws, which makes accuracy and feeding performance during this time heavily dependent on feeding

history, which is not available to the logics of the feeder's controller in short experimental characterization runs such as those described here. This dependency on feeding history during refill is caused because many feeders will modify the volumetric mode during hopper filling to a hybrid mode that dynamically changes the screw speed (rather than holding constant) based on historic feeding performance. However, this requires multiple refilling operations to occur.

To analyze the data, the mass at every 1 second was used to calculate the fed material mass for the interval. From this data the average flowrate ($\dot{m}_i$) can be calculated for each 1 second (Δt) interval:

$$\dot{m}_i = \frac{\Delta m_i}{\Delta t} \tag{4-1}$$

From all the mass flowrates at each interval a distribution can be created, and the standard deviation (σ) and relative standard deviation (RSD) can be calculated:

$$\sigma = \sqrt{\frac{\sum_{i=1}^{n}(\dot{m}_i - \overline{\dot{m}})}{n-1}} \tag{4-2}$$

$$RSD = \frac{\sigma}{\overline{\dot{m}}} \tag{4-3}$$

where $\overline{\dot{m}}$ is the arithmetic mean mass feedrate of the distribution and n is the number of samples in the distribution.

4.4.2 Characterization of powder properties in FT4

Powder samples were collected from various feeding conditions and characterized in the Freeman Technology FT4. The FT4 has a suite of tests that result in flow parameters that

are obtained through different methodologies that utilize a cylindrical vessel and various attachments. The methodologies used in these studies include dynamic flow measurements, compression measurements, and shear cell measurements. An important feature of all of these methodologies is to ensure a standardized packing condition before any of the measurements, which improves repeatability by removing consolidation effects associated with how an operator handles the powder and loads the cylindrical testing vessel. The FT4 apparatus achieves this condition with a preconditioning process which involves gentle displacement of the powder sample with a rotating helical blade that loosens and aerates the powder [64], [76].

4.4.2.1 Dynamic Flow Measurements (Flow Energy Parameters)

Dynamic flow measurements focus on the flow energy needed to displace the powder under controlled test conditions. The test investigates stability and shear sensitivity using the variable flow rate (VFR) test. This testing regime involves initially loading a sample and preconditioning it with the helical blade. Following this preconditioning is a series of 11 testing cycles, each one followed by a conditioning cycle. The first 7 conditioning cycles are carried out at the same rate with the goal of determining stability. The last 4 investigate the effect of shear rate by decreasing the rotational tip speed. Conditioning cycles are conducted in between testing cycles to remove residual compaction from any previous test cycle. The flow energy associated with confined powder flow is defined as the basic flow energy, which is often the most differentiating measurement for similar powders. The measurement that is used for the basic flow energy is from the 7^{th} testing cycle. The specific energy is the measurement of flow energy when the powder is

unconfined and is measured when the blade moves upwards during testing, where there is predominately shear with no compression.

4.4.2.2 Compression Measurements (Compressibility Parameter)

The compression test measures the compressibility and bulk density profiles of the powder. During this test, the preconditioned powder is compacted with a known normal stress. During the test the bulk density is measured as it increases due to compaction as a function of the applied normal stress. As normal stress increases the volume decreases with a larger volume change associated with more cohesive powders.

4.4.2.3 Aeration (Aerated Energy Parameters)

A second series of tests that involves dynamic flow measurements focuses on the aeration ratio. For this testing the flow energy is measured with a series of testing cycles followed by conditioning cycles, each one performed at a different aeration rate. As the aeration rate increases the flow energy decreases. The aeration ratio is the ratio of the flow energies required at any aeration rate:

$$AR_n = AE_0 / AE_n \qquad (4\text{-}4)$$

Where AE_0 is the flow energy with no aeration and AE_n is the aerated flow energy for n mm/s air velocity.

4.4.2.4 Permeability Test (Pressure Drop Parameter)

A second test that follows the compression test methodology is the permeability test. Permeability testing is used to determine how easily air can pass through a powder with increasing compaction stress. The test has a similar procedure to the compression test, but instead measures pressure drop as a function of the compaction stress.

4.4.2.5 Shear Cell Measurements (Shear Stress Parameters)

Shear cell measurements consist of three main steps: consolidation, pre-shearing, and shearing. Following preconditioning, the powder is compressed to a consolidation load with a vented piston. In order to achieve a state of uniform density that is strain independent and reproducible the sample is pre-sheared. Afterwards the normal stress is lowered, and the sample is sheared further to obtain the yield point. This pre-shear followed by shearing sequence is repeated five times at different applied normal stress to obtain a yield locus. [77]

4.5 Results

4.5.1 Volumetric Feeding Trials

4.5.1.1 Volumetric Capacity

The results from the volumetric capacity testing for the three feeders are shown in Figure 4.11. Feeding capacity was linearly dependent on the screw speed. This indicates that screw filling was consistent at all speeds of the feeder. Often, screw filling consistency for a given powder will decrease as speed increases due to the screw flights rotating faster than the powder can fill them, resulting in a proportionally smaller increase in capacity for an increase in screw speed.

As expected, the Gericke GAC232 had the largest capacity at each tested combination than the other two feeders. The KTron KT35 had the next highest, but had some overlap with the Gericke GLD87 capacity range.

Each plot of capacity versus percent screw speed was linearly fit through the origin. The results are shown in Table 4.2 and Table 4.3. All of the R^2 values were greater than 0.99

with low p-values, which indicates the linear fits are all very good. This means that only the slope is needed to determine the approximate feedrate at a screw speed for any feed tooling combination.

4.5.1.2 Volumetric Performance

In steady state feeding, the main measure of performance is the variability around the setpoint. The least consistent the feeding, the higher the variance (or the standard deviation) of the feed rate will be. To compare the performance between the feeders for different combinations of tooling, the relative standard deviation (RSD) is used. Plots of the RSD *versus* screw speed are shown in Figure 4.12. The general observation for all of the tooling combinations is that as the screw speed increases, the RSD typically decreases.

The decrease in RSD with increasing screw speed is magnified at the lower screw speeds (<50%) for both the Gericke GLD87 and Gericke GAC232, but not for the KTron KT35. The KTron KT35 is the only twin-screw feeder that was tested, and exhibited a more consistent accuracy across the range of feed rates. This occurs because the twin screw feeder applies more screw flight passes for each rotation of the screws. For each rotation rate of the single screw feeders, a single flight pass of the screw doses powder material. For the KTron KT35, using the self-cleaning concave twin-screws, there are four flight passes of the screws due to two passes for each of the screws. When the KTron KT35 is equipped with the auger screws, the flight passes are similar to the single screw feeder, as the screws are set in phase so the flight pass occurs at the same time for both screws.

The RSD as a function of screw flight pass rate is shown in Figure 4.13. In this figure, except for a few small deviations, the results for the different combinations appear to collapse onto a single curve, indicating that there is a relation between screw flight passes and feeding performance. The reason for lower screw passes resulting in higher RSD is likely due to "pulsing" of powder stream, i.e., the flights of the screw release powder intermittently as the screw rotates. The faster the rotation rate of the screws, the more frequent the powder stream pulses, which results in a more consistent stream of powder.

Another important comparison between multiple feeders and multiple combinations of tooling is the relationship between RSD *vs.* actual feedrate (Figure 4.14). From this figure, a desired feedrate can be chosen from the x-axis; the curve that displays the lowest RSD at that feedrate indicates the combination of feeder and feed tooling that performed the best in the feeding trials for that feedrate. The feeding performance of the two powders is similar for each combination of feeder and feed tooling, which is shown in the close overlap of the curves for the different powders at each feeding combination.

Comparison of different feeders is important when selecting equipment, but when only one feeder is available, the best option for optimizing performance in the feeder is based on feeding tooling. In Figure 4.14b, the RSD for the different feeding tooling in the Gericke GLD87 is shown as a function of feedrate. These plots show that the size 3 auger has better performance, but it has limited capacity. For capacities above about 40 kg/hr, the size 3 helix is the only option for this feeder with values of RSD that are comparable to the RSDs of the size 3 auger at lower speeds. So, for the Gericke GLD87, the best option is to use the size 3 auger at low speeds, and the size 3 helix extends the range of operation of the feeder to higher feedrates.

Figure 4.14c depicts the RSD *vs.* feedrate for the KTron KT35 feeder. The auger twin-screws have the poorest performance with the highest RSD. The performance differences between the screens and the case with no screen for the concave self-cleaning twin-screws are minimal. The increase in shear on the material caused with the use of the screens with no apparent benefit in feeding performance indicates the best combination of feed tooling for the KTron KT35 is with the concave twin-screws without a screen.

4.5.2 Gravimetric Feeding Trials

Gravimetric performance trials explore the real applicability of a feeder. In volumetric mode, the fluctuations are intrinsic to the feed screw as pulsation is naturally caused as a screw rotates. With gravimetric control, deviations caused by hopper emptying are minimized by adjusting the speed, which is a practical necessity for the extended running of a feeder. In Figure 4.15, the gravimetric performance of the three tested feeders is shown. These plots serve to validate that the volumetric performance is indicative of actual gravimetric performance. When overlayed with the corresponding volumetric runs, the RSD's from the gravimetric trials are very similar to that of the volumetric trials.

The gravimetric runs were tested for the best performing tooling selections from the volumetric data. Figure 4.16 shows that in the overlapping region of the operating range of the KTron KT35 and the Gericke GLD87, the KTron KT35 has better performance with both zinc oxide powders. This is not necessarily indicative of all powders, but for the zinc oxides that were tested here, there was a performance advantage to using the twin-screw design of the KTron feeder.

4.5.3 General Observations

4.5.3.1 Tooling coating by powder

During the feeding of the zinc oxide powders, it was noticed that the powder would adhere to any of the feeder's processing surfaces that came in contact with the powders, forming coating layers that often would be several millimeters thick. In the KTron KT35, it was noticed that the screws became so heavily coated that the capacity of the feeder was decreased by the reduction of the flow volume between the flights of the screw. This would occur with the auger twin screws as shown in Figure 4.17. The self-cleaning concave twin screws did not exhibit this problem. Thus, the self cleaning screws are logically a better choice for this type of powder; this enables more consistent feeding, as there is no buildup on the screws which would require to change dynamically the variables that the controller uses to predict screw speed during operation and would also decrease overall capacity, perhaps in a time-dependent fashion.

4.5.3.2 Frequency Analysis

To further analyze the data collected by the catch scales, a power spectrum of the data was obtained by using a Fast Fourier Transform technique. Figure 4.18 shows power spectra for the KTron KT35 feeder for the two powders with the coarse concave self-cleaning screws, obtained without the addition of a discharge screen for the speeds of 20% and 50% of the maximum volumetric screw speed. The rotation rate of the feed screws for the feeder at 20% and 50% of the maximum volumetric speed are 59 RPM (~1 hz) and 148 RPM (~2.5 hz) respectively. The power spectra for the two different speeds do not show dominant peaks at either of the frequencies corresponding with the rotation rate of the screws. However, if the frequencies of the screws are doubled, as the feeder is

a twin-screw design with the flights of the screws being out of phase, the double frequencies for the 20% and 50% are ~2 hz and ~5 hz. The figure shows very clear peaks, demonstrating that the rotation frequencies of the screws play a large role in the pulsation variability of the feedrate. This suggests that the performance of the feeder would be improved by increasing screw speeds or by running the feeder at higher speeds as higher frequency noise is more likely to be filtered out by the back-mixing action of subsequent unit operations such as in-line blending [62].

4.5.4 Effect of feeding conditions on powder properties

Visual inspection of the powders revealed that the screen had a significant agglomeration effect on the Norzinco zinc oxide powder. Figure 4.19 shows the effect on agglomeration caused by processing with the different discharge screen attachments in the K-Tron KT35. The first figure of each row characterizes the bulk powder before feeding, showing that the Norzinco powder has more large agglomerates than the virgin Grillo material. Processing without a screen separates the effects of the screen and the screw, and in this set of powder, it is shown that the large but weak agglomerates from bulk material are broken apart by the gentle shear of the screws. Using the coarse square screen introduces more shear than the screws alone, which causes a significant difference in the appearances of the powders. The Grillo powder remains the same in visual texture, whereas the Norzinco material starts to form fine agglomerates. This effect is increased when the fine square screen is used, where the Norzinco material forms pellet like granules that can be easily broken with gentle direct stress.

These effects were quantified using the FT4. For each of the zinc oxide grades three samples were taken for analysis in the FT4: unprocessed, low shear, and high shear. The

low shear condition was sampled from the K-Tron KT35 feeder with coarse concave screws running at low screw speed (20%) and no screen. For the high shear condition, the coarse square screen was added and a higher screw speed was used (80%). The results from the different tests in the FT4 are shown in tabulated form in Table 4.4 and in graphical form in Figure 4.20 to Figure 4.29.

Figure 4.20 displays the total energy measured using the dynamic flow measurements method (stability and variable flow rate test) on the Grillo and Norzinco zinc oxides for unprocessed bulk, a low shear feeding condition, and a high shear feeding condition. The first seven points for each plot, corresponding to the stability test, show that the behavior is fairly stable, indicating that for the amount of shear in this test there is not a significant shear sensitivity. The last four points, 8 through 11, in each plot are part of the variable flow rate test. The seventh point is the basic flowability energy, which is depicted also in Figure 4.21. This bar graph shows that the differences between the three Grillo conditions are minimal, whereas the Norzinco powder shows a significant decrease in the basic flowability energy from the unprocessed to either of the feeding-sheared conditions. This indicates that the Norzinco material is significantly more shear sensitive to the amounts of shear that are involved in the feeding process. Overall, all of the Norzinco material tends to have a higher flow energy. Since flow energy is the energy needed to displace the powder, a higher value indicates increased flow resistance. When comparing formulations with small differences, which is the case here, higher flow energy means poorer flow properties. With very different materials, this will not always be the case, as more free flowing materials often have higher densities, which requires more energy to

displace. Figure 4.22 shows the unconfined or specific energy, which shows a difference between powders but not between conditions.

Figure 4.24 shows the conditioned bulk densities for the different feeding shear conditions for both Grillo and Norzinco powders. Grillo results show that with increasing shear the conditioned bulk density (CBD) increases, whereas the Norzinco results show the opposite behavior, with a decrease in CBD as a result of shear. The Norzinco powder also shows a more significant change from unprocessed to either of the other processed conditions than Grillo powder does. The Grillo material may increase further with higher shear, whereas the Norzinco powder appears to have plateaued at a relatively low shear level.

The permeability data for the zinc oxide samples are shown in Figure 4.23. The relationship between pressure drop and applied normal stress is relatively linear aside from the first few points (~5-6 kPa) where the pores in the material are initially compressed. Figure 4.25 shows a bar graph of the pressure drops at 15 kPa normal stress for this same set of results, which easily shows the overall ordering of the plots. In general, both bowders have higher pressure drops for the higher sheared conditions, although Norzinco low shear and bulk powder have similar pressure drop. Overall the Norzinco material shows a higher resistance to gas flow.

Neither of these zinc oxide materials aerate well. Very little expansion of the powder beds was observed for any of the samples at any air velocity. Typical Aerated Energy of a powder that fluidizes well is less than 30-50 mJ, which is reached at low air velocities 1-2 mm/s. These zinc oxide powders reach a minimum energy of around 500-800 mJ,

which confirms their cohesive nature. There is an initial reduction in flow energy up to an air injection velocity of around 3-5 mm/s after which there is no further reduction in energy for higher air velocities. At this plateau, the maximum aeration occurs. As the gas flow further increases, the air does not overcome the cohesive forces and fails to separate the particles. Instead it creates channels to escape the powder bed. In a powder with low cohesive strength, the increasing air velocity would further reduce the flow energy to values that approached zero, reflecting a fully fluidized state.

Figure 4.27 shows the aeration ratios for the samples. Aside from the unprocessed Grillo sample, the aeration ratios for the samples show virtually the same rates of change of flow energy with respect to air velocity.

For both powders, the compressibility is lowest for the unprocessed powder and highest for the high shear processed powder. (See Figure 4.28) The powders behave similarly for each of the independent shear levels, but there is no significant difference between the compressibility of the powders in comparison to each other.

The shear cell results for the samples are shown in Figure 4.29. Both the powder type and processing conditions are virtually indistinguishable from one another. The shear data is often less informative than the dynamic and bulk property data for powders that contain low strength agglomerates. The yield loci do not represent clear distinctions between the different samples making interpretation less straight forward. This is due to the relatively high normal stress and pre-shearing, which removes most of the influence of processing on the samples previously observed the other lower stress testing

methodologies. The weak agglomerates that can be observed with visual inspection as shown in Figure 4.19 are unlikely to survive these high stress and shear conditions.

4.6 Conclusions

In these feeding trials, there was not a specified setpoint range, but instead the goal was to test the capabilities of the feeders, which required testing the full range. If there were a specified desired feedrate or feedrate range, the approach would change as only feeders and tooling that could potentially achieve those setpoints would be tested. As the behavior of every powder is different, there is some uncertainty in actual capacity due to powder consolidation, leading to powders exhibiting a range of densities. The estimated capacities used for capacity specification of the feeders is often based on ideal flight filling, whereas the actual powders may form bridges or coat the screws, which reduces the actual flight filling from ideal. The first set of experiments, which tested the volumetric capacity, determined actual capacity based on the powders used, which removed the "guess and test" scenario that may occur when the powder and feeder specifications are observed separately. For these zinc oxide powders the relationship between screw speed and throughput was linear, which could be fit and simply described with a single factor of slope. Some powders may not exhibit linear capacity relationships if flight filling is inconsistent with changing screw speed.

Initially, the feeding performance was evaluated with the feeder running volumetrically. This allowed for quick comparison without the added complexity of the gravimetric controller. If the gravimetric controller is improperly tuned, the feeding performance can be made worse, but normally the gravimetric control will only improve the feeding performance over what is achieved by operating the feeder volumetrically. It was found

that the relative standard deviation (RSD) of the feedrate was strongly correlated with the screw speed. Lower or better RSDs were achieved with higher screw speeds. Furthermore, the relationship between RSD to flight passes (which is directly dependent on screw speed) of the screws accounted for the differences in RSD that were observed between the single screw and twin screw feeders. The twin screw feeder tended to have better RSDs for slower screw speeds, but when translated into flight passes they were found to be mostly equivalent due to the multiple flight passes the twin screw feeder had per revolution.

After volumetric testing, gravimetric testing was completed and served as confirmation of the performance that was observed in the volumetric testing. The trials with gravimetric control are indicative of how the feeders would behave in a manufacturing process. The similarity of the materials proved to have minimal consequence on the feeder performance, but instead the most significant effect on feeding performance was found to be caused by the tooling configurations of the feeder. If the powders' flow behaviors were more different then there may have been a different conclusion.

On the other hand, the effect the feeders had on the powders themselves was significantly different for the two powders examined here. The shear sensitivity of the Norzinco zinc oxide powder was clearly evident by the changes in feeding configuration. Grillo powder exibited no visible changes and only minimal measurable changes. For the testing with the Freeman Technology FT4 device, the dynamic flow measurements were the most effective in distinguishing both the grade of powder and the treatment effects. Compressibility was able to distinguish between treatment, but not grade of powder, because the two grades had very similar changes in compressibility.

Selection of powder grade would largely depend on the acceptable change in the downstream processes as well as a cost evaluation, which was not a part of this study. On a material stability and robustness point of view, the Grillo material would likely be less problematic as the physical changes to the powder were minimal.

4.7 Figures for Chapter 4

Figure 4.1: *Visual inspection of Norzico CF8 material after spontaneous aggregation caused by tumbling in a rotating drum.*

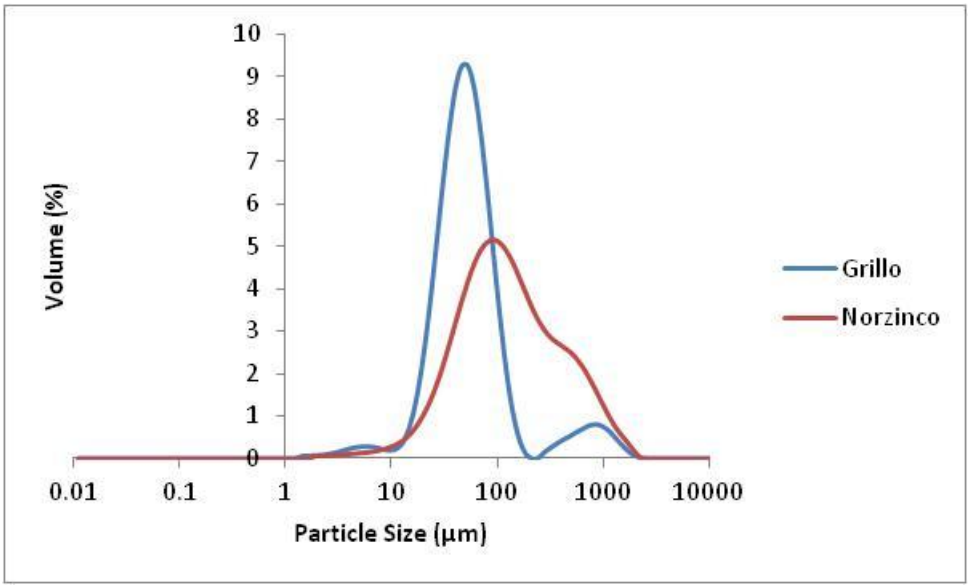

Figure 4.2: *Particle size distribution for Grillo Pharma8 and Norzinco CF8 Zinc Oxides as measured by a Malvern Mastersizer 2000.*

a.  b.  c. 

Figure 4.3: a.) KTron KT35 feeder with Schenck Accurate AccPro II catch scale. KTron KT35 feeder tooling consists of b.) 4 sets of twin screws: fine concave screw (FCS), coarse concave screw (CCS), fine auger screw (FAS), and coarse auger screw (CAS). c.) There are two screens: fine square screen (FSqS) and coarse square screen (CSqS). The feeder can also be run without a screen (NoS).

Figure 4.4: a.) Side-view of the Gericke GLD87 feeder; b.) Front view of the GLD87 with the faceplate and nozzle removed for a visual of the screw and agitator internal arrangement; c.) Various screws for the GLD87: Size 2 (Helix & Auger), Size 3 (Helix & Auger), and Size 4 (Helix & Auger); d.) Common agitator blade (top left), screw specific agitator blades (top right) and the combined agitator assembly (bottom)

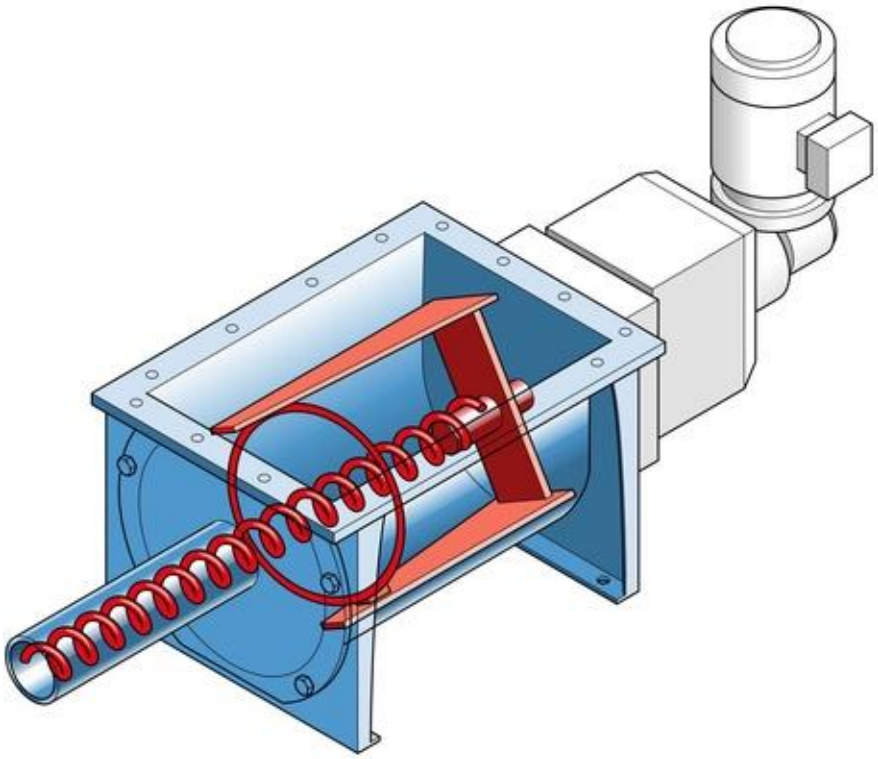

Figure 4.5: Gericke GAC232 screw and agitator setup.

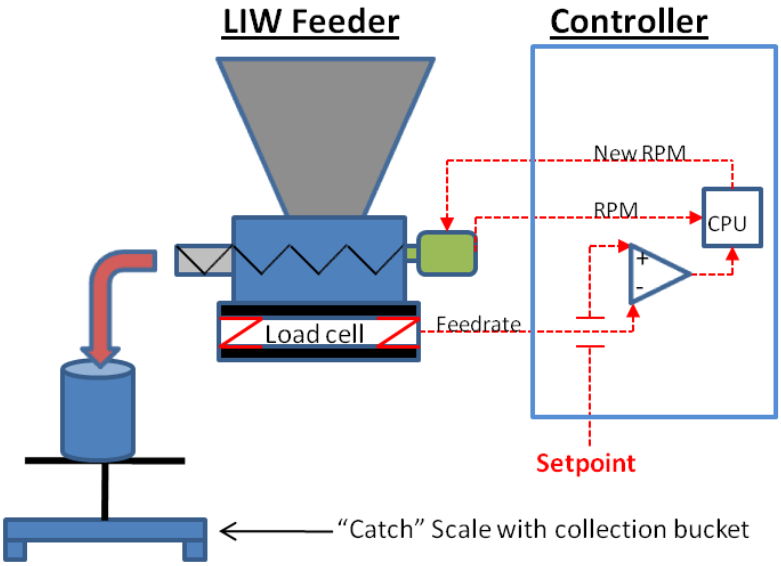

Figure 4.6: Loss-in-weight feeder characterization setup for monitoring feedrate and determining steady state performance.

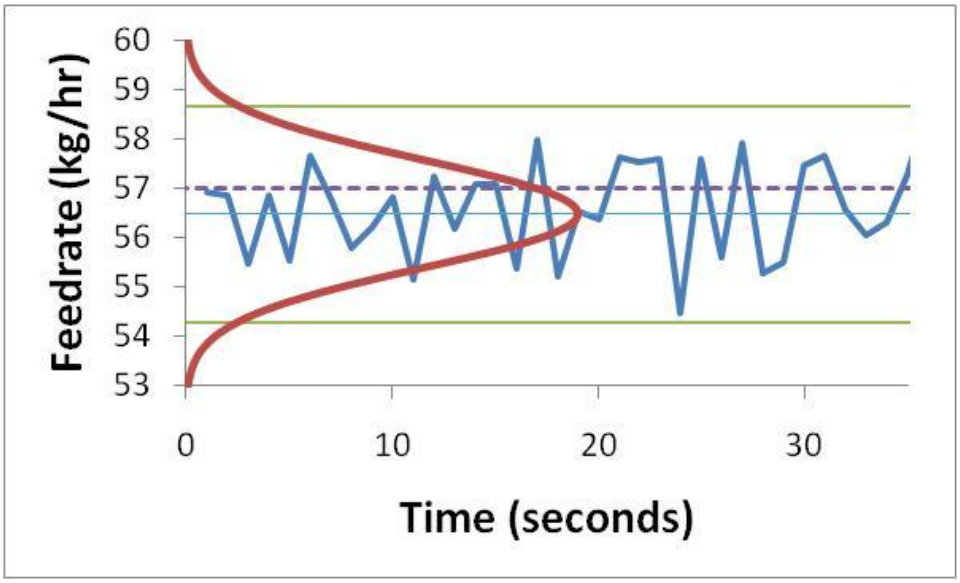

Figure 4.7: Sample catch scale data (Blue) with its normal fitted distribution (Red). Also marked with a horizontal line is the mean value (Light Blue), the setpoint (Purple), and the 2σ interval around the mean (Green).

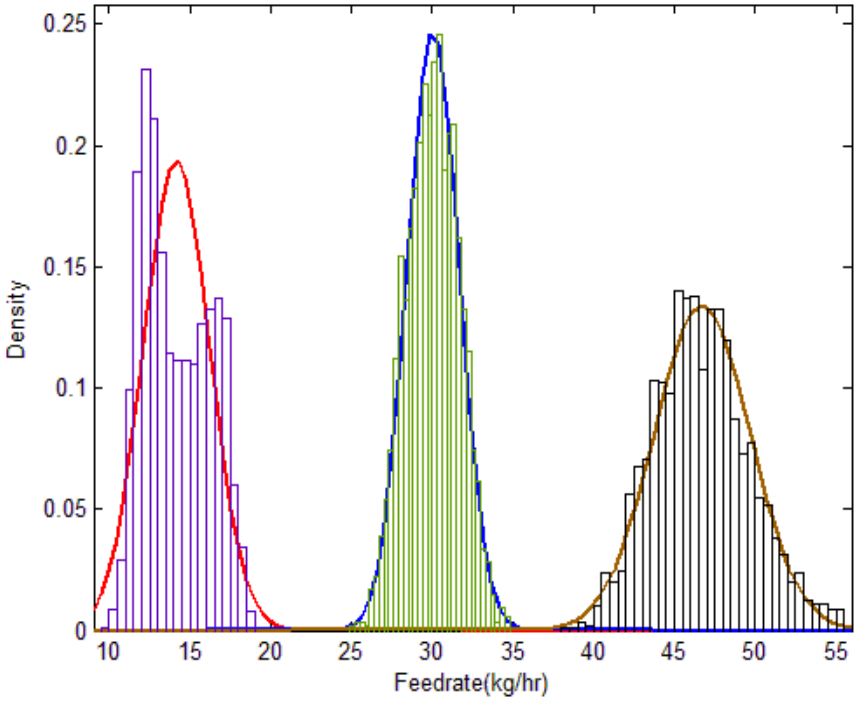

Figure 4.8: Probability distribution functions (PDF) and Gaussian fit approximations for the Gericke GLD87 feeding Norizinco powder with a size 3 helical screw for each of the following gravimetric setpoints: 14.2 kg/hr, 30.2 kg/hr, and 46.9 kg/hr. Only the PDF for the 14.2 kg/hr setpoint shows a non-Gaussian distribution.

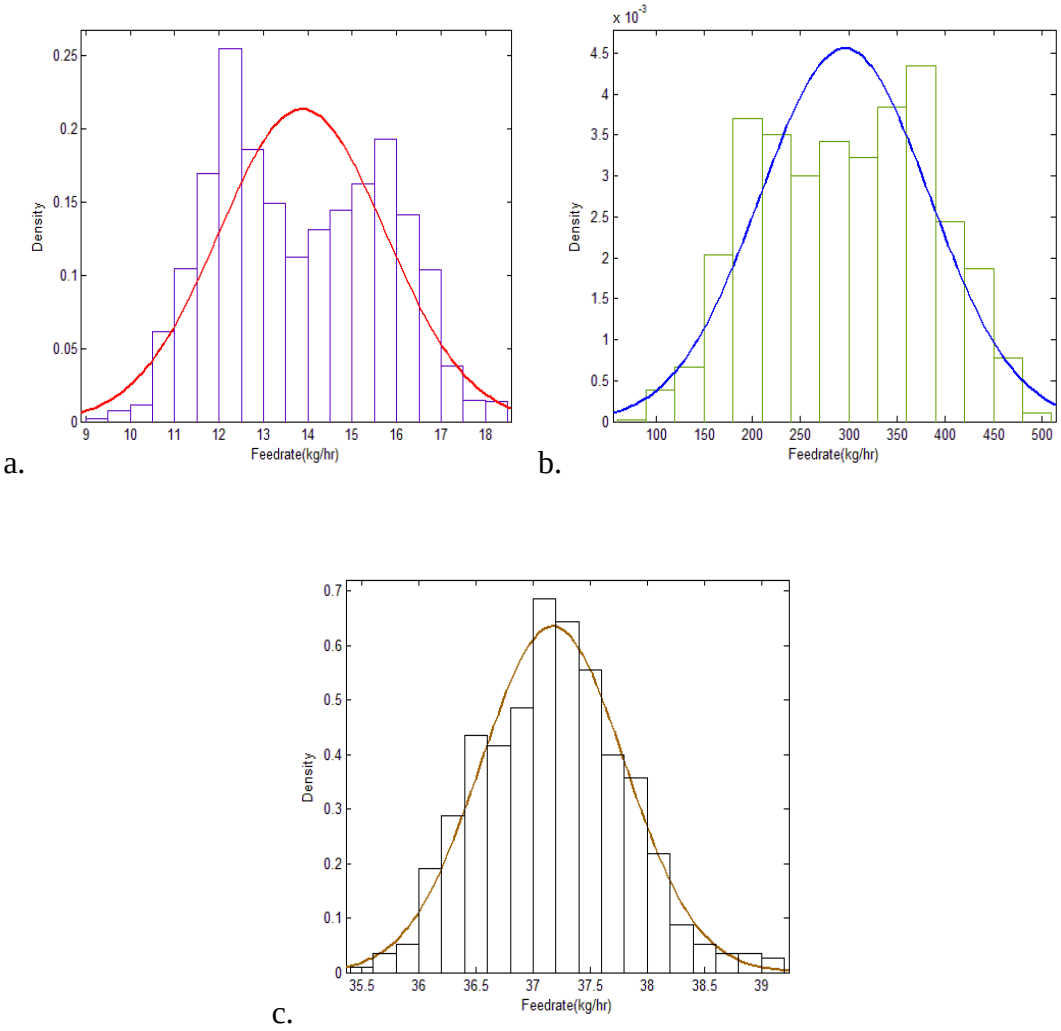

Figure 4.9: Probability distribution functions (PDF) and Gaussian fit approximations for Grillo material fed at ~20% maximum screw speed from a.) Gericke GLD87 with Helix3 screw, b.) Gericke GAC232 with Helix8 screw, and c.) K-Tron KT35 with coarse concave twin-screws.

a.

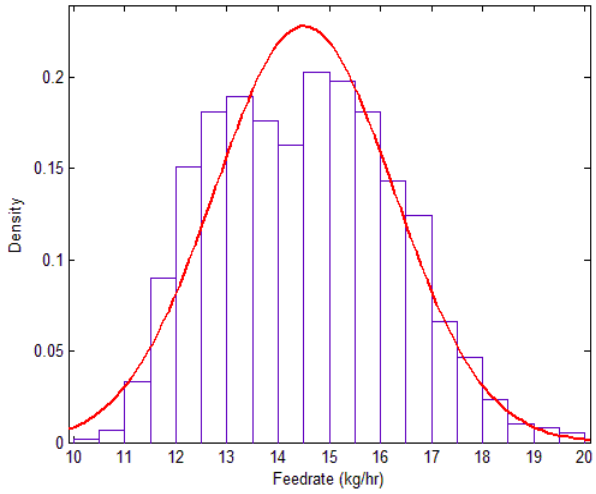

b.

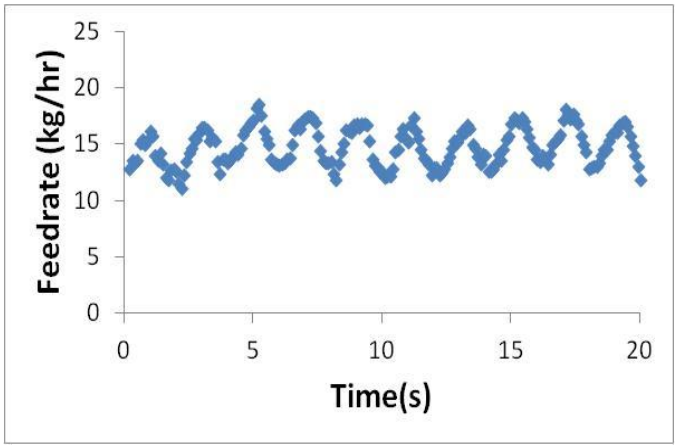

Figure 4.10: a.) Probability distribution function and b.) feedrate time series data generated from the results for the K-Tron KT35 with fine auger screw volumetrically feeding Grillo zinc oxide powder at 10% of the maximum screw speed.

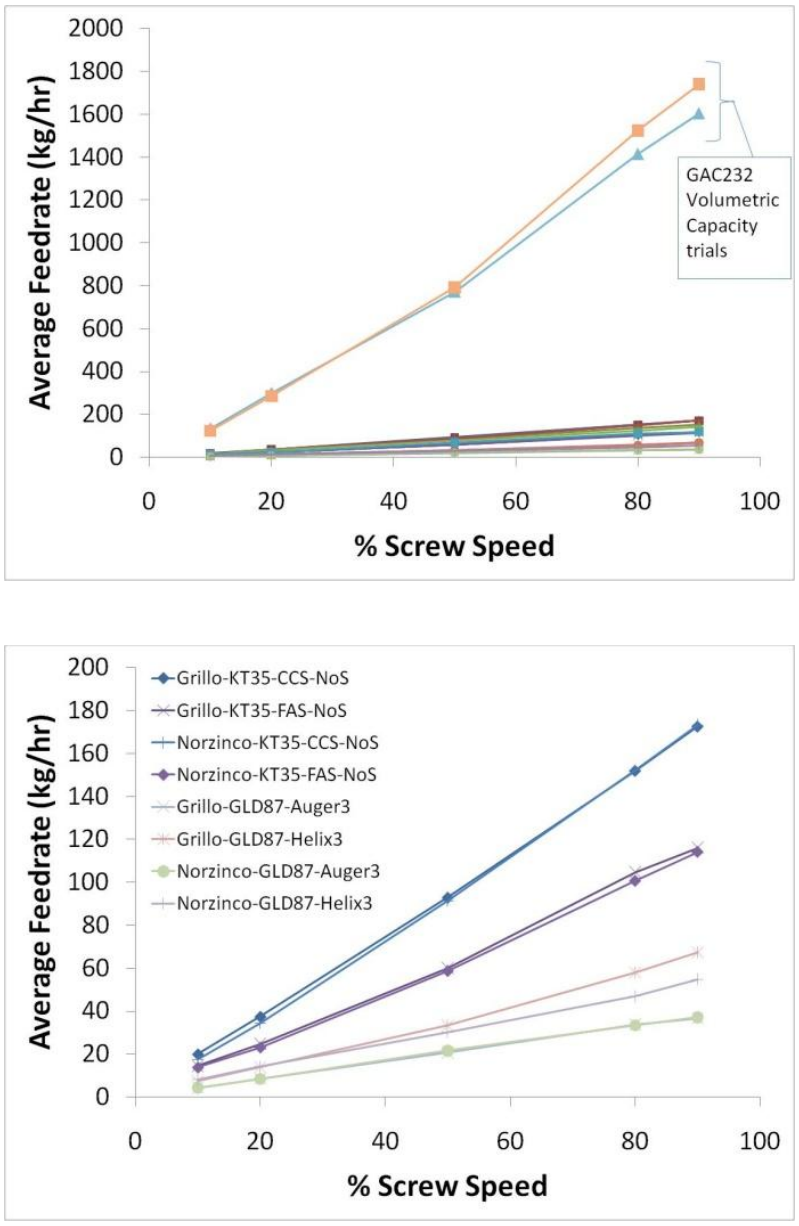

Figure 4.11: Sampling of the volumetric capacity plots (Average Feedrate versus % Screw Speed) for the Gericke GAC232 (left, squares are the Norzinco data and triangles are Grillo data) and Gericke GLD87 & KTron KT35 (on right)

a.

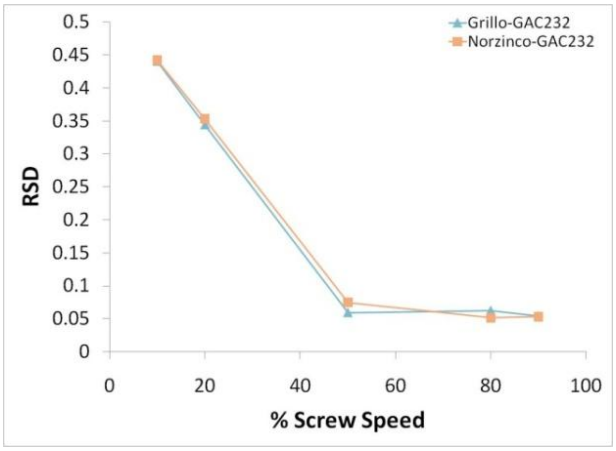

b.

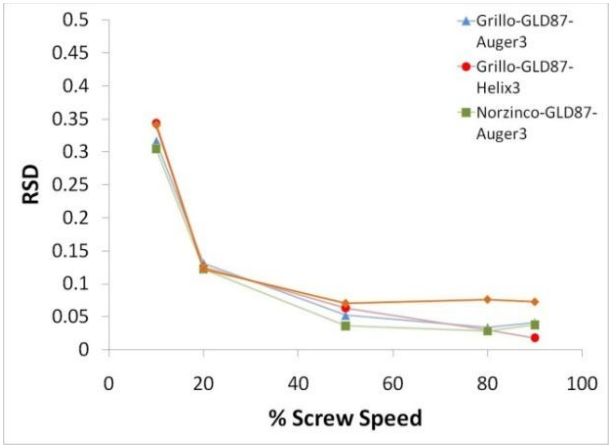

c.

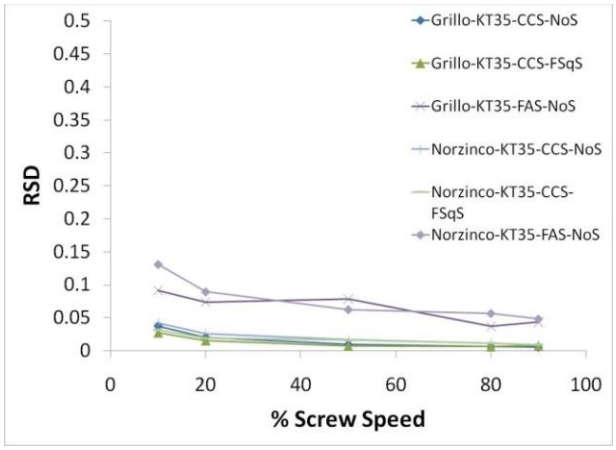

Figure 4.12: Relative standard deviation versus % screw speed for the different combinations of feed tooling and feeders (a. Gericke GAC232, b. Gericke GLD87, c. KTron KT35).

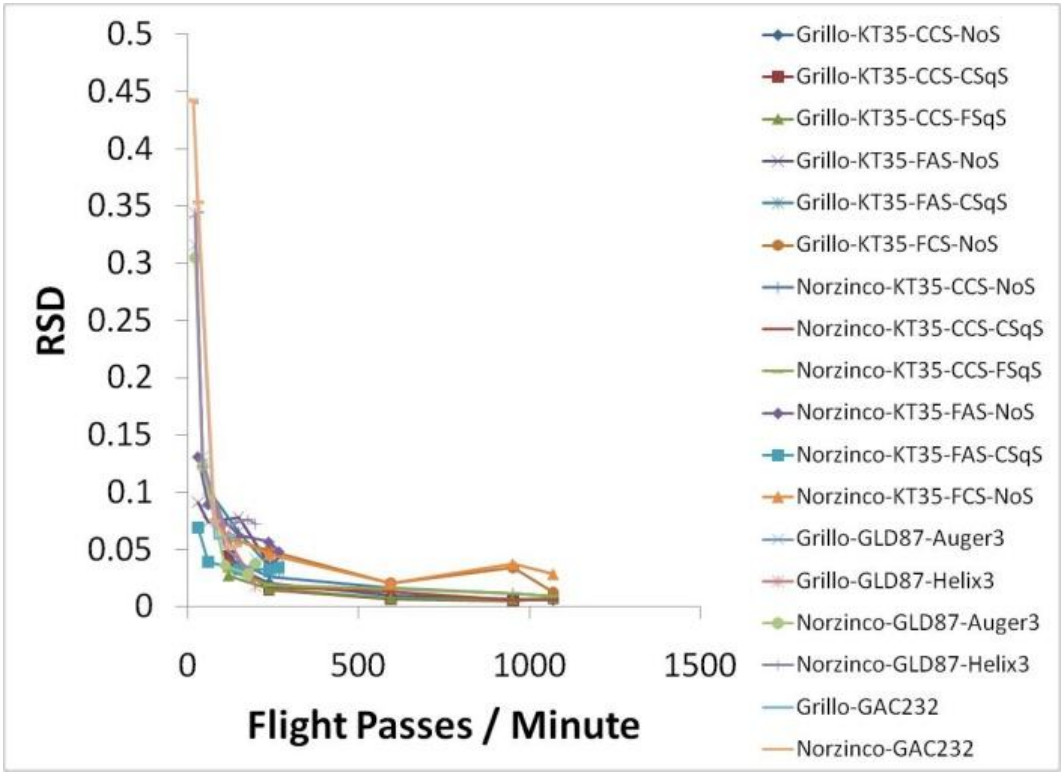

Figure 4.13: Relative standard deviation versus flight passes / minute for the 3 feeders (Gericke GAC232, Gericke GLD87, KTron KT35) feeding the two powders (Grillo Pharma8 and Norzinco CF8) with different combinations of feed tooling.

a.

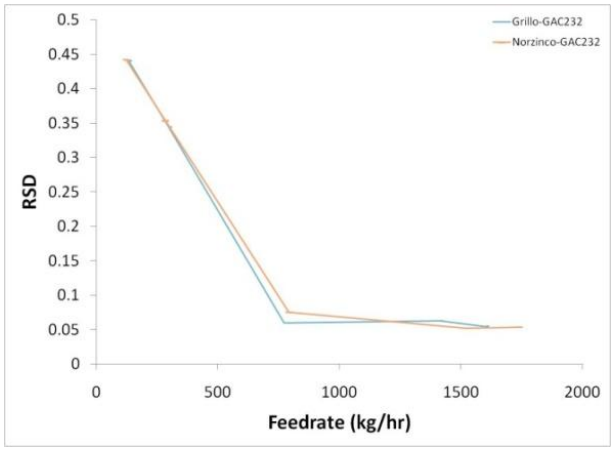

b.

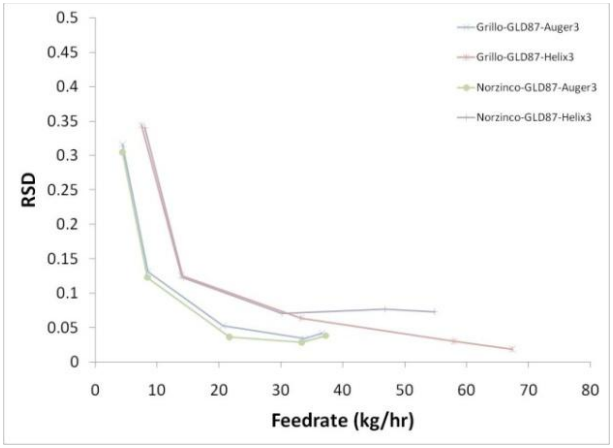

c.

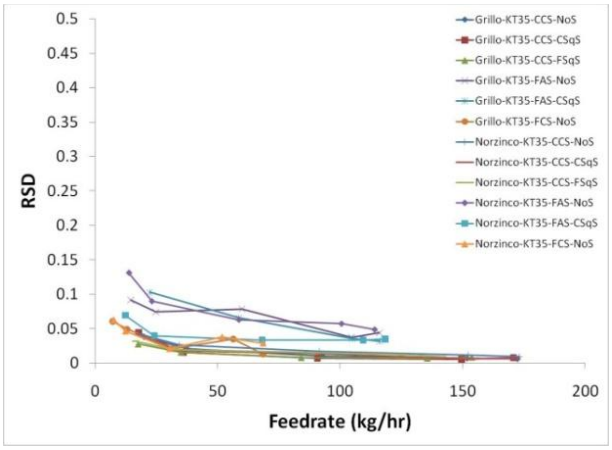

Figure 4.14: Relative standard deviation versus the feedrate for the three feeders (a. Gericke GAC232, b. Gericke GLD87, and c. KTron KT35) feeding the 2 powders (Grillo Pharma8 and Norzinco CF8) with different feed tooling.

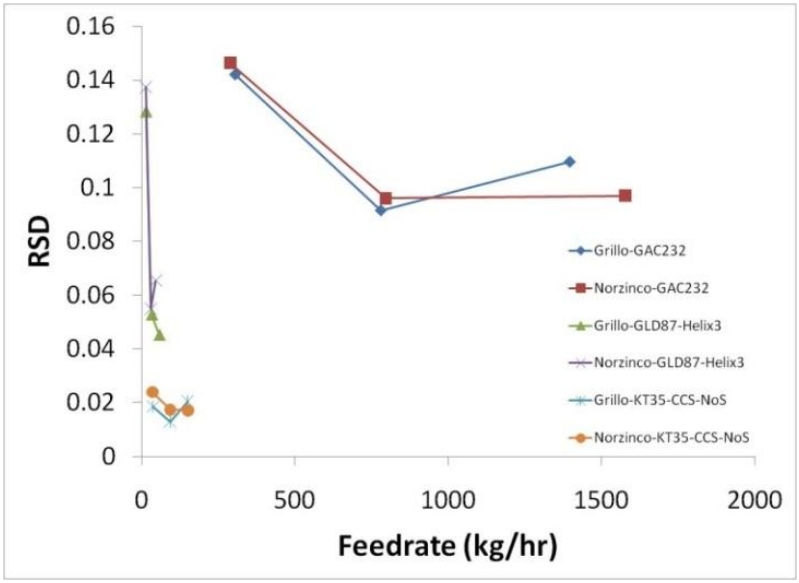

Figure 4.15: The gravimetric performance of the three tested feeders (Gericke GAC232, Gericke GLD87, and KTron KT35).

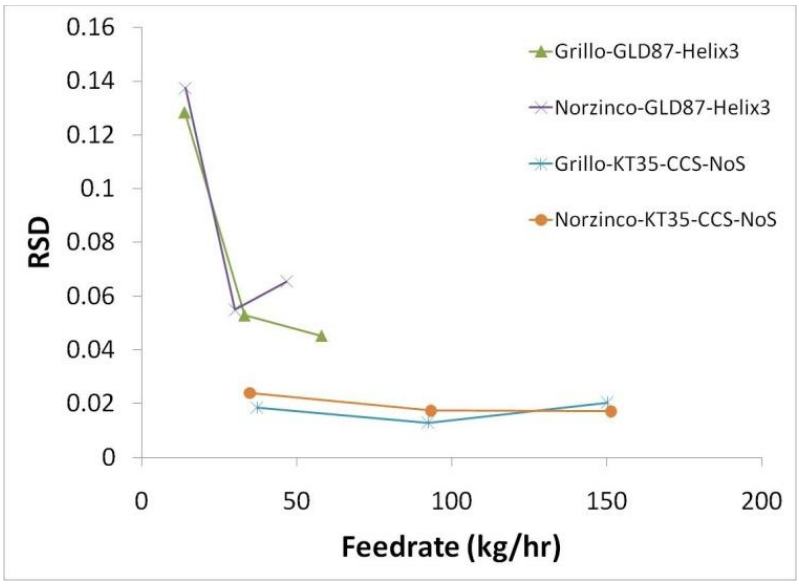

Figure 4.16: The gravimetric performance of the two smaller feeders (Gericke GLD87 and KTron KT35).

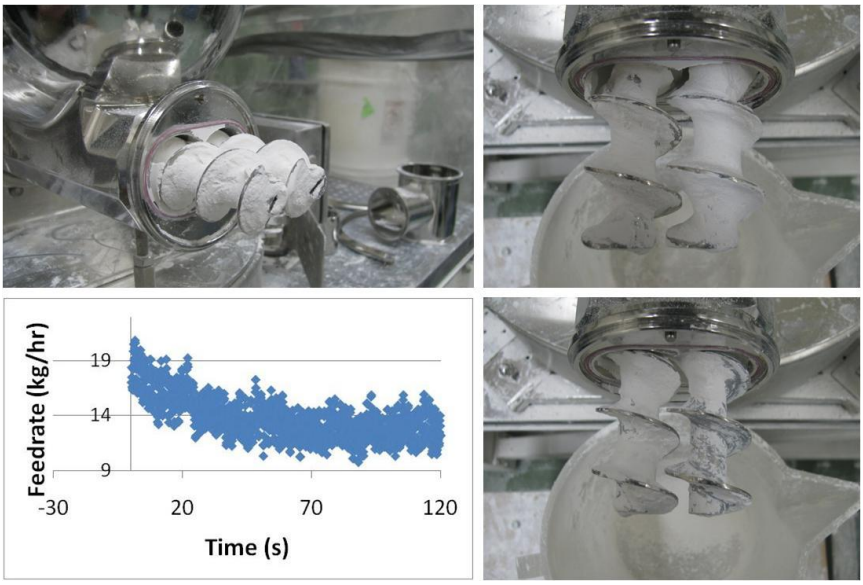

Figure 4.17: KTron KT35's fine auger twin screws become coated with zinc oxide material which reduces the feedrate.

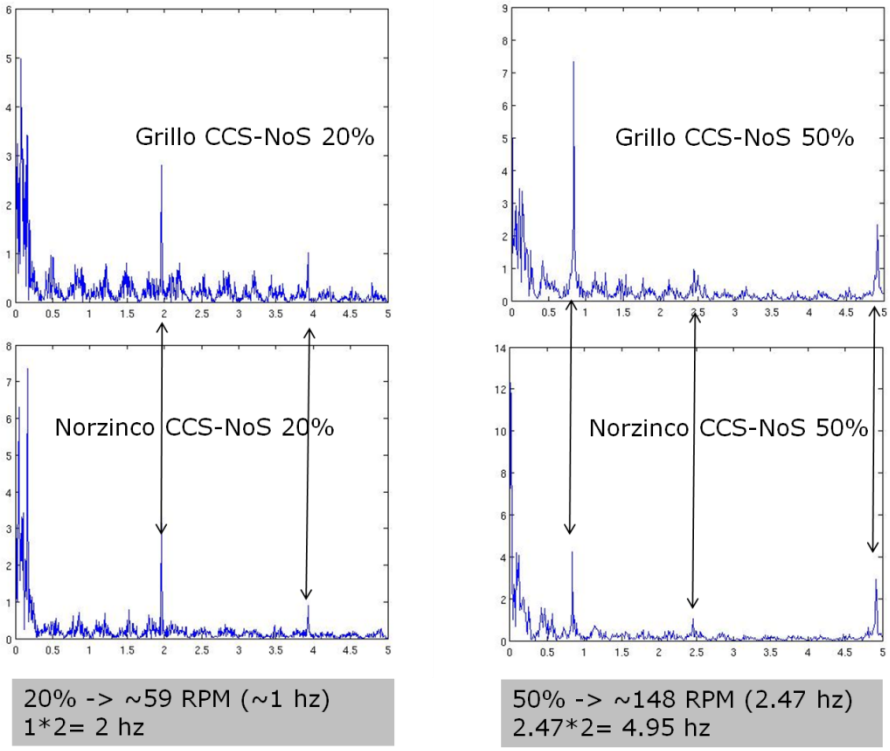

Figure 4.18: Power spectra of feedrate data for the KTron KT35 feeding at 20% and 50% of maximum screw speed with no screen and with coarse concave self-cleaning screws.

Figure 4.19: Samples showing the visual effects of feeding caused by various discharge screen conditions on zinc oxide powders. The top row is the Grillo material and the bottom row is the Norzinco material. From left to right (lowest shear to highest) is the bulk virgin powder, fed without a screen, fed with the coarse square screen, and fed with the fine square screen.

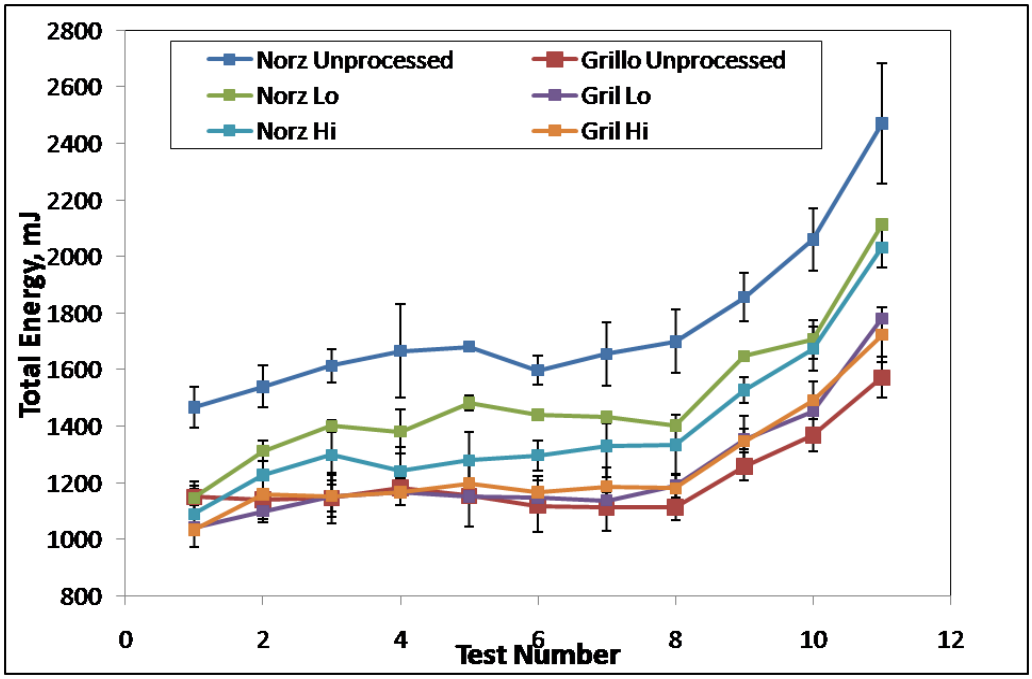

Figure 4.20: Dynamic flow measurements flowability energy profile for stability and variable flow rate testing of bulk, low shear, and high shear feeding of Grillo and Norzinco zinc oxide powders.

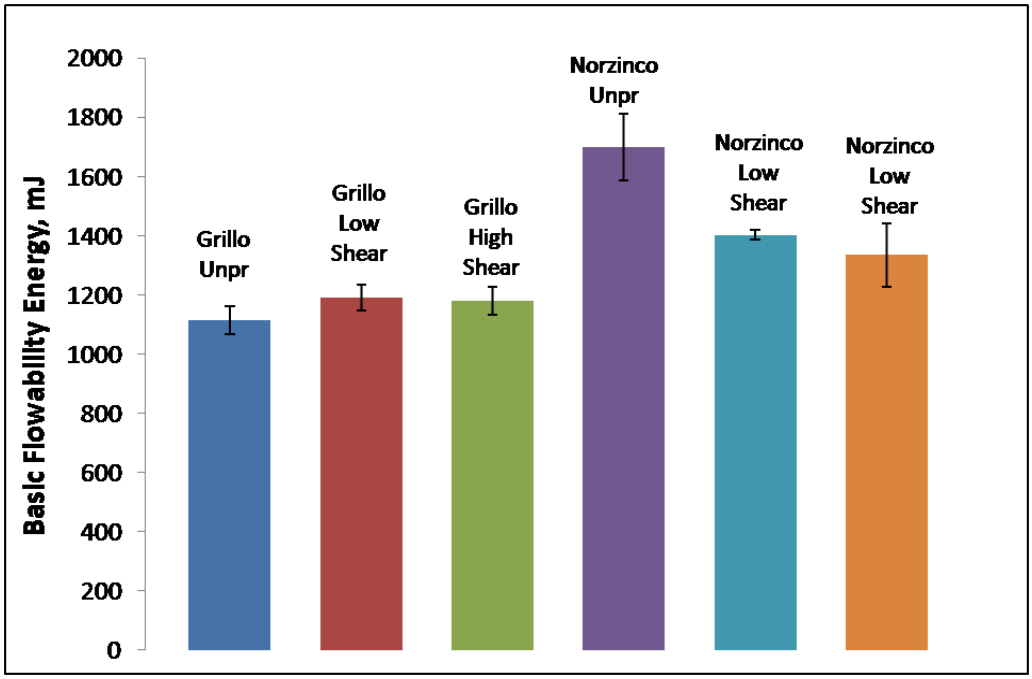

Figure 4.21: Basic Flowability Energy from the dynamic flow measurements stability test of bulk, low shear, and high shear feeding of Grillo and Norzinco zinc oxide powders.

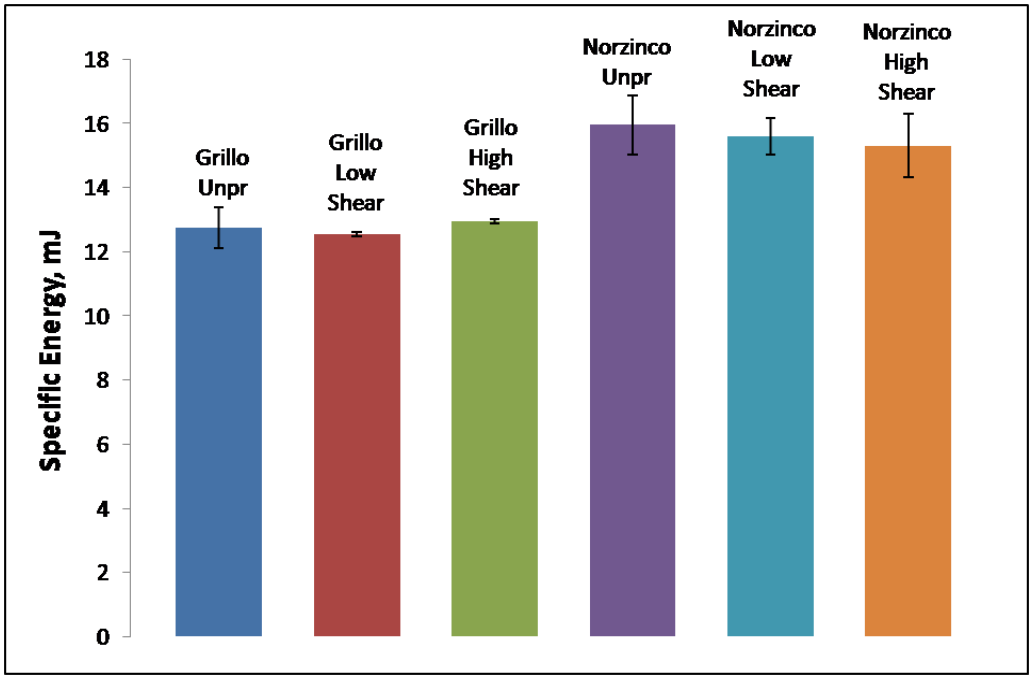

Figure 4.22: Specific Energy from the dynamic flow measurements for bulk, low shear, and high shear feeding of Grillo and Norzinco zinc oxide powders.

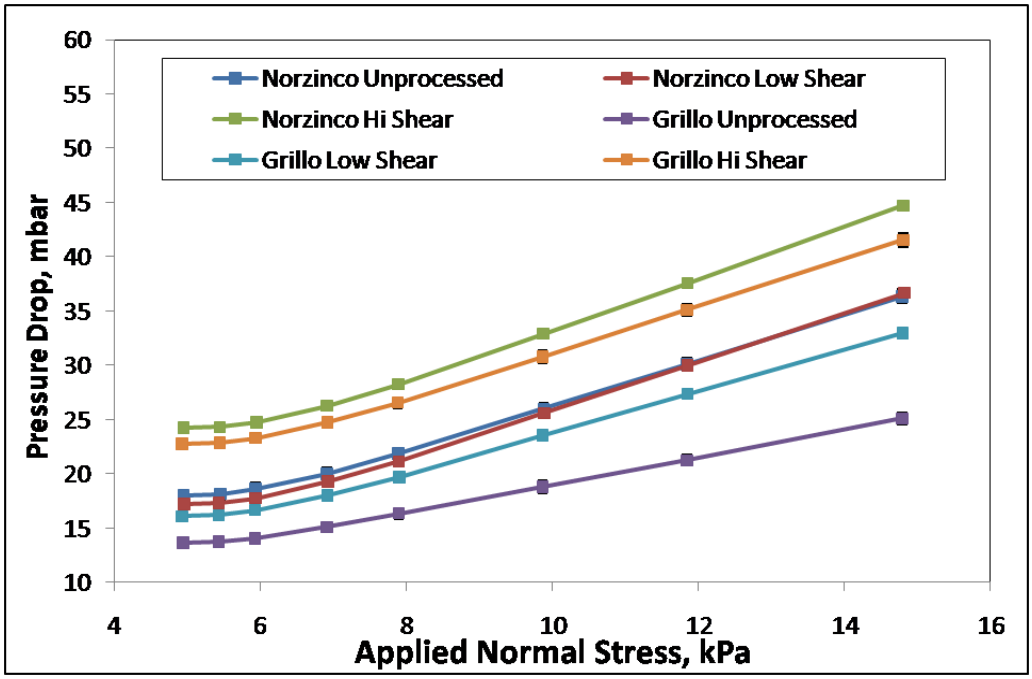

Figure 4.23: Permeability profile for bulk, low shear, and high shear feeding of Grillo and Norzinco zinc oxide powders.

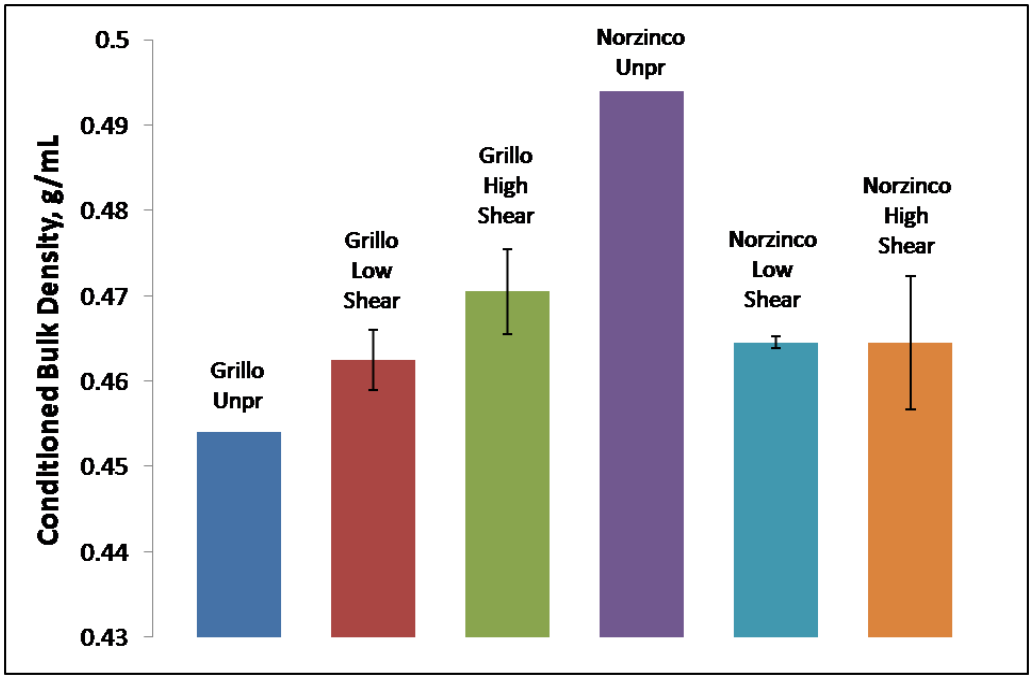

Figure 4.24: Conditioned Bulk Density for bulk, low shear, and high shear feeding of Grillo and Norzinco zinc oxide powders.

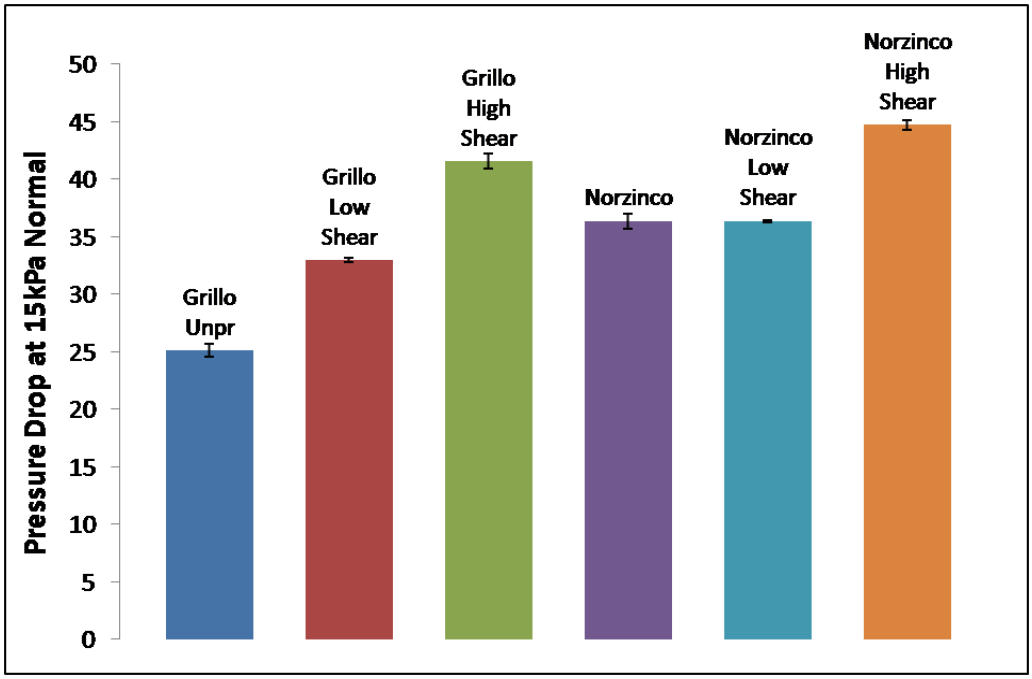

Figure 4.25: Pressure Drop @ 15kPa for bulk, low shear, and high shear feeding of Grillo and Norzinco zinc oxide powders.

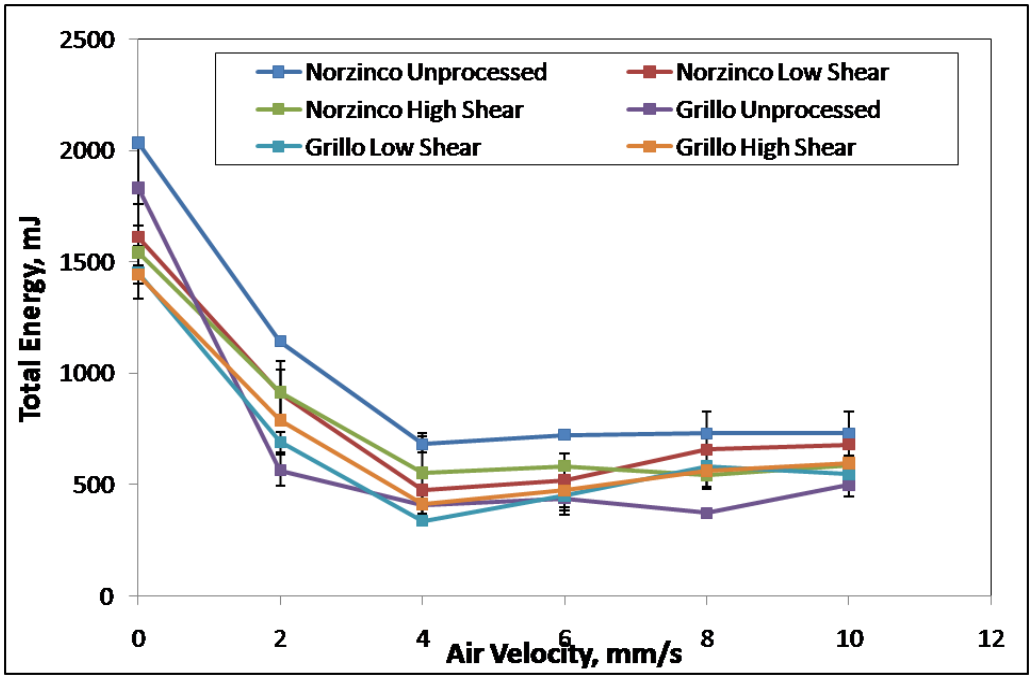

Figure 4.26: Flowability Energy of Aeration for bulk, low shear, and high shear feeding of Grillo and Norzinco zinc oxide powders.

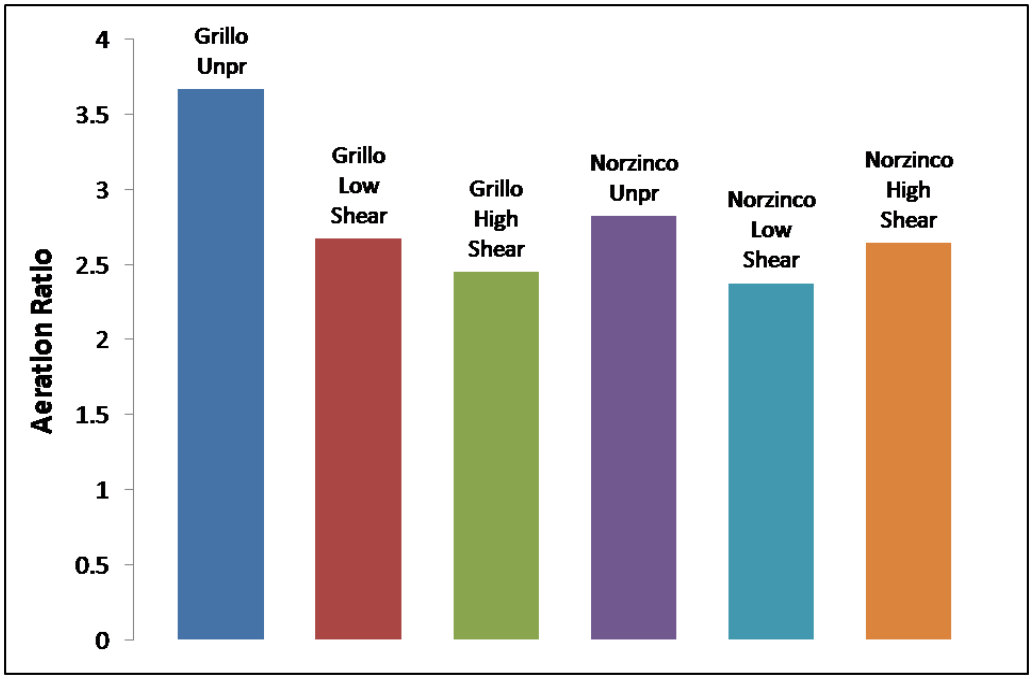

Figure 4.27: Aeration Ratio for bulk, low shear, and high shear feeding of Grillo and Norzinco zinc oxide powders.

a.

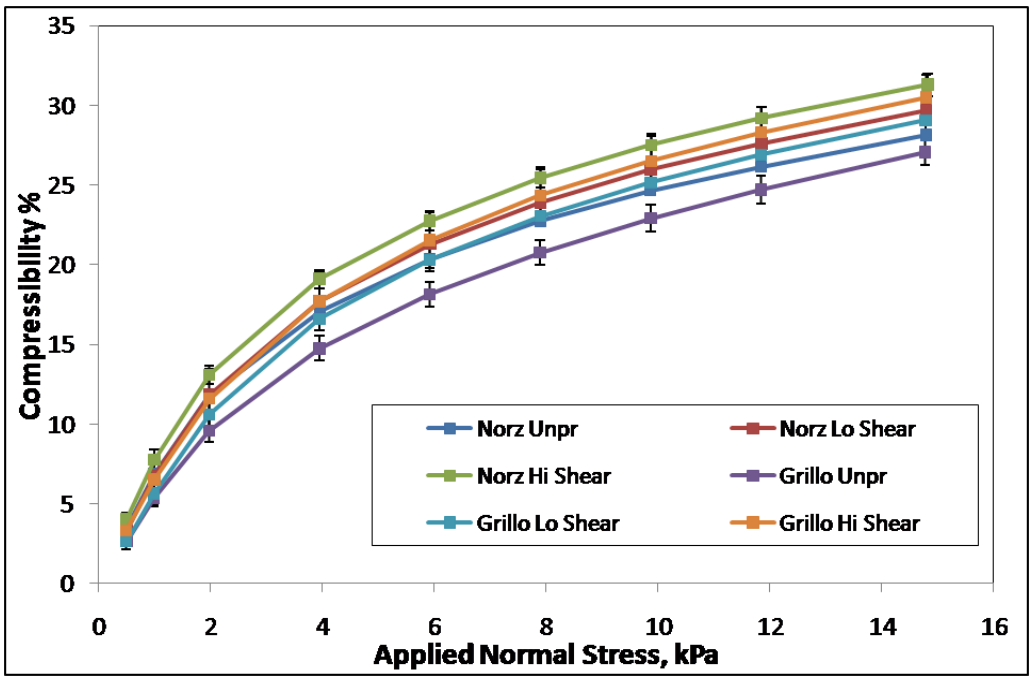

b.

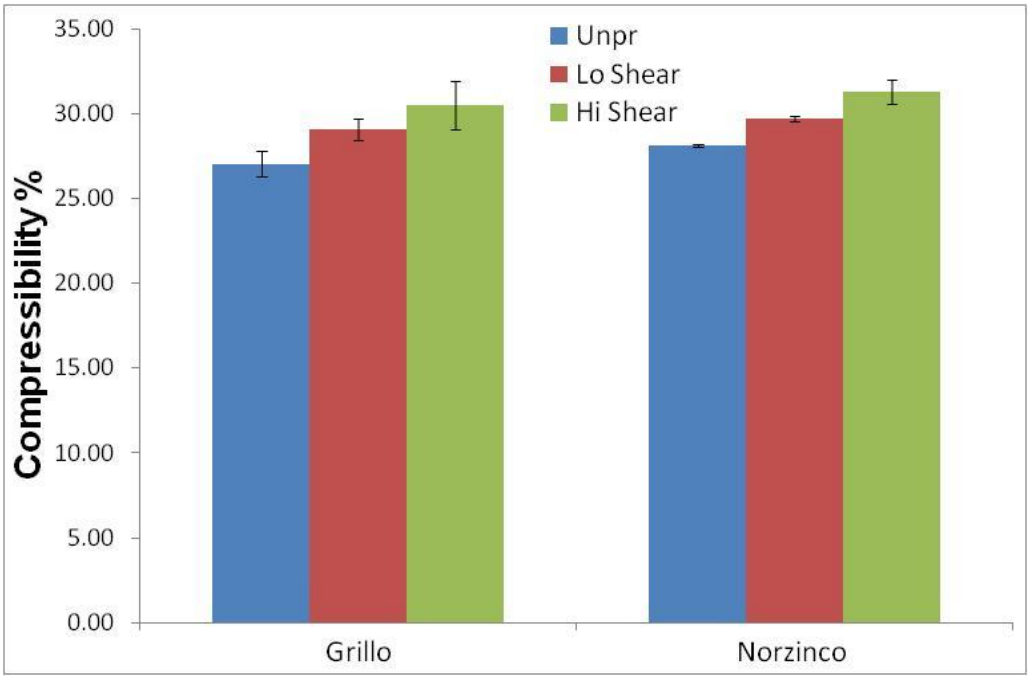

Figure 4.28: Compressibility for bulk, low shear, and high shear feeding of Grillo and Norzinco zinc oxide powders: a) as a function of Normal Stress and b) at 15 kPa Normal Stress.

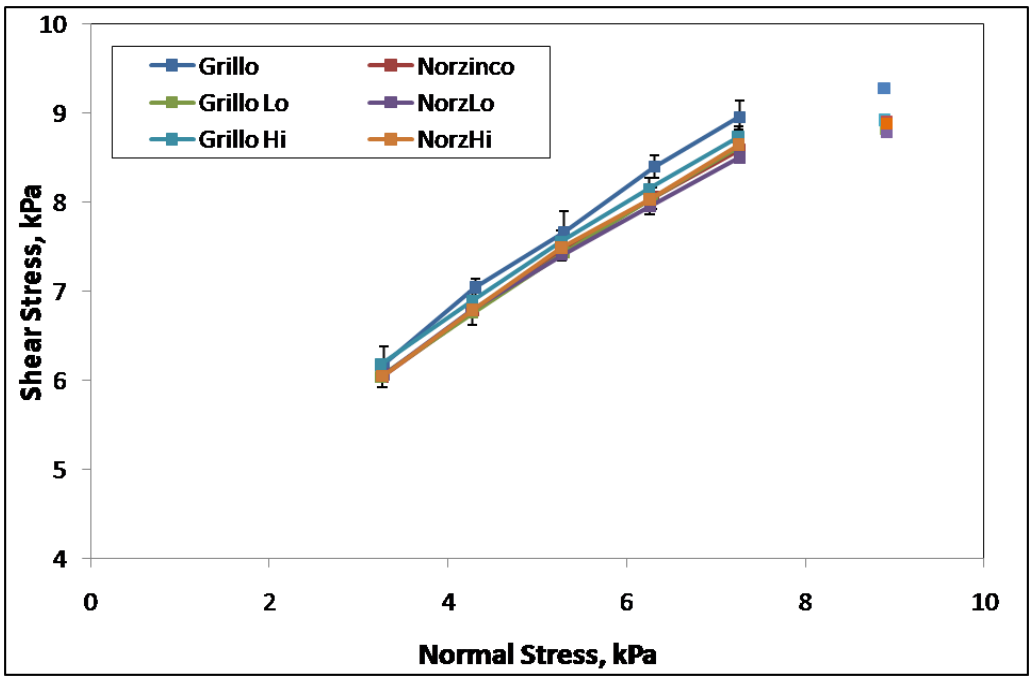

Figure 4.29: Shear Stress for bulk, low shear, and high shear feeding of Grillo and Norzinco zinc oxide powders.

4.8 Tables for Chapter 4

Table 4.1: Composition of materials as specified by the manufacturers

		Norzinco CF8	Grillo Pharma8
ZnO	%	99.9	99.9
Pb	%	0.001	0.002
Cd	%	0.001	0.0005
Cu	%	0.0001	0.0001
Fe	%	0.0005	0.0002
Mn	%	0.00001	0.0001
Cl	%	0.002	0.001
SO3	%	0.002	0.002
moisture*	%	0.2	0.25

Table 4.2: Linear fit for volumetric capacity feeder trials for Grillo Pharma8

KTron KT35

Screw	CCS	CCS	CCS	FAS	FAS	FCS
Screen	NoS	CSqS	FSqS	NoS	CSqS	NoS
Slope	1.902	1.283	0.720	1.873	1.272	1.702
Rsq	0.9999	0.9991	0.9963	0.9997	0.9937	0.9999
p	5.82E-09	2.91E-07	5.18E-06	2.57E-08	1.48E-05	1.40E-09

Gericke GLD87

Screw	Auger3	Helix3
Slope	0.415	0.727
Rsq	0.9997	0.9985
p	4.40E-08	8.00E-07

Gericke GAC232

Screw	Helix 8
Slope	17.332
Rsq	0.9971
p	3.24E-06

Table 4.3: Linear fits for volumetric capacity feeder trials for Norzinco CF8

KTron KT35

Screw	CCS	CCS	CCS	FAS	FAS	FCS
Screen	NoS	CSqS	FSqS	NoS	CSqS	NoS
Slope	1.898	1.249	0.695	1.876	1.339	1.568
Rsq	0.9995	0.9992	0.9916	0.9990	0.9994	0.9999
p	9.55E-08	2.54E-07	2.65E-05	3.67E-07	1.30E-07	6.67E-09

Gericke GLD87

Screw	Auger3	Helix3
Slope	0.418	0.603
Rsq	0.9997	0.9983
p	2.88E-08	1.08E-06

Gericke GAC232

Screw	Helix 8
Slope	18.571
Rsq	0.9941
p	1.32E-05

Table 4.4: Freeman Tech FT4 results

	Grillo						Norzinco					
	Unprocessed		Low Shear		High Shear		Unprocessed		Low Shear		High Shear	
Measurements	Value	±RSD(%)	Value	±RSD(%)	Value	±RSD(%)	Value	±RSD(%)	Value	±RSD(%)	Value	±RSD(%)
Basic Flowability Energy, BFE (mJ)	1111.50	7.32	1137.00	2.49	1187.00	5.72	1656.00	6.75	1432.00	1.48	1329.50	8.35
Stability Index, SI	0.97	4.83	1.10	1.10	1.15	3.69	1.13	1.89	1.25	2.26	1.22	2.32
Flow Rate Index, FRI	1.41	0.00	1.50	2.83	1.46	1.94	1.45	1.95	1.51	0.47	1.53	4.62
Specific Energy, SE (mJ/g)	12.75	4.99	12.55	0.56	12.95	0.55	15.95	5.76	15.60	3.63	15.30	6.47
Conditioned Bulk Density, CBD (g/ml)	0.45	0.00	0.46	0.76	0.47	1.05	0.49	0.00	0.47	0.15	0.47	1.67
Aerated Energy, AE_{10}	499.00	10.49	544.50	8.18	595.00	13.79	728.00	13.40	678.50	0.31	584.50	5.44
Aerated Energy, AE_{20}	563.00	12.56	689.50	6.67	788.00	1.79	1142.50	1.05	910.50	11.26	914.50	15.08
Aeration Ratio, AR_{10}	3.67	1.03	2.67	0.00	2.45	13.17	2.82	14.54	2.37	9.49	2.65	13.17
Pressure Drop, PD_{15} (mbar)	25.10	2.25	32.95	0.64	41.55	1.53	36.35	1.75	36.65	0.19	44.70	0.95
Compressibility, CPS_{15} (%)	27.05	2.88	29.05	2.19	30.50	4.64	28.15	0.25	29.70	0.48	31.30	2.26
Shear Stress, $\tau_{7.9}$ (kPa)	8.34	2.03	8.19	0.95	8.22	0.26	8.30	2.90	8.14	2.69	8.33	1.44
Shear Stress, $\tau_{3.9}$ (kPa)	6.48	3.49	6.30	5.28	6.61	2.46	6.18	5.72	6.34	0.33	6.36	6.23

Chapter 5. FEEDRATE DEVIATIONS CAUSED BY HOPPER REFILL OF LOSS-IN-WEIGHT FEEDERS

5.1 Summary

A gravimetric feeder does not monitor and control the feedrate during hopper refill, which often results in deviations from setpoint. This refill problem is a known issue to feeder manufacturers, and they have developed many methods to attempt to address it, including: refill modes that have a variable screw speed during refill [34], redundant refill [35] and/or feeder systems [36] that try to bypass the issues.

All the methods or systems mentioned above may work to reduce or eliminate the issue. However, these patented techniques do not always eliminate the problem and often involve purchasing extra equipment. The work discussed in this chapter focuses on using pre-commissioning testing to observe the effects and issues during refill as well as developing a method for quantifying the effects so that it can be used for optimizing refill scheduling. By using a gain-in-weight catch scale, which collects and weighs material as it is fed, deviations from the feed setpoint can be monitored during hopper refill even when the internal feeder loadcell is not reliable. It has been observed that size of refill has a significant impact on feeder consistency and performance.

5.2 Equipment

5.2.1 Loss-in-Weight Feeders

During normal gravimetric control, a loss-in-weight feeder compensates for changes in powder densityby directly regulating the mass feedrate. [4] Using the difference in

weight measured by the platform divided by time, the controller can determine the instantaneous feedrate:

$$\left(\frac{\Delta w_{feeder}}{\Delta t}\right) = -\dot{m}_{feed} \tag{5-1}$$

This feedrate is compared to the desired setpoint by the controller which adjusts the speed of the screw in order to maintain the feedrate setpoint. However, this equation is not true when the feeder undergoes hopper replenishment.

5.2.1.1 Operation during hopper refill

Eventually, as the hopper empties the powder needs to be replenished. See Figure 5.2. In order to maintain continuity of operation, the hopper is refilled while the feeder is operating. During refill the feeder must be switch to non-gravimetric operation where screw speed is instead controlled volumetrically. The reason for the switch in operation mode is because the change in weight with time during refill includes the mass flow of material refilling the feeder, $\dot{m}_{refill}$, in addition to the mass being fed from the feeder, $\dot{m}_{feed}$. The instantaneous rate of change of mass as observed by the feeder's loadcells during refill is represented by the following equation:

$$\left(\frac{\Delta w_{feeder}}{\Delta t}\right)_{refill} = \dot{m}_{refill} - \dot{m}_{feed} \tag{5-2}$$

This indicates that there are two unknown mass flows, whereas there is only one measurement. The net hopper weight measured by the feeder's internal loadcell confounds the two feed streams. To distinguish the feedrate for each of these varying streams would require more information about one of the streams. Hence, the feeder

must operate in volumetric mode, which leads to feedrate inconsistencies, in particular as the feeder is refilled and flight filling varies due to an increase in the weight of the powder above the screws.

5.2.1.2 Gericke GAC232 feeder and Gericke RA bin discharger

The Gericke GAC232 is the larger feeder tested in this study. It is a single screw feeder that has an agitator that rotates around the dispensing screw. There are interchangeable screws and nozzles, which allow for a large operating range of 1.3 to 27,000 liters / hour. The screw size tested for this feeder was a metering tool size 8 helix, which has a feeding rate range of 160 to 3,200 liters / hr. The maximum rotation rate of the screw is 157 RPM with the operating range of 32 to 126 RPM (20 to 80% of the maximum). For the refill testing of this feeder, the gravimetric setpoint was 840 kg/hr.

A Gericke type RA bin discharger was used for automatic refill of the large Gericke GAC232 feeder (See Figure 5.3). The bin discharger has an agitator on the bottom with a manually adjustable compressed air gate valve, which can open and close to allow the material in the agitated bin to replenish the feeder mounted below. When the level of powder in the feeder is depleted to the point where a refill was required, the feeder enters refill mode (not gravimetrically controlled). At the beginning of the refill mode, the feeder triggers the gate valve of the bin discharger to open, allowing material to enter the feeder's hopper. When the feeder reaches the pre-set maximum fill level, the signal requesting refill ceases. The refill system is then closed. After a short settling time, the feeder returns to gravimetric operation.

5.2.1.3 K-Tron KT35 twin screw feeder

The K-Tron KT35 twin screw loss-in-weight feeder's design is described in detail in Chapter 2. Testing with the KTron KT35 feeder was completed with manual refilling, using a conical hopper placed above the feeder that would discharge a premeasured refill into the feeder's hopper. Similar to automatic refill, the feeder is operated in gravimetric mode until its hopper empties to the pre-set minimum level. At this point, the feeder enters refill mode and requests refill. At that time, an operator needs to manually add the premeasured charge of material. After the manual refill, the level of material in the hopper rises above the preconfigured refill stop level, causing the feeder to return to gravimetric control. A pre-set wait period before returning to gravimetric control includes a settling time, allowing for vibrations caused by the operator's refilling action to dissipate, thereby avoiding disturbances to the feeder's built-in loadcell.

5.2.1.4 K-Tron KT20 twin screw feeder

The K-Tron KT20 twin screw loss-in-weight feeder's design consists of a twin-shaft feeder mounted on a weigh bridge. It functions identical to the K-Tron KT35 except it has a smaller diameter of screws, 20mm instead of 35mm. At the maximum speed, the screw rate is 154 RPM (170 RPM @ 110% is also achievable by over-speeding).

Refilling with this feeder was examined using two different automatic refilling systems: a vacuum refilling apparatus or the K-Tron KT35 operating in volumetric mode. The vacuum refilling system (See Figure 5.4) was calibrated to fill with a specific amount of material. When a refill was requested, the K-Tron KT20 triggered the butterfly valve to open, releasing the charge of material in the vacuum refilling system, which would occur suddenly and rapidly. The K-Tron KT35 served as a more rate controlled refilling

system with the K-Tron KT20 requesting a refill from the KT35, which instructed the KT35 to dispense material volumetrically at ~400 kg/hr until the hopper of the KT20 was filled.

5.2.2 Catch Scale

5.2.2.1 Schenck Accurate AccPro II

For characterization of the KTron KT35 feeder's performance, a Schenck Accurate AccPro II was used as a catch scale. As mentioned in previous chapters, AccPro II uses a PC Excel program that obtains weight readings from a 7 kg strain gage loadcell through the Schenck DISOBOX summing box. The DISOBOX uses a 24 bit Analog Devices A/D converter to obtain the weight readings every 0.1 seconds. These readings are obtained and stored by the AccPro II application.

5.2.2.2 Mettler Toledo scales

For the large Gericke GAC232 a Mettler WMHC600 was used as the catch scale. The Mettler WMH scales are platform scales that communicate via RS232/422 to a Labview program which monitors the load cell every 1 second for a maximum of 15 minutes.

5.3 Methods

5.3.1 Catch Scale "Gain-in-Weight" Method

To measure the output flow of the feeder, a bucket on a catch scale was used to collect the fed material. A catch scale was needed because the internal load cell measurement is not a reliable measurement during refill. Although the catch scale software includes built-in data analysis that runs in real time, only the raw mass readings are used for post-processing and analysis. By using a gain-in-weight catch scale, which collects and

weighs material as it is fed, the feedrate can be monitored during refill. The instantaneous change in rate of mass observed by the catchscale is represented by the following equation:

$$\left(\frac{\Delta w_{catchscale}}{\Delta t}\right) = \left(\frac{\Delta w_{catchscale}}{\Delta t}\right)_{refill} = \dot{m}_{feed} \qquad (5\text{-}3)$$

The mass feedrate, $\dot{m}_{feed}$, is perceived by the catch scale as gain-in-weight, which is similar to loss-in-weight, but has the opposite sign. The catch scale is only dependent on the feed stream from the feeder and is completely independent from the refill stream, unlike the internal loadcell of the feeder. This lack of dependence on the refill stream means this equation is the same regardless of whether the feeder is operating in gravimetric or volumetric (for refill) mode.

The catch scale experimental setup is shown in Figure 5.5. This setup is similar to the one described in detail in Chapter 2 [61] which investigated steady state feeding. The primary difference between this experimental setup and the one in Chapter 2 is the refilling prehopper above the feeder, although the purpose of the catch scale is the same, which is to measure the feeding performance independent of the internal load cell of the feeder.

Refill scheduling was investigated for three different hopper replenishment amounts. When the material depleted to the predefined lower hopper fill level, the feeder was refilled up to 80%. The examined lower hopper fill levels were: 20, 40, and 60% of the maximum. To prevent overfilling, the upper fill level was set to 80%, which allows extra headroom to accomodate for powder that may be in freefall or a highly aerated state. The

feeders are programmed to wait a short configurable delay before returning to gravimetric control, to enable freefalling powder to settle, vibrations to dampen out, and other disturbances immediately follow material replenishment to die out.

For the feeder refill trials described above, the gravimetric setpoint of the feeder was set to approximately 50% of the maximum capacity. Flow variability and setpoint deviation were observed and recorded. The generalized test procedure was as follows:

1. Initially fill the feeder
2. Operate the feeder until lower hopper level is reached
3. Initiate refill while the feeder is operating
4. After refill continue monitoring the feeder collecting feedrate deviations caused by refill and the subsequent baseline performance.

In order to collect data that is representative of the refill process, the feeders were operated for an extended amount of time, which required periodically changing the bucket on the catch scale. Since bucket changing disturbs the measurements of the catch scale, the bucket changes were scheduled during the normal steady state feeding, ensuring feedrate data collected during and immediately after refill was not interrupted.

5.3.2 Fitting Baseline

To evaluate the effects of refill, a baseline for variability in steady operation must first be determined. The baseline is used to determine typical variability observed for normal steady state feeding operation without refill disturbances. The baseline only includes the fluctuations caused by the powder flow properties and the feeder tooling. This enables separate analysis of the deviations caused by refill. As discussed in Chapter 2, baseline

characterization requires eliminating the effects of disturbances in the collected feedrate data such as those caused by machine startup/shutdown, catch scale bucket changes, etc.

The effects of disturbances were rigorously filtered out of the original data set. This data filtering consisted of removing 3 seconds of data before, after, and including any deviations caused by a disturbance, which resulted in a total of 6 seconds in addition to the perceived duration of the disturbance. The 3 seconds before and after allowed adequate time for settling and stabilization. Disturbances can be detected in the data set by setting appropriate bounds that the steady-state feedrate data points should remain within. The feeder is using gravimetric control, which means the feedrate should not be deviating more than 10% from the setpoint. This is a modest set of bounds as the feeder typically controls the feedrate more precisely than 10% deviations. However, these margins will detect significant physical disturbances.

By comparing the distribution of the original unfiltered data with the filtered baseline data it was possible to further optimize the filtering procedure. The initial filtering of an extra 6 seconds in addition to each disturbance resulted in a roughly filtered data set that had an average feedrate representative of the quasi-steady behavior and an approximated standard deviation. The average feedrate and standard deviation of the data set was used as a first pass on the unfiltered data with the bounds of filtering being three standard deviations around the average feedrate. New average and standard deviation values were calculated and reapplied iteratively for filtering until both the average and standard deviation reached a limit and remained unchanged. This filtering method was discussed in further detail in a Chapter 2 [61].

Because the effect of refill is the focus of this Chapter (See Figure 5.6a), the ±3σ-multipass filtering, as described in Chapter 2, is used only on the steady state data (time periods where refill is not taking place) to establish a baseline (See Figure 5.6b). The feedrate data collected during the time periods of refill is not processed by the filter and remains unfiltered, as this filter would remove this important data. Figure 5.6c is a sample of filtered data. Since bucket change times are carefully scheduled in the steady state region, the filtering algorithm removed the deviations caused by bucket changes, leaving only the baseline behavior and refill-caused deviations.

5.3.3 Quantifying Deviation

The variability of the feed rate due to refill can be characterized in multiple ways. In this dissertation, flow rate deviations were quantified by: magnitude of the maximum deviation, time feedrate is away from setpoint, and total deviation of material fed in excess (or in defect) of set point (see Figure 5.7). The best value for quantifying the effect of deviation depends on the application and subsequent unit operations.

If the sensitivity of a unit operation is constrained by a maximum feedrate, the maximum deviation may be the best quantifying method to use. The maximum deviation is calculated by subtracting the peak of the deviation from the average feedrate (See Figure 5.7a), and is represented by the following equation:

$$\Delta\dot{m} = \dot{m}_{\max} - \overline{\dot{m}} \qquad (5\text{-}4)$$

where $\dot{m}_{\max}$ is the maximum feedrate (at the peak) and $\overline{\dot{m}}$ is the mean feedrate calculated from steady state feeding. This value is the quickest and easiest method for comparing multiple refill deviations or detect out of specification material. Because it has no time

dependence, its quantity only represents a deviation in feedrate, but does not contain information on the length of the time of the deviation.

In cases where a unit operation is affected also by the duration of the deviation, the time the feedrate is out of specification may be useful for quantifying the deviation. This method uses an upper bound for detection that should be equal to the value that represents an out of specification feed rate. In this case, it was defined at being 3 standard deviations (SD) above the mean feedrate. As discussed, the SD was determined by the steady state feeding signal. The duration of the perturbation is defined as the period that begins when the feedrate first exceeds the boundary and ends when the feedrate returns within range (See Figure 5.7b), and is represented by the following equation:

$$\Delta t_{OOS} = t_{OOS,final} - t_{OOS,initial} \qquad (5\text{-}5)$$

where $t_{oos,initial}$ and $t_{oos,final}$ are the initial and final times where the flow rate is out of specification. The time the feedrate is out of specification is useful, because short pulses may not have a significant effect on a robust system, although if the deviation occurs for an extended period of time, it may cause disruption or failure.

The total amount of excess powder fed during a perturbation is also a useful parameter, because it captures both the magnitude and duration of the deviation. This quantity, total deviation, is calculated by determining the area between the feedrate boundary for out of specification material (3 standard deviations about the mean) and the feedrate profile (See Figure 5.7c), and can be represented with the following equation:

$$m_{excess} = \int_{t_{OOS,initial}}^{t_{OOS,final}} \left[\dot{m}_{feed}(t) - \left(\overline{\dot{m}} + 3\sigma \right) \right] dt \quad (5\text{-}6)$$

where $\dot{m}_{feed}(t)$ is the feedrate data, $\overline{\dot{m}}$ is the mean feedrate calculated from steady state feeding, σ is the standard deviation, $t_{oos,intial}$ is the inital time of out of specification material, and $t_{oos,final}$ is the final time of out of specification material.

5.4 Results

5.4.1 Effect of Refill Scheduling

During steady state feeding, gravimetric control adjusts the screw speed for changes in the flight filling of the screw. During refill, the feeder is not operating in gravimetric mode, but instead in volumetric mode, where the screw speed is not controlled. The rapid increase of the fill level in the hopper causes densification of the powder and increased pressure, forcing material into the flights of the screw. This increased flight filling causes overfeeding.

Figure 5.8 shows catch scale feedrate data that was collected from the Gericke GAC232 feeder dispensing Grillo Pharma8 zinc oxide at a setpoint of 840kg/hr. In this figure, the vertical green lines represents when the gate valve opened, and the vertical red line represents when it closed. During this feeding there were three different hopper refill operations, which were initiated at 20%, 40%, and 60% of total fill level by volume. The first hopper replenishment was the largest, which refilled the hopper from 20% to 80% of the hopper fill. This refill was the most extreme case and resulted in largest deviation from the setpoint, resulting in instantaneous feedrates that rose as high as

~1200 kg/hr. The mid-sized refill occured when the hopper was depleted to 40% of the fill level and then filled to 80%. This refill had a less significant deviation from setpoint, but still reached feedrate levels of ~1000 kg/hr. The smallest refill was triggered at the low hopper level of 60% and finished at 80%. This resulted in deviations that were barely noticeable over the baseline fluctuations.

A similar series of refill experiments with the same Grillo zinc oxide material were also performed using a smaller twin-screw feeder, the K-Tron KT35. Figure 5.9 shows four plots of the catch scale-collected feedrate data for different feeding and refill conditions. For each condition, the same three refill levels were investigated. The largest triggering at 20% hopper fill level, then 40% hopper fill level, and the smallest at 60% hopper fill level. The effect of rate of refill was investigated and can be observed by comparing Figure 5.9a to Figure 5.9b or Figure 5.9c to Figure 5.9d. For the two plots on the left (Figure 5.9a and Figure 5.9c), the powder is quickly dumped into the hopper, whereas for the plots on the right (Figure 5.9b and Figure 5.9d), the powder is poured slowly during refill. When the powder was quickly dumped to refill the feeder, it resulted in sharp, large spikes in feedrate that deviated from setpoint more substantially than when the refill was completed more slowly.

The effect of using a discharge screen can be examined by comparing the plots on the top having no screen (Figure 5.9a and Figure 5.9b) with those on the bottom having the coarse square screen (Figure 5.9c and Figure 5.9d). The discharge screen adds resistance to the flow out of the feeder as well as breaks up the powder leading to a more consistent exit density. This ultimately creates less deviation due to hopper refill.

5.4.2 Repeatability

To test for repeatability, multiple refills at each hopper fill level were performed. The feedrate data collected by the catch scale are shown in Figure 5.10. Each plot in the figure shows a series of 5 refills, all performed at the same hopper fill level. The settling time was 10 seconds for the first 3 refills, but was reduced to 5 seconds for the last two refills. The settling time was reduced to determine if the longer settling time had any effect on the deviations. A longer settling time increases the time that the feeder remains in volumetric mode. There was no significant difference, indicating that there is no improvement when the feeder returns to gravimetric control almost immediately after refill. It also indicates that these deviations occur mostly while the feeder is still being refilled and not immediately following refill.

Figure 5.10a displays the feedrate data for hopper refills initiated at 20% hopper fill level, Figure 5.10b shows refills initiated at 40% hopper fill level, and Figure 5.10c shows feed rate observed for the smallest refill pulse, initiated at 60% of the hopper fill level. Results for all three conditions are displayed in Figure 5.10d, which shows each of the figures plotted together on the same time scale.

It is apparent that deviations are larger when the hopper is refilled at lower fill levels. The advantage of refilling the hopper more frequently at a higher fill level is that the deviations are much smaller. However, this requires a more demanding refill schedule: refills occured every ~4.5 minutes when initiated at 20%, every ~3 minutes for 40%, and every ~1.5 minutes when refilled at 60%.

The methods of quantifying deviations in Section 5.3.3 were used for the different refill levels. Results are shown in Figure 5.11. Figure 5.11a shows the maximum deviation from flow rate set point observed during refill for each refill level. Figure 5.11b shows the total amount of time the powder stream is out of specification for each refill cycle. Figure 5.11c shows the total amount of excess powder delivered during each refill cycle. In each of these quantifying plots, the values of the performance indicators at each level are highly repeatable and show obvious trends. It is clear that all three performance indicators decrease with smaller, more frequent refills. The refill starting at 60% had the least impact on the output feed stream.

5.4.3 Effect of Material Properties

The effect of refill level and repeatability was also investigated for a blend of semi-fine acetaminophen and 0.25% silica. The feedrate data for this blend was dosed from the K-Tron KT35 for several repeated manual refills as shown in Figure 5.12 and Figure 5.13. Figure 5.12 shows the deviations from feedrate setpoint caused by the largest of the refills, where the low level that triggered refill was 20%, and the feeder was refilled until reaching 80% hopper fill level. The deviations vary greatly because the powder fluidizes and occasionally flushes through the screws of the feeder, leading to large uncontrolled amounts of powder being dispensed. This is in contrast to the results shown for zinc oxide in Figure 5.10, which overfed because of increases in density caused by the compressive force exerted by refilling material.

When the hopper is filled more frequently with a smaller amount of material, the deviation reduced until it became nearly undetectable at the highest fill level of 60% (see Figure 5.13 and Figure 5.14). The maximum deviation and total amount fed in excess

reduced sharply from the 20% to 40% hopper fill level. The difference in maximum deviation and total amount fed in excess were not as large for the change from 40% to 60% initial fill level. The time of deviation showed a more gradual reduction across all low hopper fill levels.

The behavior of the hopper refilling differed between the acetaminophen blend and the zinc oxide. Figure 5.14 shows the quantified deviations for both the zinc oxide and the acetaminophen / 0.25% silica blend. Although the zinc oxide also showed decreasing deviations for more frequent refilling at the highest fill level, the deviations were still significant when compared to the baseline fluctuations. This indicates that when comparing the two tested materials the acetaminophen / 0.25% silica blend was significantly more sensitive to hopper fill level than the zinc oxide. This was especially noticable at the lower fill levels, where the acetaminophen blend showed uncontrolled flooding. Aside from the 20% fill level where the acetaminophen blend flushed through the feeder, the range of deviations were relatively similar in magnitude for the two materials. Maximum deviation and total deviation both showed a significant deviation for the powder flushing, and due to the acetaminophen blend having smaller deviations at the higher fill levels, the plots cross between 20% and 40% hopper fill level. The time of deviation for both powders showed similar changes. A noteworthy difference was that the time of deviations for the zinc oxide remained out of specification for about 20 seconds longer at the three refill levels. The compressive effect that lead to increased density in the zinc oxide is longer lasting than the flushing behavior of the acetaminophen blend. There was no visual evidence of powder flushing at the higher fill levels for the acetaminophen blend, indicating the cause of the deviations were likely due to the same

compressive density raising effect that caused the deviations observed in the zinc oxide tests.

5.4.4 Investigation of Refill Method

The effect of rate of refill discussed in section 5.4.1 revealed that the modality of the refilling operation (not just its magnitude) can have an important role on deviation reduction. To further investigate the effect of refill method, the hopper replenishment of a smaller K-Tron KT20 was tested. High rate refilling with the automatic vacuum refill system was compared to rate controlled refilling, utilizing the K-Tron KT35 as an automatic refill system. The powder used for testing was Fast Flo Lactose, and the feedrate setpoint was 20 kg/hr.

The feedrate results for both refill methods are shown in Figure 5.16. The refills from the automatic vacuum refill system were quick and delivered the powder with a high intensity of impulse. As shown in Figure 5.16a, this refill modality resulted in deviations even when the feeder was refilled very frequently (at 60% fill level). The deviations during refill can be clearly seen in the plot at ~550 and ~1100 seconds. When using the K-Tron KT35 as the refill device (See Figure 5.16b), the two refills were at ~550s and ~1100s, but no discernable deviations were observed in the feedrate data. The lower refill rate of the K-Tron KT35 resulted in lower compressive forces that did not cause significant density changes of the powder in the hopper. However, the high rate automatic vacuum refill system, which dumps a sudden charge of powder, caused significant compressive force which resulted in feedrate deviations.

5.5 Conclusions

Continuous processing requires a steady, consistent, and non-stop feedstream of powder. The use of gravimetric loss-in-weight feeders with limited hopper size inevitably means the feed hoppers will need to be refilled often, leading to potentially large deviations from feedrate setpoint. When designing the refill apparatus and scheduling of hopper refill, it is necessary to utilize the knowledge of such deviations to mitigate and minimize them. By quantifying the size of the deviations, it is possible to compare multiple feeder / refill system configurations and refilling schedules in order to select the optimal setup.

By refilling the feeders more frequently with less material, the feeders perform better. However, this results in the feeder functioning in volumetric mode a longer fraction of the time. In volumetric mode, the feeder is essentially blind to changes in screw filling or powder density. In order to minimize this potential problem, it is best to select a refilling regime that both minimizes the deviations as well as the number of refills needed. The quantity of refills should be based on reducing the deviations from feedrate setpoint to a level that is acceptable to the unit operations downstream of the feeder. This requires an understanding of the downstream process and acceptable variability.

Alternatively, in cases where even small levels of variability are unacceptable, the refilling system should be designed to gently refill the feeder. This requires more control over the refilling stream, which also demands a specialized refilling apparatus. In the case shown in this study, where a volumetic feeder is used to control the refill rate, this will also require a refilling system to refill the volumetric feeder. This leads to a higher initial equipment cost. However, where increased control over fluctuations is necessary, this may be the preferred option.

5.6 Figures for Chapter 5

a.

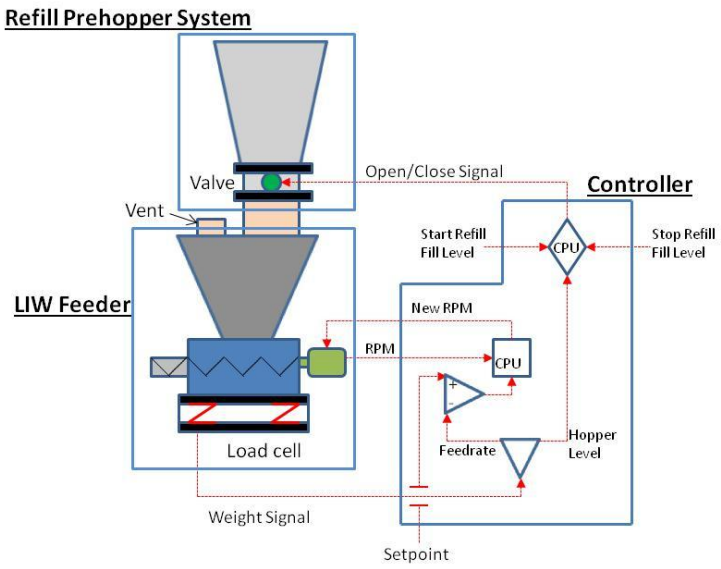

b.

Figure 5.1: a.) Diagram of the main components of a loss-in-weight feeder including a refill system and gravimetric controller with labels for the main control signals. b.) Photograph of a Gericke GLD87 feeder in a testing setup with an attached automatic refill system located on the platform above.

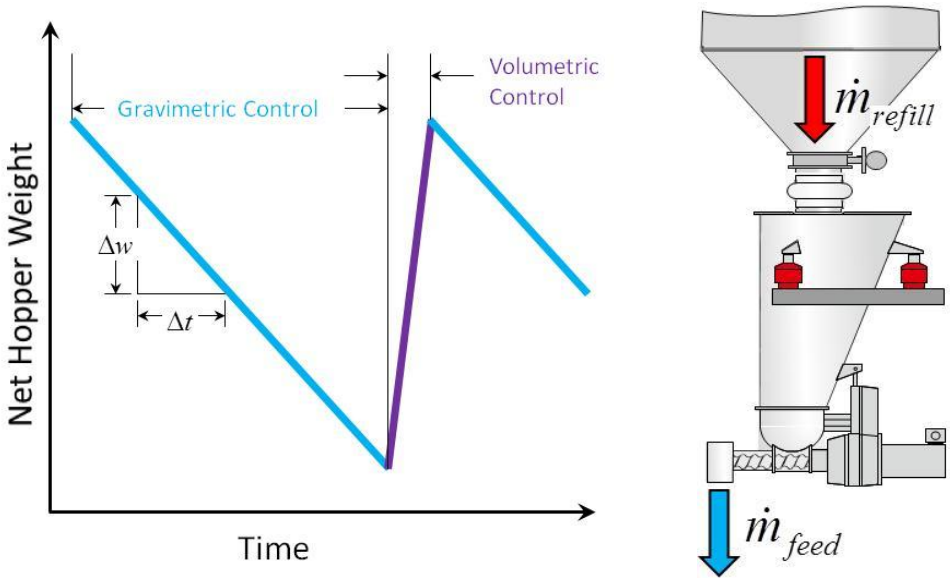

Figure 5.2: Loss-in-weight operating principle dipicting the loss-in-weight feeding cycle created by periodic hopper refill.

Figure 5.3: Gericke Type RA bin discharger which has a agitator blade and a gate to dispense material from a bin.

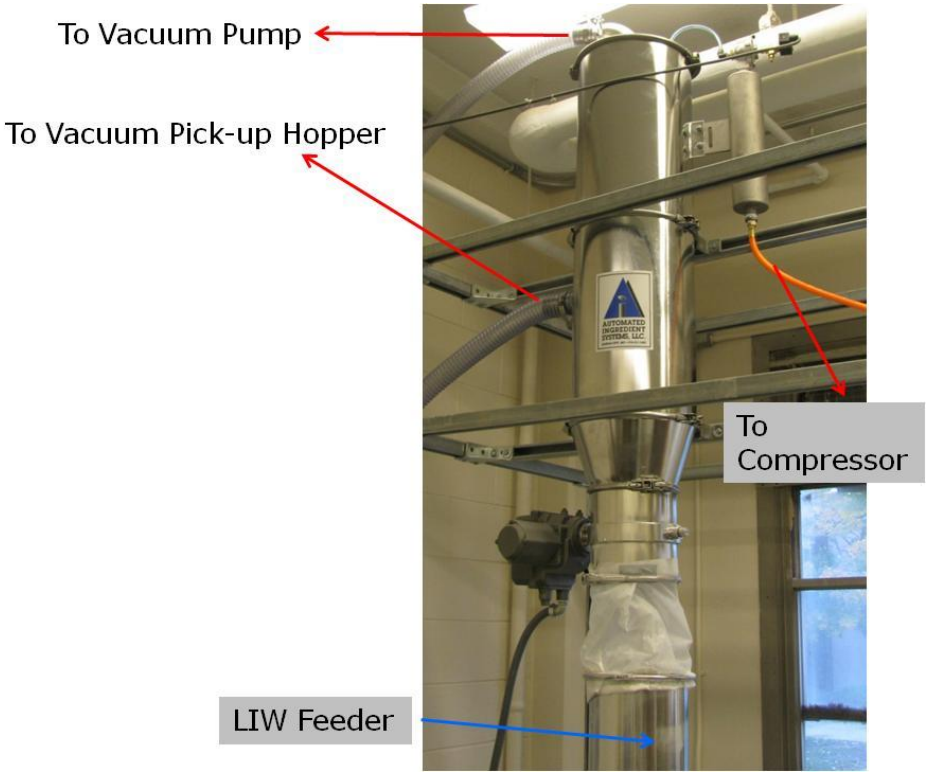

Figure 5.4: Automatic Vacuum Refill System

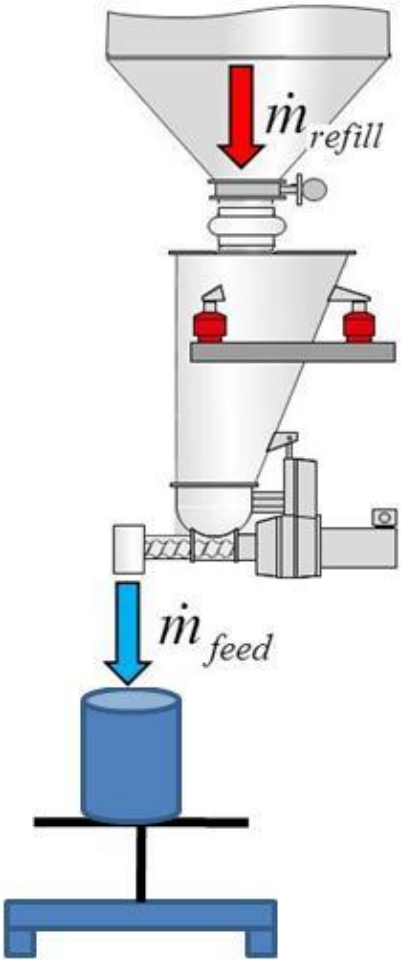

Figure 5.5: Depiction of the experimental setup using a gain-in-weight bucket on a catch scale to monitor the feeding performance during the refill process.

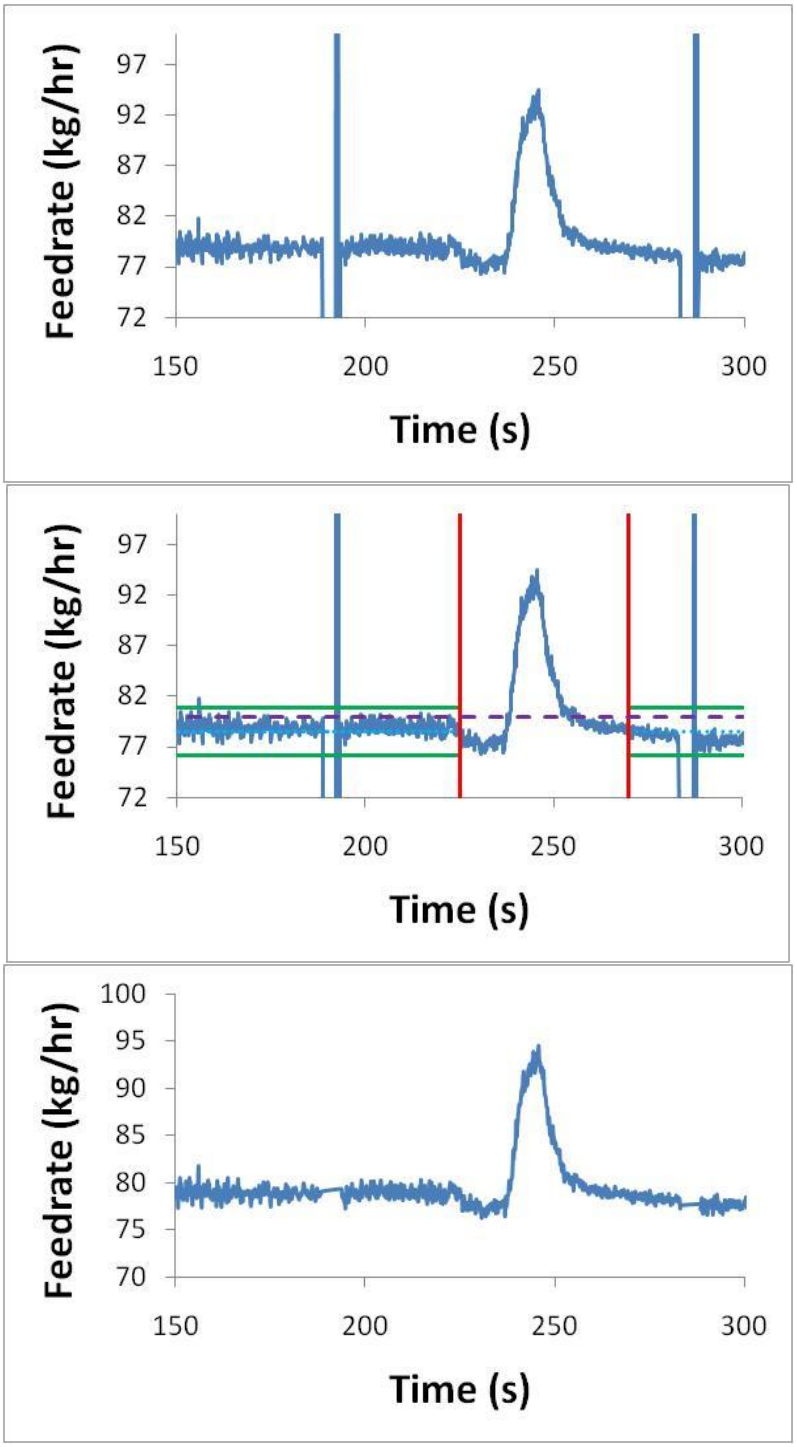

Figure 5.6: Example data of the filtering of feeder hopper refill trials

a.

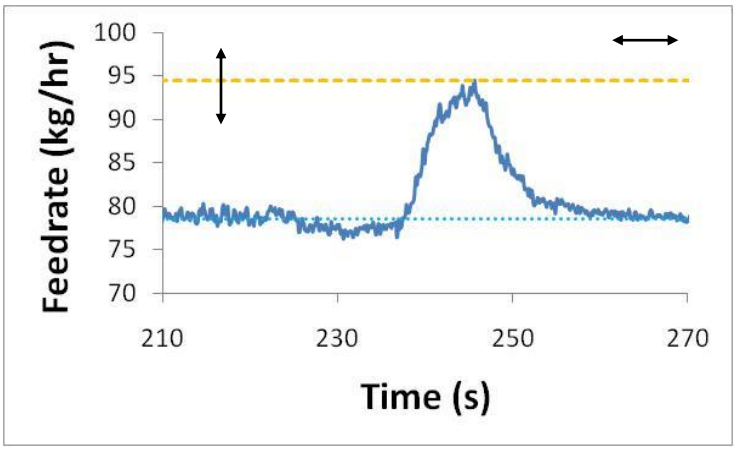

b.

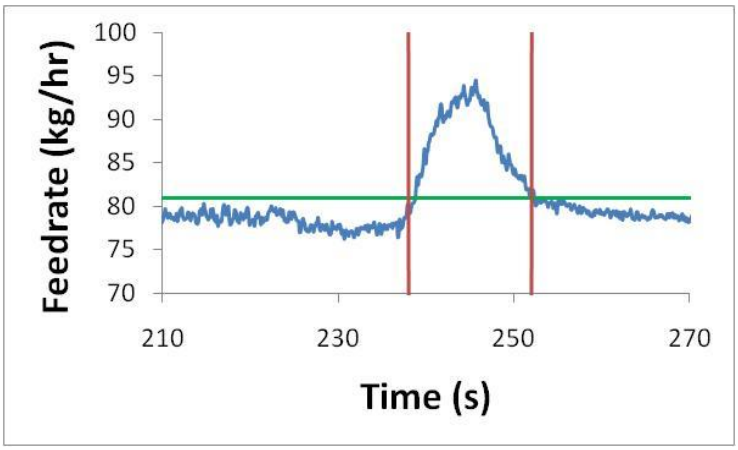

c.

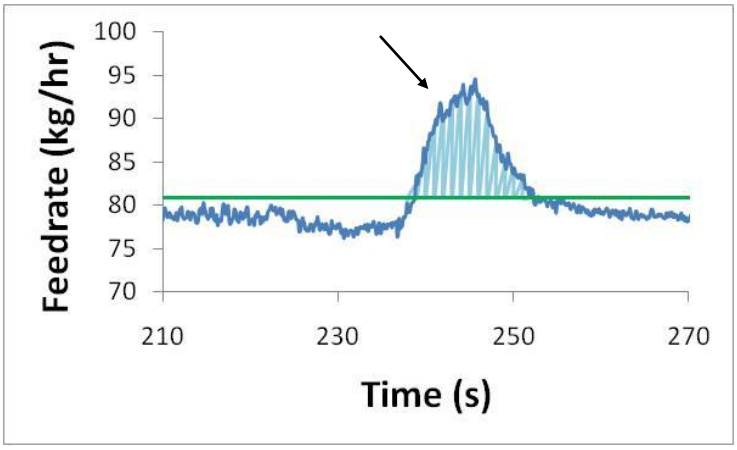

Figure 5.7: Methods for quantifying the deviation from setpoint: a.) magnitude of the maximum deviation, b.) the time that the feedrate is out of specification, and c.) the total deviation / powder fed in excess

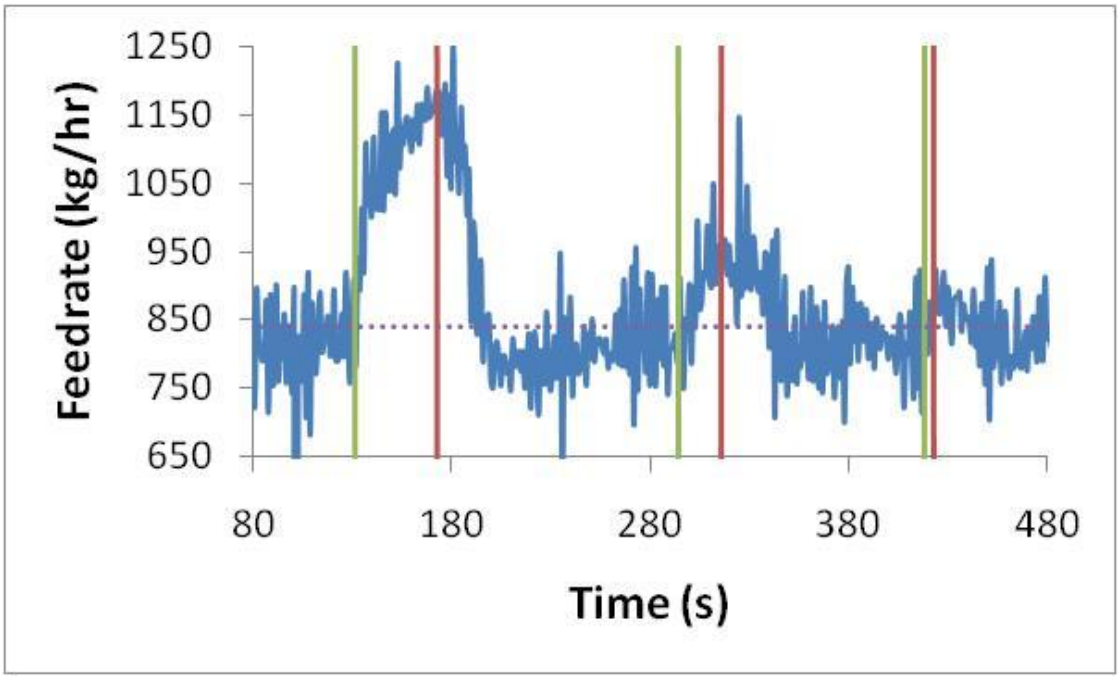

Figure 5.8: Deviations from setpoint caused by hopper refill in a Gericke GAC232 feeding zinc oxide powder using three different low hopper levels: 20%, 40%, and 60%.

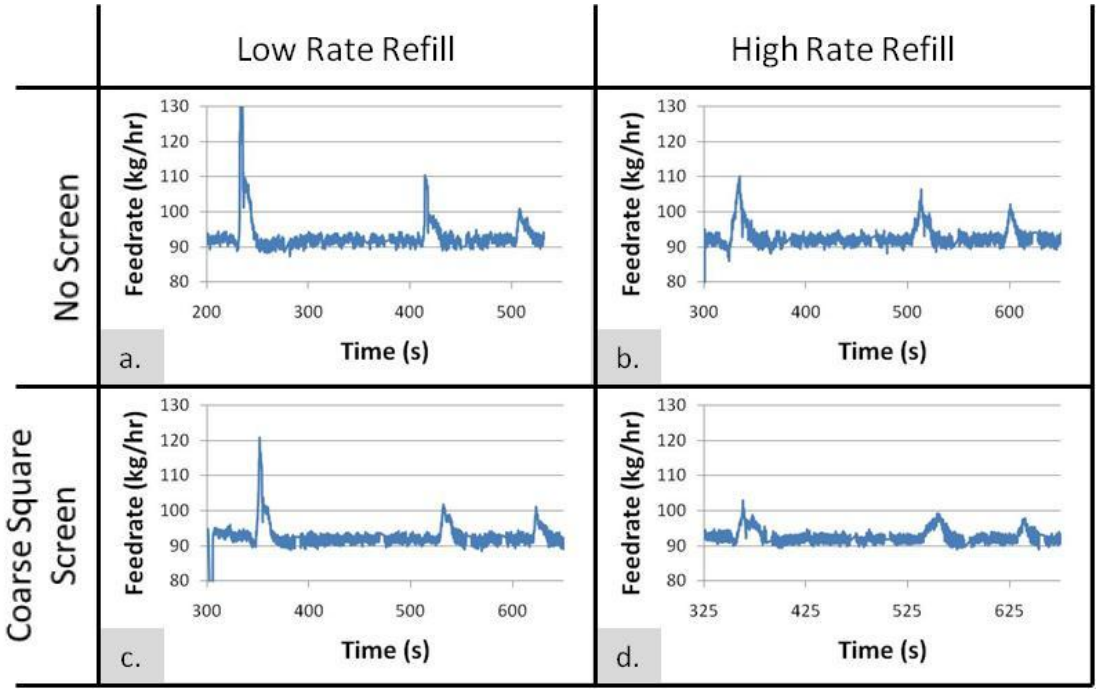

Figure 5.9: Catch scale data for the feedrate data from the KTron KT35 feeding Grillo Pharma8 under different conditions: a. No screen, low rate refill; b. No screen, high rate refill; c. Coarse square screen, low rate refill; d. Coarse square screen, high rate refill. In each picture, the spike on the left is caused by refilling the hopper when it is at the 20% fill level, the spike in the middle corresponds to refill at the 40% level, and the spike on the right is observed when the hopper is refilled at the 60% fill level.

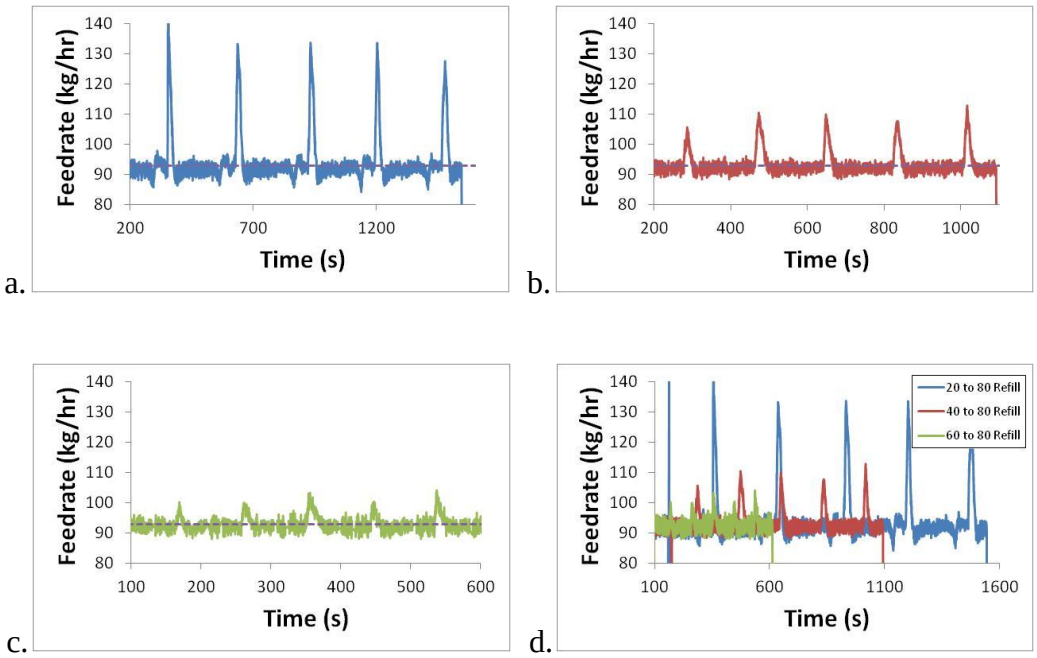

Figure 5.10: Catch scale feedrate data for several series of 5 repeated manual refills of the KTron KT35 feeding Grillo Pharma8 zinc oxide at 3 refill levels. a.) 20% to 80% hopper refill; b.) 40 to 80% hopper refill; c.) 60 to 80% hopper refill; d.) plot of all series for time scale reference. The first 3 refills in each series has a settling time of 10 seconds, whereas the last 2 refills of each has a reduced settling time of 5 seconds.

a.

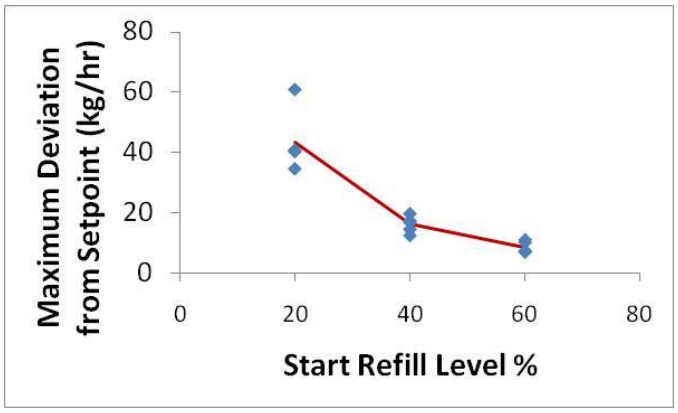

b.

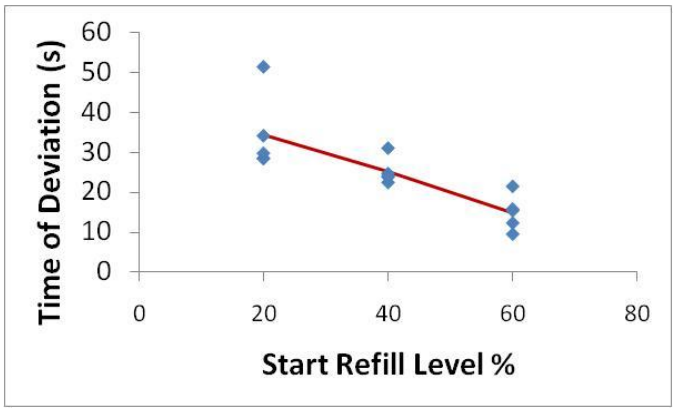

c.

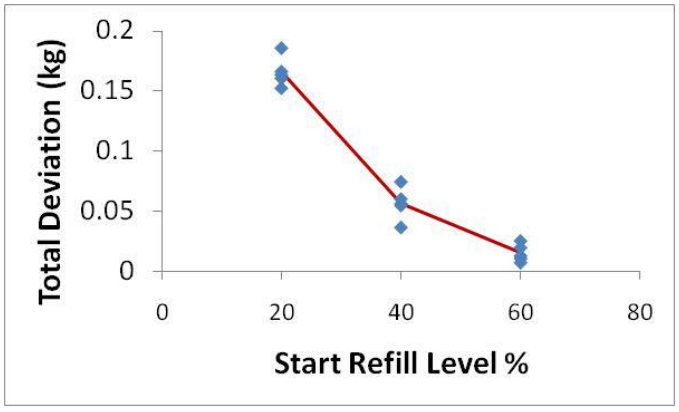

Figure 5.11: Performance indicators extracted from the catch scale feedrate data (shown in Figure 5.10) for series of 5 repeated manual refills of the KTron KT35 feeding Grillo Pharma8 at 3 refill levels. a.) The maximum deviation from setpoint, b.) total time of deviation, and c.) total deviation (total amount of excess powder delivered per refill) all decrease as the refill is performed at higher hopper fill levels.

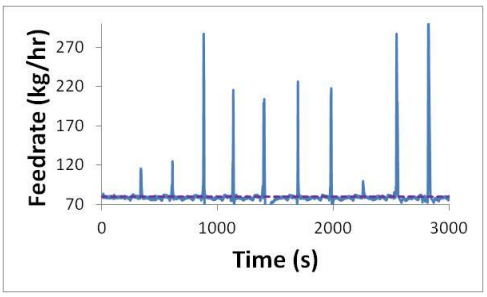

Figure 5.12: Catch scale feedrate data for several series of 10 repeated manual refills of the KTron KT35 feeding a Semi-Fine Acetaminaphen and 0.25% silica blend for 20% to 80% hopper fill refills. Scaled to show the large variation in deviations caused by flushing.

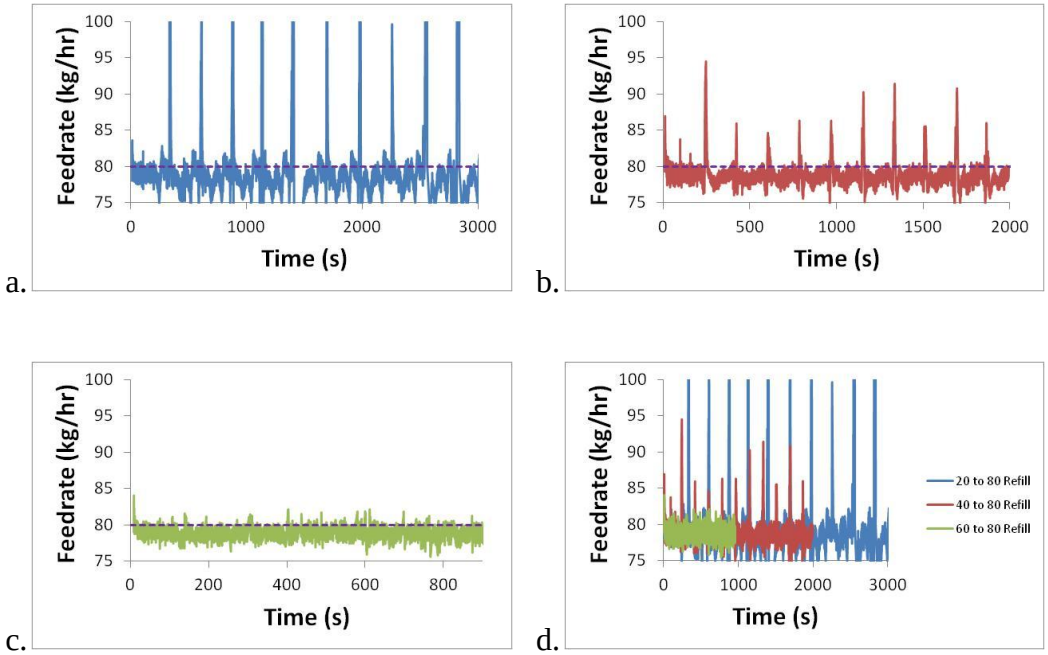

Figure 5.13: Catch scale feedrate data for several series of 10 repeated manual refills of the KTron KT35 feeding a Semi-Fine Acetaminaphen and 0.25% silica blend at 3 refill levels. a.) 20% to 80% hopper refill; b.) 40 to 80% hopper refill; c.) 60 to 80% hopper refill; d.) plot of all series for scale reference.

a.

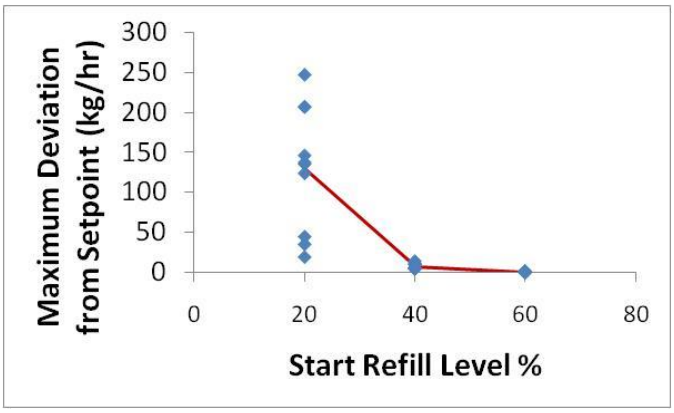

b.

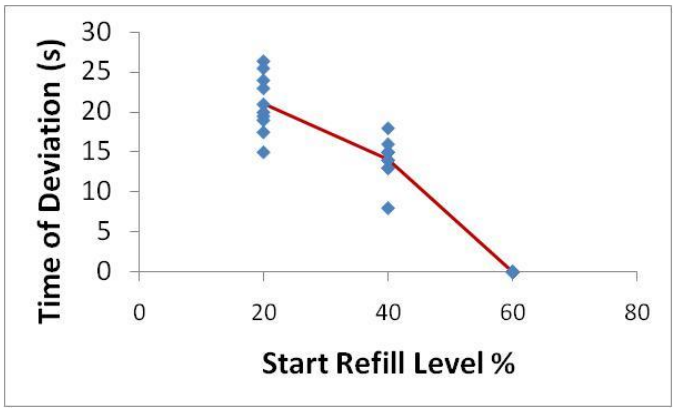

c.

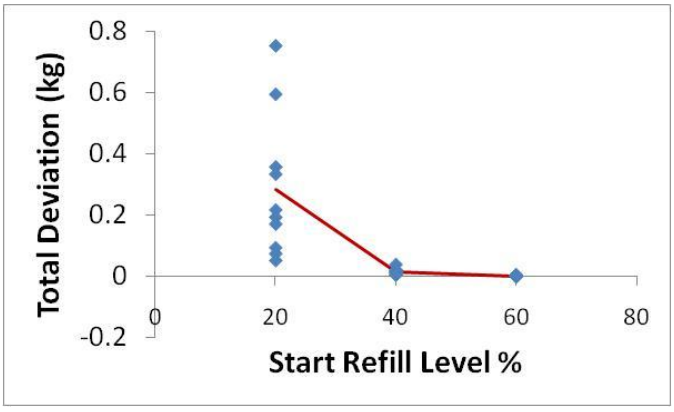

Figure 5.14: Performance indicators extracted from the catch scale feedrate data (shown in Figure 5.13) for series of 10 repeated manual refills of the KTron KT35 feeding Semi-fine Acetaminaphen and 0.25% silica blend at 3 refill levels. a.) The maximum deviation from setpoint, b.) total time of deviation, and c.) total deviation (total amount of excess powder delivered per refill all decrease as the refill is performed at higher hopper fill levels.

a.

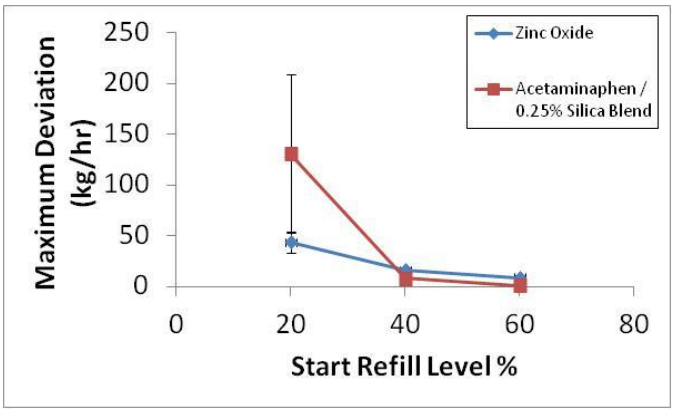

b.

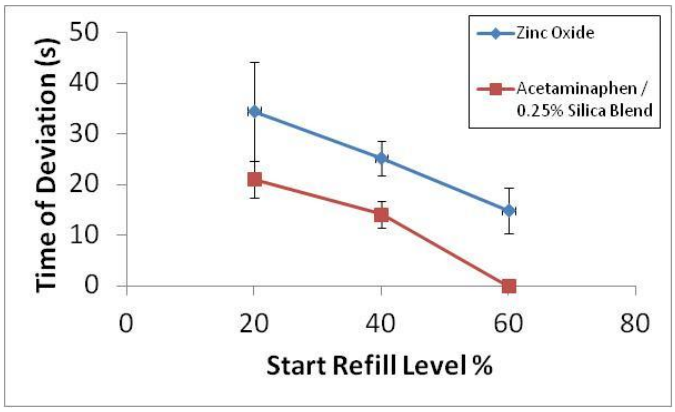

c.

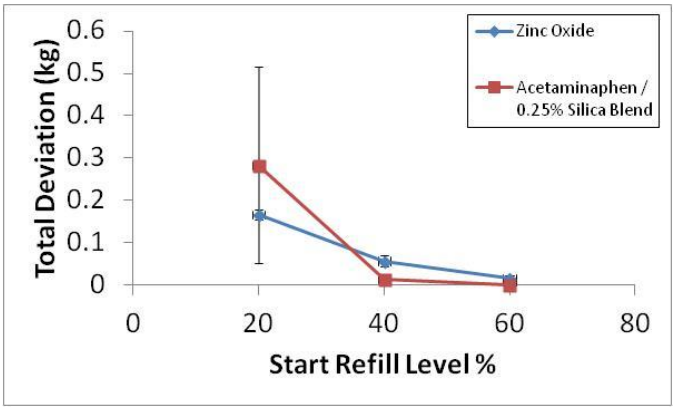

Figure 5.15: Performance indicators extracted from the catch scale feedrate data for the KTron KT35 feeding zinc oxide as well as for the feeding of Semi-fine Acetaminaphen and 0.25% silica blend at 3 refill levels. a.) The maximum deviation from setpoint, b.) total time of deviation, and c.) total deviation (total amount of excess powder delivered per refill).

a.

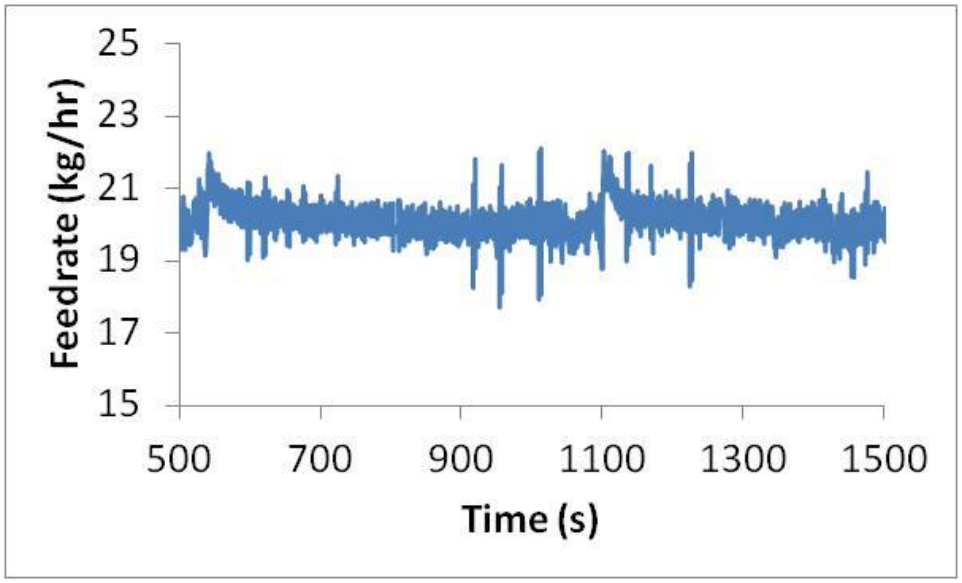

b.

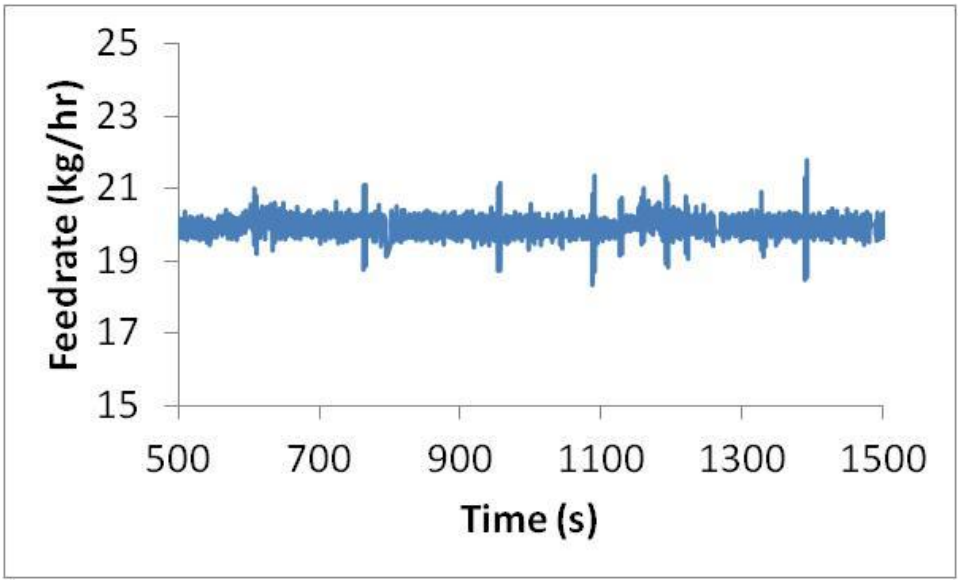

Figure 5.16: Feedrate data during 60-80% hopper refills of the K-Tron KT20 using a.) an automatic vacuum refill system and b.) the K-Tron KT35 setup as a volumetric screw refill system.

Chapter 6. TRACEABILITY OF RAW MATERIALS WITHIN CONTINUOUS PHARMACEUTICAL MANUFACTURING

6.1 Introduction

One of the main approaches to modernizing and improving pharmaceutical manufacturing has been developing continuous processing, which has gained attention of both the industry and regulatory authorities [3], [53], [54], [78]–[83]. Continuous manufacturing has many advantages over traditional batch, which have been embraced by other industries [2], [3]. Continuous processing equipment has a much smaller footprint leading to lower equipment costs. Because all the processing steps are interconnected, no intermediate storage is needed, lowering the necessary material inventory. Unlike batch processing, the smaller scale and ability to process different amounts of material simply by changing the production time makes continuous systems versatile in both the clinical and commercial scale without the need for scale-up.

Continuous systems with automation and process control result in high quality (low variability) products, whereas batch processing is far less understood, resulting in fluctuation and an unpredictable product quality [3]. Segregation has been shown to be prominent on batch systems, yet continuous systems have demonstrated the ability to process segregating mixtures without issue [84]. A continuous system handles smaller portions of material at any given moment, increasing material monitoring scrutiny. This is impossible for large-scale batch processes with a similar throughput. Utilizing product and process understanding with properly implemented online PAT, continuous manufacturing readily fits the criteria needed to enable real time release testing (RTRt) leading to rapid and reliable batch release of high quality product. In spite these vast

advantages, continuous manufacturing also has significant challenges. If implemented incorrectly, continuous manufacturing will lead to failure.

Two notable challenges are batch definition and raw material traceability, both required by regulation. [85] This chapter presents a method based on the residence time distribution (RTD), which can be used to solve both of these challenges. The RTD is also used to examine the sensing frequency, with the goal of defining a sensing speed that would ensure that any unacceptable content uniformity variations would be detected and handled. As a case study, a simplified quality risk management process, including assessment and control, was completed for a direct compression case study, which identified high risk content uniformity issues and reduced them through redesign that improved system robustness.

In chemical processing fields, the residence time distribution (RTD) is used to describe how a material travels inside the unit operations of a continuous process system. RTD is a critical yet underutilized tool in pharmaceutical process understanding, quality assurance, and equipment and sensing design. Although traditionally applied to fluid systems [8], there have been many publications showing this same probability based time distribution also applies to granular or powder systems. [10], [86]–[93]

6.2 Continuous Manufacturing System

The model system used for the methods developed in this work is the prototype continuous direct compaction (DC) manufacturing system, which was developed and built by the Engineering Research Center for Structured Organic Particulate Systems (ERC-SOPS, http://www.ercforsops.org/) located at Rutgers University. A photo and model of the continuous manufacturing platform are shown in Figure 6.1a and Figure

6.1b, and a simplified model highlighting the unit operations is shown in Figure 6.1c. The continuous DC system was constructed on a 3-tiered scaffolding platform, which has multiple loss-in-weight feeders on the highest level. The feeders supply the multiple components of formulation through to a Quadro Comil, which is located on the middle level and serves a triple purpose. The Comil sieves breaking large agglomerates, performs initial high shear mixing, and ensures intimate contact of poorly flowing ingredients with glidants, thus improving blend flow properties. Also on the middle level, the Comil's exit passes milled material to a Glatt continuous mixer, which consists of a horizontally rotating shaft with triangular shaped paddles that mix the blend as it travels through the tubular body. Following the mixer is a Kikusui tablet press, which compresses the blended formulation into tablets at the ground floor level.

6.3 Methods

6.3.1 Residence Time Distribution (RTD) Experiments

The residence time distribution (RTD) can be easily obtained for all unit operations in a continuous line with a tracer response experiment performed for each unit operation separately, and for the mechanically integrated line as well. In this testing, a pulse or step change of tracer is added to the inlet of the continuous equipment, and the response of the tracer concentration profile at the outlet is measured. The concentration measurements can be recorded using online spectroscopy, or samples can be collected for off-line measurement. In either case, it is important that the tracer concentration be readily measureable by an analytical technique. Additionally, the presence of the tracer should not impact the flow properties of the bulk material for which the RTD measurements are being taken, because the RTD is highly dependent on the flow behavior of the material

within the apparatus. Any significant changes to the flow behavior will cause the measured RTD not to be representative of the material.

For tracer pulse tests, the response will be a concentration profile, C(t), that has the same shape as the residence time distribution, E(t). The RTD can be calculated by normalizing the concentration profile by the area underneath the profile:

$$E(t) = \frac{C(t)}{\int_0^\infty C(t)dt} \tag{6-1}$$

It is important that the data set for the concentration profile be complete and include the entire tail. If the profile is not complete or the tail is very long, the RTD will be inaccurate. If this occurs, it is possible to extrapolate the tail as an exponential decay, which will improve accuracy of an incomplete dataset. [94]

The tracer pulse technique also relies on the ability to add a pulse that is as close to instantaneous as possible. If this is not possible or the residence time is very short, this can also add inaccuracies. However, when correctly applied this method is the most direct method for determining the RTD. [94]

If the pulse technique is not reliable, an alternative is the step change technique. For tracer step change tests, the response will be a concentration profile with the same shape as the cumulative distribution function (CDF), F(t). To calculate the CDF, the concentration profile needs to be normalized so that the initial value is 0 and the final value is 1:

$$F(t) = \frac{C(t) - C_{initial}}{C_{final}} \tag{6-2}$$

where $C_{initial}$ and C_{final} are the intial and final tracer concentrations. Typically the initial tracer concentration would be 0, which simplifies this equation to:

$$F(t) = \frac{C(t)}{C_{tracer}} \tag{6-3}$$

The cumulative distribution function (step response) and residence time distribution (pulse or point response) are related by the following equations:

$$F(t) = \int_0^t E(t)dt \tag{6-4}$$

$$E(t) = \frac{dF(t)}{dt} \tag{6-5}$$

A residence time distribution has several moments that can be used to characterize its shape. For this study only the first two integer moments are used, respectively the mean residence time and the variance (square of standard deviation). The equations for the mean residence time and the variance are as follows:

$$\tau = \int_0^\infty tE(t)dt \tag{6-6}$$

$$\sigma^2 = \int_0^\infty (t-\tau)^2 E(t)dt \tag{6-7}$$

The mean residence time can be used to quantify the center of the residence time distribution, whereas the standard deviation is used for determining the width. These moment values are useful for describing the shape of a distribution without relying on the entire distribution.

6.3.2 Residence Time Distribution Fitting

Continuous unit operations vary dramatically in both function and geometry, and correspondingly the residence time distribution (RTD) of any unit operation is equally as varied. This has resulted in the development of many RTD models, some of which may not be appropriate for solids unit operations.

However, the examples shown in this work use the "stirred tanks in series" model, which is an empirical model based on equally-sized continuously stirred tank reactors (CSTRs) placed in series (see Figure 6.2). The model for a CSTR assumes a mixed vessel with perfect back-mixing. However, placing CSTRs in series results in a model for realistic mixing. Figure 6.3 shows a range of residence time distributions modeled with tanks in series. The number of tanks in this figure range from 1 up to infinity. A larger number of tanks in series results in a more narrow distribution. An infinite number of CSTRs in series is equivalent to a plug-flow tubular reactor (PFR), which does not have any axial mixing and is represented by a pulse response.

Generalizing the model for tanks in series results in the follow equations for RTD [94]:

$$E(t) = \frac{t^{n-1}}{(n-1)!\left(\frac{\tau}{n}\right)^n} e^{\left(\frac{-nt}{\tau}\right)} \qquad (6\text{-}8)$$

where τ is the mean residence time and n is the number of CSTRs. The concentration profile for the pulse response testing is similarly generalized by:

$$C(t) = C_0 E(t) = C_0 \frac{t^{n-1}}{(n-1)!\left(\frac{\tau}{n}\right)^n} e^{\left(\frac{-nt}{\tau}\right)} \qquad (6\text{-}9)$$

where C_0 depends on the amount of material added in the pulse.

The RTD experimental data was fit to the tanks in series model using a built-in Matlab function, "lsqcurvefit", which is a least squares curve fitting function based on the trust region reflective least squares algorithm described by Coleman *et al.* [95], [96]. The concentration profile defining parameters (C_0, τ, and n) are determined by this least squares technique, which seeks these values while minimizing the sum of squares (SS) error between estimated and experimental values:

$$SS = \min_X \sum_i \left(C(X, t_i) - C_i\right)^2 \tag{6-10}$$

where $C(X,t_i)$ is the estimated concentration, t_i and C_i represent the *i*th points from the experimentally collected time and concentration datasets, and X is the parameter set for the model:

$$X = [C_0, \tau, n] \tag{6-11}$$

6.3.3 Convolution

A residence time distribution can be used to trace the passage of materials through a continuous flow system. Since the RTD is the pulse or point response of the system, if the system response is linear (i.e., if the tracer does not modify the flow properties of the blend) any point in time will behave and spread through the system just like a pulse of equal magnitude. A measured input stream could be represented with a string of discrete values representing the fluctuations in the stream. Using the convolution integral for mixing:

$$C_{out}(t) = \int_0^t C_{in}(t - t')E(t')dt' = \int_0^t C_{in}(t')E(t - t')dt' \qquad (6\text{-}12)$$

or the convolution equation:

$$C_{out}(t) = C_{in}(t) * E(t) \qquad (6\text{-}13)$$

it is possible to predict the outlet of a unit operation as long as the concentration of the inlet stream, $C_{in}(t)$, and the RTD, E(t), are both known. This can be extended to a series of unit operations by calculating the overall RTD recursively, for example, for two unit processes, as:

$$E(t) = E_1(t) * E_2(t) \qquad (6\text{-}14)$$

where $E_1(t)$ is the RTD from a first unit operation and $E_2(t)$ is from a second operation.

This convolution technique is depicted in Figure 6.4 and Figure 6.5. In Figure 6.4a, the first RTD, $E_1(t)$, is discretized with approximations for the time interval of 2.4s, where the discrete version of the RTD is now represented by a sequence of bars. Figure 6.4b shows the second RTD, $E_2(t)$, which is scaled for each of the elements in the discrete approximation from Figure 6.4a and are plotted in Figure 6.4c. For example, the first element is 0 when t=0, which is why the peak of $E_2(t)$, 0.36 at t=5s, results in the scaled response of 0 at 5s. The second element, which is 0.0378 at t=2.4s, results in a product of 0.033 (0.36*0.0378*2.4), which is the value shown for the peak of the scaled response at t=7.4 (5s + 2.4s). This was repeated for all of the elements in the discrete approximation, while the time was offset by 2.4s for each subsequent approximation, which was the time interval. These are then summed, and are shown in Figure 6.4d overlayed with the solution from the Matlab 'conv' function, which uses a smaller time interval than the 2.4s

interval used for the example. Figure 6.5 shows a plot of the two unit operation RTDs, $E_1(t)$ and $E_2(t)$, with their convoluted solution or overall RTD, which is both more broad and has a longer mean residence time.

The Matlab function's generalized definition is*:*

$$E(t_k) = \sum_j E_1(t_j) E_2(t_k - t_j + \Delta T) \Delta T \qquad (6\text{-}15)$$

where ΔT is the time interval for the two RTDs and t_k and t_j are the *k*th and *j*th points of the time array.

6.3.4 Traceability of Raw Materials in Continuous Processing Systems

The overall process RTD can be determined using the mathematical tool of convolution in combination with the residence time distributions (RTD) for each unit operation. Figure 6.6 shows a process flow diagram for a direct compaction continuous manufacturing system. After the feeders at the top, the first unit operation is a mill, which has a short and narrow RTD. Next is the continuous blender, which has significant back-mixing and therefore a broader residence time distribution. Finally is the tablet press, which has an even longer residence time due to the feed hopper and the feed frame, but only a small amount of back mixing in the feed frame. Combining these three unit operations through the convolution technique yields an overall system RTD, which is both longer and wider than any of the individual unit operations. This overall system RTD can be used to trace raw materials across the entire system, all the way to the tablets.

The RTD modeling of the system predicts the evolution of any process upset so that it may easily be captured downstream, making it a useful predictive tool for risk

management. This enables the use of controls to mitigate content uniformity risks in the form of dynamic process changes or rejection of out of specification material, effectively reducing variability, narrowing the composition distribution of accepted product, and improving overall product quality.

For simplicity of this depiction in Figure 6.6, the RTD of the feeders and feeder refill system is not shown, but to trace raw material back to a drum, this will require mapping those unit operations as well. The method for this or other continuous systems is the same. The RTD for each feeder will be unique to the equipment and powder used under the actual operation conditions used. Because of this, each component will have a separate overall system residence time distribution. This would be the case anytime multiple streams are combining. For example, consider a process to create a bi-layer tablet. The process would involve separate blending of the blend used to make each side of the tablet, usually in unequal proportion and having different composition (i.e., a different API) causing the ingredients in the two sides to have different RTDs. However, RTDs vary monotonically with respect to material properties and processing conditions, and thus the development for predictive correlations for RTDs is entirely feasible [97].

6.4 "Batch" Definition

One of the early barriers to developing and implementing continuous processing was, and to some extent remains, the uncertainty of regulatory compliance. One of the main concerns is the ability to trace materials by batch and lot, a regulatory requirement. According to 21 CFR 210 [98], the definitions of batch and lot are:

Batch - "A specific quantity of a drug or other material that is intended to have uniform character and quality, within specified limits, and is produced according to a single manufacturing order during the same cycle of manufacture."

Lot - "a batch, or specific identified portion of a batch, having uniform character and quality within specified limits' or, in the case of a drug product produced by continuous process, it is a specific identified amount produced in a unit of time or quantity in a manner that assures its having uniform character and quality within specified limits."

The regulatory definition of batch has no stipulation or requirement as to the method of manufacture, and in fact the definition of lot specifically includes continuous processing. It is still necessary to define batch and lot to comply with various aspects of current good manufacturing practice [85], [99]. Compliance requires:

- Batch production and control records
- Laboratory conformance testing and release
- Investigation of failures or discrepancies
- Recall procedures

While both batch and lot are defined, precise specification of each are left to the manufacturer's discretion and design. For a continuous manufacturing process, specification may be based on: production time period, amount of material, variation in production, or maintenance cycles. A variation in production, such as a change in feedstock lot, may be the most appropriate method as a batch is "intended to have uniform character and quality" [98].

In a batch process, the "batches" are physically separated into enclosed vessels, making batch identification straightforward (See Figure 6.7a). In continuous manufacturing, a physically separated "batch" does not exist, instead a continuous non-stop stream of product is generated. The lack of a physical barrier in a continuous process causes the boundaries between batches to become confounded because of back-mixing across the system. A naive and unrealistic view of batch specification for a continuous processing might assume that there is no back-mixing. However, this is only true for an ideal plug flow system (See Figure 6.7b), in which an arbitrary boundary would suffice and then the identification would be similar to that of batch processing. Such a plug flow system, however, would have no back mixing capabilities, and therefore would be unable to eliminate any variability entering the system due to either material properties or processing conditions. Thus, substantial back-mixing would be an intrinsic characteristic of any robust and effective continuous manufacturing process, and batch definition must address its presence.

Therefore, in a realistic continuous system (See Figure 6.7c), which would have some amount of back-mixing, materials would comingle between subsequent batches. Although there is no specific regulatory conformance problem with using an arbitrary division, it must be determined how many batches are affected by any potential manufacturing inconsistency. Additional procedures would need to be developed to address these inconsistencies. See Figure 6.7c for an example. In this case, if there were a need to recall "Batch 3", then it must be assumed that the recall must also apply to "Batch 2" and "Batch 4". As the batches may be quite large, this would result in a large amount of recalled or rejected material. To solve this problem, smaller batches could be

used, resulting in less material loss, but increased release-related testing. With any batch size, experimental qualification of the equipment must be determined to properly identify the batches that should be considered adulterated.

An alternative to drawing an arbitrary line between batches in a continuous system would be to separate the interface region between batches and define the batch as the material between the interfaces. See Figure 6.8. In the case where batches are specified by a component lot change, this method would ensure that each batch contains only a single feedstock lot. Removing the interface is analogous to the removal of the first and last parts of a batch made by batch processing, which is often performed to maintain uniform quality. However, the need to do this in batch processing is due to actual quality problems, such as blend segregation. In continuous manufacturing, such quality problems are minimized, and thus the possible need to discard the interface is entirely a regulatory compliance issue.

In continuous processing, the size of the interface between batches can be minimized using experimentally measured RTDs. Since the RTD represents the pulse response of the system, it can be applied to represent the point response from a feedstock lot change, which behaves exactly like a tracer step change. For example, given the RTD measured from a continuous blender shown in Figure 6.9a, the cumulative distribution function (CDF), F(t), shown in Figure 6.9b can be derived. The CDF represents the fraction of new feedstock that will exit in the outlet stream as a function of time. For instance, the value is 0 at t=0, meaning none of the new feedstock will be exiting. When the value of the CDF becomes 1, the old feedstock has completely exited and only the new feedstock

would be exiting. The old feedstock would follow the inverse washout profile, represented by:

$$W(t) = 1 - F(t) \tag{6-16}$$

Using 0.5% and 99.5%, which are shown by the vertical lines in both Figure 6.9a,b, the boundaries were defined. At a time of 30 seconds, the new feedstock would start to appear at the outlet of the system. At 160 seconds, the last of the old feedstock has left the system and the outlet only contains the new feedstock. Therefore, the material exiting from 30s to 160s could be discarded as the transition interface. The material before and after this time interval becomes two different and separate batches. The result is a short 130 second long interface. At a total processing throughput for a formulation of 30kg/hr, the discarded interface would amount to about 1 kg of material. This is modest compared to the often used procedure of discarding the first and last portions of large batch-processed batches.

6.5 Results

6.5.1 Identifying Sources of Disturbances

A quality risk management process should include the assessment, control, communication, decisions, and review of risks to the quality of the drug product across the product lifecycle. [41] In the work presented here, the focus is specifically on the first two parts, assessment and control as they relate to content uniformity. A risk assessment includes identifying hazards, estimating the risk, and evaluation. Although there are an infinite number of hazards that can occur in any process, risk is based on both the probability and severity of the hazards.

In a continuous direct compaction line, the highest probability for content uniformity risk is at the feeders and blender. Assuming the blend is uniform at the exit of the blender, there is a very low risk of content uniformity issues arising. A properly designed continuous blender should have no dead zones and should have enough radial mixing to blend multiple components into a uniform mixture. The real issue is typically not the blender, but instead the composition of the inlet stream. If the ingredients in the inlet streams are not entering the blender at the correct ratios, no amount of blending will correct the composition of the blend. The feeders and the downspout from the feeders are the most likely cause of content uniformity risks.

The recommended feeders for pharmaceutical continuous processing are loss-in-weight feeders, which use internal gravimetric control based on load cell measurements. Gravimetric control greatly reduces the risk of feeder error. However, a few hazards that may arise and have been identified as the following:

- Poor load cell calibration can cause the feeder to dispense at the wrong rate with the feeder's controller unable to detect an issue. This is an operator error that will require system shutdown to correct. Detection depends on downstream PAT or monitoring the feeder's drive speed. A calibration problem may be indicated by significant deviation from the historic behavior of the feeder's screw speed while the reported load cell measurements remain within range.
- Some feeder fluctuation (See Figure 6.10a) is unavoidable. Fluctuation can be minimized with proper design, but still poses a potential risk.
- Disturbances can lead to deviations (i.e. hopper refill). See Figure 6.10b. The most common cause of significant deviations in the feedrate of the feed stream is

caused during hopper refill. When refilling, the feeders temporarily operate in volumetric mode and therefore do not correct for the density changes associated with hopper refill. This can be minimized with refill scheduling optimization, but still needs to be considered a potential risk. [100]

- Downspout accumulation (See Figure 6.10c) can cause a sudden rise in concentration of a component if accumulated material suddenly breaks off and falls. This typically indicates a design problem and requires redesign. However small accumulation may still occur.
- Feeder bearding (See Figure 6.10d) can also pose a risk when the material suddenly discharges and falls.

This above list of common feeding hazards is not exhaustive. Depending on the formulation and process, there may be other unlisted hazards, or the ones listed here may not be relevant. The cases displayed in Figure 6.10 are all extreme cases, and will not necessarily occur to the same degree with every powder. These can be summarized into two difference cases that require analysis: fluctuations and pulse disturbances.

6.5.2 Feeder Fluctuations and Filterability of the Mixer

Due to the intrinsic nature of feeders, there will be some degree of variability in the feed stream. This variability can be minimized through feeder and tooling selection, [5], [61], [101], but in any case these fluctuations need to be quantified, and the system needs to be designed to handle these unavoidable variations. Typically feeders would feed individual components into a continuous blender, blending them into a homogenous mixture through radial mixing. If the blender were a perfect plug flow mixer, then the variations from the feeders will pass through the blender causing variations in content uniformity.

Axial mixing within the blender enables a secondary function of smoothing or filtering out feeder variability. The degree to which this occurs depends on the residence time distribution (RTD) of the blender and the magnitude and frequency of the fluctuations from the feeder.

The relations between the feeder and the blender can be evaluated using the Fourier series analysis demonstrated by Gao *et al.* [62] This paper defines the filterability, which quantifies a blender's variance reduction ratio as a function of the frequencies of fluctuations. The filterability function can be derived from any residence time distribution. Similarly, the feed stream from a feeder can also be transformed into the frequency domain. [61], [101]

The effect of residence time distribution on an incoming feedstream is shown in Figure 6.11 and Figure 6.12. Figure 6.11a shows a very narrow RTD and Figure 6.12a shows a broad distribution. Using the same feedstream, a bi-modal sine wave with frequencies of 0.05hz and 0.1hz, results in very different behavior as shown in Figure 6.11b and Figure 6.12b. For the narrower distribution, the bi-modal sine wave is only shifted in the time scale, but the shape is nearly identical before and after the blender. For the broad distribution, which has significantly more back-mixing, the higher frequency is filtered out, and the amplitude of the lower frequency is reduced. These results are more clearly reflected in the frequency domain plots of Figure 6.11d and Figure 6.12d.

For the filtering ability plots in Figure 6.11c and Figure 6.12c, a value of 1 indicates that fluctuations will pass through, and a value of 0 indicates that the fluctuation has been spread, and therefore reduced in magnitude. Figure 6.11c shows the filtering ability for

the narrow distribution, which will not filter out most fluctuations with frequencies longer than 0.15 Hz. In contrast, Figure 6.12c shows the filtering ability for the broad distribution, which filters most fluctuations above 0.05 Hz.

The effect of changing the parameters of the tanks in series model are shown in Figure 6.13 and Figure 6.14. Figure 6.13a shows the residence time distributions as the number of tanks was increased from 1, which resembles a CSTR, up to infinity, which resembles that of a PFR. As the number of tanks was increased, the variance of the distribution decreases, which is indicated by a narrower distribution. Figure 6.13b shows that as the number of tanks increased the ability to filter fluctuations decreased, which is indicated by the filterability increasing towards a value of 1.

Figure 6.14a shows the effect of increasing mean residence time on the shape of the residence time distribution. The mean residence time was increased from 1 to 25 using the tanks in series model. Due to the arrangement of parameters within the equation of the model, an increase in mean residence time also increases the variance, which is shown by the broadening of the distribution. This resulted in a significant amount of back-mixing, which improved the ability to filter fluctuations as shown in Figure 6.14b. Since the tanks in series model is a mono-modal distribution, the filtering ability tends to decrease down to 0 with increasing frequency. This indicates that lower frequencies are more likely to pass through, whereas higher frequencies will be smoothed and filtered out entirely.

6.5.3 Traceability of Pulse Disturbances

6.5.3.1 Simulated Pulse Disturbances

With the potential hazards identified, the next step of a quality risk assessment is the analysis and evaluation. For content uniformity, out of specification product is of high risk due to severity and thus would need to be addressed. For most of the hazards identified above, the result is a sudden pulse-like addition of a component, which may cause a significant deviation from product content specification. Using the residence time distributions for each unit operation and the system as a whole, the significance of any pulse addition can be quantified via simulation.

Consider a pulse input into the mill, such as from feeder bearding or downspout accumulation breaking off and falling. Figure 6.15a shows the response of a 0.25g pulse into a direct compaction system with an overall throughput of 30 kg/hr and a nominal active pharmaceutical ingredient (API) concentration of 6%. The API pulse in the feed stream occured at 300s with the response from the mill immediately following. The spike in API concentration after passing through the blender occured between 325s and 375s, which added a significant amount of spreading due to back-mixing. Finally, the tablets exited between 800s and 900s. This resulted in tablets within specification, <7.5% (125% of 6%), meaning that no action was needed. However if the pulse was increased to 1g, as shown in Figure 6.15b, there would be tablets out of specification (OOS). In this case, the OOS material should be removed from the product stream.

If material testing indicates a high probability of one of the identified hazards rather than a rare exceptional event, then the system should be designed to handle that hazard. Figure 6.16 shows the results for a system where the blade pattern in the continuous

blender was changed, which caused it to have a broader residence time distribution. This resulted in a more robust system that could handle a 1g pulse of the API without generating OOS product.

6.5.3.2 Sampling Frequency / Adequate PAT

Online process analytical technology is crucial for control of any continuous manufacturing process. However, its implementation is not as simple as adding sensors to measure properties of the blend at various stages in the system. Measurement needs to be meaningful, which requires a measurement that is representative and timely. In batch manufacturing, the challenge is typically obtaining a measurement that is representative of the batch, because sensors or sampling are very localized. In continuous manufacturing, timely measurements are the larger challenge.

It is important to highlight a critical difference between a batch process and a continuous process. A batch process varies with time, whereas a continuous process varies primarily with respect to the spacial dimension. This means that the measurement at a fixed location in a batch process will be different at the beginning as opposed to the end. In a continuous process, this is not the case. If a sensor was fixed at the entrance to a continuous blender, the sensor would see the individual unmixed components throughout the entire processing time. If the sensor was fixed at the exit of the blender, the sensor would see a fully mixed blend after a short steady-state startup time and until the line is shutdown. A sensor in a batch process only measures the final blend at the end of processing, whereas a continuous process conducts many measurements of small sections of the final blend throughout processing. Therefore, the measurements from the

continuous process are more representative of the entire product stream (and therefore, of entire batches).

In a continuous system, the most meaningful measurement is to characterize the intensity and frequency of fluctuations in the process stream. This means the sensors must be fast enough to detect any of these disturbances, ensuring nothing important passes the sensor undetected. This would be equivalent to a high concentration pocket or a segregated section not being detected in a batch process, due to the section not being within a sampling region. To ensure that this does not occur in continuous processing requires investigating how a fluctuation would spread in the process. The most difficult fluctuations to detect in a feed stream are narrow pulses, but as they progress along the system, pulses are spread based on the residence time distribution (RTD). Thus, the RTD contains the information needed to design the sensing system in order to ensure that pulse fluctuations do not travel through the system undetected

Figure 6.17 shows an example residence time distribution from the continuous blender. In this plot, the mean (68.8s) is represented with a single vertical red line, and the standard deviation (22.4s) is represented with two green vertical lines spaced on either side of the mean by the value of the standard deviation. It is logical to assume detection of the downstream response is easier than detecting the pulse disturbance itself. If the system were “plug flow”, the perturbation would be largely unchanged as it travels along the system, meaning that a pulse into the system would result in a pulse response. This would be difficult to detect without a very rapid measurement. Fortunately this is not the case, and the sampling frequency only needs to be fast enough to catch a disturbance equivalent in shape to the RTD. A reasonable approach is to use a sampling or

measurement regime that results in three to five measurements across the time interval represented by double the width of the RTD, which is quantified by its standard deviation. The following equations can then be used to define the maximum time between sampling and the minimum sampling frequency:

$$\tau_{sampling} = \frac{2\sigma}{n_{samples}} \tag{6-17}$$

$$f_{sampling} = \frac{1}{\tau_{sampling}} = \frac{n_{samples}}{2\sigma} \tag{6-18}$$

where $n_{samples}$ represents the number of samples and σ is the standard deviation of the RTD. For the RTD represented in Figure 6.17 this would result in a sampling time of 8.96s to 14.93s or a sampling frequency of 0.7 to 0.1 Hz. Utilizing high frequency PAT sensors as defined by Equation (6-18) would ensure adequate sensing to determine the approximated shape of the RTD. Aided by a simple peak detection algorithm most significant spikes can be easily detected.

However, using 125% concentration as an upper limit for detection with a binary pass or fail outcome may result in smaller anomalies passing the PAT system undetected, resulting in small amounts of superpotent product unless the sampling frequency is extremely high. Figure 6.18 shows the pulse response to various size pulses that result in differing amounts of superpotent product. The percentages for out of specification (OOS) product were calculated based on an assumed "batch" size based on 15 minutes (900s) of continuous processing. Large deviations such as the one that results in 5% OOS product, as shown in Figure 6.18, will easily be detected as there will be several measurements indicating OOS material. Whereas the smaller deviations, 1% and 2% OOS, do not exceed 125% API concentration by much nor for very long, making online detection a challenge.

Figure 6.19 shows the percent chance of detection for various deviations, resulting in 1%, 2% and 5% OOS product, as a function of increasing sampling rate. With increasing sampling frequency, the probability of detection increases and eventually reaches 100%

for all three cases. Since the larger deviations are easier to detect, the detection percent is highest for 5% OOS at any sampling frequency, which is followed by 2% OOS, and finally 1% OOS. The chance of detection reaches 100% at the following sampling frequencies (and sampling time intervals) for the various deviations: 0.022 Hz (45s) for 5% OOS, 0.056 Hz (18s) for 2% OOS, and 0.111 Hz (9s) for 1% OOS. This means that at any of these sampling rates there is 100% coverage for deviations of that respective size. However, as the percent of OOS material decreases closer to 0% the ability to detect these very small deviations requires infinitely faster sensing.

To increase the ability of slower or less accurate PAT sensors to detect OOS material, the upper limit for binary pass/fail criteria should be lowered. To detect a deviation at even the smallest deviation above 125% requires sensing the limit where a single point reaches 125%. Figure 6.20 shows this limiting concentration profile that peaks at 125% API concentration and shares the shape of the RTD displayed in Figure 6.17. Lowering the upper limit to 121.75% results in material that exceeds the limit for 22.4s, which is also the standard deviation of the RTD. Assuming a sampling frequency as defined by Equation (6-18), would ensure that a few measurements are made during this interval allowing for adequate detection. Figure 6.21a shows a depiction of the material that would fail if the upper limit were reduced to 121.75%, and Figure 6.21b shows the corresponding chance of detection plotted as a function of increasing sampling frequency. The chance of detection reaches 100% at the following sampling frequencies (and sampling time intervals) for the various deviations: 0.02 Hz (50s) for 5% OOS, 0.036 Hz (28s) for 2% OOS, and 0.042 Hz (24s) for 1% OOS. For comparison, the similar plots for the case using 125% as the upper limit are also shown, but as dotted lines. For the smaller deviations, 1% and 2% OOS, the improved detection ability is dramatic, whereas the larger deviation, 5%, has less improvement.

The advantage of the continuous measurements of PAT versus sampling of a batch after processing is shown in Figure 6.22. The sampling frequency for the continuous PAT measurements were translated into number of samples based on an assumed 15 minutes of processing for a batch allowing for direct comparison to a batch with a similar amount of OOS material. The batch curve assumes the sampling is completely random, differing

from the continuous case which utilizes PAT. The PAT sensors have a set sampling frequency, which ensures that each measurement is observing a different section of material. Therefore, the sampling coverage and ability to detect all deviations will rapidly approach 100%, at which point no deviation will pass the sensors undetected. To reach this same amount of coverage, a completely random or batch process will require orders of magnitude more samples. An initial comparison of continuous versus batch processing made from this plot is that there will be more correctly failed batches for a continuous process. However, this is not entirely the case, as these PAT sensor measurements allow downstream batch correction, such as a rejection chute, ensuring batches that would have failed do not contain any OOS material and therefore are of higher quality than batch processing with random sampling could ever achieve.

6.6 Conclusions

Methods were presented to address challenges of batch definition, raw material traceability, and adequate PAT sensor frequency as it pertains to continuous manufacturing with reference to regulatory requirements and guidances that offer little explanation on sensible implementation. Although batch definition is left open for the manufacturer to specify, other requirements, such as recording specific identification for each component within the batch records, makes production changes, such as a feedstock lot change, a favorable factor for specification. To minimize crossover between batches, it was suggested to measure residence time distribution to quantify and define reasonable boundaries to remove the interface between batches, which may contain multiple batches of components.

To access and control risks associated with content uniformity, higher probability hazards were identified, categorized, and investigated. Solutions to these potential risks were presented where raw material traceability was a prevalent focus and a significant part of the solution. Residence time distribution (RTD) play an important role in raw material traceability as it characterizes the spreading of the materials through the system. Thus, a disturbance could be predictively tracked through the entire continuous system, allowing for downstream control or even removal of the affected material.

An important requirement of any PAT instrumentation is the reliability of the measurements, which includes a sensing frequency high enough to detect all significant disturbances. Since pulse disturbances would require an extremely fast sensor for detection, it was suggested that a downstream sensor could be used. This would not require such high frequency sensing, but instead would only need sensing fast enough to detect the downstream response, which would have the shape of the RTD. This resolves the potential issue of OOS material passing through to the product undetected, and also setup up some of the conditions needed for real time release testing (RTRt). RTRt also requires verification that the measurements from PAT instrumentation reflect the testing results that would be collected in traditional batch release testing.

Although the methods described focus on direct compaction, they apply to any continuous processing system. To apply these methods to other continuous formulating techniques requires only minor changes. Together, the methods presented in this work bring continuous processing in the pharmaceutical industry to the point of understanding for actual commercial installations.

6.7 Figures for Chapter 6

a.  b. 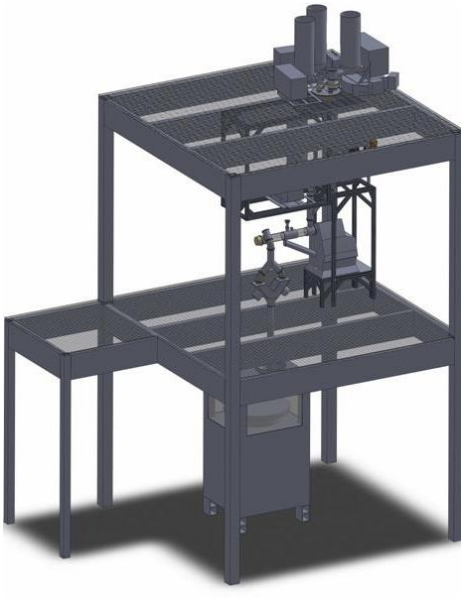

c. 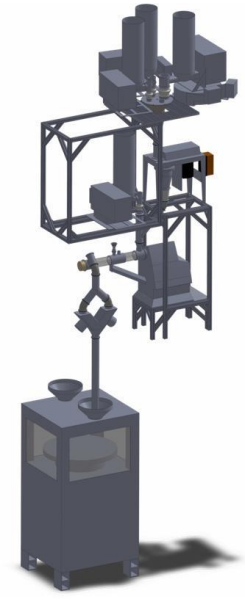

Figure 6.1: ERC-SOPS Prototype Direct Compaction Line located at Rutgers University: a.) Photo of the platform, b.) Model of the platform, c.) Simplified model of the system showing the connected unit operations without the scaffolding.

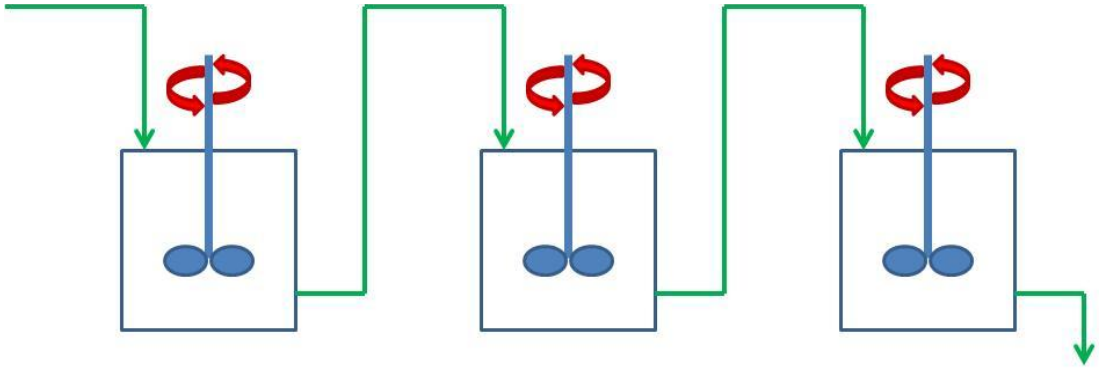

Figure 6.2: Depiction of the tanks in series model where n=3.

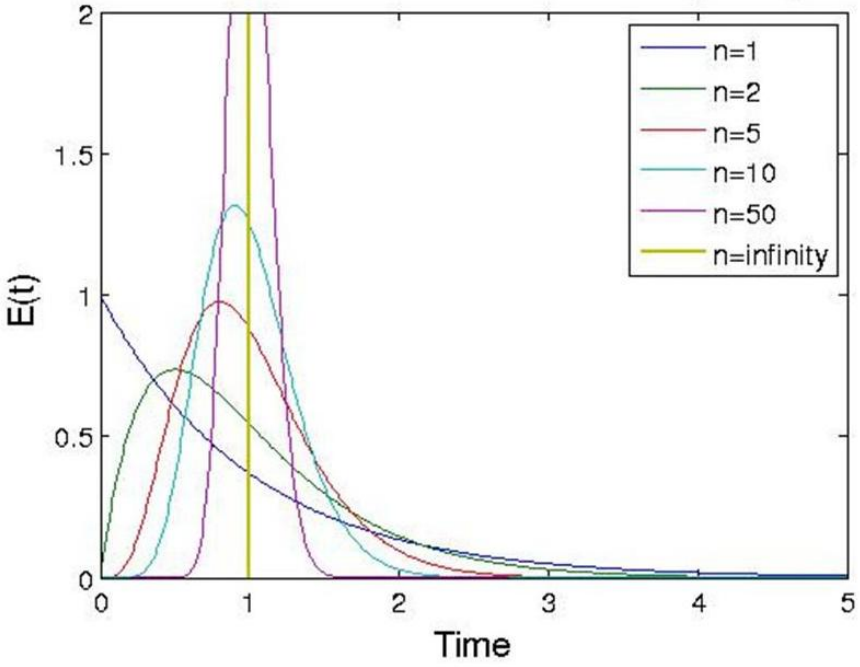

Figure 6.3: Residence time distributions for tanks in series model having a mean residence time of 1 and a number of tanks ranging from 1 to infinity.

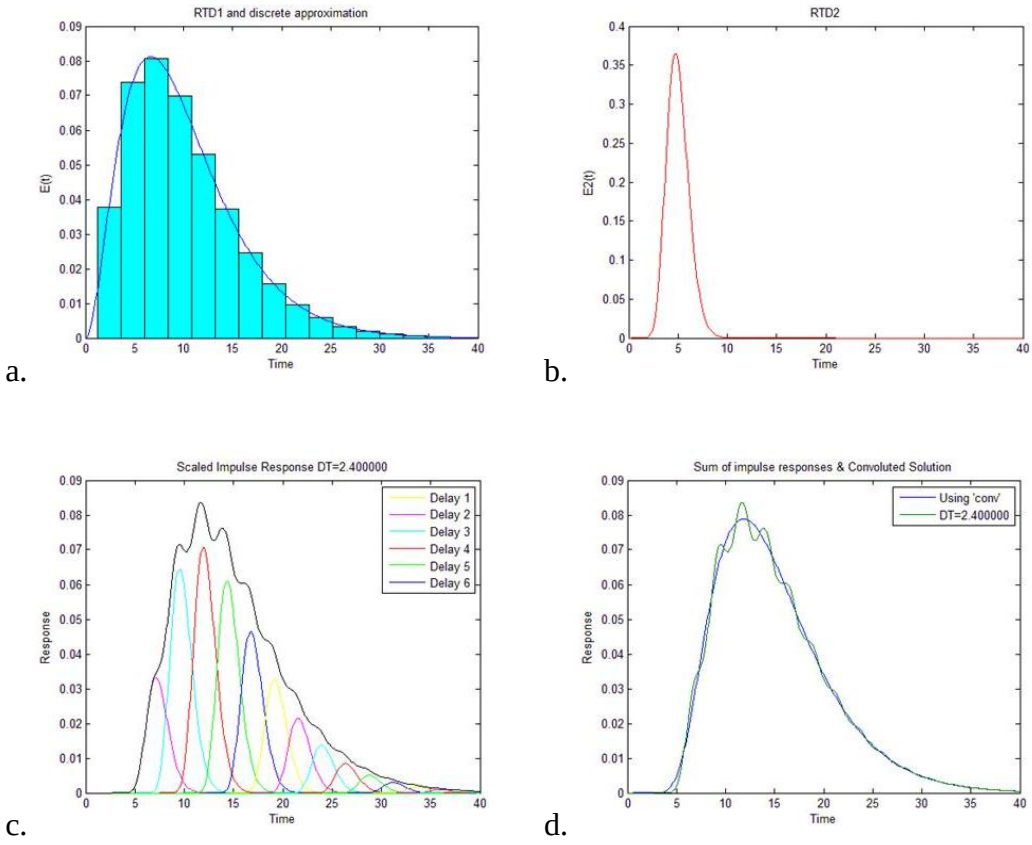

a. b.

c. d.

Figure 6.4: Visual representation of the convolution technique for two residence time distributions (RTD), E1 and E2. a.) Discrete approximation of E1, b.) E2, c.) E1's Discrete approximation-scaled responses of E2 and their sum d.) Sum of impulse responses for a time interval of 2.4s and result from convolution function.

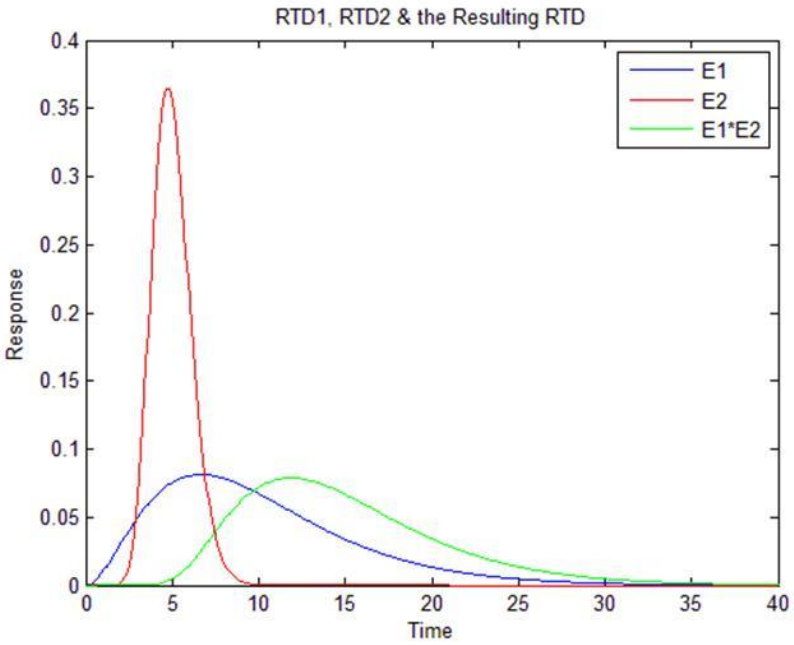

Figure 6.5: Representation of the convolution of two residence time distributions (RTD), E1*E2, plotted with the two component RTDs, E1 and E2.

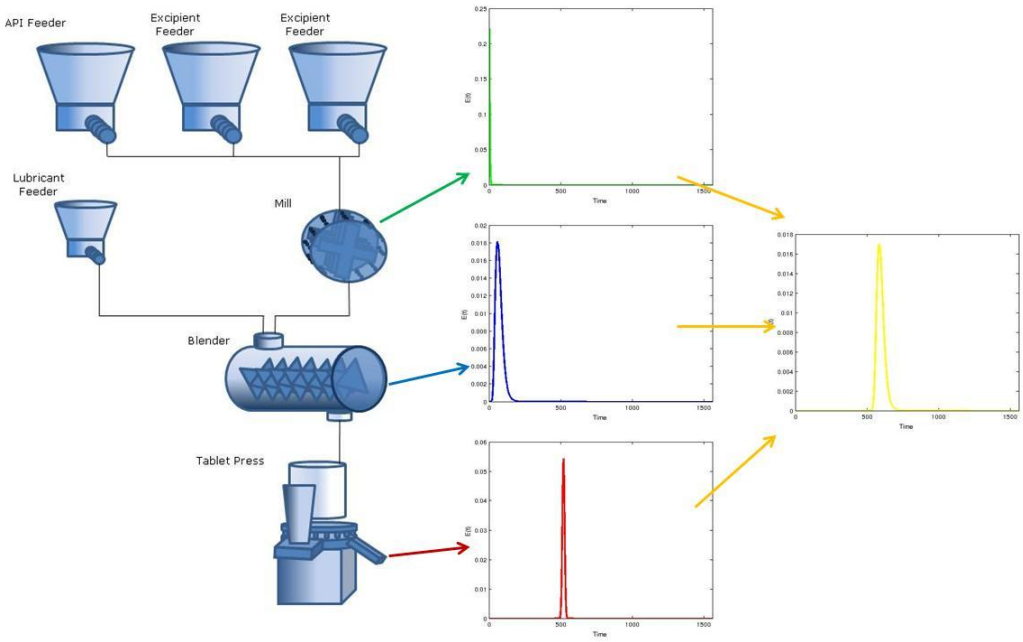

Figure 6.6: Residence time distribution of the individual unit operations and overall system.

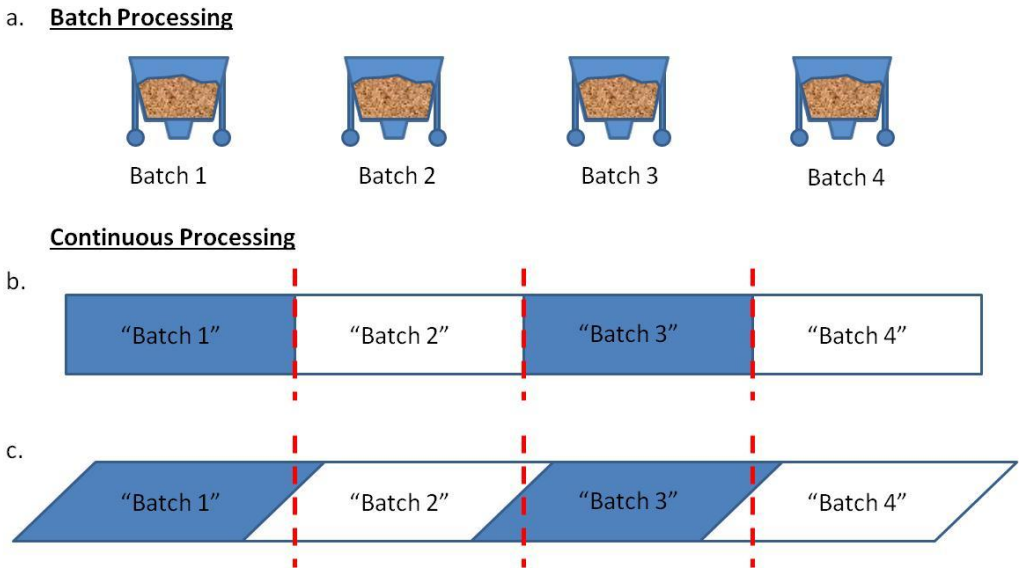

Figure 6.7: Visual comparison of batch definition for: a.) "Traditional" Batch processing, b.) Continuous "Plug Flow" Processing, and c.) Realistic (non-plug flow) Continuous Processing. The dotted-lines represent arbitrary divisions between batches.

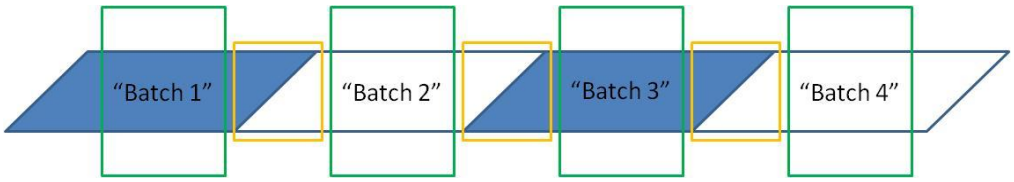

Figure 6.8: Depiction of batch definition for continuous processing, which removes the interface regions (in yellow boxes) between batches. The remaining material between these regions then become the batches (in green boxes).

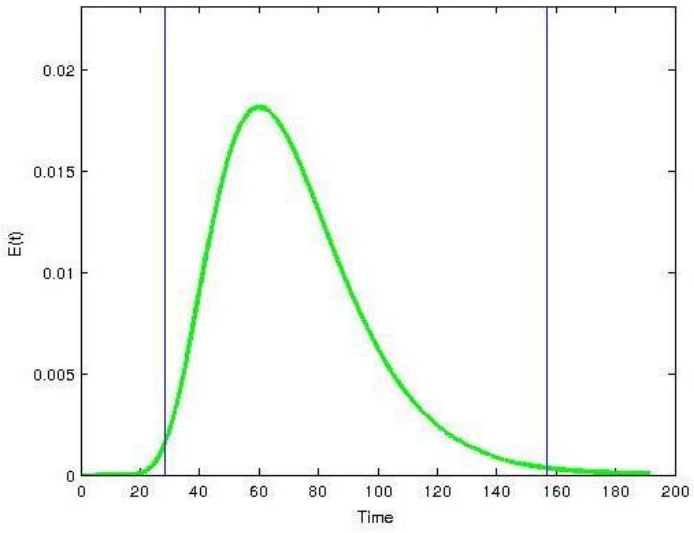

a.

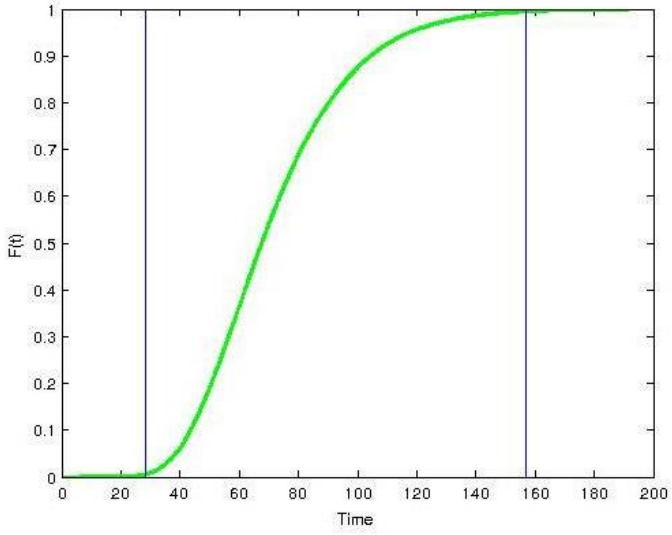

b.

Figure 6.9: Define the boundaries of a batch for a continuous process by using: a.) residence time distribution (RTD) and b.) cumulative distribution function (CDF). The boundaries shown here are 0.5% and 99.5%, which may not be the ideal values, but were chosen to demonstrate this exercise.

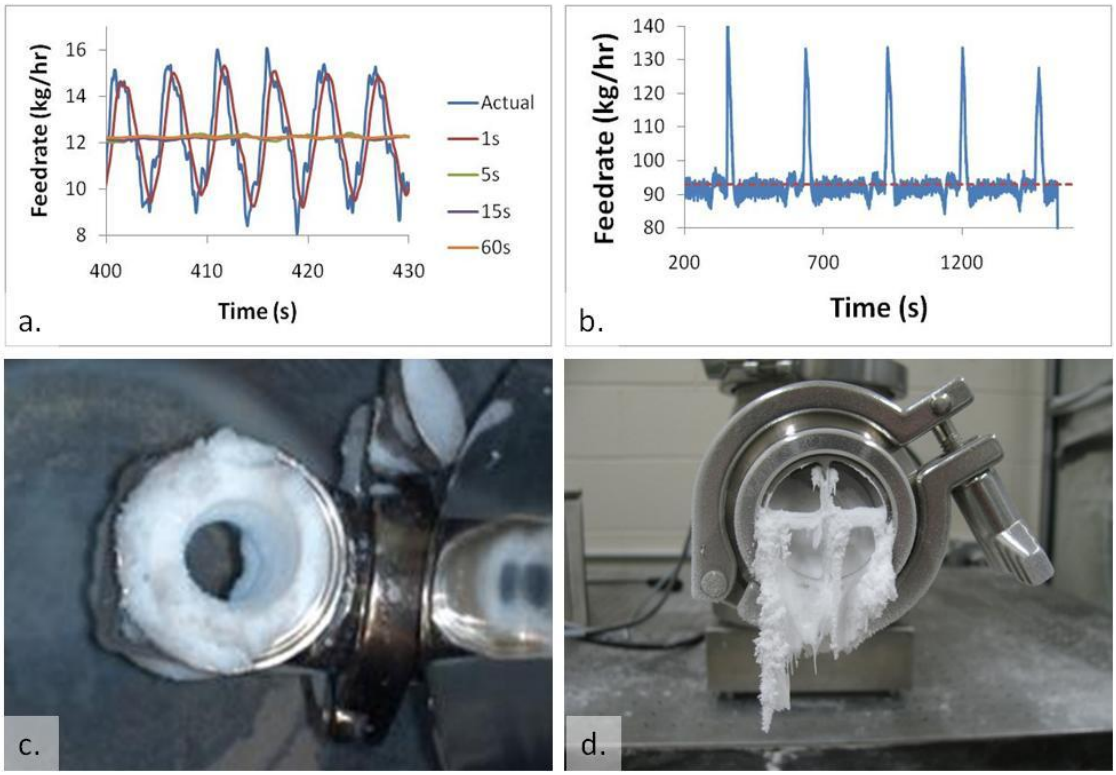

Figure 6.10: Sources of content uniformity variability: a.) Feeder Fluctuations, b.) Deviations caused by refill, c.) Downspout accumulation, d.) Feeder Bearding.

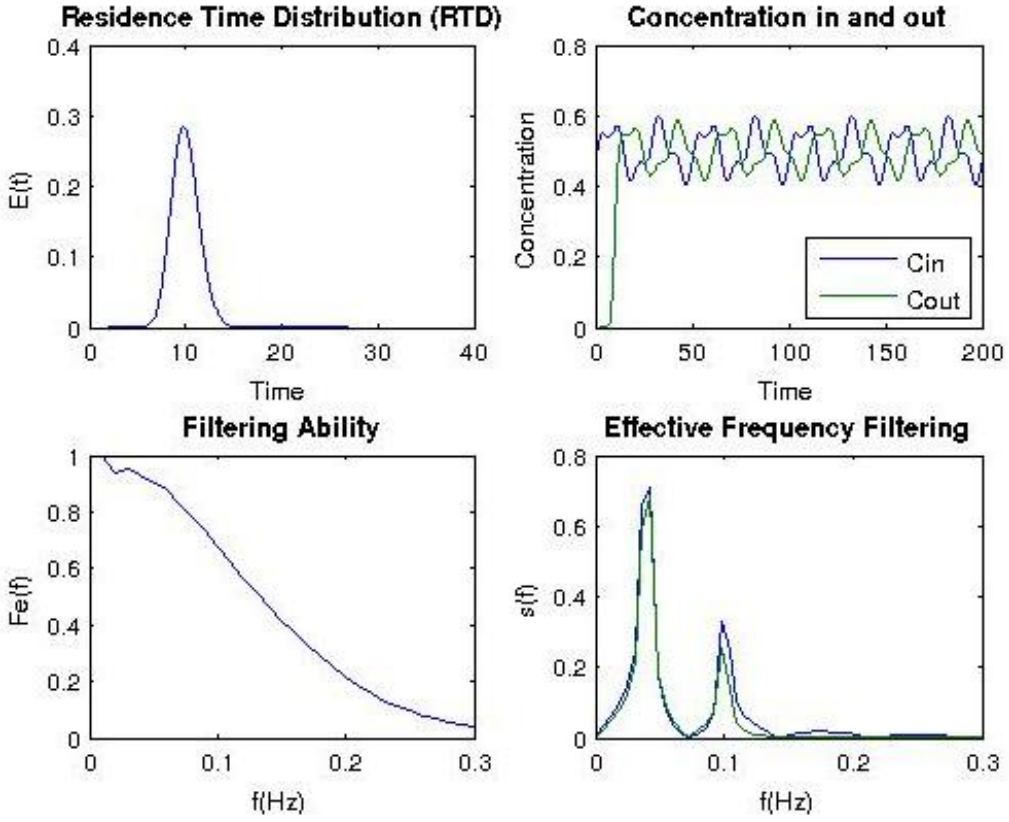

Figure 6.11: Simulated results for a bi-modal sine wave feed stream being fed to a blender with a narrow residence time distribution (in comparison to Figure 6.12). a.) residence time distribution, b.) concentration profiles for the inlet and outlet of the blender, c.) calculated filtering ability of the blender as a function of frequency, d.) frequency domain of inlet and outlet streams.

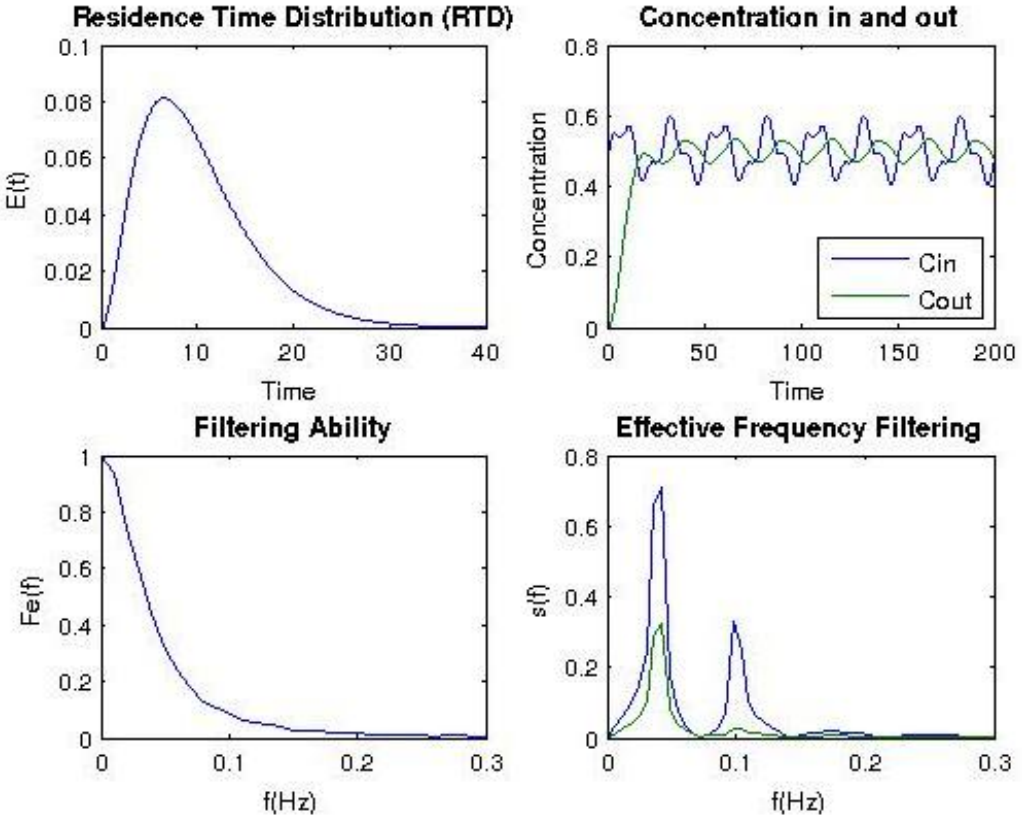

Figure 6.12: Simulated results for a bi-modal sine wave feed stream being fed to a blender with a broad residence time distribution (in comparison to Figure 6.11). a.) residence time distribution, b.) concentration profiles for the inlet and outlet of the blender, c.) calculated filtering ability of the blender as a function of frequency, d.) frequency domain of inlet and outlet streams.

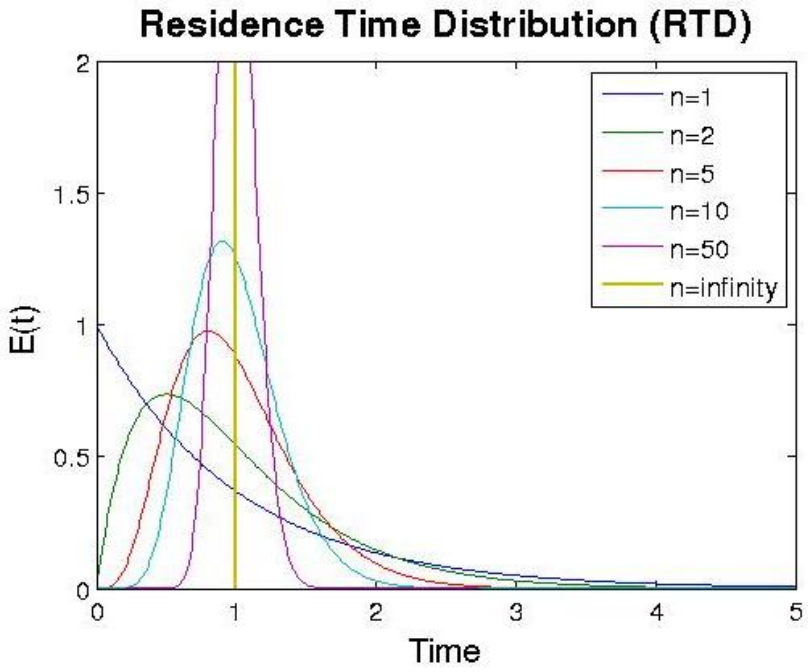

a.

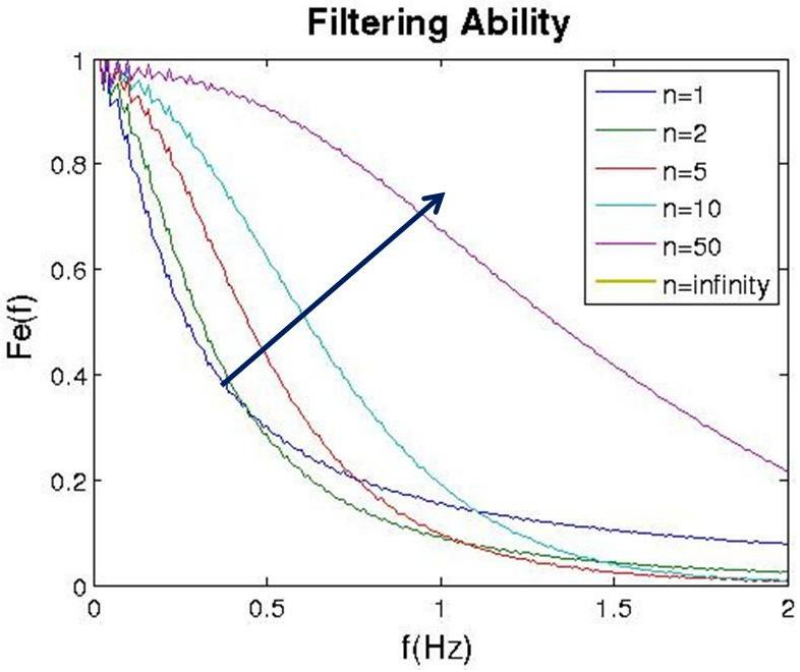

b.

Figure 6.13: Effect of changing number of tanks in the tanks in series model: a.) residence time distribution, b.) ability to filter fluctuations of different frequencies.

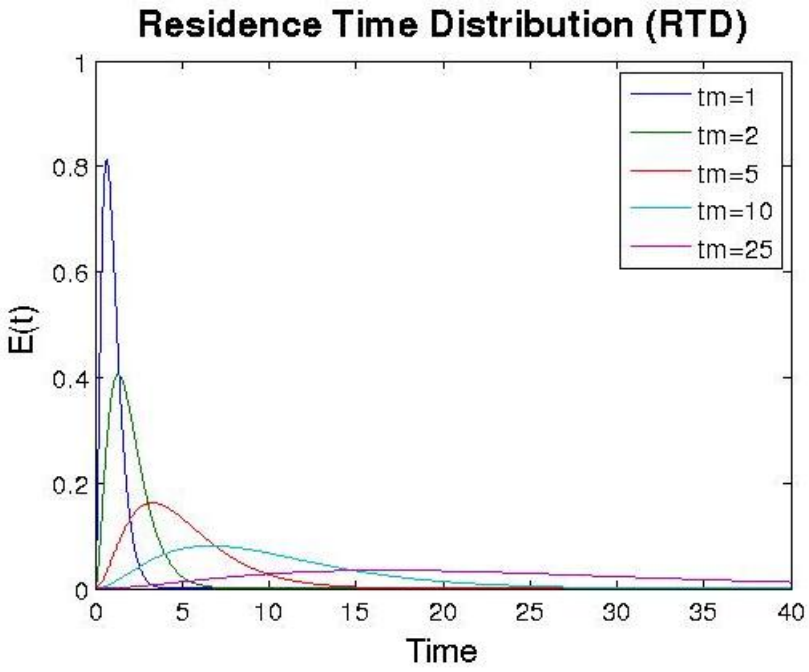

a.

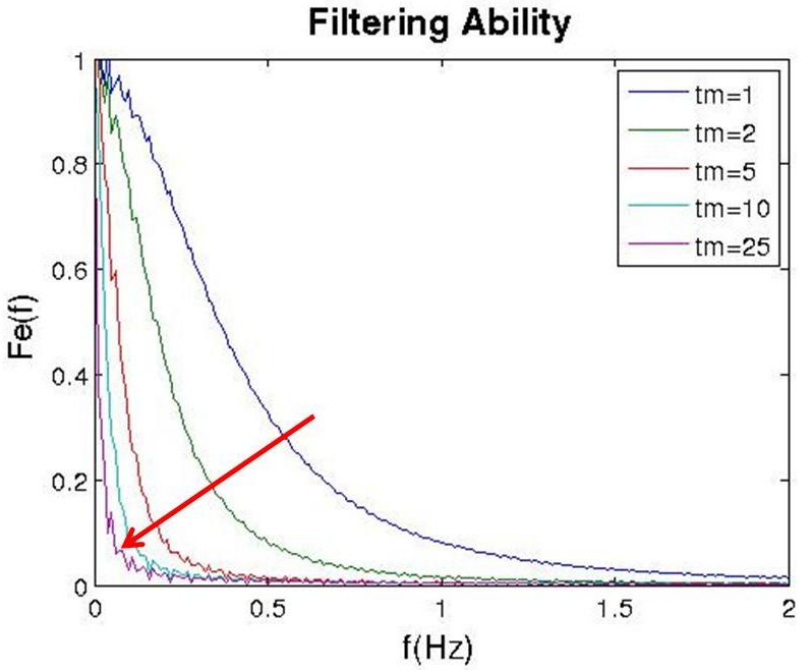

b.

Figure 6.14: Effect of changing the mean residence time in the tanks in series model: a.) residence time distribution, b.) ability to filter fluctuations of different frequencies.

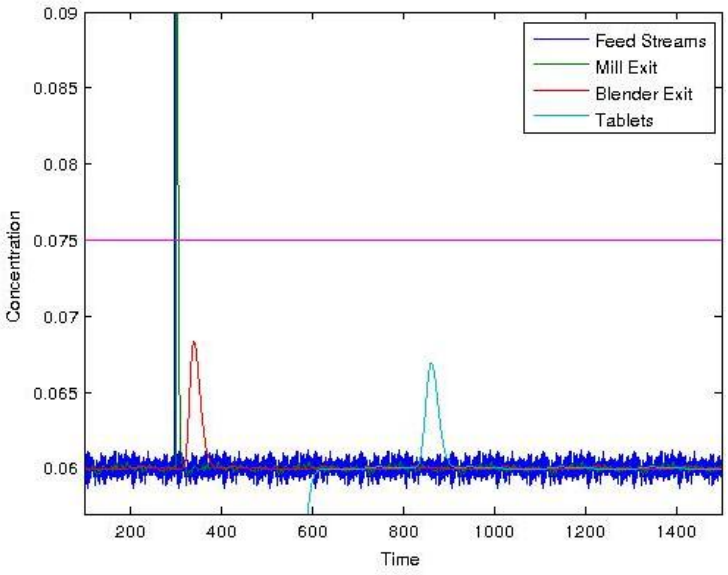

a.

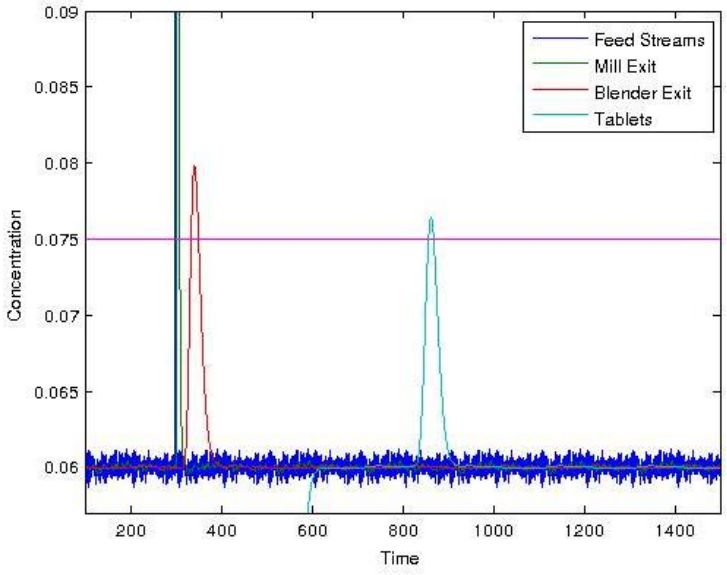

b.

Figure 6.15: Simulation results showing the active pharmaceutical ingredient (API) concentration profile for the various unit ops and their response to a pulse of API added to the entrance to the mill. The blender has a mean residence time of 41.6 seconds and a standard deviation of 12seconds. The size of the pulse is: a.) 0.25g, b.) 1g

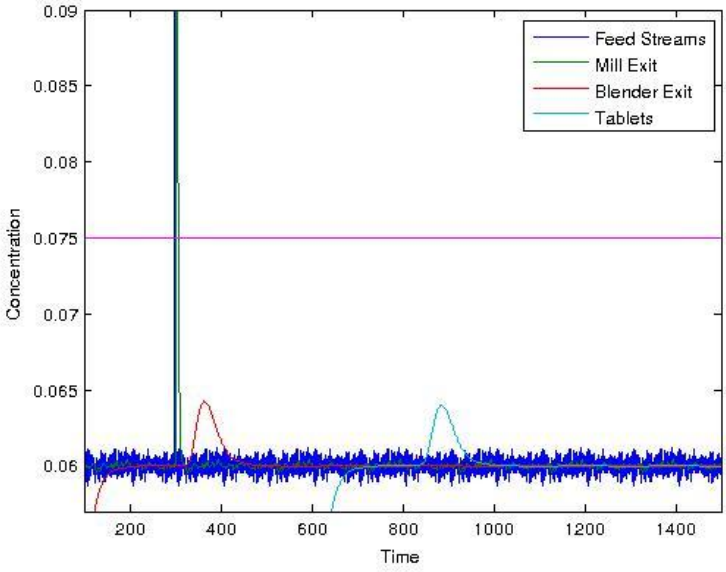

Figure 6.16: Simulation results showing the active pharmaceutical ingredient (API) concentration profile for the various unit ops and their response to a 1g pulse of API added to the entrance to the mill. The blender has a mean residence time of 71.7s and a standard deviation of 24.9s.

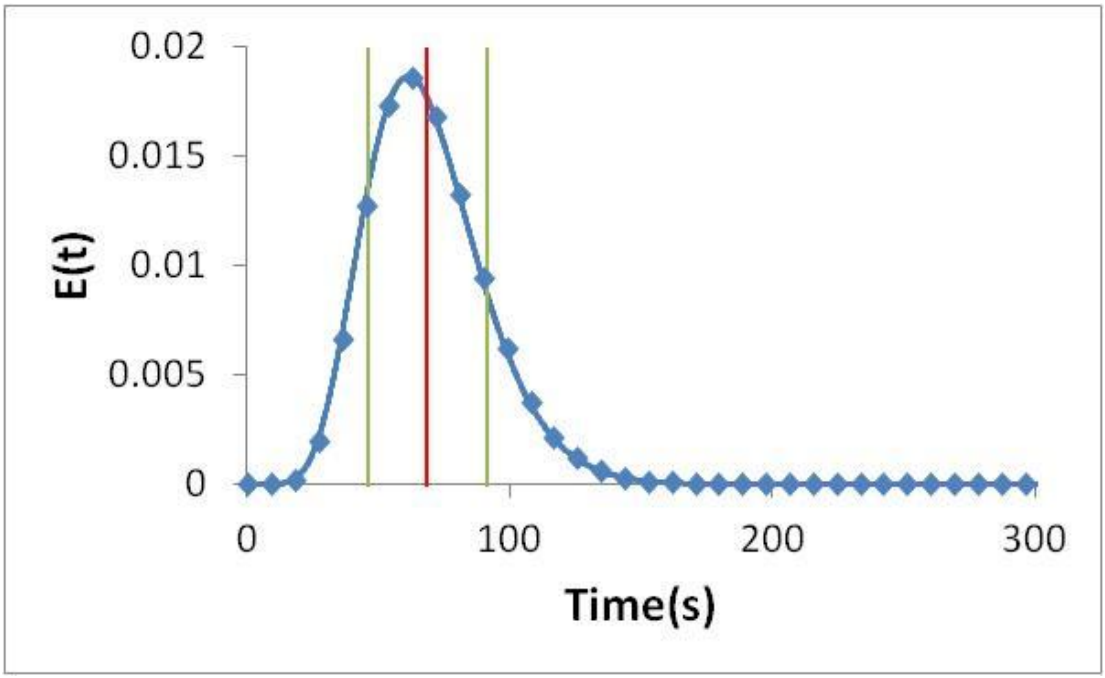

Figure 6.17: Residence time distribution with vertical lines representing the mean (68.8s in red) and standard deviation (22.4s in green). The sampling interval represented by the diamonds is 8.96s, which was selected based on using 5 points across double the standard deviation.

a.

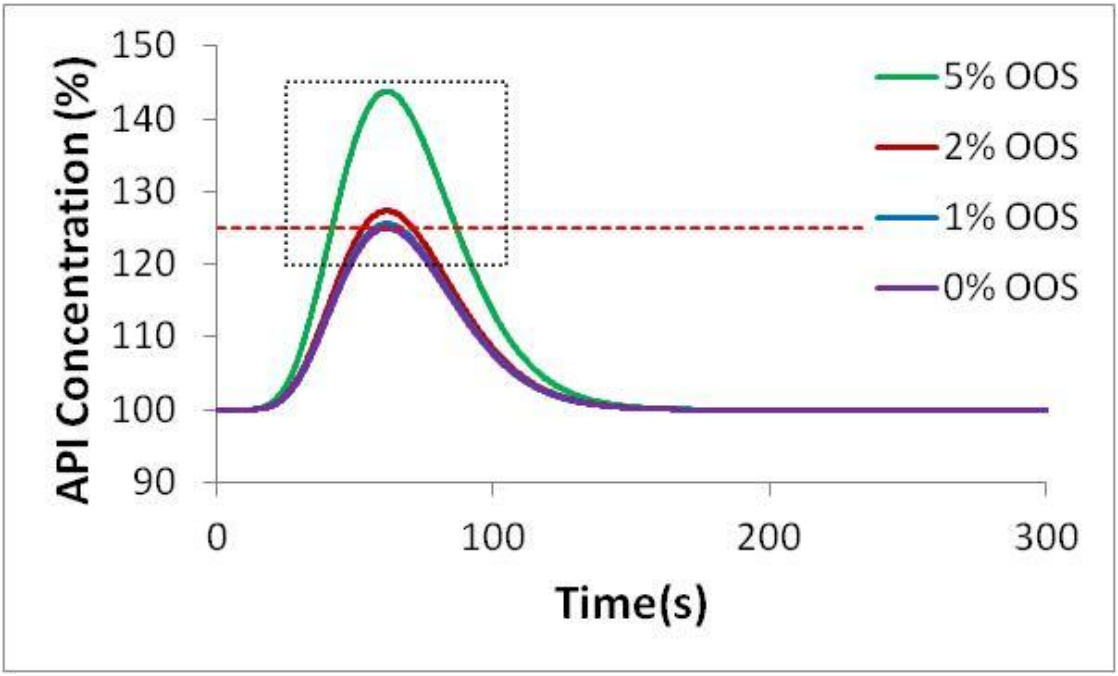

b.

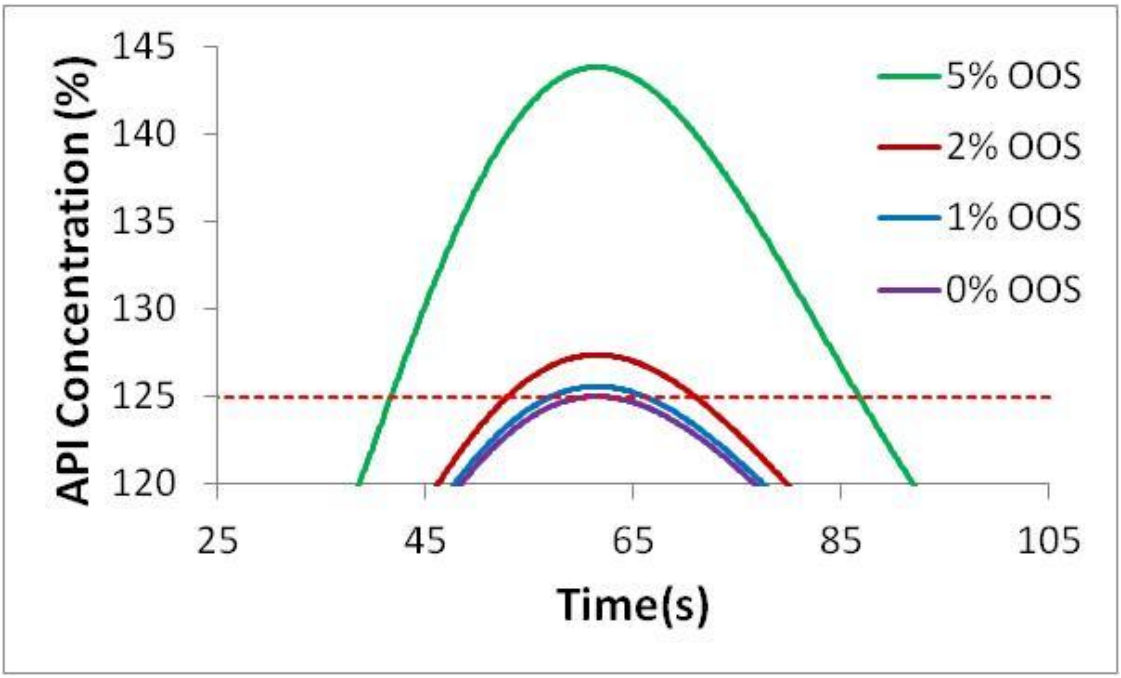

Figure 6.18: a.) API concentration pulse response resulting in various amounts of OOS material with a pass/fail value of 125% API concentration. b.) Zoomed version for better resolution of the peak.

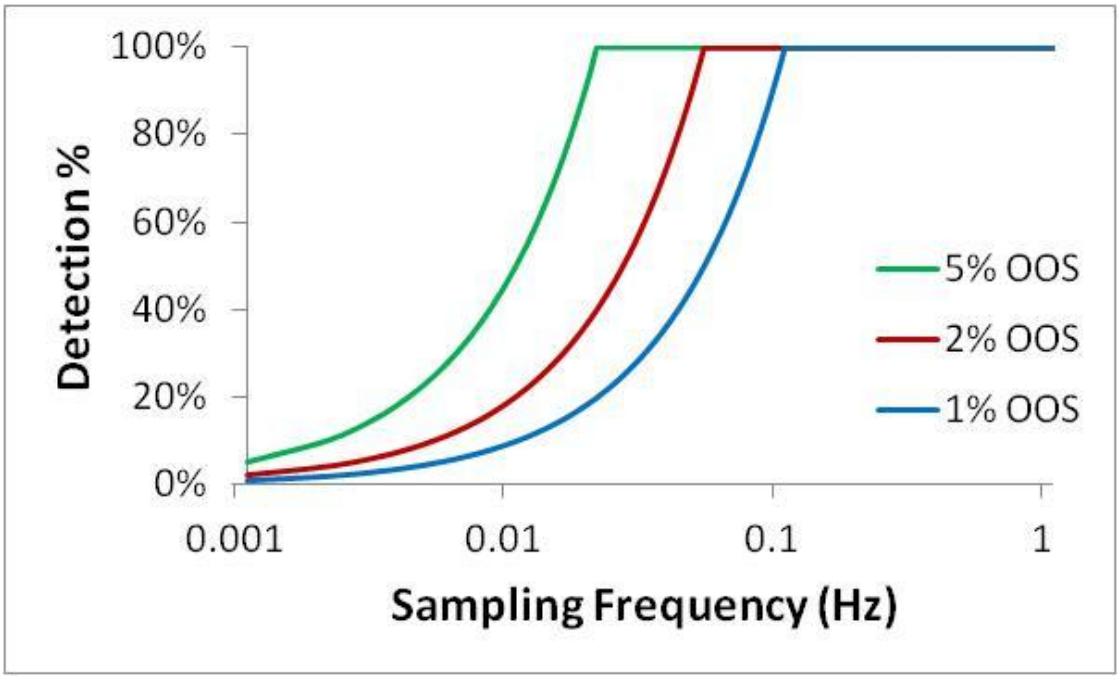

Figure 6.19: Probability of detection as a function of sampling frequency for pulses resulting in various amount of OOS material: 1%, 2%, and 5%

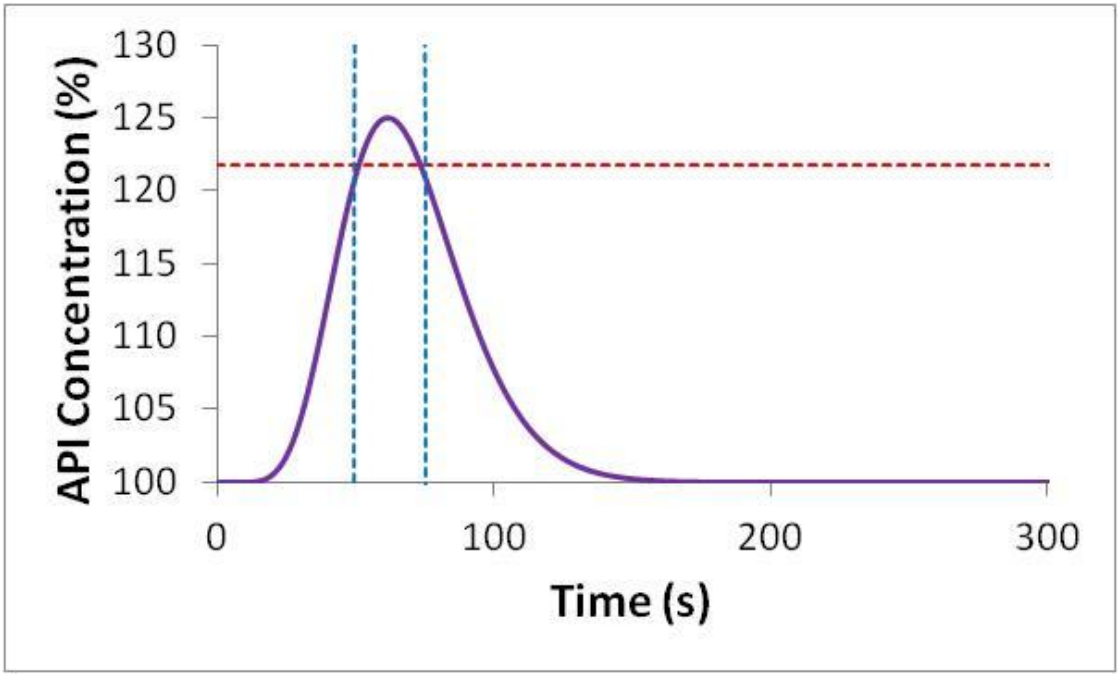

Figure 6.20: Concentration profile for a pulse response resulting in a peak of 125% concentration. The red horizontal dotted line indicates a 121.75% limit and the two vertical blue dotted lines indicate the width of the standard deviation (22.4s) of the corresponding RTD, which is show in Figure 6.17.

a.

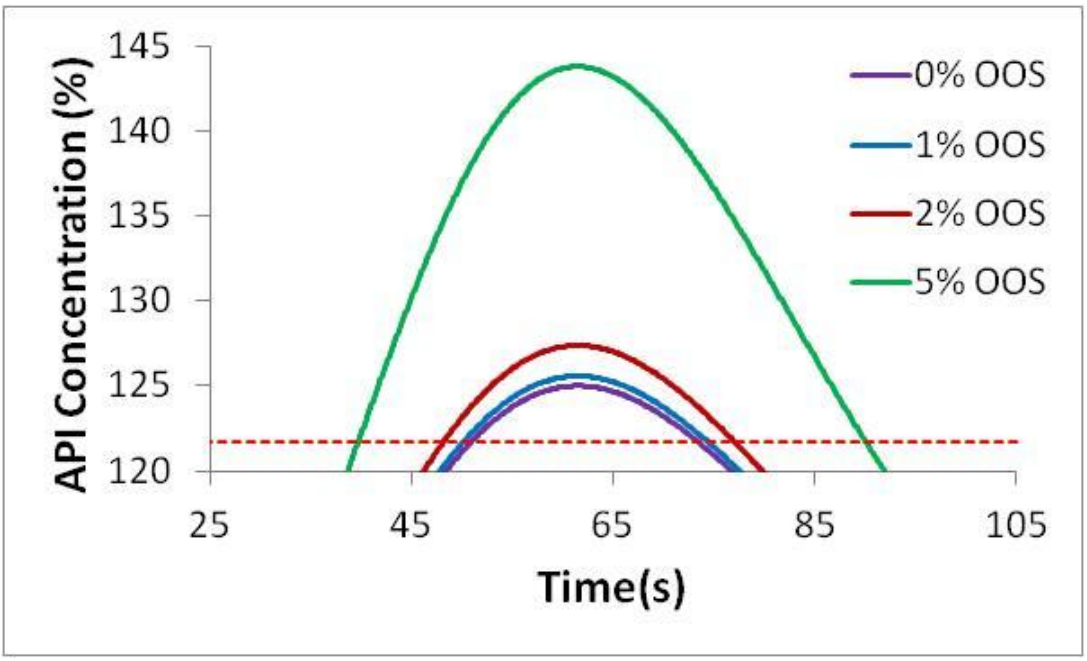

b.

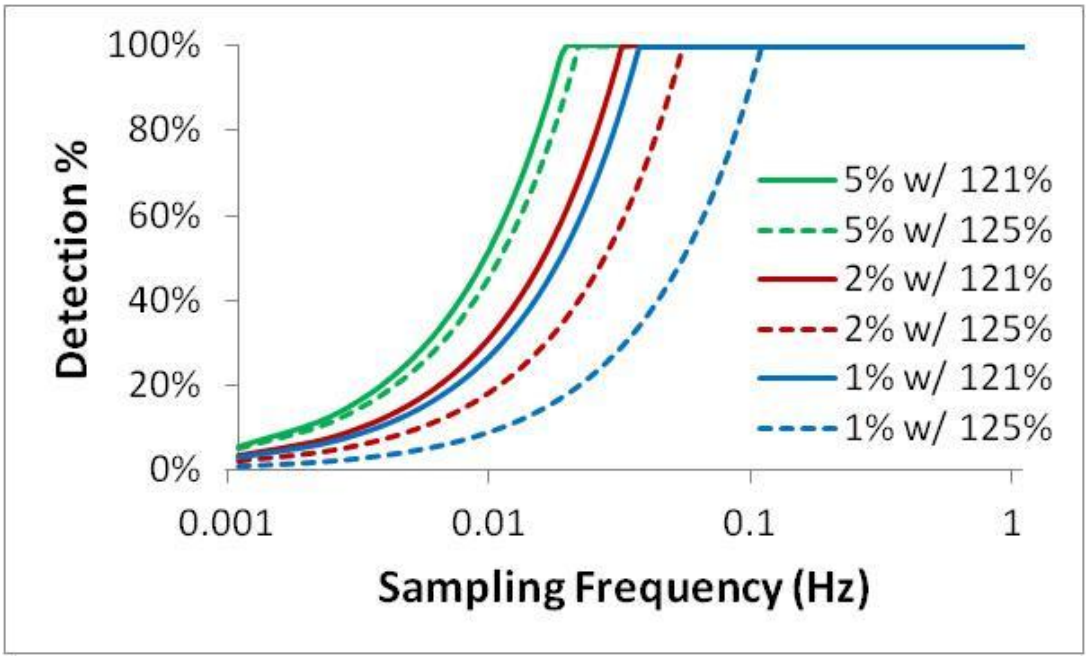

Figure 6.21: a.) API concentration pulse response resulting in various amounts of OOS material with a pass/fail value of 121.75% API concentration. b.) Probability of detection as a function of sampling frequency for pulses resulting in various amount of OOS material: 1%, 2%, and 5% for both 121.75% limit and 125% limit. OOS material is determined by 125% limit in both cases.

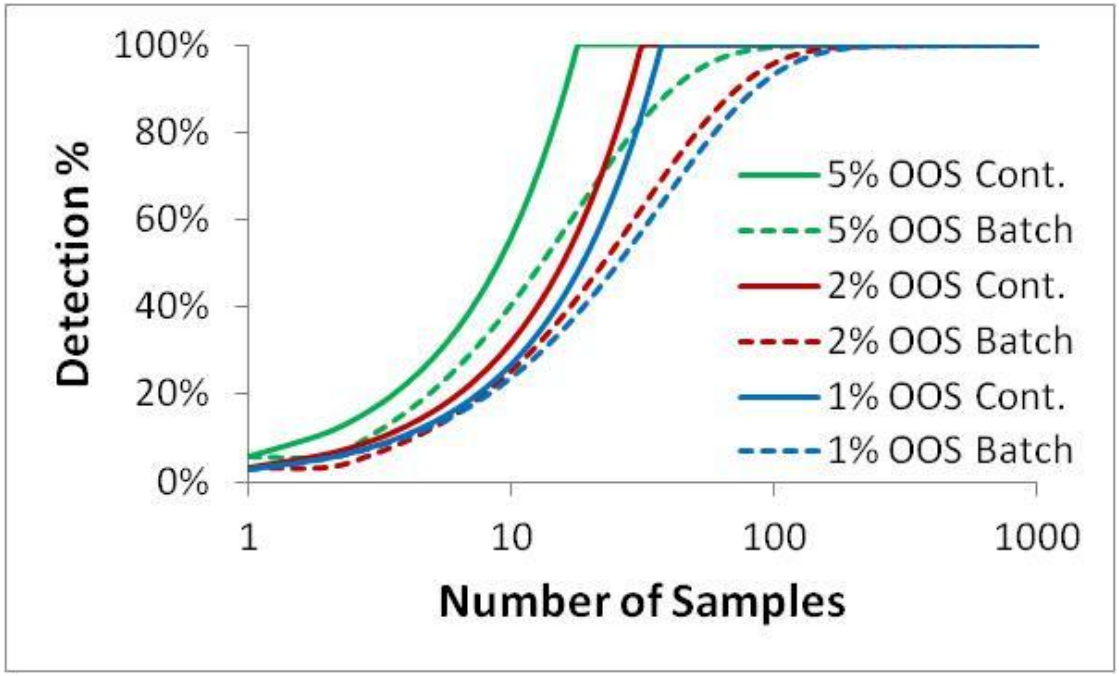

Figure 6.22: Probability of detection as a function of sampling frequency for pulses resulting in various amount of OOS material: 1%, 2%, and 5% for both a continuous process with online PAT (solid lines) and a batch process (dotted lines) with offline random sampling. OOS material is specified by an upper limit of 125% concentration, and the limit used for detection is 121.75% concentration.

Chapter 7. CONCLUSIONS AND RECOMMENDATIONS

7.1 Conclusions

This dissertation work is divided into four research aims. The first research aim is focused on the development of a method for characterization of feeding equipment and was detailed in Chapter 2. The experimental setup utilized a catch scale which collected the material dispensed from the feeder and recorded the mass as a function of time, which could be used to calculate the feedrate profile. The algorithm used for optimized filtering of irrelevant disturbances utilized a multipass iterative technique, which minimized the amount of removed data. This resulted in filter datasets that were used for determining the parameters that are useful for evaluating and comparing feeding consistency and performance, relative standard deviation and mean of the feed rate. This standardized method for characterizing feeding performance with an external loadcell removed biases of using the internal loadcells of the feeders. Although the values from the feeders' internal load cells are available, the filtering algorithms are proprietary and may vary significantly between the different feeders.

The second aim is focused on determining the steady state performance of the feeders for various operating conditions. This aim was addressed in two powder feeding trial case studies: components of a pharmaceutical formulation (Chapter 3) and grades of zinc oxide (Chapter 4). In the pharmaceutical formulation feeding trials, the multiple components of a direct compaction continuous manufacturing formulation were examined and optimized. This required individually optimizing the feeder and tooling selection of each of the five components: API, Prosolv HD90, Crospovidone,

Magnesium Stearate, and Colloidal Silicon Dioxide. The Prosolv HD90 and crospovidone easily resulted in optimal feeding conditions, whereas the other components presented some challenges. The API displayed flow issues, leading to clogging of the small holes of the screens. The magnesium stearate exhibited shear sensitivity; increasing shear of the powder due to mechanical hopper agitation resulted in drifting feeding performance (relative standard deviation). Colloidal silicon dioxide exhibited extreme electrostatic issues that render most tooling options unsuitable for consistent operation. Although the components are part of a formulation meant for direct compaction, the techniques can be applied to the sizing and tooling selection of a feeder for any set of powders.

The second case study investigated the optimization of feeding zinc oxide using three different feeders (Gericke GLD87, Gericke GAC232, and K-Tron KT35). Two comparable zinc oxide grades (Grillo Pharma8 and Norzinco CF8) were investigated. Quantified by the relative standard deviation of the feedrate, the feeding performance of these two zinc oxide materials was similar when comparing each other using the same feeding configuration. However, the performance was significantly affected by screw speed and tooling configuration. Differences in the powders were found to be driven by the difference in shear sensitivity. The Norzinco powder was the more shear-sensitive of the two and showed considerably more material degradation than the Grillo material. The use of discharge screens is not recommended with these materials, because the increased shear further degraded the materials. Samples were taken during the feedihng trials for each material and tested in the Freeman Tech FT4 powder rheometer. The FT4 tests that showed the greatest sensitivity for determining differences between feeding

conditions were the dynamic flow measurements, which resulted in the flow energy parameters, and the compression tests.

The third aim focused on investigation of the effects of powder feeder refilling and was covered in Chapter 5. To evaluate the effect of refill, the methods developed in Chapter 2 were modified. This required catch scale bucket planning to occur during the steady state feeding and not filtering out the effects of refill. The baseline determination used the filtering algorithm as described in Chapter 2. Three techniques for quantifying the deviation from setpoint were also developed: magnitude of the maximum deviation, the time that the feedrate is out of specification, and the total deviation or the amount of powder fed in excess of the setpoint. The main results show that the level the hopper refill is started is the most significant factor that can be used in mitigating the deviation caused during hopper replenishment. The use of discharge screens also showed a small improvement in the feeding accuracy. Another potentially useful method of reducing deviations during refill is to use refilling systems that have a lower more controlled rate of refill that gently replenishes the feed hopper rather than the high rate refilling of some replenishment systems. A larger volumetric feeder could be used as a rate controlled refill system.

The fourth aim focused on the downstream effects of feeding and were investigated in Chapter 6. Using the residence time distribution for the various unit operations in a continuous direct compaction system, the expected filtering or smoothing effect of feedrate fluctuations can be determined. The easiest unit operation to adjust the residence time distribution is the continuous blender, which makes it the ideal unit operation for adding robustness to pulse disturbances from the feeder. This chapter also focuses on the

regulatory requirements as they pertain to continuous processing. Methods for defining batches and adequate sensor frequency determination were also presented. All of the methods are based on sound engineering and mathematical principles of residence time distribution. All of the methods were discussed with a direct compaction manufacuring line in mind, but the techniques can easily be applied to other continuous manufacturing routes.

7.2 Recommendations for future work

7.2.1 Powder properties database correlation

One recommendation for future work for loss-in-weight feeding should move towards predictive measurements. For example, there would be much value in the creation of a powder properties database that could be used to predict the optimal feeder and tooling selection. Figure 7.1 shows the relative standard deviation (RSD) of feedrate for the K-Tron KT35 dosing fastflo lactose, avicel102, and ceolus. Ceolus is the most cohesive and results in the highest RSDs. The next most cohesive is Avicel102, which has the next highest RSD as well. Fastflo lactose was the most free flowing and had the lowest RSD. The cohesive nature of the powders can be quantified by the flow index from the gravimentric displacement rheometer (GDR) or the dilation ratio from a tumbling drum. Figure 7.2 shows the results of plotting the same RSD values as a function of flow index or dilation. The trending shows increased RSD for as both indicators of cohesivity increase, indicating more freeflowing materials having better feeding consistency. This same properties database correlation studies can be applied to the entire continuous manufacturing line, potentially enabling blend and tablet property predictions.

7.2.2 Residence time distribution (RTD) studies

The residence time distribution of the various unit operations of a continuous processing system is an important part of understanding the process and is essential for traceability of both disturbances and raw material lot changes. In the work presented in Chapter 6, methods utilizing RTD were presented with a direct compaction line used as an example system. However, there are many other manufacturing routes, such as wet granulation or dry granulation, which operate with very different unit operations. Furthermore, the work in Chapter 6 explores a limited set of experimental data in a design space that is very large. The goal for the future of this RTD work should be to further explore the design space of the multiple manufacturing routes in order to populate models based off of process inputs. Predictive process models, incorporating RTD models, programmed into a flowsheet modeling software, such as gPROMS, would greatly improve upon how processes are designed. This ideally would provide the modeling necessary for a proactive designing rather than reactive, which requires more experimentation.

7.2.2.1 RTD of the feeders

Whereas most unit operations have some RTD studies, feeders have not been investigated and are often not viewed as an important unit operation for study. To further understand the feeders and achieve raw material traceability back to the drum, it is necessary to understand the residence time distribution of the feeders. It is expected, that there will be a significant difference depending on the design of the feeders. For example, a mechanically agitated feeder would be expected to have more backmixing than a feeder that is agitated through only vibration or massaging paddles. As the residence time distribution would likely vary from the front to back of the feeder, the tracer response

should be completed using a tracer step changer rather than a pulse response test. Figure 7.3 shows a depiction of the expected RTD model that will be representative of the feeders. The hopper part of the feeder is expected to be nearly plug flow, whereas the bottom feeding bowl is expected to have significantly more backmixing due to the agitator.

7.2.2.2 RTD of Hoppers

The simplest form of a feeder consists of a feeding mechanism and a bulk material hopper. Similar to feeders, the residence time of hoppers have not been studied, yet they are often attached to various unit operations as a collection vessel for material queued within the device. Decoupling the hopper as its own unit operation would provide better process understanding.

7.2.2.3 Multi-tracer RTD studies

An assumption that is often made with RTD studies is that all the components move through similarly with the same RTD. This seems like a reasonable assumption, because a simple material balance of the system assumes that what comes into the system will eventually leave. However, this may not always be the case, as materials that are highly segregating or that may adhere to the walls of the apparatus, it is possible a accumulation behavior may arise. Due to the finite size of the devices accumulation will be limited, and will likely result in a pseudo steady state eventually being achieved, where accumulation eventually equals zero or oscillates. A simple study observing different tracers in the same system could resolve this unknown of whether all components have the same RTD. Furthermore, it would be useful to identify mechanisms such as segregation or wall selectivity that may cause materials to have differing RTDs.

7.2.3 Optimizing the Blender

The performance of the blender can be dramatically changed by the configuration and design of the blender. The shape of the residence time distribution effects the robustness of the blender and its ability to handle inlet fluctuations. Using a very broad residence time distribution may smooth larger fluctuations, however, a larger amount of backmixing also complicates traceability issues by making batches harder to separate. Therefore, there is an optimization problem that needs to be solved. Based on the fluctuations of the inlet streams, the residence time distribution should be shaped to provide just enough fluctuation dampening, while also minimizing the amount of backmixing. However, these are not the only constraints. Although axial mixing may be of interest for minimizing the effect on inlet fluctuations, it is also important to have adequate radial mixing, which will result in a well mixed blend.

7.2.4 Sensing Frequency with Measurement Error

Chapter 6 introduced a method for defining sampling frequency based on the RTD. However, the method assumed that measurement error was very low. With a higher measurement error, the ability to detect any deviation with a single measurement decreases. See Figure 7.4 for a depiction of the effect of measurement error. To ensure a reasonable amount of certainty in the measurements, multiple measurements may be required, resulting in a higher sensing frequency.

7.3 Figures for Chapter 7

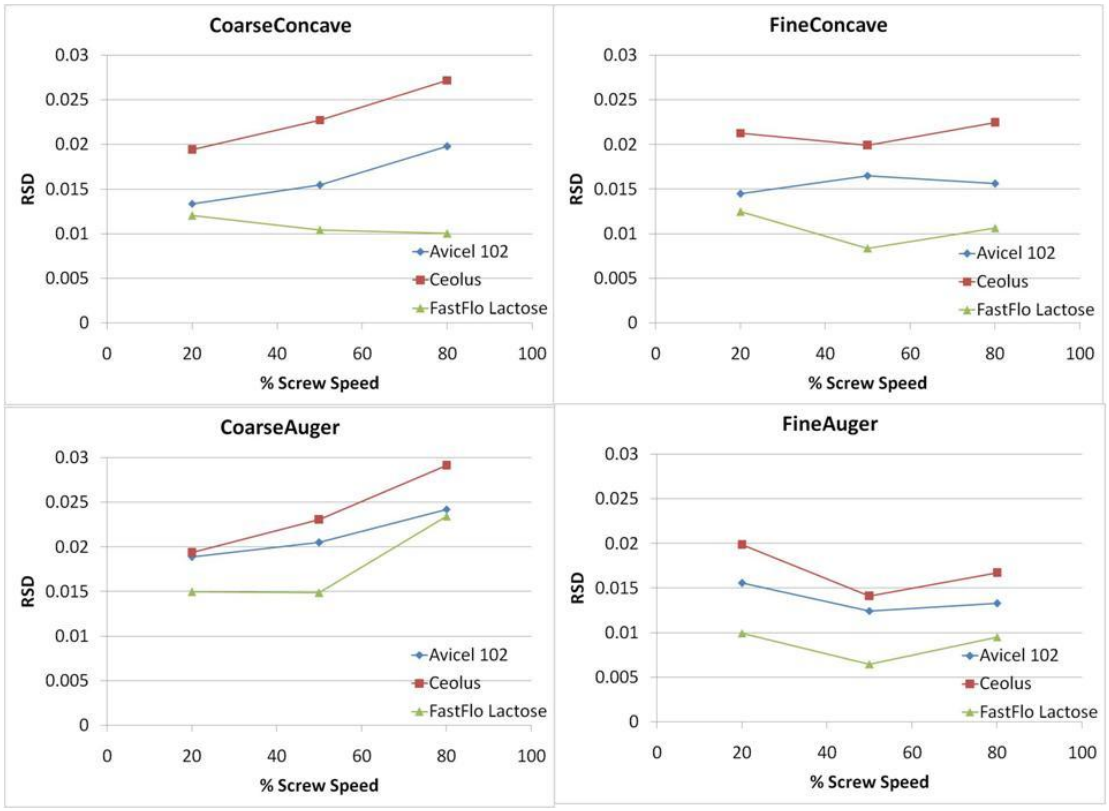

Figure 7.1: Relative standard deviation of feedrate for the feeding of fastflo lactose, avicel 102, and ceolus in the K-Tron KT35 without a discharge screen and using: a.) coarse conave screws, b.) fine concave screws, c.) coarse auger screws, d.) fine auger screws.

a.

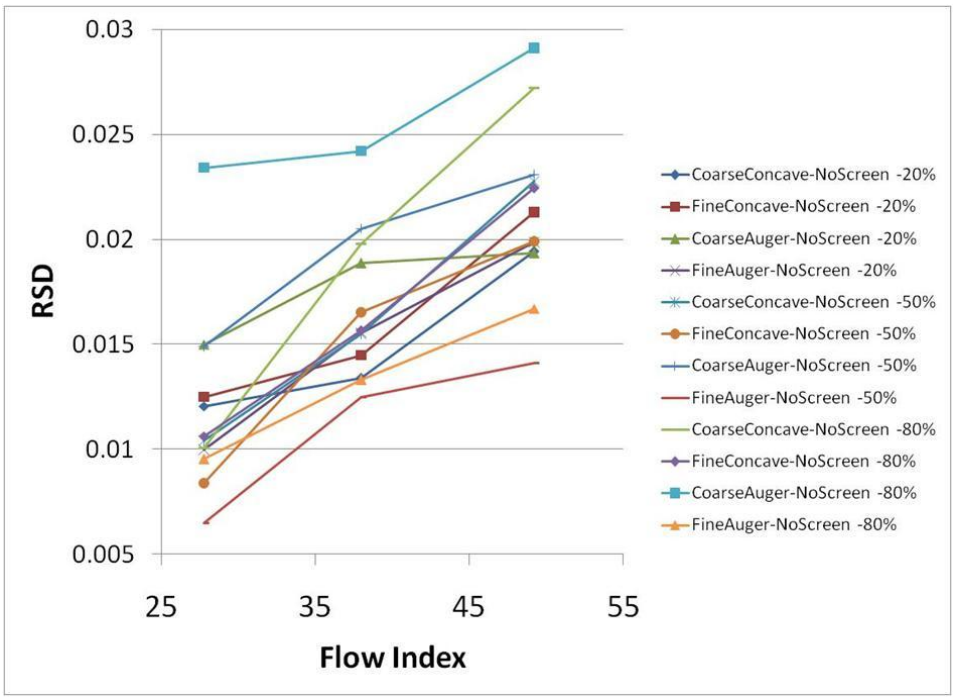

b.

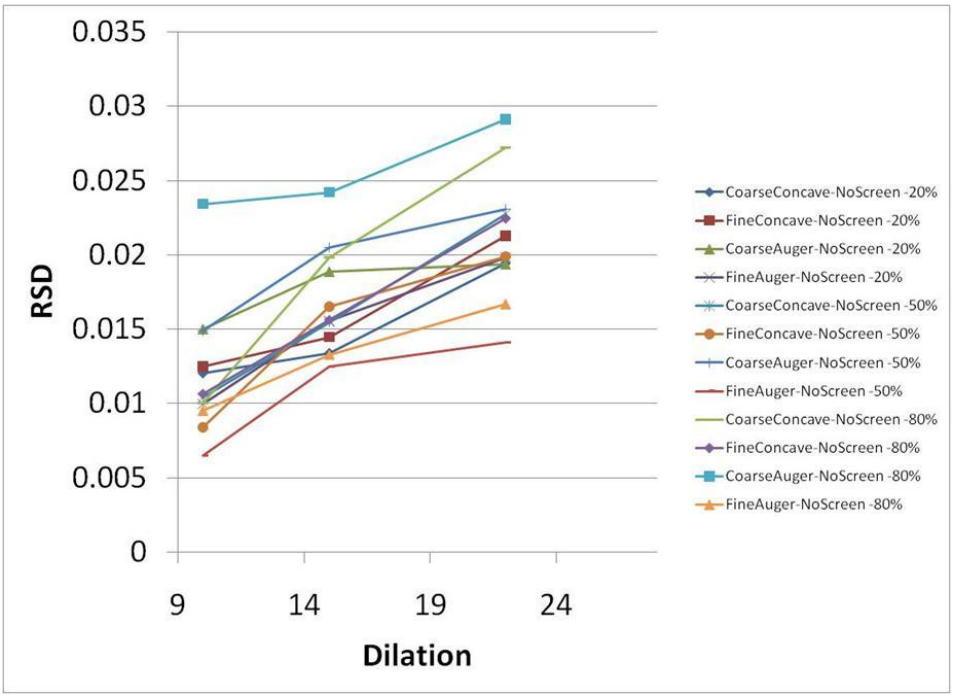

Figure 7.2: Relative standard deviation (RSD) of feedrate plotted as a function of: a.) gravimetric displacement rheometer (GDR) measured flow index and b.) dilation number from a tumbling drum.

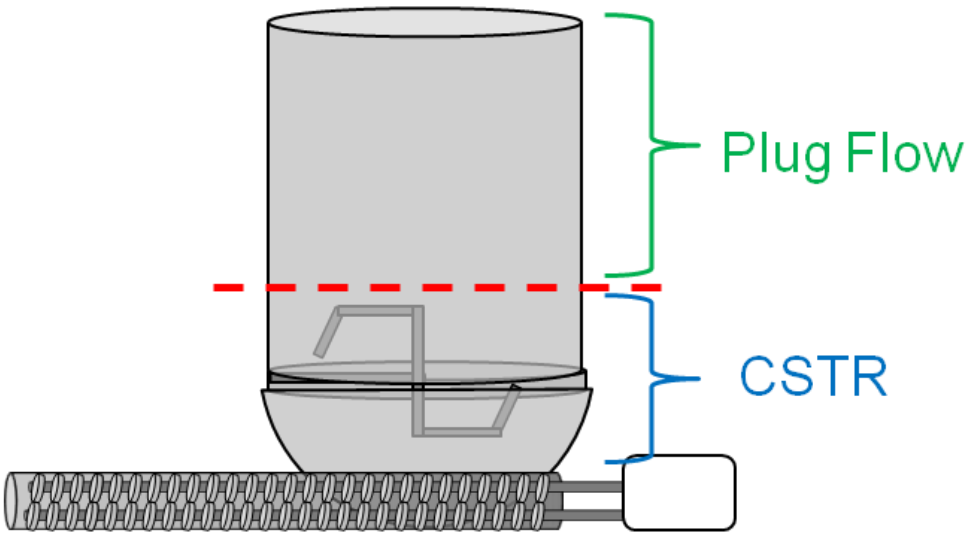

Figure 7.3: Mixing regions within a mechanically agitated screw feeder.

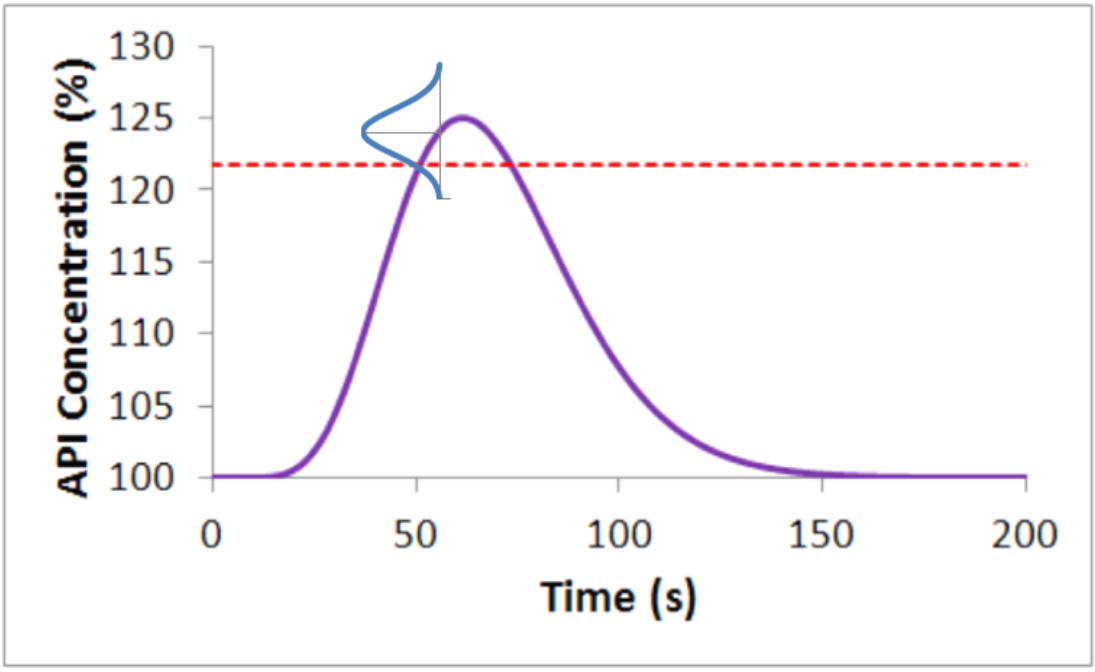

Figure 7.4: Dipiction showing the effect of sensing error on determining pass/fail sensing. The purple curve represents the pulse response of the system. The red dotted line represents a pass/fail limit. The sensing error is represented by a blue gaussian curve.

REFERENCES

[1] S. D. Schaber, D. I. Gerogiorgis, R. Ramachandran, J. M. B. Evans, P. I. Barton, and B. L. Trout, "Economic Analysis of Integrated Continuous and Batch Pharmaceutical Manufacturing: A Case Study," *Ind. Eng. Chem. Res.*, vol. 50, no. 17, pp. 10083–10092, Sep. 2011.

[2] A. Goršek and P. Glavič, "Design of Batch Versus Continuous Processes: Part I: Single-Purpose Equipment," *Chem. Eng. Res. Des.*, vol. 75, no. 7, pp. 709–717, Oct. 1997.

[3] K. Plumb, "Continuous Processing in the Pharmaceutical Industry: Changing the Mind Set," *Chem. Eng. Res. Des.*, vol. 83, no. 6, pp. 730–738, Jun. 2005.

[4] M. Hopkins, "LOSS in weight feeder systems," *Meas. Control*, vol. 39, no. 8, pp. 237–240, 2006.

[5] V. Kehlenbeck and K. Sommer, "Possibilities to improve the short-term dosing constancy of volumetric feeders," *Powder Technol.*, vol. 138, no. 1, pp. 51–56, Nov. 2003.

[6] G. Tardos and Q. Lu, "Precision dosing of powders by vibratory and screw feeders: an experimental study," *Adv. Powder Technol.*, vol. 7, no. 1, pp. 51–58, 1996.

[7] R. Weinekotter and L. Reh, "Continuous Mixing of Fine Particles," *Part. Part. Syst. Charact.*, vol. 12, no. 1, pp. 46–53, 1995.

[8] P. V. Danckwerts, "Continuous flow systems: Distribution of residence times," *Chem. Eng. Sci.*, vol. 2, no. 1, pp. 1–13, Feb. 1953.

[9] J. C. Williams and M. A. Rahman, "Prediction of the performance of continuous mixers for particulate solids using residence time distributions: Part II. Experimental," *Powder Technol.*, vol. 5, no. 5, pp. 307–316, Apr. 1972.

[10] L. Pernenkil and C. L. Cooney, "A review on the continuous blending of powders," *Chem. Eng. Sci.*, vol. 61, no. 2, pp. 720–742, Jan. 2006.

[11] J. C. Williams and M. A. Rahman, "Prediction of the performance of continuous mixers for particulate solids using residence time distributions Part I. Theoretical," *Powder Technol.*, vol. 5, no. 2, pp. 87–92, Jan. 1972.

[12] J. Dai, H. Cui, and J. R. Grace, "Biomass feeding for thermochemical reactors," *Prog. Energy Combust. Sci.*, vol. 38, no. 5, pp. 716–736, Oct. 2012.

[13] S. Yang and J. R. G. Evans, "Metering and dispensing of powder; the quest for new solid freeforming techniques," *Powder Technol.*, vol. 178, no. 1, pp. 56–72, Sep. 2007.

[14] E. C. Abdullah and D. Geldart, "The use of bulk density measurements as flowability indicators," *Powder Technol.*, vol. 102, no. 2, pp. 151–165, Mar. 1999.

[15] E. R. Nowak, J. B. Knight, E. Ben-Naim, H. M. Jaeger, and S. R. Nagel, "Density Fluctuations in Vibrated Granular Materials," *Phys Rev E*, vol. 57, p. 1971, 1998.

[16] S. F. Edwards and D. V. Grinev, "Statistical mechanics of vibration-induced compaction of powders," *Phys. Rev. E*, vol. 58, no. 4, pp. 4758–4762, Oct. 1998.

[17] K. J. Shinners, B. N. Binversie, R. E. Muck, and P. J. Weimer, "Comparison of wet and dry corn stover harvest and storage," *Biomass Bioenergy*, vol. 31, no. 4, pp. 211–221, Apr. 2007.

[18] J. Dai and J. R. Grace, "A model for biomass screw feeding," *Powder Technol.*, vol. 186, no. 1, pp. 40–55, Aug. 2008.

[19] J. B. Myhre and S. Ludescher, "Apparatus and method for controlling flow rate in vibratory feeders," 5341307, 23-Aug-1994.

[20] J. C. Homer, III, J. R. Walsh, and D. P. Ratcliffe, "System for checking the calibration of gravimetric feeders and belt scales ...," 5686653, 11-Nov-1997.

[21] N. Somsuk, T. Wessapan, and S. Teekasap, "Design and Development of a Rotary Airlock Valve for Using in Continuous Pyrolysis Process to Improve Performance," *Adv. Mater. Res.*, vol. 383–390, pp. 7148–7154, Nov. 2011.

[22] T. Sato and Y. Kumamoto, "Adaptive PI control with feed-forward compensator for a weigh feeder," in *Networking, Sensing and Control, 2009. ICNSC'09. International Conference on*, 2009, pp. 428–433.

[23] T. Sato, "Design of a GPC-based PID controller for controlling a weigh feeder," *Control Eng. Pract.*, vol. 18, no. 2, pp. 105–113, 2010.

[24] N. Araki, T. Sato, Y. Kumamoto, Y. Iwai, and Y. Konishi, "Design of weigh feeder control system using extremum-seeking method," in *Asian Control Conference, 2009. ASCC 2009. 7th*, 2009, pp. 250–255.

[25] L. Manci, "Energy Assisted Gravity Flow - Overview of Vibrational Effects on Bulk Solids and Storage Vessels," *Proc. Tech. PROGRAM POWDER BULK SOLIDS Conf. Exhib.*

[26] J. Zhang, Z. Yuan, and X. Wei, "An automatic shake mechanism for the biomass pyrolysis feeding system," *Powder Technol.*, vol. 207, no. 1–3, pp. 348–352, Feb. 2011.

[27] H. Heinrici, L. Toerner, and J. Biebel, "Apparatus for the metered discharge of bulk material from a flexible supply ...," 5735439, 07-Apr-1998.

[28] C. S. Papazoglou and D. L. Pyle, "Air-assisted flow from a bed of particles," *Powder Technol.*, vol. 4, no. 1, pp. 9–18, Nov. 1970.

[29] T. Fahlenbock, "Design Considerations for Refilling and Venting Continuous Loss-in-Weight Feeders." Brabender Technologie Inc.

[30] B. G. Liptak, *Instrument Engineers' Handbook, Fourth Edition, Volume One: Process Measurement and Analysis*. CRC Press, 2003.

[31] K-Tron, "K-Tron Operating Instruction: KSU-II/KCM-KD Operation for LWF, WBF, PID, SFM and VOL Applications." Pitman, NJ: K-Tron, 2006.

[32] I. Ghebre-Sellassie and C. Martin, *Pharmaceutical extrusion technology*. New York: M. Dekker, 2003.

[33] H. F. G. Jr, E. M. M. III, and J. R. W. Jr, *Extrusion: The Definitive Processing Guide and Handbook*. William Andrew, 2004.

[34] D. H. Wilson and J. M. Loe, "Apparatus and method for improving the accuracy of a loss-in-weight feeding ...," 4524886, 25-Jun-1985.

[35] P. Aalto and J.-P. Bjrklund, "Loss-in-weight feeder control," 6446836, 10-Sep-2002.

[36] D. H. Wilson and K. W. Bullivant, "Loss-in-weight gravimetric feeder," 4579252, 01-Apr-1986.

[37] L. Abboud and S. H. S. R. of T. W. S. Journal, "New Prescription For Drug Makers: Update the Plants," *Wall Street Journal*, 03-Sep-2003.

[38] FDA, "Pharmaceutical CGMPs for the 21st Century—a risk-based approach," *Final Rep. Rockv. MD*, 2004.

[39] FDA, "Guidance for Industry: PAT - a framework for innovative pharmaceutical development, manufacturing and quality assurance." Food and Drug Administration, 2004.

[40] ICH, "Guidance for Industry: Q8(R2) Pharmaceutical Development." Food and Drug Administration, 20-Nov-2009.

[41] ICH, "Guidance for Industry: Q9 Quality Risk Management." Food and Drug Administration, 01-Jun-2006.

[42] ICH, "Guidance for Industry: Q10 Pharmaceutical Quality System." Food and Drug Administration, 07-Apr-2009.

[43] J. C. Berridge, "PQLI ®: Current Status and Future Plans," *J. Pharm. Innov.*, vol. 4, no. 1, pp. 1–3, Mar. 2009.

[44] C. Potter, "PQLI Application of Science- and Risk-based Approaches (ICH Q8, Q9, and Q10) to Existing Products," *J. Pharm. Innov.*, vol. 4, no. 1, pp. 4–23, Mar. 2009.

[45] T. Garcia, G. Cook, and R. Nosal, "PQLI Key Topics - Criticality, Design Space, and Control Strategy," *J. Pharm. Innov.*, vol. 3, no. 2, pp. 60–68, Jun. 2008.

[46] A. W. Alexander, B. Chaudhuri, A. Faqih, F. J. Muzzio, C. Davies, and M. S. Tomassone, "Avalanching flow of cohesive powders," *Powder Technol.*, vol. 164, no. 1, pp. 13–21, May 2006.

[47] B. Chaudhuri, A. Mehrotra, F. J. Muzzio, and M. S. Tomassone, "Cohesive effects in powder mixing in a tumbling blender," *Powder Technol.*, vol. 165, no. 2, pp. 105–114, Jul. 2006.

[48] A. Faqih, B. Chaudhuri, F. J. Muzzio, M. S. Tomassone, A. Alexander, and S. Hammond, "Flow - induced dilation of cohesive granular materials," *AIChE J.*, vol. 52, no. 12, pp. 4124–4132, 2006.

[49] A. Faqih, B. Chaudhuri, A. W. Alexander, C. Davies, F. J. Muzzio, and M. Silvina Tomassone, "An experimental/computational approach for examining unconfined cohesive powder flow," *Int. J. Pharm.*, vol. 324, no. 2, pp. 116–127, Nov. 2006.

[50] U. Erdem, "A Guide to the specification and procurement of industrial process weighing systems," *Meas. Control*, vol. 36, no. 1, pp. 25–29, 2003.

[51] M. Frigo and S. G. Johnson, "FFTW: an adaptive software architecture for the FFT," in *Proceedings of the 1998 IEEE International Conference on Acoustics, Speech and Signal Processing, 1998*, 1998, vol. 3, pp. 1381 –1384 vol.3.

[52] K. R. Wilburn, "The business case for continuous manufacturing of pharmaceuticals," Thesis, Massachusetts Institute of Technology, 2010.

[53] H. Leuenberger, "New trends in the production of pharmaceutical granules: batch versus continuous processing," *Eur. J. Pharm. Biopharm.*, vol. 52, no. 3, pp. 289–296, Nov. 2001.

[54] G. Betz, P. Junker-Bürgin, and H. Leuenberger, "Batch And Continuous Processing In The Production Of Pharmaceutical Granules#," *Pharm. Dev. Technol.*, vol. 8, no. 3, pp. 289–297, 2003.

[55] S. Buchholz, "Future manufacturing approaches in the chemical and pharmaceutical industry," *Chem. Eng. Process. Process Intensif.*, vol. 49, no. 10, pp. 993–995, Oct. 2010.

[56] R. Singh, F. Boukouvala, E. Jayjock, R. Ramachandran, M. Ierapetritou, and F. Muzzio, "Flexible multipurpose continuous processing of pharmaceutical tablet manufacturing process," *GMP News Eur. Compliance Acad. ECE*, 2012.

[57] R. Singh, M. Ierapetritou, and R. Ramachandran, "An engineering study on the enhanced control and operation of continuous manufacturing of pharmaceutical tablets via roller compaction," *Int. J. Pharm.*, vol. 438, no. 1–2, pp. 307–326, Nov. 2012.

[58] R. Singh, M. Ierapetritou, and R. Ramachandran, "System-wide hybrid MPC–PID control of a continuous pharmaceutical tablet manufacturing process via direct compaction," *Eur. J. Pharm. Biopharm.*

[59] R. Singh, M. Ierapetritou, and R. Ramachandran, "Hybrid advanced control of flexible multipurpose continuous tablet manufacturing process via direct compaction," in *Computer Aided Chemical Engineering*, vol. Volume 32, Andrzej Kraslawski and Ilkka Turunen, Ed. Elsevier, 2013, pp. 757–762.

[60] R. Singh, F. Boukouvala, E. Jayjock, R. Ramachandran, M. Ierapetritou, and F. Muzzio, "Flexible multipurpose continuous processing," *Pharm Process*, vol. 27, no. 6, pp. 22–25, 2012.

[61] W. E. Engisch and F. J. Muzzio, "Method for characterization of loss-in-weight feeder equipment," *Powder Technol.*, vol. 228, no. 0, pp. 395–403, Sep. 2012.

[62] Y. Gao, F. Muzzio, and M. Ierapetritou, "Characterization of feeder effects on continuous solid mixing using fourier series analysis," *AIChE J.*, vol. 57, no. 5, pp. 1144–1153, 2011.

[63] R. Freeman and X. Fu, "Characterisation of powder bulk, dynamic flow and shear properties in relation to die filling," *Powder Metall.*, vol. 51, no. 3, pp. 196–201, 2008.

[64] R. Freeman, "Measuring the flow properties of consolidated, conditioned and aerated powders — A comparative study using a powder rheometer and a rotational shear cell," *Powder Technol.*, vol. 174, no. 1–2, pp. 25–33, May 2007.

[65] A. Vasilenko, B. J. Glasser, and F. J. Muzzio, "Shear and flow behavior of pharmaceutical blends — Method comparison study," *Powder Technol.*, vol. 208, no. 3, pp. 628–636, Apr. 2011.

[66] A. M. N. Faqih, A. Mehrotra, S. V. Hammond, and F. J. Muzzio, "Effect of moisture and magnesium stearate concentration on flow properties of cohesive granular materials," *Int. J. Pharm.*, vol. 336, no. 2, pp. 338–345, May 2007.

[67] S. Dawoodbhai and C. T. Rhodes, "The Effect of Moisture on Powder Flow and on Compaction and Physical Stability of Tablets," *Drug Dev. Ind. Pharm.*, vol. 15, no. 10, pp. 1577–1600, Jan. 1989.

[68] D. Geldart, "Types of gas fluidization," *Powder Technol.*, vol. 7, no. 5, pp. 285–292, May 1973.

[69] H. Hou and C. C. Sun, "Quantifying effects of particulate properties on powder flow properties using a ring shear tester," *J. Pharm. Sci.*, vol. 97, no. 9, pp. 4030–4039, 2008.

[70] A. Al-Tounsi, R. Puyane, and M. S. J. Hashmi, "Compaction of agglomerated zinc oxide powder," *J. Mater. Process. Technol.*, vol. 37, no. 1–4, pp. 543–550, Feb. 1993.

[71] R. Kaiser, "The agglomeration of zinc oxide powders," Massachusetts Institute of Technology, 1962.

[72] Z. L. Wang, "Zinc oxide nanostructures: growth, properties and applications," *J. Phys. Condens. Matter*, vol. 16, no. 25, pp. R829–R858, Jun. 2004.

[73] A. Moezzi, A. M. McDonagh, and M. B. Cortie, "Zinc oxide particles: Synthesis, properties and applications," *Chem. Eng. J.*, vol. 185–186, pp. 1–22, Mar. 2012.

[74] H. P. Meissner, A. S. Michaels, and R. Kaiser, "Spontaneous Pelletization in Fine Powders," *Ind. Eng. Chem. Process Des. Dev.*, vol. 3, no. 3, pp. 197–201, Jul. 1964.

[75] J. S. Shrimpton and M. Danby, "Effect of poly-dispersity on the stability of agglomerates subjected to simple fluid strain fields," *Powder Technol.*, vol. 228, pp. 241–249, Sep. 2012.

[76] R. E. Freeman, J. R. Cooke, and L. C. R. Schneider, "Measuring shear properties and normal stresses generated within a rotational shear cell for consolidated and non-consolidated powders," *Powder Technol.*, vol. 190, no. 1–2, pp. 65–69, Mar. 2009.

[77] J. W. Carson and H. Wilms, "Development of an international standard for shear testing," *Powder Technol.*, vol. 167, no. 1, pp. 1–9, 2006.

[78] P. Poechlauer, J. Manley, R. Broxterman, B. Gregertsen, and M. Ridemark, "Continuous Processing in the Manufacture of Active Pharmaceutical Ingredients

and Finished Dosage Forms: An Industry Perspective," *Org. Process Res. Dev.*, Sep. 2012.

[79] L. Proctor, P. J. Dunn, J. M. Hawkins, A. S. Wells, and M. T. Williams, "Continuous Processing in the Pharmaceutical Industry," in *Green Chemistry in the Pharmaceutical Industry*, P. J. Dunn, A. S. Wells, and M. T. Williams, Eds. Wiley-VCH Verlag GmbH & Co. KGaA, 2010, pp. 221–242.

[80] M. Warman, "Continuous Processing in Secondary Production," *Chem. Eng. Pharm. Ind. RD Manuf.*, pp. 837–851, 2011.

[81] F. Boukouvala, V. Niotis, R. Ramachandran, F. J. Muzzio, and M. G. Ierapetritou, "An integrated approach for dynamic flowsheet modeling and sensitivity analysis of a continuous tablet manufacturing process," *Comput. Chem. Eng.*, vol. 42, no. 0, pp. 30–47, Jul. 2012.

[82] R. Ramachandran, J. Arjunan, A. Chaudhury, and M. G. Ierapetritou, "Model-Based Control-Loop Performance of a Continuous Direct Compaction Process," *J. Pharm. Innov.*, vol. 6, no. 4, pp. 249–263, Dec. 2011.

[83] S. Chatterjee, "FDA Perspective on Continuous Manufacturing," presented at the IFPAC Annual Meeting, Baltimore, MD, Jan-2012.

[84] F. Muzzio, "Avoiding Blend Segregation in Continuous Manufacturing," presented at the IFPAC - 2014, Arlington, VA, 24-Jan-2014.

[85] FDA, *CFR Part 211: Current Good Manufacturing Practice for Finished Pharmaceuticals*. US Food and Drug Administration, Rockville, MD, www. fda. gov, 21.

[86] Y. Gao, A. Vanarase, F. Muzzio, and M. Ierapetritou, "Characterizing continuous powder mixing using residence time distribution," *Chem. Eng. Sci.*, vol. 66, no. 3, pp. 417–425, Feb. 2011.

[87] Y. Gao, F. J. Muzzio, and M. G. Ierapetritou, "A review of the Residence Time Distribution (RTD) applications in solid unit operations," *Powder Technol.*, vol. 228, no. 0, pp. 416–423, Sep. 2012.

[88] K. Marikh, H. Berthiaux, V. Mizonov, E. Barantseva, and D. Ponomarev, "Flow Analysis and Markov Chain Modelling to Quantify the Agitation Effect in a Continuous Powder Mixer," *Chem. Eng. Res. Des.*, vol. 84, no. 11, pp. 1059–1074, Nov. 2006.

[89] K. Marikh, H. Berthiaux, C. Gatumel, V. Mizonov, and E. Barantseva, "Influence of stirrer type on mixture homogeneity in continuous powder mixing: A model case and a pharmaceutical case," *Chem. Eng. Res. Des.*, vol. 86, no. 9, pp. 1027–1037, Sep. 2008.

[90] A. T. Harris, J. F. Davidson, and R. B. Thorpe, "Particle residence time distributions in circulating fluidised beds," *Chem. Eng. Sci.*, vol. 58, no. 11, pp. 2181–2202, Jun. 2003.

[91] P. M. Portillo, M. G. Ierapetritou, and F. J. Muzzio, "Characterization of continuous convective powder mixing processes," *Powder Technol.*, vol. 182, no. 3, pp. 368–378, Mar. 2008.

[92] O. S. Sudah, A. . Chester, J. . Kowalski, J. . Beeckman, and F. . Muzzio, "Quantitative characterization of mixing processes in rotary calciners," *Powder Technol.*, vol. 126, no. 2, pp. 166–173, Jul. 2002.

[93] G. R. Ziegler and C. A. Aguilar, "Residence time distribution in a co-rotating, twin-screw continuous mixer by the step change method," *J. Food Eng.*, vol. 59, no. 2–3, pp. 161–167, Sep. 2003.

[94] H. S. Fogler, *Elements of Chemical Reaction Engineering*. Pearson Education Internat., 2006.

[95] T. F. Coleman and Y. Li, "On the convergence of interior-reflective Newton methods for nonlinear minimization subject to bounds," *Math. Program.*, vol. 67, no. 1–3, pp. 189–224, Oct. 1994.

[96] T. F. Coleman and Y. Li, "An Interior Trust Region Approach for Nonlinear Minimization Subject to Bounds," *SIAM J. Optim.*, vol. 6, no. 2, pp. 418–445, May 1996.

[97] A. U. Vanarase, J. G. Osorio, and F. J. Muzzio, "Effects of powder flow properties and shear environment on the performance of continuous mixing of pharmaceutical powders," *Powder Technol.*, vol. 246, pp. 63–72, Sep. 2013.

[98] FDA, *CFR Part 210 Current Good Manufacturing Practice in Manufacturing, Processing, Packing, or Holding of Drugs; General*. US Food and Drug Administration, Rockville, MD, www. fda. gov, 21.

[99] C. Moore, "Continuous Manufacturing - FDA Perspective on Submissions and Implementation," presented at the PQRI Workshop on Sample Sizes for Decision Making in New Manufacturing Paradigms, Bethesda, MD, 13-Sep-2011.

[100] W. E. Engisch and F. Muzzio, "Hopper Refill of Loss-in-Weight Feeding Equipment," presented at the 2010 AIChE Annual Meeting, Salt Lake City, UT, 10-Nov-2010.

[101] W. E. Engisch and F. Muzzio, "Method for Characterization of Loss-in-Weight Feeder Equipment," presented at the 2009 AIChE Annual Meeting, Nashville, TN, 10-Nov-2009.